



Universiteit
Leiden
The Netherlands

Molecular and cellular characterization of cardiac overload-induced hypertrophy and failure

Umar, S.

Citation

Umar, S. (2009, June 18). *Molecular and cellular characterization of cardiac overload-induced hypertrophy and failure*. Retrieved from <https://hdl.handle.net/1887/13860>

Version: Corrected Publisher's Version

License: [Licence agreement concerning inclusion of doctoral thesis in the Institutional Repository of the University of Leiden](#)

Downloaded from: <https://hdl.handle.net/1887/13860>

Note: To cite this publication please use the final published version (if applicable).

Molecular and Cellular Characterization
of Cardiac Overload-induced
Hypertrophy and Failure

Soban Umar

COLOPHON

The studies described in this thesis were performed at the department of Cardiology of the Leiden University Medical Center, Leiden, The Netherlands.

Copyright © 2009 Soban Umar, Leiden, The Netherlands. All rights reserved. No part of this thesis may be reproduced or transmitted, in any form or by any means, without prior permission of the author.

Cover:

α -actinin stained neonatal rat cardiomyocyte photographed by Soban Umar, Leiden, The Netherlands.

Layout:

Soban Umar, Leiden, The Netherlands.

Printing:

Gildeprint Drukkerijen, Enschede, The Netherlands.

ISBN: 978-90-9024298-9

Molecular and Cellular Characterization of Cardiac Overload-induced Hypertrophy and Failure

PROEFSCHRIFT

ter verkrijging van

de graad van Doctor aan de Universiteit van Leiden,
op gezag van de Rector Magnificus prof.mr. P.F. van der Heijden,
volgens besluit van het College voor Promoties
te verdedigen op donderdag 18 juni 2009
klokke 15:00 uur

door

Soban Umar

geboren te Multan, Pakistan

in 1979

PROMOTIECOMISSIE

Promotor: Prof. Dr. A. van der Laarse

Copromotores: Dr. D.E. Atsma
Dr. P. Steendijk

Referent: Dr. A.A. Voors (Univ. Groningen)

Overige leden: Prof. Dr. E.E. van der Wall
Prof. Dr. M.J. Schalij
Prof. Dr. D.L. Ypey

LIST OF CONTENTS

Chapter 1

General introduction and outline of the thesis.

Submitted for publication

Chapter 2

Integrin stimulation-induced hypertrophy in neonatal rat cardiomyocytes is NO-dependent.

Molecular and Cellular Biochemistry 2009;320:75-84

Chapter 3

Myocardial collagen metabolism in failing hearts before and during cardiac resynchronisation therapy.

European Journal of Heart Failure 2008;10:878-883

Chapter 4

Activation of signaling molecules and matrix metalloproteinases in right ventricular myocardium of rats with pulmonary hypertension.

Pathology – Research and Practice 2007;203:863-872

Chapter 5

Novel approaches to treat pulmonary arterial hypertension.

Submitted for publication

Chapter 6

Stem cells from rats with pulmonary hypertension reduce pulmonary parenchymal damage, medial hypertrophy of pulmonary arterioles, and right ventricular hypertrophy in rats with pulmonary hypertension.

Submitted for publication

Chapter 7

Intravenous cell therapy with mesenchymal stem cells from donor rats with pulmonary hypertension reduces right ventricular pressure overload and reverses right ventricular hypertrophy in recipient rats with pulmonary artery hypertension.

Submitted for publication

Chapter 8

An exploration of the role of Kv channels in excitability of right ventricular cardiomyocytes from normal adult rats.

Chapter 9

Summary, conclusions, future perspectives and Samenvatting.

List of publications**Acknowledgements****Curriculum Vitae**

CHAPTER 1

General Introduction and Outline of the Thesis

Soban Umar

Part of this introduction is submitted for publication

General Introduction and Outline of Thesis

I. Normal Function

The heart contains two fluid pumps: the right heart pumps blood through the lungs and the left heart pumps blood through the rest of the body. Upon exercise, the heart can adapt its output through a unique property, being the length-dependent force generation. One pump cycle has four phases: the filling phase that has started with opening of the atrioventricular valve while the output valve is closed, the isovolumetric contraction phase occurring with both valves closed, the ejection phase during which the output valve is open whereas the atrioventricular valve is still closed, and the isovolumetric relaxation phase occurring with both valves closed (see Figure 1). During filling of the chamber the enlargement of the chamber by the incoming blood mass occurs at low filling pressures (≈ 5 mmHg), which demonstrates the compliance of the chamber during diastole. During systole the chamber shows a progressive stiffness, necessary to expel a mass of blood from the chamber in an artery with quite high blood pressure.

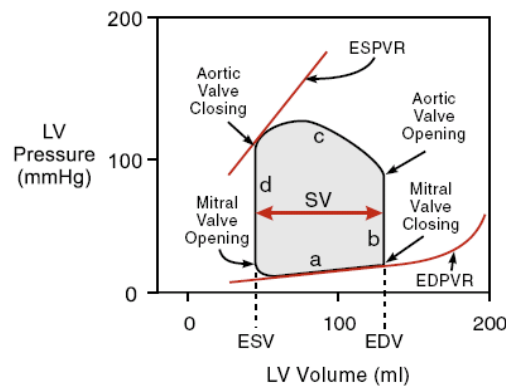


Figure 1. The pressure-volume loop describing one contractile cycle of the left ventricle. The four phases distinguished by the pressure-volume loop are the filling phase (a), isovolumetric contraction phase (b), the ejection phase (c), and the isovolumetric relaxation phase (d). ESV and EDV represent left ventricular end-systolic and end-diastolic volumes, respectively. SV represents stroke volume. ESPVR (the end-systolic pressure-volume relationship) represents the line that connects all end-systolic points of loops generated during changes of preload.

Thus, myocardial tissue should have compliant passive properties, given by relaxed cardiomyocytes and the extracellular matrix (ECM), whereas during systole the myocardial tissue should be stiff which is produced particularly by

contracted cardiomyocytes. The myocardial tissue consists of cardiomyocytes (≈ 75 vol%), interstitium (≈ 15 vol%), and capillaries, venules and arterioles (≈ 10 vol%).

For proper cardiomyocyte function, calcium homeostasis is of utmost importance. Ca^{2+} ions are released from the SR upon Ca^{2+} influx through the sarcolemmal L-type Ca^{2+} channels associated with phase 2 of the action potential. The Ca^{2+} release channels of the SR are blocked by ryanodine and are called the ryanodine receptors (RyR). Ca^{2+} release from the SR causes a rise of intracellular Ca^{2+} concentration ($[\text{Ca}^{2+}]_i$) leading to formation of cross-bridges between myosin and actin, and contraction. Subsequent uptake of Ca^{2+} by the SR via the Ca^{2+} -ATPase pumps (SERCA) restores low diastolic Ca^{2+} concentrations, leading to relaxation [1].

ECM Composition, Synthesis and Degradation

The ECM is a network composed of fibrillar collagens, basement membrane components and proteoglycans. The major part of the ECM is synthesized by interstitial fibroblasts that are—in number—the most abundant cells in the myocardium. The ECM provides a scaffold for cardiomyocytes, fibroblasts, endothelial cells, and the vasculature to align and build a network. The weave of ECM proteins behaves quite elastic at stretch, but becomes stiff if stretched fully. Collagens type I and type III are the predominant interstitial collagens in the myocardium that generate structural integrity for the adjoining cardiomyocytes, providing the means by which cardiomyocyte shortening is translated into overall ventricular pump function. The network of collagen fibers exists at three levels: endomysium, epimysium and perimysium (see Figure 2). Endomysium surrounds individual muscle fibers, while the epimysium network surrounds a group of muscle fibers. The perimysium consists of thick, spiral-shaped bundles of collagen that connect epimysial and endomysial networks.

Basement membrane components include laminin, entactin, fibronectin, collagen type IV and fibrillin. Fibronectin and laminin are important for cell adhesion and cell-cell interaction. Proteoglycans include chondroitin sulfate dermatan sulfate, and heparan sulfate. Syndecans are transmembrane proteoglycans, with a family of four members, syndecan-1 to -4. The main protein constituents of ECM of vascular tissue are collagen and elastin, with elastin being the most abundant protein in large arteries that are continually subjected to pulsatile pressures.

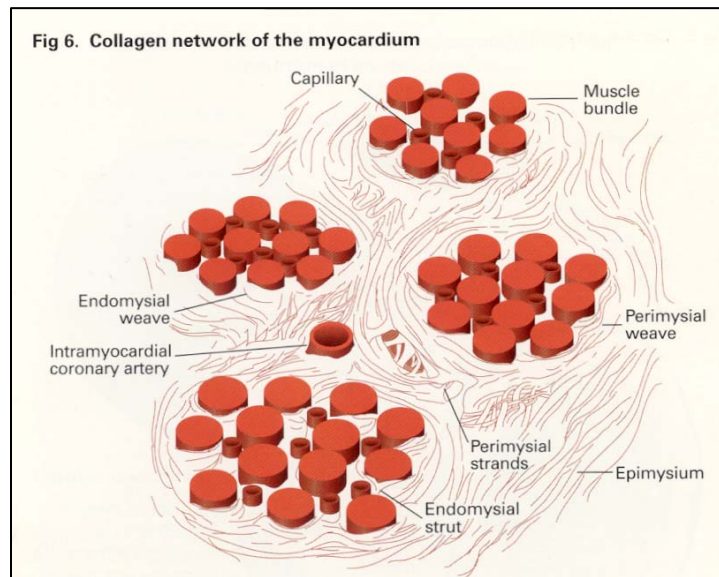


Figure 2. Collagen network of the myocardium (ref. 2).

Matrix Metalloproteinases

ECM integrity is maintained by a balance in the activity of matrix metalloproteinases (MMPs) (see Table), and their tissue inhibitors (TIMPs). The proenzymes of MMPs are secreted by several cell types, including cardiomyocytes. Proenzymes may be converted into active enzymes by other MMPs (e.g. by MMP14, or MT1-MMP) or by proteinases such as urokinase. Inflammatory cytokines, such as interleukin-1 β , interleukin-6, and tumor necrosis factor- α , decrease collagen synthesis by cardiac fibroblasts, whereas anti-inflammatory cytokines, such as transforming growth factor- β , are potent stimulants of collagen synthesis. Cytokines also influence the synthesis and secretion of proMMPs, and MMPs are capable to process or activate cytokines from a latent form into an active form. This way, a complex feedback loop may occur whereby high MMP activity leads to increased cytokine bioactivity, further contributing to ECM remodeling.

MMPs are Ca²⁺ and Zn²⁺-dependent proteases that are primarily synthesized as inactive zymogens (proMMPs), requiring activation by the removal of an amino-terminal propeptide domain either by autoproteolysis or processing by another MMP or serine protease. To date, 24 MMPs have been identified in vertebrates and classified in a number of ways; numerically, according to ECM substrate specificity, or based on shared functional domains (see Table 1). Beyond the ECM proteins, MMPs are now recognized to have non-ECM substrates including a number of growth factors and cytokines. Localization of a protease is an

important determinant in its actions. Membrane-type MMPs (MT-MMPs) are covalently linked to the cell membrane. Some of the secreted MMPs also localize to the cell surface by binding to an integrin [3], cell surface hyaluronon receptor CD44 [4], through interaction with cell surface associated heparin sulfate proteoglycans, collagen type IV, or the extracellular matrix metalloproteinase inducer (EMMPRIN) [5]. In the myocardium, MMPs are expressed by fibroblasts [6] and cardiomyocytes [7], and primarily function extracellularly [5]. In cardiomyocytes MMP2 is present where it colocalizes with troponin I and α -actinin along the Z-lines of the sarcomere [7,8].

Table. Matrix metalloproteinases in vertebrate tissues, including descriptive name and molecular weight of proenzyme and active enzyme.

MMP number	Descriptive name	Mol. weight (latent/active)	Substrate
MMP1	collagenase	52/43 kDa	collagens (I, II, III, VII), basement membrane proteins
MMP2	gelatinase A	72/62 kDa	fragments of a number of collagens (I, III, IV, V)
MMP3	stromelysin	52/43 kDa	fibronectin, laminin, collagens (II, IV, IX)
MMP7	matrilysin	28/19 kDa	
MMP8	collagenase 2	75/55 kDa	
MMP9	gelatinaseB	92/82/65 kDa	fragments of a number of collagens (I, IV, V)
MMP10	stromelysin 2	52/44 kDa	
MMP11	stromelysin 3	51/46 kDa	
MMP12	macrophage elastase	52/20 kDa	
MMP13	collagenase 3	52/42 kDa	collagens (I, II, III)
MMP14	MT1-MMP	64/54 kDa	fibronectin, gelatin, laminin-I, fibrillar collagen
MMP15	MT2-MMP	71/61 kDa	
MMP17	MT4-MMP	62/51 kDa	

Besides MMPs, certain metalloproteinases also contain a unique integrin-binding domain. These enzymes are called A Disintegrin And Metalloproteinase (ADAM).

To date, 34 ADAMs have been identified in a variety of species, with 19 in humans [9]. These membrane-anchored enzymes bring about the shedding of numerous cell surface and matrix-bound proteins and are thus also called sheddases [10]. Among the cell surface molecules processed by ADAMs are growth factors, including heparin-binding epidermal growth factor (HB-EGF), and transforming growth factor- α (TGF α), and cytokines, such as TNF α , IL-1 and IL-6 [11]. These molecules are known to influence myocardial remodeling by introducing hypertrophy and/or apoptosis. Thus, the diversity of substrates now linked to metalloproteinase activity show that the role of MMPs and ADAMs in the myocardium extends beyond ECM degradation to their involvement in cardiac structure, function and response to injury by regulating the release of ligands critical to cardiomyocyte hypertrophy and apoptosis.

Activity of MMPs is controlled by a series of endogenous inhibitors. TIMPs are specific MMP inhibitors in the tissue compartment and have a complex role. They reversibly inhibit activated MMPs through binding with MMPs in a 1:1 stoichiometry. There are four TIMPs in vertebrates. TIMP1 and TIMP3 are transcriptionally induced by growth factors and cytokines, while TIMP2 and TIMP4 are mostly constitutively expressed. TIMP1, TIMP2 and TIMP4 are present in soluble form, while TIMP3 binds to the ECM via heparin sulfate proteoglycans within the ECM [12]. TIMPs efficiently inhibit MMPs albeit with different specificity and affinity. In addition to inhibiting a broad spectrum of MMPs, TIMP-3 is also an effective inhibitor of ADAMs, as well as ADAMs with thrombospondin domain (e.g. ADAMTS-4 and ADAMTS-5) [13]. TIMP1 reportedly inhibits ADAM-10 and ADAMTS-1 [14].

Besides MMPs and ADAMs there is a protein called Extracellular MMP Inducer, abbreviated by EMMPRIN, also known under the name of basigin and CD147. It has been demonstrated that EMMPRIN is a cell surface glycoprotein that belongs to the immunoglobulin superfamily. It forms a complex with $\alpha_3\beta_1$ -integrin [15]. It is highly expressed on the surface of tumor cells and stimulates adjacent fibroblasts or tumor cells to produce MMPs. EMMPRIN also stimulates expression of vascular endothelial growth factor (VEGF) and hyaluronan, which leads to angiogenesis and anchorage-independent growth/multidrug resistance, respectively [16].

Collagen synthesis in tissues is coupled to the release of aminoterminal propeptide of type I procollagen (**PINP**) and aminoterminal propeptide of type III procollagen (**PIIINP**) in blood. Collagen degradation in tissues is coupled to the release of carboxyterminal cross-linked telopeptide of type I collagen (**CITP** or **ICTP**) in blood (see Figure 3) [17].

The natriuretic peptides and NO, both of which function via the second messenger cGMP, demonstrate anti-fibrotic actions by inhibiting collagen synthesis and by stimulating MMP activity. On the other hand, norepinephrine, angiotensin II and endothelin-1 directly stimulate fibroblast proliferation and collagen synthesis, thereby increasing myocardial fibrosis [18,19]. In addition, aldosterone stimulates collagen synthesis in cardiac fibroblasts *in vitro* and in rat hearts *in vivo* [20,21].

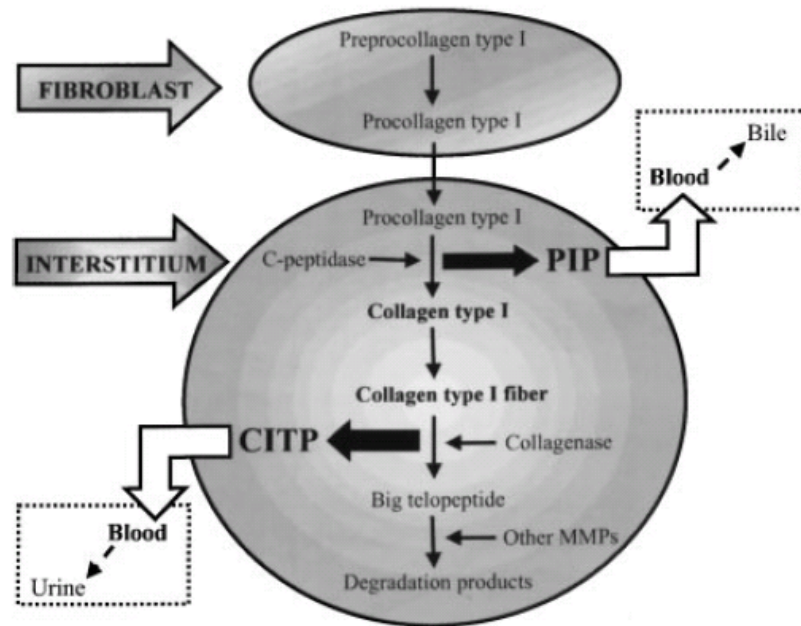


Figure 3. Schematic overview of collagen synthesis and degradation (ref. 17)

Excessive collagen synthesis leads to stiffness of the chambers and consequent impairment of diastolic properties, whereas overdigestion of the ECM results in myocyte-to-myocyte slippage and subsequent ventricular dilatation [22]. The connections of ECM and cardiomyocytes are located at the integrins.

Integrins and Integrin Signaling

Myocardial tissue comprises of fibers of serially coupled cardiomyocytes with parallel running capillaries embedded in a weave of extracellular matrix, mainly composed of collagen. The cardiomyocytes bind to the extracellular matrix by integrin receptors. Integrins are transmembranous heterodimeric receptors composed of an α - and a β -subunit. At the integrin receptors, the extracellular forces (via extracellular matrix), e.g. myocardial stretch, are transferred to the cell where the cellular cytoskeleton, including microfilaments, microtubules and intermediate filaments, maintains the shape and structure of the cell. The cytoplasmic terminus of integrin interacts with the cytoskeleton via a number of proteins that are part of the molecular machinery initiating the signaling response. These proteins include talin, vinculin, α -actinin, paxillin, filamin, zyxin, p130CAS, Src, focal adhesion kinase (FAK) and melusin. FAK is a cytoplasmic tyrosine kinase playing a major role in integrin signaling [23]. Clustering of integrins leads

to the recruitment of FAK to the cell-matrix adhesions and results in activation of FAK via autophosphorylation at Tyr-397. Even soluble integrin receptor ligands, the so called RGD peptides that contain the -Arg-Gly-Asp- sequence, could induce FAK phosphorylation in cardiomyocytes [24].

Several groups have demonstrated that soluble integrin receptor ligands cause a decrease of the L-type calcium currents or a decrease of $[Ca^{2+}]_i$ in arteriolar smooth muscle cells [25-27]. The $\alpha_5\beta_1$ integrin appears to regulate a Tyr-phosphorylation cascade involving Src and several focal adhesion proteins that control the function of the L-type Ca^{2+} channels [28].

Chan *et al.* reported that pretreatment with ryanodine (blocker of the ryanodine receptor (RyR) of the SR) completely eliminated the RGD-induced Ca^{2+} response, suggesting a role of integrin signaling and downstream effects on RyR, leading to Ca^{2+} release from the SR [29]. This result was corroborated by Van der Wees *et al.* who demonstrated that the RGD-induced Ca^{2+} release from SR is blocked by a NOS inhibitor, L-NMMA, while integrin stimulation by RGD was associated with elevation of intracellular NO, probably by NOS1, a NO-synthase isoform that is localized to the SR [30].

Ingber and colleagues proposed that upon extracellular forces integrins and cytoskeleton reorganise to form focal adhesions that transfer mechanical signals across the cell surface [31]. At these focal adhesion complexes several components of the cell's signal transduction systems are organised, including tyrosine kinases, inositol lipid kinases, ion channels, and certain growth factor receptors [32]. Signaling activities that have been shown to be modulated by mechanical distortion or fluid shear stress and to be mediated by integrins of focal adhesions in the cell include Src, focal adhesion kinase (FAK), extracellular receptor kinase-1 and -2 (ERK1/2), Shc, Grb2, protein kinase C (PKC), nuclear factor- κ B (NF- κ B), Akt, phosphatidyl-3-P kinase (PI3K), Ca^{2+} ions, cAMP, various stress-sensitive ion channels, actin polymerisation, and expression of genes encoding platelet derived growth factor (PDGF), endothelin-1 (ET1), and sterol regulatory element-binding protein-1 (reviewed in [33]). In skeletal muscle cyclic mechanical stretch induced the expression of β_{1D} -integrin, which, in turn, stimulated NO production and activated the downstream signaling proteins of the integrin pathway, FAK and RhoA. Activated FAK was assessed by FAK phosphorylation at Tyr397 and activated RhoA was assessed by activity assay. Stimulated NO production was considered to be due to NOS3 activation [34].

NO-Synthases and NO

NO-synthase (NOS) catalyzes the conversion of L-arginine to L-citrulline + nitric oxide (NO). In the heart three NOS isoforms are present: NOS1, or neuronal NOS (nNOS), NOS2, or inducible NOS (iNOS), and NOS3, or endothelial NOS (eNOS). NOS1 and NOS3 are constitutively present enzymes and their enzyme activity is Ca^{2+} -dependent [35]. NOS2 is absent in the healthy heart, but its expression is induced by inflammation, mediated through cytokine-inducible transcription factors, such as IFN regulatory factor-1 and NF- κ B to elements within the NOS2 promoter [36,37]. Massive quantities of NO generated by NOS2 induced by exogenously interleukin- 1β , interferon- γ and lipopolysaccharide (LPA)

added to neonatal rat cardiomyocytes are shown to be toxic [38]. NOS2's enzyme activity is Ca^{2+} -independent.

As will be seen in the following paragraphs dealing about NOS isoforms and sub-cellular NOS compartmentalization, NO produced by a specific NOS isoform does not act as a freely diffusible messenger within the cardiomyocyte. In the tissue NO has two main effects: (*i*) NO stimulates the activity of guanylate cyclase, an enzyme that produces cGMP from GTP, and (*ii*) NO nitrosylates tyrosine residues in proteins and thiol-groups of cysteine in proteins. Upon nitrosylation proteins may change their properties, comparable to (but different from) the changes induced by phosphorylation, isoprenylation, geranyl-geranylation and palmitoylation [39-41]. Cellular proteins that may undergo S-nitrosylation are L-type Ca^{2+} channel [42-44], Kv1.5 channel [45], Ca^{2+} -activated ATPase of the sarcoplasmic reticulum (SR) [46], and the ryanodine receptor-2 of the SR [47,48]. This NO-induced post-translational modification of proteins serves as a major effector of NO bioactivity and an important mode of cellular signal transduction. Animals deficient in S-nitrosoglutathione reductase (GSNOR) show increased steady-state levels of circulating S-nitrosylated proteins at basal conditions and elevations of S-nitrosothiols in tissues following challenge by cytokines [49,50]. Thus, formation of S-nitrosothiols and their subsequent clearance are characteristics of NO-related signaling, and have analogies in phosphorylation of proteins by kinases and subsequent dephosphorylation by phosphatases. Thus, S-nitrosothiol turnover is considered to contribute to physiologic signaling. The systems affected most by GSNOR deficiency include the liver, immune system, and cardiovascular system.

NO exerts anti-apoptotic effects by S-nitrosylating and thereby inhibiting caspases 3 and 9, the kinase activities of both apoptosis signaling kinase-1 and c-Jun N-terminal kinase, and the transcriptional activity of jun [51-55].

NOS3

Under normal circumstances NO exerts several direct functions in the myocardium which are probably not related to the vasodilatory function of NO, such as acceleration of relaxation [56,57]. This effect is attributed to cGMP-dependent, protein kinase (PKG)-mediated phosphorylation of troponin I, leading to a reduction in myofilament Ca^{2+} sensitivity [58-60]. Apparently, these effects are exerted by stimulated NO release from vascular NOS3, as studies in hearts from NOS3^{-/-} mice have not shown changes in myocyte relaxation [61], nor LV diastolic function [62], nor force-frequency response [63]. Myocardial NOS3 is mostly localized at the sarcolemmal and T-tubular caveolae, sites where caveolin-3 is also localized and where several signal transduction pathways have been shown to be modulated by NO [64]. Thus, sarcolemma-bound NOS3 inhibits the L-type Ca^{2+} channel and attenuates the β -adrenergic receptor-stimulated increase in myocardial contractility [62,65]. In mice with cardiomyocyte-specific NOS3 overexpression the line with highest level of transgenic NOS3 protein expression had increased heart weights. All lines displayed depressed LV peak systolic pressures, which was partially reversed by administration of L-NAME, suggesting

a net negative inotropic effect of NOS3-derived NO due to a blunted myofilament Ca^{2+} sensitivity [66].

NOS3 has been reported to co-purify with RyR [67] and to increase RyR open probability (P_o) and the amplitude of the calcium transient under conditions of sustained myocardial stretch via a cGMP-independent mechanism [68].

Angiotensin-converting enzyme (ACE) inhibitors have been shown to enhance NOS3 expression and NO bioavailability (reviewed in [69]). Such a mechanism may contribute to the beneficial effects of ACE inhibitors in patients with heart failure. Moreover, NOS3 plays an important anti-atherogenic role: NOS3-derived NO inhibits (*i*) proliferation of rat aortic smooth muscle cells in a cGMP dependent way [70], (*ii*) monocyte adhesion to aortic endothelial cell monolayers [71], and (*iii*) collagen-induced platelet aggregation [72]. However, Garg & Hassid reported that NO from NO-donors like S-nitroso-N-acetylpenicillamine and isosorbide dinitrate, administered to BALB/c 3T3 fibroblasts, decreased DNA-synthesis and cell proliferation in these cells, without any effect on cGMP accumulation [73].

NOS2

Upregulation of NOS2 by interleukin- 1β and interferon- γ increases apoptosis in neonatal rat cardiomyocytes by a process that is independent of guanylate cyclase activation and cGMP [74]. These authors also demonstrated that cytokine-induced apoptosis and peroxynitrite-induced apoptosis of cardiomyocytes are prohibited by treatment with a peroxynitrite scavenger. Generally spoken, NOS2-derived NO is considered to have detrimental effects on the myocardium. Mice with myocardial NOS2 overexpression suffered from cardiac fibrosis, cardiomyocyte death, cardiac hypertrophy, and cardiac dilatation. While a few NOS2-overexpressing mice developed overt heart failure, most animals died suddenly from atrioventricular block and asystole [75]. These data suggest that increased myocardial NOS2 activity is capable of initiating a process of cardiac remodeling that is characterized by ventricular hypertrophy, dilatation and sudden cardiac death.

NOS1

Myocardial NOS1 is normally localized at the sarcoplasmic reticulum (SR) membrane vesicles, where it influences the activities of calcium-handling genes [76,77]. The ryanodine receptor (RyR2) of the SR is also regulated by FKBP12 subunits, calmodulin, and protein kinases [78].

Myocardial NOS1 stimulates SR Ca^{2+} release and reuptake, facilitating Ca^{2+} -induced Ca^{2+} release and potentiation of the cardiac force-frequency response [63,79], probably by S-nitrosylation of calcium-handling proteins.

Accordingly, in NOS1^{-/-} mice β -adrenergic receptor stimulation elicits a smaller LV inotropic response compared to control mice [65,80]. NOS1^{-/-} mice had increased basal contraction, both in isolated LV cardiomyocytes as in their hearts in vivo. NOS1 disruption increased Ca^{2+} current and prolonged the slow time constant of inactivation of I_{Ca} significantly, leading to an increased Ca^{2+} influx and a greater

calcium load in SR in NOS1^{-/-} cardiomyocytes [77]. Also the Ca²⁺ transient peak amplitude was greater in NOS1^{-/-} cardiomyocytes than in cardiomyocytes from wild-type mice. The contractile response to β-adrenergic stimulation was greatly enhanced in NOS1^{-/-} cardiomyocytes as well as in cardiomyocytes from wild-type mice treated with a specific NOS1 inhibitor, vinyl-L-N-5-(1-imino-3-butenyl)-L-ornithine (L-VNIO) [81].

NOS1 inhibits xanthine oxidoreductase activity, both enzymes co-localizing in the SR. Thus, in NOS1^{-/-} mice xanthine oxidoreductase-mediated production of oxyradicals (ROS) is increased, leading to depression of myocardial excitation-contraction coupling [82]. NOS1 deletion or inhibition leads to increased Ca²⁺ current through the L-type Ca²⁺ channels and reduction in SR SERCA2A activity, leading to increase of contraction and impairment of relaxation [57]. However, the positive force-frequency relationship in wild type mice is considerably attenuated in NOS1^{-/-} mice, which suggests that NOS1-derived NO may enhance the force-frequency relationship [63]. This suggestion was rejected when the same authors found out that the force-frequency relationship in NOS1^{-/-} mice normalized upon administration of allopurinol, an inhibitor of xanthine oxidoreductase [82]. Thus, Khan and coworkers concluded that a ROS-mediated reduction in myofilament Ca²⁺ sensitivity may be the mechanism underlying the reduced force-frequency relationship in NOS1^{-/-} mice [82].

Isolated cardiomyocytes from mice with myocardial-specific overexpression of NOS1 demonstrated lower Ca²⁺ current density, lower amplitude of the Ca²⁺ transient, and lower amplitude of cell shortening, while their hearts in vivo revealed reduced contractility as judged from lower LV ejection fraction and lower dP/dt_{max} compared to nontransgenic littermates [83].

NO activates skeletal and cardiac ryanodine receptors, thereby regulating force in striated muscle [84]. NO-induced S-nitrosylation of ryanodine receptor-2 of the SR can increase the RyR open probability (P_o) through this mechanism [47,48]. There is evidence that S-nitrosylation of RyR2 and the L-type Ca²⁺ channel is preferentially mediated by NOS1-derived NO [85]. However, also NOS3 has been reported to co-purify with RyR [67] and to increase P_o of RyR as well as the amplitude of the calcium transient under conditions of sustained stretch via a cGMP-independent mechanism [68].

Like many signaling proteins, the activity of NOS1 can be regulated by phosphorylation. If phosphorylated by calcium calmodulin-dependent protein kinase II (CaMKII), NOS1 activity diminished, but after phosphorylation by protein kinase C (PKC) NOS1 activity demonstrated a modest increase [86].

II. Hypertrophy

Upon continuous overload of the heart, either by pressure or by volume, the myocardial tissue undergoes adaptation-like reactions of which growth is the most prominent. This myocardial growth is mainly produced by growth of the existing cardiomyocytes (cell hypertrophy), whereas the non-myocytes of the myocardium, e.g. the fibroblasts, undergo hyperplasia to keep non-myocyte density more or less constant. Other reactions observed upon initiating myocardial hypertrophy is the expression of genes encoding proteins that were expressed in the fetal stage

only, such as atrial natriuretic factor in ventricular tissue and α -skeletal muscle-actin in ventricular tissue, whereas several other genes are downregulated (e.g. Ca^{2+} -activated ATPase of the sarcoplasmic reticulum [87]) or upregulated (e.g. Na^+ , Ca^{2+} -exchanger, β -myosin heavy chain). Although gene expression profiles in hypertrophied myocardium of rats subjected to pressure overload and to volume overload are similar for several genes, such as increased expression of B-type natriuretic peptide, lysyl oxidase-like protein-1 and metallothionein-1, other genes had overload-specific expression changes [88].

The hypertrophic ventricle suffers, due to a thicker wall, from impaired diastolic filling, leading to higher filling pressures.

A special type of cardiac hypertrophy is the hypertrophy usually observed in athletes of endurance sports, such as elite cyclists. These athletes have a “physiologic” hypertrophy that serves their exercise well, being large chambers that can fill with large volumes of blood and with preserved contractile properties. At rest, these athletes have a cardiac output that is produced by ≈ 40 beats per minute.

A cell model of mechanical loading is the *in vitro* mechanical stretch model of cultured NRCMs. Upon stretch of these cells intracellular Ca^{2+} concentration increases [89], thereby activating several Ca^{2+} -dependent processes, such as calcineurin activation [90]. This Ca^{2+} /calmodulin-activated phosphatase is responsible for dephosphorylation of NFAT3 leading to nuclear translocation and transcriptional activation of numerous hypertrophy genes [91].

ECM Composition, Synthesis and Degradation

The extent of ECM remodeling depends partly on a balance between pro-inflammatory and anti-inflammatory cytokines, which can be differentially activated depending on the type of myocardial insult or the stage of disease progression. Pressure overload-induced myocardial stress is associated with increased concentrations of inflammatory cytokines. Components of the ECM, such as fibronectin, laminin and collagens I and III, are upregulated during *in vivo* hypertrophy [92-94]. Also, several matricellular proteins in the ECM are upregulated during cardiac hypertrophy, such as osteopontin and tenascin [95,96]. The extent of ANP expression in rat cardiomyocyte cultures that were stimulated with an α_1 -adrenoceptor agonist appeared to be highly dependent of the ECM components present in the coating of the culture dishes, such as fibronectin and laminin [97].

In hypertensive heart disease, fibrous tissue accumulation in the myocardium leads to myocardial dysfunction and heart failure. To assess efficacy of therapeutic strategies changes in myocardial collagen turnover should be monitored. To this purpose, the use of serological markers of collagen turnover, such as aminoterminal propeptide of type I procollagen (PINP), aminoterminal propeptide of type III procollagen (PIIINP) and carboxyterminal cross-linked telopeptide of type I collagen (CITP or ICTP), are extremely useful. The plasma level of PINP is significantly correlated to the collagen volume fraction in the myocardium of spontaneously hypertensive rats [98] and in the myocardium of hypertensive patients [99]. Treatment of spontaneously hypertensive rats with

quinapril [98] or losartan [100] led to (*i*) reduction of myocardial fibrosis, (*ii*) lower collagen volume fraction in the myocardium, (*iii*) lower plasma PINP concentrations, and (*iv*) a tendency to increased plasma ICTP concentrations. In hypertensive patients, treatment with losartan led to (*i*) lower collagen volume fraction in the myocardium, and (*ii*) lower plasma PINP concentrations [101]. As normally collagen synthesis is in equilibrium with collagen degradation [102], situations that disturb this equilibrium, like long-standing hypertension, are associated with abnormalities in either plasma PINP or PIIINP levels and/or abnormalities in plasma ICTP and/or MMP levels, and/or TIMP levels. In patients with hypertrophic cardiomyopathy myocardial collagen turnover is enhanced compared with controls, as reflected by higher levels of PINP, ICTP, MMP2, MMP9, and TIMP-1 in plasma of patients compared to plasma of controls [103]. The higher the plasma PIIINP level, the smaller was the LV end-diastolic diameter [103]. Quality of LV diastolic function, represented by the difference in duration between transmitral forward wave (A) and pulmonary venous retrograde (Ar) wave, was (*i*) directly related to plasma MMP1 and MMP2 levels, and (*ii*) inversely related to plasma PINP levels [103]. Although increased levels of MMP1 and MMP2 in plasma of patients with hypertrophic cardiomyopathy would compensate for increased plasma PINP and PIIINP levels, the increased plasma TIMP-1 level may explain why, in general, myocardial collagen turnover is enhanced in the patients associated with LV diastolic dysfunction.

Integrins and Integrin Signaling

In pressure-overload hypertrophy myocardial expression of integrins was increased markedly. The most abundantly expressed integrin in ventricular tissue, integrin β_{1D} , was upregulated together with integrin α_1 , α_5 , and α_7 . ANP mRNA was increased 6-fold, and myocardial concentrations of phosphorylated FAK, ERK1 and ERK2 were elevated [104]. In rat cardiomyocytes in vitro α_1 -adrenergic stimulation resulted in cardiomyocyte hypertrophy, increased protein levels of integrin β_{1D} by a factor of 3-4, and rapid and sustained phosphorylation of FAK [105]. Also β_3 -integrin plays a role in cardiac hypertrophy. In pressure-overloaded rat RV β_3 -integrin, c-Src and FAK associate in a cytoskeleton-bound complex [106]. Stimulation of β_3 -integrin by **Arg-Gly-Asp** containing peptide in isolated adult cardiomyocytes triggers (*i*) activation of c-Src accompanied by binding to p130CAS and phosphorylation of FAK on Tyr925 [107] and (*ii*) activation of p70S6 kinase [108]. FAK has an important role in hypertrophic growth of cardiomyocytes. Upon pressure-overload myocardial FAK tyrosine phosphorylation is increased, associated with activation of c-Src and a number of downstream adapter and signaling proteins such as p130CAS, GRBS, PI3K and ERK1/2 [24,105,109-113]. Also mechanical stretch activates FAK and ERK1/2 [110,114]. FAK signaling also plays a key role in cardiomyocyte hypertrophy induced by α_1 -adrenoceptor stimulation [105,111], endothelin-1 [112], and angiotensin II [115], all three being well known hypertrophic stimuli acting via G protein coupled receptors. Phenylephrine-mediated ANP expression is attenuated by the dominant negative FAK mutant, FRNK [105] and by a dominant negative form of integrin β_{1D} [97]. By overexpression of β_1 -integrin in rat

cardiomyocyte cultures that were stimulated with an α_1 -adrenoceptor agonist, protein synthesis and ANP expression increased ≈ 2 -fold [97].

In response to increased hemodynamic load, ligand binding of integrins in the cardiomyocytes leads to their clustering. To propagate integrin signaling, focal adhesion complexes enriched in adapter and signaling molecules are subsequently assembled, leading to activation of pathways that are known to be implicated in the hypertrophic response. Studies that have used myocardial hypertrophy-inducing stimuli, like stretch [110], endothelin-1 [112], and phenylephrine [111], implicate a prominent role for integrins, integrin-dependent FAK multicomponent signaling complex, and downstream Tyr-phosphorylation of signaling molecules. The responses to these stimuli appear to be dependent of the type of ECM protein and the type of integrin receptor. Cultured neonatal rat ventricular myocytes that were stretched on deformable silicone sheet coated with collagen caused activation of the prepro-B-type-natriuretic peptide (preproBNP) gene promoter that was dependent of the presence of the integrin subunits β_1 , β_3 and $\alpha_v\beta_5$ [116]. Stretch of cardiomyocytes can cause hypertrophy and induction of gene expression [117-120], as well as phosphorylation of FAK [121] and activation of the Ras/ERK1/2 pathway [119,122]. In pressure-overloaded rat heart, Franchini and coworkers observed a time-dependent increase in (i) FAK phosphorylation at Tyr397, (ii) c-Src phosphorylation at Tyr416, (iii) co-immunoprecipitation of FAK with actin, and (iv) phosphorylation of ERK/2 and Akt [109].

Overexpression of integrin β_{1D} or FAK triggers hypertrophy in NRCMs [105].

NO-Synthases and NO

NOS3

NOS3 normally generates NO, which can have antihypertrophic influences. However, pressure load results in NOS3 uncoupling associated with reduced tetrahydrobiopterin levels, transforming NOS3 activity to favor ROS generation [123]. In cardiomyocytes isolated from pressure-overloaded hearts NOS3 has reduced activity and expression [124]. Inhibition of endogenous NO formation induces myocardial hypertrophy [125]. Upon inhibition of NOS3-derived NO formation, adult rat ventricular cardiomyocytes showed an increase in protein synthesis and cell size [126], which confirms an earlier report demonstrating that NOS3^{-/-} mice have hypertension and left ventricular hypertrophy [127]. In NOS3^{-/-} mice pressure overload induced more severe left ventricular hypertrophy, LV dysfunction and myocardial fibrosis than in wild-type mice [128]. But if NOS3 was restored in the hearts of NOS3^{-/-} mice, pressure overload by aortic constriction caused less LV hypertrophy and dysfunction than observed in NOS3-deficient mice [129]. Contradictory reports about the effects of NOS3 and NOS3-deficiency on pressure-overload LV hypertrophy and dysfunction have been published [123,130]. The former authors stipulated that NOS3 expression can have deleterious effects due to its uncoupling during pressure-overload, leading to

oxidant stress [123]. The latter authors stated that ANP production, associated with pressure overload, may prevent hypertrophy in NOS3-deficient mice [130]. Cardiac-specific overexpression of NOS3 attenuates the LV hypertrophy induced by isoproterenol infusion [131] and the LV hypertrophy induced by coronary artery occlusion [132].

NOS1

In cardiomyocytes isolated from pressure-overloaded hearts NOS1 undergoes upregulation [133].

NOS2

Mice with aortic constriction have induction of myocardial NOS2 expression and LV hypertrophy. NOS2-deficient mice demonstrated –upon aortic constriction– much less hypertrophy, dilatation, fibrosis and dysfunction, than wild-type mice with aortic constriction [134].

III. Heart Failure

Compensated hypertrophy is often seen to undergo a transition to heart failure [135]. Thus, although neurohumoral stimuli are accumulating to stimulate the heart to higher achievements, the heart is not able to do so leading to increased filling pressures and venous congestion. The failing heart has undergone many changes, the most prominent being changes in the calcium handling proteins [136]. The changing geometry, architecture and properties of the chamber are generally indicated as (adverse) chamber remodeling, in severe cases associated with atrioventricular valve insufficiency, dyssynchronous contractions of the chamber's wall segments, and rhythm disturbances. An important mediator of ventricular remodeling is the neurohumoral activation of the heart by the sympathetic nervous system and the renin-angiotensin-aldosterone system (RAAS). Full recognition of their deleterious influences on the heart has led to the foundation of the cornerstones of heart failure therapy: β -blockers and ACE-inhibitors (or angiotensin receptor type 1-blockers).

In the myocardial tissue the ECM undergoes a series of changes due to (*i*) myocardial collagen accumulation, (*ii*) collagen fibril disruption, (*iii*) altered arrangement and reduced cross-linking between collagen fibers, and (*iv*) synthesis of proteins that are not present in the healthy myocardium. To the latter group of proteins belong tenascin-C [137], thrombospondin-2 [138], matrix Gla protein [139], and osteopontin [139]. The volume percentage of ECM in failing myocardial tissue is usually increased, which is often accompanied by increased serum levels of aminoterminal propeptide of type I procollagen (PINP) and aminoterminal propeptide of type III procollagen (PIIINP), two propeptides that are liberated from the tissue upon collagen type I and type III synthesis. At the same time serum levels of carboxyterminal cross-linked telopeptide of type I collagen (ICTP) are low, representing a low rate of collagen degradation [17]. These

changes in ECM composition are ascribed to the myocardial fibroblasts that are stimulated by high plasma levels of catecholamines, angiotensin-II and aldosterone. High levels of collagen degrading enzymes, such as collagenases, may lead to increases in LV dimensions and subsequent cardiomyocyte slippage that may contribute to progressive LV remodelling [22]. In an animal model of hypertensive heart disease, increased expression of collagenases coincided with the transition from hypertrophy to heart failure [140].

During cardiac overload, calcium homeostasis becomes disturbed leading to an increase of diastolic $[Ca^{2+}]_i$ and a decrease of systolic $[Ca^{2+}]_i$. One of the underlying mechanisms is a decreased activity of SERCA. Recently, also the changes in cardiac RyR (RyR2) function are becoming elucidated. RyR2 comprises a tetramer composed of 4 RyR2 monomers, each binding 1 molecule of FKBP12.6 (also known as calstabin-2) [141]. Other proteins binding to the RyR2/FKBP12.6 complex are protein kinase A (PKA), the protein phosphatases PP1 and PP2A, and the anchoring protein mAKAP. In failing hearts phosphorylation of RyR2 by PKA causes dissociation of FKBP12.6 from the channel resulting in altered channel function manifested as an increased open probability (P_o) of RyR2 [142]. Secondly, RyR2 may become S-nitrosylated by SR-associated NOS1, which may influence P_o [47]. In failing cardiomyocytes an increased diastolic $[Ca^{2+}]_i$ and an increased Na^+,Ca^{2+} -exchanger (NCX) may stimulate an electrogenic Na^+ influx leading to early and delayed afterdepolarizations, underlying life-threatening arrhythmias. In this respect it is worthwhile mentioning that fish oils, such as EPA and DHA, protect against lethal arrhythmias and reduce P_o of RyR [143]. Moreover, several mutations in the human RyR2 gene are associated with stress-induced ventricular tachycardia, leading to sudden cardiac death. In molecular and cellular studies these mutations exhibit gain-of-function Ca^{2+} -release properties following cell stimulation [144].

ECM Composition, Synthesis and Degradation

The oxidative stress in the failing heart, in combination with high plasma levels of catecholamines, angiotensin-II, aldosterone, and endothelin-1, induces the synthesis of several MMPs and TIMPs, via transcription factor binding elements in their promoters, like binding sites for NF- κ B, AP-1, Ets, and GATA. Also pro-inflammatory cytokines may activate transcription factors, leading to induction of MMPs and TIMPs [145]. Besides transcriptional regulation, ROS can also post-transcriptionally activate MMPs, e.g. by activating proMMPs. In failing hearts of patients with ischemic cardiomyopathy (ICM) or idiopathic dilated cardiomyopathy (DCM) protein and mRNA expression of TIMP1 and TIMP3 were reduced, but TIMP2 expression was unchanged [146]. These alterations were associated with increases in myocardial MMP1, MMP2, MMP9, MMP13 and MMP14 protein concentrations [147-151]. Right ventricular biopsies from hearts of patients with DCM demonstrated an inverse correlation between myocardial MMP2 and TIMP2 levels and the LV ejection fraction [152]. In patients with progressive heart failure, myocardial MMP1 and TIMP1 concentrations were significantly elevated compared to donor hearts [153]. In myocardium of patients with hypertensive

heart disease TIMP1 levels correlated with extent of fibrosis. This inhibitive effect on collagenase activity was associated with increased rates of collagen synthesis [154].

In myocardium of patients with heart failure several inflammatory cytokines, such as IL-1 β , IL-6 and TNF α are elevated [155]. These increased proinflammatory cytokines can directly decrease collagen synthesis and procollagen mRNA expression in cardiac fibroblasts, while increasing the mRNAs of several MMPs as well as increasing the activities of several MMPs [156]. Activation of MMP activities by proinflammatory cytokines is amplified by the decreased expression of TIMPs by these cytokines [157]. The stimulating effect of proinflammatory cytokines on MMPs are attenuated by NO [158].

In myocardial biopsies from 20 patients with dilated cardiomyopathy (DCM), 5 patients with hypertrophic obstructive cardiomyopathy (HOCM), and 5 nonfailing donor hearts (control) DCM was associated with increased concentrations of ADAM-10, -15 and -17, while HOCM was associated with increased concentrations of ADAM-12 and -17, as compared to their respective concentrations in control myocardium [159].

In LV myocardium of 19 patients with aortic stenosis (AS) who underwent aortic valve replacement EMMPRIN mRNA contents were significantly higher than in myocardial tissue of 12 nonused donor hearts with normal LV function [160].

Plasma of patients with congestive heart failure (CHF) showed increased concentrations of tenascin-C and MMP9, that declined upon cardiac resynchronization therapy in patients who responded to this therapy by a decrease of LV end-systolic volume [137]. In addition, plasma of patients with CHF showed a 3-fold increase in MMP9/TIMP1 ratio and a 16-fold increase in MMP9/TIMP2 ratio, compared to plasma of a healthy reference population [161]. Another study reported higher circulating MMP2 in patients with severe CHF than in those with mild CHF, while in both groups circulating MMP2 levels were higher than in controls [162]. If MMP activities were inhibited with an MMP inhibitor, LV dilatation was attenuated in (i) the infarcted mouse heart [163], (ii) an animal model of cardiac volume overload due to an arteriovenous fistula [164] and (iii) a rat model of progressive heart failure, the spontaneously hypertensive heart failure rat [165].

In the heart's reaction to overload Janicki and coworkers recognized three phases. The **intitial phase** is characterized by an increased MMP activity associated with degradation of fibrillar collagen and development of progressive cardiomyocyte hypertrophy. In the **following phase**, the compensated phase, myocardial MMP activity and collagen concentration return to normal, while cardiomyocyte hypertrophy continues. The **final phase**, the decompensated phase, is attained once the compensatory mechanisms are exhausted and heart failure develops. This phase is characterized by elevated MMP activity, marked ventricular dilatation and prominent fibrosis [166]. During the decompensated phase, myocardial collagen content builds up despite elevated MMP activity due to massive collagen synthesis that is stimulated by multiple factors, including cytokines, angiotensin II, and high wall tension. The collagen synthesized may differ from that in the healthy heart with respect to type (e.g., type III instead of type I) and extent of collagen cross-linking.

These three phases were not observed in a porcine model of pacing-induced supraventricular tachycardia. In this model heart failure was induced that was progressive in the first 21 days after onset of pacing. During this period LV myocardial sections showed progressively lower collagen content and progressively higher activities of MMP1, MMP2 and MMP3, associated with progressively lower % fractional shortening of LV segments and progressively higher LV end-diastolic dimensions [167]. In patients with dilated cardiomyopathy the degree of diastolic dysfunction was associated with plasma PIIINP concentrations independently of LV volume and ejection fraction [168]. In these patients plasma PIIINP concentrations were correlated to *(i)* tissue collagen content [169], and *(ii)* poor outcome [170]. In patients with congestive heart failure resulting from LV systolic dysfunction event-free survival was predicted by plasma PIIINP level, LV ejection fraction and a restrictive mitral filling pattern [171].

Integrins and Integrin Signaling

As integrins trigger intracellular signaling pathways activating the cardiomyocyte hypertrophy program, mechanical signals and their integrin receptors likely contribute to transcriptional regulation of MMPs [172], expression of “fetal” genes, such as brain natriuretic peptide gene [173], and expression of genes encoding ECM proteins [174]. In a mouse model, cardiac-specific deletion of the integrin β_1 gene results in myocardial fibrosis and cardiac failure [175]. In myocardial biopsies taken from hearts of patients with ischemic cardiomyopathy there was a loss of integrin β_1 D by 36%, a loss of FAK by 54%, a loss of phosphorylated FAK by 49%, and a loss of phosphorylated AKT by 44%, compared to myocardial tissue from individuals without cardiac disease [176]. Apparently, these results are not specific for failing myocardium, since myocardial biopsies taken from hearts of patients with idiopathic dilated cardiomyopathy were not altered with respect to integrin β_1 D, FAK, FAK-P and AKT-P, as compared to myocardial tissue from individuals without cardiac disease [176]. In hearts of patients with ischemic cardiomyopathy the integrin β_1 mRNA concentration was unchanged compared to control hearts. The possibility that integrin β_1 D has been shedded from the sarcolemma was tested and found to be unlikely as the observed loss of integrin β_1 D in hearts with ischemic cardiomyopathy was not associated with an increase of a 55-kD integrin fragment [176].

NO-Synthases and NO

Dysregulation of NO and increased oxidative and nitrosative stress are implicated in the pathogenesis of heart failure [177,178]. Peroxynitrite is a reactive oxidant that is produced from the reaction of NO with superoxide anion and impairs cardiovascular function through multiple mechanisms, including activation of MMPs and nuclear enzyme poly(ADP-ribose) polymerase (PARP).

The induction of cytokines in the failing myocardium, such as IL6 and TNF α , induce the expression of NOS2 [37]. At the same time the production of reactive

oxygen species (ROS) is stimulated by NADPH oxidases, probably induced by increased angiotensinII levels [179].

The combination of abundance of ROS, impaired antioxidant defense mechanisms (superoxide dismutase, catalase and glutathione peroxidase) and reduced concentrations of antioxidants (vitamin E, ascorbic acid, glutathione) contribute to a state of oxidative stress, that together with increased NO formation, leads to formation of peroxynitrite [180,181]. By a process called NOS uncoupling, a monomeric form of NOS may become a source for myocardial ROS rather than NO [182-184]. The generation of peroxynitrite has been demonstrated in various forms of acute heart failure and chronic heart failure in both animals and humans [185, Table 2 of ref. 177] and in neonatal rat ventricular cardiomyocytes in culture peroxynitrite had detrimental effects [38]. Rats with chronic renal failure demonstrated marked elevations of blood pressure, plasma malondialdehyde, plasma nitrotyrosine, and tissue nitrotyrosine abundance, associated with depressed vascular tissue NO production and reduced immunodetectable NOS proteins in the vascular, renal and cardiac tissues [186].

Peroxynitrate has many effects [187], one of which being the induction of MMPs [188]. Overexpressing glutathione peroxidase [189] or administering tetrahydrobiopterin to decrease myocardial superoxide anion production [123] decreased myocardial MMP abundance.

In isolated aortic rings from rats with infarction-induced heart failure acetylcholine-induced vasodilatation was attenuated leading to a shift of the effect-dose curve to higher doses of acetylcholine [190].

NOS3

In cardiomyocytes isolated from canine hearts with hypertrophic cardiomyopathy NOS3 and caveolin have reduced expression [191]. Seddon and coworkers stated that *“to date it remains unclear whether constitutive myocardial NOS3 activity plays a role in regulating myocardial function in remodeled or failing hearts”* [57]. Although several groups reported a reduction of myocardial NOS3 expression and activity in failing myocardium of human hearts [192,193], other groups reported increased myocardial NOS3 expression and activity in failing myocardium of human hearts [194]. In biopsies taken from human failing hearts Fukuchi and coworkers demonstrated higher expression of NOS3 in cardiomyocytes of patients who were on β -blocker therapy than in cardiomyocytes of patients who were treated with β -adrenoceptor agonists [195]. Other groups found no change in LV NOS3 protein expression in infarcted mouse myocardium compared to sham-operated mouse myocardium [80], nor changes in myocardial NOS3 expression and activity in rats with volume overload-induced heart failure, compared to healthy rats [196].

Transgenic upregulation of myocardial NOS3 expression in mice with myocardial infarction was associated with a beneficial effect on LV remodeling [132]. NOS3 gene delivery protected mice with acute myocardial infarction against cardiac remodeling, myocardial fibrosis, apoptosis, and oxidative stress [197]. Apparently, NOS3 may counterbalance the deleterious effects of increased ROS in ischemia/reperfusion. Overexpression of human NOS3 in mice protected against myocardial infarction-induced congestive heart failure, including less pulmonary

edema and improved 1-month survival, compared to wild-type mice with myocardial infarction of equal size [198]. Correspondingly, NOS3 deletion had either detrimental effects (such as increased long-term mortality) or to have no significant impact on the development of LV failure in mice with myocardial infarction [199,200].

Oxidant stress from NOS3 uncoupling was reported to be responsible for pressure-overload LV remodeling and failure [123].

NOS2

Cardiomyocytes from patients and experimental animals with CHF have increased expression of NOS2 [192,195,196,201-203]. However, Stein and coworkers found no NOS2 mRNA in 28 of 30 failing human hearts, nor any NOS2 immunoreactivity in these hearts [194]. Only in failing hearts from patients with sepsis these investigators detected NOS2 protein expression [204]. NOS2 expressed in failing hearts is considered to lead to nitrosative stress, a pathophysiologic situation characterized by accumulation of S-nitrosylated proteins to hazardous levels. In addition, abundant NOS2-derived NO serves as a source of myocardial reactive oxygen species (ROS) that contribute to LV hypertrophy and dilatation [134]. Thus, myocardial NOS2-derived NO contributes to a cardiomyopathy phenotype that may exhibit a lethal brady-arrhythmia [75]. In myocardial biopsies from 22 patients with end-stage heart failure (8 patients with dilated cardiomyopathy and 14 patients with ischemic heart disease) Vejlstrup and coworkers detected NOS2 predominantly in vascular endothelium and smooth muscle cells, regardless of the etiology. Only in 4 of 22 patients with end-stage heart failure NOS2 was found in cardiomyocytes, associated with the sarcolemma [202]. In myocardial biopsies of 24 patients with end-stage heart failure NOS2 mRNA as well as NOS2 activity were increased. Myocardial NOS2 activity was inversely correlated with the inotropic response to isoproterenol [192]. This attenuation of inotropic effects to isoproterenol was associated with an accelerated relaxation in the failing hearts. The use of a general NOS inhibitor, L-NMMA, enhanced the inotropic effects of the failing hearts to β -adrenergic stimulation. In LV endomyocardial biopsies taken from 20 patients with dilated cardiomyopathy NOS2 mRNA and NOS3 mRNA concentrations correlated linearly with LV stroke volume and LV stroke work [205]. An intracoronary infusion of substance P, which releases NO from the coronary endothelium, increased LV stroke volume and LV stroke work, and shifted the LV end-diastolic pressure-volume relationship to the right, representing a concomitant increase in LV preload reserve [205]. Fukuchi and coworkers found that in biopsies of 28 failing human hearts increased NOS2 activity was mainly associated with infiltrated macrophages rather than with cardiomyocytes [195].

In mice with myocardial infarction myocardial NOS2 expression is increased associated with higher NO production and higher nitrotyrosine levels, leading to myocardial dysfunction and increased mortality. NOS2^{-/-} mice with myocardial infarction had better contractility and lower mortality than wild-type mice with acute myocardial infarction [206]. Other studies corroborated the deleterious effects of NOS2-derived NO on infarcted myocardium. Sam and coworkers found that in NOS2-deficient mice late after myocardial infarction contractile dysfunction

was attenuated and apoptotic cell death was reduced [207]. However, Jones and coworkers reported that in NOS2-deficient mice severe congestive heart failure was not attenuated compared to wild-type mice with myocardial infarction [208]. Liu and coworkers found that myocardial infarction-induced increase in LV chamber dimension and the decrease in LV ejection fraction were less severe in NOS2^{-/-} mice compared to wild-type mice [209]. Also myocardial concentrations of nitrotyrosine and 4-hydroxy-2-nonenal, markers for ROS, were lower in infarcted NOS2^{-/-} mice compared to wild-type mice with myocardial infarction, indicating reduced oxidative stress by lack of NOS2-derived NO.

As mentioned before, induction of NOS2 by cytokines was found to cause cardiomyocyte apoptosis [74]. The increased expression of NOS2 in myocardium of animals and patients with heart failure [192,201-203] may be responsible for increased numbers of apoptotic cardiomyocytes observed in myocardium of animals and patients with heart failure [210,211].

NOS1

Myocardial NOS1 expression and activity have been reported to be increased following experimental myocardial infarction in rats [212,213], in mice [80], in human failing hearts [193], and in spontaneously hypertensive rats [191]. In failing LV myocardium NOS1 was found to be translocated from SR to the sarcolemma where NOS1 associates with caveolin-3 [193,212,213]. Irreversible activation of the RyR by oxidants leads to Ca²⁺ leak from SR, depressed calcium stores in the SR, and a heart failure phenotype [214].

Increased activity of NOS1 in failing myocardium does not necessarily translate in higher NO production rates, particularly if tetrahydrobiopterin levels and other cofactors are falling short. Then NOS1 uncoupling may occur, leading to ROS generation. In plasma of patients with congestive heart failure elevated concentrations of biomarkers reflecting oxidative stress have been observed [215]. Plasma concentrations of lipid peroxides increased with increasing NYHA classes of heart failure [216] and plasma concentrations of malondialdehyde-like material and plasma thiols correlated with LV ejection fraction negatively and positively, respectively [217].

Upon translocation to the sarcolemma, NOS1 exerts NOS3-like effects, such as inhibition of β -adrenergic receptor-stimulated increase in inotropy [212].

Inhibition of NOS1 enhanced the inotropic and lusitropic response to β -adrenergic stimulation in failing rat hearts but had no significant effect in sham-operated rats. Accordingly, myocardial NOS1 overexpression may contribute to the depressed β -adrenergic inotropic responsiveness observed in heart failure [213]. In NOS1^{-/-} mice acute myocardial infarction caused more severe LV remodeling and impaired β -adrenergic reserve and increased mortality compared with wild-type mice with similar infarct size [80,218]. On the basis of these results Casadei suggested that NOS1-derived NO may delay the development of heart failure after myocardial infarction [219]. Since NOS1 suppresses xanthine oxidoreductase (XOD) activity under normal conditions, NOS1 deletion causes XOD activation and oxidative stress. In infarcted NOS^{-/-} mice, oxidative stress is probably responsible for β -adrenergic hyporesponsiveness, depressed

myofilament responses to activator calcium, more intense hypertrophy of cardiomyocytes, adverse LV remodeling, and increased mortality [82,218,220].

In failing LV myocardium NOS1 was found to be translocated from SR to the sarcolemma where NOS1 associates with caveolin-3 [193,212, 213]. Following ischemia/reperfusion female mice exhibited increased NOS1 in association with caveolin-3 and increased S-nitrosylation of the L-type Ca^{2+} channel. Functionally, this led to decreased L-type Ca^{2+} current with reduced Ca^{2+} entry into the cell, which in turn protected the cell from calcium overload injury [221]. Due to translocation of NOS1 from SR to the sarcolemma of failing cardiomyocytes, suppression of XOD activity is relieved, which contributes to oxidative stress. S-nitrosylation of RyR2 is now considered to be beneficial for proper RyR2 function. In NOS1^{-/-} mice cardiomyocytes were found to have higher diastolic Ca^{2+} concentrations compared to wild-type mice, suggesting diastolic Ca^{2+} leakage from SR. This Ca^{2+} leak from SR through RyR2 was associated with diminished S-nitrosylation and increased S-oxidation of RyR2 [222]. These authors concluded that the hyponitrosylation of RyR2 in NOS1-deficient mice is responsible for Ca^{2+} leakage from SR, leading to an arrhythmogenic phenotype. In infarcted NOS1^{-/-} mice worse remodeling and survival occurred despite an increased NOS3 expression [218]. The finding that tissue NO production was not elevated in these mice may be explained by NOS3 uncoupling contributing to nitroso-redox imbalance [223].

When both NOS1 and NOS3 genes are deleted, concentric hypertrophy is observed associated with interstitial fibrosis, impairment of LV diastolic properties, and high mortality [224].

Hearts of transgenic mice with cardiomyocyte-specific NOS1 overexpression subjected to pressure-overload by aortic constriction developed hypertrophy with thicker LV walls, less LV dilatation, and better preserved LV fractional shortening than hearts of wild-type mice with aortic constriction. Cardiomyocytes isolated from NOS1-overexpressing hearts with aortic constriction had higher amplitude of intracellular Ca^{2+} transients and higher SR Ca^{2+} load than cardiomyocytes isolated from hearts of wild-type mice with aortic constriction [225]. The negative effects of NOS1-knockout in conjunction with the positive effect of NOS1-overexpression on cardiomyocyte function before and during overload strongly suggest that cardiomyocyte NOS1 plays an important role in cell protection, particularly during conditions of cardiac volume or pressure overload.

IV. Experimental Models of Myocardial Hypertrophy and Heart Failure

Neonatal Rat Ventricular Cardiomyocytes (NRVCs) *in vitro*

The monolayer of NRVCs has proven to be a very useful cell preparation to study growth-promoting effects of conditions or substances on NRVCs *in vitro*. The capacity of pro-hypertrophic stimuli can be studied in terms of (i) increase in cell volume, (ii) expression of “fetal” genes, and (iii) sarcomeric organization. Simpson and colleagues have shown that α_1 -adrenoceptor stimulation has potent

pro-hypertrophic effects on NRVCs mediated by protein kinase C and downstream signaling proteins [226-229]. Other pro-hypertrophic conditions or substances that have been tested in NRVCs *in vitro* are endothelin-1 [230], angiotensin II [231,232], myotrophin [233], and stretch [118,234-236].

Ventricular Pressure Overload *in vivo*

By inducing an increased afterload on left or right ventricle, the myocardium will undergo hypertrophy, characterized by (*i*) increased size of cardiomyocytes [237,238], (*ii*) increased number of interstitial fibroblasts to keep the fibroblast density more or less constant [238,239], and (*iii*) expression of “fetal” genes, such as the genes encoding ANP, skeletal α -actin and β -myosin heavy chain [240-242]. Even animals born with hypertension, the spontaneously hypertensive rats (SHR), have cardiac hypertrophy.

Due to multiple changes in gene expression a hypertrophic ventricle will undergo failure sooner or later [243], characterized by either ventricular dilatation, also referred to as ventricular remodeling, or myocardial fibrosis that opposes ventricular filling, also referred to as diastolic failure. Even SHRs will spontaneously develop heart failure at an age of 12-18 months [244].

Pressure overload of the RV is produced by either constriction of the pulmonary artery or induction of pulmonary artery hypertension (PAH).

Monocrotaline-Induced Pulmonary Hypertension

Mechanism and Pathology of Pulmonary Toxicity of Monocrotaline

Monocrotaline (MCT), a pyrrolizidine alkaloid derived from *Crotalaria spectabilis*, causes a pulmonary vascular syndrome in rats characterized by proliferative pulmonary vasculitis, pulmonary artery hypertension (PAH), and cor pulmonale. Current lines of evidence of the pathogenesis of MCT-induced pneumotoxicity indicate that MCT is activated to one or more reactive metabolites in the liver, particularly a MCT pyrrole called dehydromonocrotaline [245-247], and is then transported by red blood cells to the lung [248], where it initiates endothelial injury [249,250]. The endothelial injury does not appear to be acute cell death but rather a delayed functional alteration that leads to smooth muscle cell proliferation in the media of pulmonary arteriolar walls by unknown mechanisms. The role of inflammation in the progression of MCT-induced pulmonary vascular disease is uncertain. Both perivascular inflammation and platelet activation have been proposed as processes contributing to the response of the vascular media [247]. MCT and dehydroMCT are known to be toxic to a variety of domestic and laboratory animals and to humans. Major pathological effects induced by MCT poisoning include hepatic cirrhosis and megalocytosis, venoocclusive disease, PAH, and RV hypertrophy. There is a positive correlation between progressive PAH, thickening of the medial wall of small pulmonary arteries and arterioles, and RV hypertrophy as a function of time [251].

Characterization of Right Ventricular Function during Monocrotaline-induced Pulmonary Hypertension in the Intact Rat

Besides RV hypertrophy, the primary response to MCT treatment is RV dilatation, i.e. increases of RV end-systolic and end-diastolic volumes and, consequently, a decrease of RV ejection fraction. The dose-dependent RV hypertrophy strongly correlates with MCT-induced pressure overload, but, despite this increased muscle mass, RV wall stress gradually increases, ultimately leading to RV decompensation [252]. Interestingly, RV end-systolic elastance and end-diastolic stiffness did not change significantly, even when corrected for myocardial muscle mass, suggesting that intrinsic myocardial function was not importantly altered. The unchanged RV diastolic stiffness was consistent with the absence of changes in fibrosis and the fact that filling pressures remained relatively normal. However, end-systolic and end-diastolic pressure-volume relationships showed a tendency to be shifted toward larger volumes, suggesting myocyte slippage as a potential mechanism for dilatation. In addition, early active relaxation, as reflected by τ , was severely depressed in the group of rats treated with 80 mg MCT/kg body weight, consistent with severe RV hypertrophy [252]. Using an orthogonal three-lead system, Henkens and coworkers recorded ECGs from rats with MCT-induced PAH at baseline, and 14 and 25 days after MCT administration [253]. Baseline ECGs of controls and MCT rats were similar, and ECGs of controls did not change over time. In MCT rats, ECG changes were already present on day 14 but more explicit on day 25: increased RV electromotive forces decreased mean QRS-vector magnitude and changed QRS-axis orientation. Important changes in action potential duration distribution and repolarization sequence were reflected by a decreased spatial ventricular gradient magnitude and increased QRS-T spatial angle. On day 25, RV hypertrophy was found, but not on day 14. They concluded that developing PAH was characterized by early ECG changes preceding RV hypertrophy, whereas severe PAH was marked by profound ECG changes associated with anatomical and functional changes in the RV. Three-dimensional ECG analysis appears to be very sensitive to early changes in RV afterload [253].

V. Purpose of the Study

We hypothesized that pressure overload is “felt” by the myocardium through stretch-like effects imposed on integrins, the receptor by which cardiomyocytes are attached to the ECM. In the cell model of NRVCs *in vitro*, we activate the integrins by administration of a Arg-Gly-Asp (RGD) containing pentapeptide to test whether integrin stimulation leads to NRVC hypertrophy. Any pro-hypertrophic effect of RGD-containing pentapeptide on NRVCs is compared with the well-known pro-hypertrophic effects of α_1 -adrenoceptor stimulation with phenylephrine (**chapter 2**).

Ventricular failure is associated with a disturbed myocardial collagen turnover. In patients with heart failure, myocardial collagen turnover can be assessed by plasma concentrations of PINP, PIIINP, and ICTP that either represent measures of collagen synthesis (PINP, PIIINP) or collagen degradation (ICTP). We set out to investigate the effects of cardiac resynchronization therapy (CRT) on myocardial collagen turnover in patients with heart failure by comparing PINP, PIIINP and ICTP concentrations in plasma obtained at baseline and after 6 months of CRT (**chapter 3**).

As it is known for some time that MCT-induced PAH and RV failure were associated with activation of MMPs in RV myocardium, we first set out to investigate whether NO plays any role in PAH-induced RV hypertrophy and failure. To that purpose, two doses of MCT were used that produced RV hypertrophy only and RV hypertrophy and subsequent RV failure, respectively (**chapter 4**).

Which experimental treatments of PAH have been described? In **chapter 5** we review the novel approaches to treat pulmonary artery hypertension, particularly in experimental animals.

PAH is a life-threatening disease with an important pulmonary component that may provide a target to direct therapy. We set out to investigate whether MCT-induced PAH and subsequent RV failure can be treated with bone marrow-derived mesenchymal stem cells (MSCs) obtained from donor rats with PAH caused by injection of MCT 28 days earlier. At day 14 after MCT injection, recipient rats are treated with i.v. administration of MSCs from rats that had a MCT injection 28 days earlier (**chapters 6 and 7**).

In **chapter 6** the effects of stem cell therapy to rats with PAH on pulmonary pathology, incl. hypertension, are examined. In **chapter 7** the effects of stem cell therapy to rats with PAH on RV function and structure are examined, including changes in myocardial extracellular matrix composition.

Cardiomyocytes isolated from RV myocardium of rats with and without PAH have been investigated electrophysiologically to explore PAH-related changes in excitability. In **chapter 8** we report on cardiomyocyte excitability properties dependent on Kv-channel expression, because these channels have been proposed to play an important role in PAH-related arrhythmias. We define the control excitability properties of RV cardiomyocytes from rats without PAH and make a provisional comparison with myocytes from PAH-rats in the discussion of this study.

By using *in vitro* cell preparations, rat hearts *in vivo* and *ex vivo*, and human plasma samples our goal is to characterize (*i*) the signaling pathways that are activated by pro-hypertrophic stimuli, (*ii*) changes in the ECM that are typical for heart failure, and (*iii*) the effects of cell therapy with MSCs on RV function, RV myocardial structure, and RV cardiomyocyte electrophysiology of rat hearts with MCT-induced PAH.

References

1. Bers DM. Cardiac excitation-contraction coupling. *Nature* 2002; 415: 198-205.
2. Weber KT, Brilla CG. Myocardial fibrosis, aldosterone, and antialdosterone therapy: Evolving concept in the management of congestive heart failure. Searle and Co., 1991.
3. Brooks PC, Strömblad S, Sanders LC, et al. Localization of matrix metalloproteinase MMP-2 to the surface of invasive cells by interaction with integrin $\alpha_v\beta_3$. *Cell* 1996; 85: 683-93.
4. Yu Q, Stamenkovic I. Localization of matrix metalloproteinase 9 to the cell surface provides a mechanism for CD44-mediated tumor invasion. *Genes Dev* 1999; 13: 35-48.
5. Sternlicht MD, Werb Z. How matrix metalloproteinases regulate cell behavior. *Annu Rev Cell Dev Biol* 2001; 17: 463-516.
6. Chapman RE, Scott AA, Deschamps AM, et al. Matrix metalloproteinase abundance in human myocardial fibroblasts: effects of sustained pharmacologic matrix metalloproteinase inhibition. *J Mol Cell Cardiol* 2003; 35: 539-48.
7. Coker ML, Doscher MA, Thomas CV, et al. Matrix metalloproteinase synthesis and expression in isolated LV myocyte preparations. *Am J Physiol Heart Circ Physiol* 1999; 277: H777-H787.
8. Wang W, Schulze CJ, Suarez-Pinzon WL, et al. Intracellular action of matrix metalloproteinase-2 accounts for acute myocardial ischemia and reperfusion injury. *Circulation* 2002; 106: 1543-9.
9. Seals DF, Courtneidge SA. The ADAM family of metalloproteases: multidomain proteins with multiple functions. *Genes Dev* 2003; 17: 7-30.
10. Werb Z, Yan Y. A cellular striptease act. *Science* 1998; 282: 1279-80.
11. Black RA, Rauch CT, Kozlosky CJ, et al. A metalloproteinase disintegrin that releases tumour-necrosis factor- α from cells. *Nature* 1997; 385: 729-33.
12. Yu W-H, Yu SC, Meng Q, et al. TIMP-3 binds to sulfated glycoaminoglycans of the extracellular matrix. *J Biol Chem* 2000; 275: 31226-32.
13. Kashiwagi M, Tortorella M, Nagase H, et al. TIMP-3 is a potent inhibitor of aggrecanase 1 (ADAM-TS4) and aggrecanase 2 (ADAM-TS5). *J Biol Chem* 2001; 276: 12501-4.
14. Tortorella MD, Burn TC, Pratta MA, et al. Purification and cloning of aggrecanase-1: a member of the ADAMTS family of proteins. *Science* 1999; 284: 1664-6.
15. Berditchevski F, Chang S, Bodorova J, et al. Generation of monoclonal antibodies to integrin-associated proteins. Evidence that $\alpha_3\beta_1$ complexes with EMMPRIN/BASIGIN/OX47/M6. *J Biol Chem* 1997; 272: 29174-80.
16. Nabeshima K, Iwasaki H, Koga K, et al. Emmprin (basigin/CD147): matrix metalloproteinase modulator and multifunctional cell recognition molecule that plays a critical role in cancer progression. *Pathol Int* 2006; 56: 359-67.
17. Lopez B, Gonzalez A, Varo N, et al. Biochemical assessment of myocardial fibrosis in hypertensive heart disease. *Hypertension* 2001; 38: 1222-6.
18. Calderone A, Thaik CM, Takahashi N, et al. Nitric oxide, atrial natriuretic peptide, and cyclic GMP inhibit the growth-promoting effects of norepinephrine in cardiac myocytes and fibroblasts. *J Clin Invest* 1998; 101: 812-8.
19. Schultz JJ, Witt SA, Glascock BJ, et al. TGF- β 1 mediates the hypertrophic cardiomyocyte growth induced by angiotensin II. *J Clin Invest* 2002; 109: 787-96.
20. Brilla CG, Zhou G, Matsubara L, et al. Collagen metabolism in cultured adult rat cardiac fibroblasts: Response to angiotensin II and aldosterone. *J Mol Cell Cardiol* 1994; 26: 809-20.
21. Brilla CG, Weber KT. Mineralocorticoid excess, dietary sodium, and myocardial fibrosis. *J Lab Clin Med* 1992; 120: 893-901.

22. Olivetti G, Capasso JM, Sonnenblick EH, *et al.* Side-to-side slippage of myocytes participates in ventricular wall remodeling acutely after myocardial infarction in rats. *Circ Res* 1990; 67: 23-34.
23. Schlaepfer DD, Hauck CR, Sieg DJ. Signaling through focal adhesion kinase. *Progr Biophys Mol Biol* 1999; 71: 435-78.
24. Laser M, Willey CD, Jiang W, *et al.* Integrin activation and focal complex formation in cardiac hypertrophy. *J Biol Chem* 2000; 275: 35624-30.
25. D'Angelo G, Mogford JE, Davis GE, *et al.* Integrin-mediated reduction in vascular smooth muscle $[Ca^{2+}]_i$ induced by RGD-containing peptide. *Am J Physiol Heart Circ Physiol* 1997; 272: H2065-H2070.
26. Mogford JE, Davis GE, Platts SH, *et al.* Vascular smooth muscle $\alpha_v\beta_3$ integrin mediates arteriolar vasodilation in response to RGD peptides. *Circ Res* 1996; 79: 821-6.
27. Wu X, Mogford JE, Platts SH, *et al.* Modulation of calcium current in arteriolar smooth muscle by $\alpha_v\beta_3$ and $\alpha_5\beta_1$ integrin ligands. *J Cell Biol* 1998; 143: 241-52.
28. Wu X, Davis GE, Meininger GA, *et al.* Regulation of the L-type calcium channel by $\alpha_5\beta_1$ integrin requires signaling between focal adhesion proteins. *J Biol Chem* 2001; 276: 30285-92.
29. Chan WL, Holstein-Rathlou NH, Yip KP. Integrin mobilizes intracellular Ca^{2+} in renal vascular smooth muscle cells. *Am J Physiol Cell Physiol* 2001; 280: C593-C603.
30. Van der Wees CGC, Bax WH, van der Valk EJM, *et al.* Integrin stimulation induces calcium signalling in rat cardiomyocytes by a NO-dependent mechanism. *Pflügers Arch – Eur J Physiol* 2006; 451: 588-95.
31. Wang N, Butler JP, Ingber DE. Mechanotransduction across the cell surface and through the cytoskeleton. *Science* 1993; 260: 1124-7.
32. Miyamoto S, Teramoto H, Coso O, *et al.* Integrin function: molecular hierarchies of cytoskeletal and signaling molecules. *J Cell Biol* 1995; 131: 791-805.
33. Ingber DE. Mechanical signaling and the cellular response to extracellular matrix in angiogenesis and cardiovascular physiology. *Circ Res* 2002; 91: 877-87.
34. Zhang SJ, Truskey GA, Kraus WE. Effect of cyclic stretch on β_{1D} -integrin expression and activation of FAK and RhoA. *Am J Physiol Cell Physiol* 2007; 292: C2057-C2069.
35. Wang Y, Marsden PA. Nitric oxide synthases: gene structure and regulation. *Adv Pharmacol* 1995; 34: 71-90.
36. Xie Q-W, Nathan C. The high-output nitric oxide pathway: role and regulation. *J Leukocyte Biol* 1994; 56: 576-82.
37. Nathan C. Inducible nitric oxide synthase: what difference does it make? *J Clin Invest* 1997; 100: 2417-23.
38. Keira N, Tatsumi T, Matoba S, *et al.* Lethal effect of cytokine-induced nitric oxide and peroxynitrite on cultured rat cardiac myocytes. *J Mol Cell Cardiol* 2002 ;34 :583-96.
39. Mannick JB, Schonhoff CM. Nitrosylation: the next phosphorylation? *Arch Biochem Biophys* 2002; 408: 1-6.
40. Martinez-Ruiz A, Lamas S. S-nitrosylation: a potential new paradigm in signal transduction. *Cardiovasc Res* 2004; 62: 43-52.
41. Hess DT, Matsumoto A, Kim SO, *et al.* Review. Protein S-nitrosylation: purview and parameters. *Nat Mol Cell Biol* 2005; 6: 150-66.
42. Campbell DL, Stamler JS, Strauss HC. Redox modulation of L-type calcium channels in ferret ventricular myocytes. Dual mechanism regulation by nitric oxide and S-nitrosothiols. *J Gen Physiol* 1996; 108: 277-93.
43. Hu H, Chiamvimonvat N, Yamagishi T, *et al.* Direct inhibition of expressed cardiac L-type Ca^{2+} channels by S-nitrosothiol nitric oxide donors. *Circ Res* 1997; 81: 742-52.
44. Sun J, Picht E, Ginsburg KS, *et al.* Hypercontractile female hearts exhibit increased S-nitrosylation of the L-type Ca^{2+} channel α_1 subunit and reduced ischemia/reperfusion injury. *Circ Res* 2006; 98: 403-11.

45. Nunez L, Vaquero M, Gomez R, *et al.* Nitric oxide blocks hKv1.5 channels by S-nitrosylation and by a cyclic GMP-dependent mechanism. *Cardiovasc Res* 2006; 72: 80-9.
46. Lokuta AJ, Maertz NA, Vadakkadath Meethal S, *et al.* Increased nitration of sarcoplasmic reticulum Ca²⁺-ATPase in human heart failure. *Circulation* 2005; 111: 988-95.
47. Xu L, Eu JP, Meissner G, *et al.* Activation of the cardiac calcium release channel (ryanodine receptor) by poly-S-nitrosylation. *Science* 1998; 279: 234-7.
48. Eu JP, Xu L, Stamler JS, *et al.* Regulation of ryanodine receptors by reactive nitrogen species. *Biochem Pharmacol* 1999; 57: 1079-1084.
49. Liu L, Hausladen A, Zeng M, *et al.* A metabolic enzyme for S-nitrosothiol conserved from bacteria to humans. *Nature* 2001; 410: 490-4.
50. Liu L, Yan Y, Zeng M, *et al.* Essential roles of S-nitrosothiols in vascular homeostasis and endotoxic shock. *Cell* 2004; 116: 617-28.
51. Dimmeler S, Haendeler J, Nehls M, *et al.* Suppression of apoptosis by nitric oxide via inhibition of interleukin-1 β -converting enzyme (ICE)-like and cysteine protease protein (CPP)-32-like proteases. *J Exp Med* 1997; 185: 601-7.
52. Nikitovic D, Holmgren A, Spyrou G. Inhibition of AP-1 DNA binding by nitric oxide involving conserved cysteine residues in Jun and Fos. *Biochem Biophys Res Commun* 1998; 242: 109-12.
53. Mannick JB, Hausladen A, Liu L, *et al.* Fas-induced caspase denitrosylation. *Science* 1999; 284: 651-4.
54. Park HS, Huh SH, Kim MS, *et al.* Nitric oxide negatively regulates c-Jun N-terminal kinase/stress-activated protein kinase by means of S-nitrosylation. *Proc Natl Acad Sci USA* 2000; 97: 14382-7.
55. Park HS, Yu JW, Cho JH, *et al.* Inhibition of apoptosis signal-regulating kinase 1 by nitric oxide through a thiol redox mechanism. *J Biol Chem* 2004; 279: 7584-90.
56. Paulus WJ, Bronzwaer JG. Nitric oxide's role in the heart: control of beating or breathing? *Am J Physiol Heart Circ Physiol* 2004; 287: H8-H13.
57. Seddon M, Shah AM, Casadei B. Cardiomyocytes as effectors of nitric oxide signaling. *Cardiovasc Res* 2007; 75: 315-26.
58. Paulus WJ, Vantrimpont PJ, Shah AM. Paracrine coronary endothelial control of left ventricular function in humans. *Circulation* 1995; 92: 2119-26.
59. Shah AH, Spurgeon HA, Sollott SJ, *et al.* 8-Bromo-cGMP reduces the myofilament response to Ca²⁺ in intact cardiac myocytes. *Circ Res* 1994; 74: 970-8.
60. Layland J, Li J-M, Shah AM. Role of cyclic GMP-dependent protein kinase in the contractile response to exogenous nitric oxide in rat cardiac myocytes. *J Physiol (Lon)* 2002; 540: 457-67.
61. Martin SR, Emanuel K, Sears CE, *et al.* Are myocardial eNOS and nNOS involved in the β -adrenergic and muscarinic regulation of inotropy? A systematic investigation. *Cardiovasc Res* 2006; 70: 97-106.
62. Gyurko R, Kuhlencordt P, Fishman MC, *et al.* Modulation of mouse cardiac function in vivo by eNOS and ANP. *Am J Physiol Heart Circ Physiol* 2000; 278: H971-H981.
63. Khan SA, Skaf MW, Harrison RW, *et al.* Nitric oxide regulation of myocardial contractility and calcium cycling: independent impact of neuronal and endothelial nitric oxide synthases. *Circ Res* 2003; 92: 1322-9.
64. Shaul PW. Regulation of endothelial nitric oxide synthase: location, location, location. *Annu Rev Physiol* 2002; 64: 749-74.
65. Barouch LA, Harrison RW, Skaf MW, *et al.* Nitric oxide regulates the heart by spatial confinement of nitric oxide synthase isoforms. *Nature* 2002; 416: 337-40.
66. Brunner F, Andrew P, Wölkart G, *et al.* Myocardial contractile function and heart rate in mice with myocyte-specific overexpression of endothelial nitric oxide synthase. *Circulation* 2001; 104: 3097-102.

67. Martinez-Moreno M, Alvarez-Barrientos A, Roncal F, *et al.* Direct interaction between the reductase domain of the endothelial nitric oxide synthase and the ryanodine receptor. *FEBS Lett* 2005; 579: 3159-63.
68. Vila-Petroff MG, Kim SH, Pepe S, *et al.* Endogenous nitric oxide mechanisms mediate the stretch dependence of Ca^{2+} release in cardiomyocytes. *Nat Cell Biol* 2001; 3: 867-73.
69. Linz W, Wohlfart P, Schölkens BA, *et al.* Review. Interactions among ACE, kinins and NO. *Cardiovasc Res* 1999; 43: 549-61.
70. Cornwell TL, Arnold E, Boerth NJ, *et al.* Inhibition of smooth muscle cell growth by nitric oxide and activation of cAMP-dependent protein kinase by cGMP. *Am J Physiol Cell Physiol* 1994; 267: C1405-C1413.
71. Bath PMW, Hassall DG, Gladwin A-M, *et al.* Nitric oxide and prostacyclin. Divergence of inhibitory effects on monocyte chemotaxis and adhesion to endothelium in vitro. *Arterioscler Thromb* 1991; 11: 254-60.
72. Radomski MW, Palmer RMJ, Moncada S. An L-arginine/nitric oxide pathway present in human platelets regulates aggregation. *Proc Natl Acad Sci USA* 1990; 87: 5193-7.
73. Garg UC, Hassid A. Nitric oxide-generating vasodilators inhibit mitogenesis and proliferation of BALB/c 3T3 fibroblasts by a cyclic GMP-dependent mechanism. *Biochem Biophys Res Commun* 1990; 171: 474-9.
74. Arstall MA, Sawyer DB, Fukazawa R, *et al.* Cytokine-mediated apoptosis in cardiac myocytes: The role of inducible nitric oxide synthase induction and peroxynitrite generation. *Circ Res* 1999; 85: 829-40.
75. Mungrue IN, Gros R, You X, *et al.* Cardiomyocyte overexpression of iNOS in mice results in peroxynitrite generation, heart block, and sudden death. *J Clin Invest* 2002; 109: 735-43.
76. Xu KY, Huso DL, Dawson TM, *et al.* Nitric oxide synthase in cardiac sarcoplasmic reticulum. *Proc Natl Acad Sci USA* 1999; 96: 657-62.
77. Sears CE, Bryant SM, Ashley EA, *et al.* Cardiac neuronal nitric oxide synthase isoform regulates myocardial contraction and calcium handling. *Circ Res* 2003; 92: e52-e59.
78. Meissner G. Molecular regulation of cardiac ryanodine receptor ion channel. *Cell Calcium* 2004; 35: 621-8.
79. Danson EJ, Choate JK, Paterson DJ. Cardiac nitric oxide: Emerging role for nNOS in regulating physiological function. *Pharmacol Therap* 2005; 106: 57-74.
80. Dawson D, Lygate CA, Zhang MH, *et al.* nNOS gene deletion exacerbates pathological left ventricular remodeling and functional deterioration after myocardial infarction. *Circulation* 2005; 112: 3729-37.
81. Ashley EA, Sears CE, Bryant SM, *et al.* Cardiac nitric oxide synthase 1 regulates basal and β -adrenergic contractility in murine ventricular myocytes. *Circulation* 2002; 105: 3011-6.
82. Khan SA, Lee K, Minhas KM, *et al.* Neuronal nitric oxide synthase negatively regulates xanthine oxidoreductase inhibition of cardiac excitation-contraction coupling. *Proc Natl Acad Sci USA* 2004; 101: 15944-8.
83. Burkard N, Rokita AG, Kaufmann SG, *et al.* Conditional neuronal nitric oxide synthase overexpression impairs myocardial contractility. *Circ Res* 2007; 100: e32-e44.
84. Stoyanovsky D, Murphy T, Anno PR, *et al.* Nitric oxide activates skeletal and cardiac ryanodine receptors. *Cell Calcium* 1997; 21: 19-29.
85. Jaffrey SR, Erdjument-Bromage H, Ferris CD, *et al.* Protein S-nitrosylation: a physiological signal for neuronal nitric oxide. *Nat Cell Biol* 2001; 3: 193-7.
86. Nakane M, Mitchell J, Förstermann U, *et al.* Phosphorylation by calcium calmodulin-dependent protein kinase II and protein kinase C modulates the activity of nitric oxide synthase. *Biochem Biophys Res Commun* 1991; 180: 1396-1402.
87. Prasad AM, Ma H, Sumbilla C, *et al.* Phenylephrine hypertrophy, Ca^{2+} -ATPase (SERCA2), and Ca^{2+} signaling in neonatal rat cardiac myocytes. *Am J Physiol Cell Physiol* 2007; 292: C2269-C2275.

88. Miyazaki H, Oka N, Koga A, *et al.* Comparison of gene expression profiling in pressure and volume overload-induced myocardial hypertrophies in rats. *Hypertens Res* 2006; 29: 1029-45.
89. Ruwhof C, van Wamel JT, Noordzij LA, *et al.* Mechanical stress stimulates phospholipase C activity and intracellular calcium ion levels in neonatal rat cardiomyocytes. *Cell Calcium* 2001; 29: 73-83.
90. Zobel C, Rana OR, Saygili E, *et al.* Mechanisms of Ca²⁺-dependent calcineurin activation in mechanical stretch-induced hypertrophy. *Cardiology* 2007; 107: 281-90.
91. Molkentin JD, Lu JR, Antos CL, *et al.* A calcineurin-dependent transcriptional pathway for cardiac hypertrophy. *Cell* 1998; 93: 215-28.
92. Samuel JL, Barrieux A, Dufour S, *et al.* Accumulation of fetal fibronectin mRNAs during the development of rat cardiac hypertrophy induced by pressure overload. *J Clin Invest* 1991; 88: 1737-46.
93. Villarreal FJ, Dillmann WH. Cardiac hypertrophy-induced changes in mRNA levels for TGF- β_1 , fibronectin, and collagen. *Am J Physiol Heart Circ Physiol* 1992; 262: H1861-H1866.
94. Farhadian F, Contard F, Corbier A, *et al.* Fibronectin expression during physiological and pathological cardiac growth. *J Mol Cell Cardiol* 1995; 27: 981-90.
95. Schellings MWM, Pinto YM, Heymans S. Matricellular proteins in the heart: possible role during stress and remodeling. *Cardiovasc Res* 2004; 64: 24-31.
96. Schaper J, Speiser B. The extracellular matrix in the failing human heart. *Basic Res Cardiol* 1992; 87(suppl 1): 303-9.
97. Ross RS, Pham C, Shai S-Y, *et al.* Integrins participate in the hypertrophic response of rat ventricular myocytes. *Circ Res* 1998; 82: 1160-72.
98. Diez J, Panizo A, Gil MJ, *et al.* Serum markers of collagen type I metabolism in spontaneously hypertensive rats: relation to myocardial fibrosis. *Circulation* 1996; 93: 1026-32.
99. Querejeta R, Varo N, Lopez B, *et al.* Serum carboxy-terminal propeptide of procollagen type I is a marker of myocardial fibrosis in hypertensive heart disease. *Circulation* 2000; 101: 1729-35.
100. Varo N, Iraburu MJ, Varela M, *et al.* Chronic AT₁ blockade stimulates extracellular collagen type I degradation and reverses myocardial fibrosis in spontaneously hypertensive rats. *Hypertension* 2000; 35: 1197-1202.
101. Lopez B, Querejeta R, Varo N, *et al.* Usefulness of serum carboxy-terminal propeptide of procollagen type I to assess the cardioreparative ability of antihypertensive treatment in hypertensive patients. *Circulation* 2001; 104: 286-91.
102. Laurent GL. Dynamic state of collagen: pathways of collagen degradation in vivo and their possible role in regulation of collagen mass. *Am J Physiol Cell Physiol* 1987; 252: C1-C9.
103. Lombardi R, Betocchi S, Losi MA, *et al.* Myocardial collagen turnover in hypertrophic cardiomyopathy. *Circulation* 2003; 108: 1455-60.
104. Babbitt CJ, Shai S-Y, Harpf AE, *et al.* Modulation of integrins and integrin signaling molecules in the pressure-loaded murine ventricle. *Histochem Cell Biol* 2002; 118: 431-9.
105. Pham CG, Harpf AE, Keller RS, *et al.* Striated muscle-specific β_{1D} -integrin and FAK are involved in cardiac myocyte hypertrophic response pathway. *Am J Physiol Heart Circ Physiol* 2000; 279: H2916-H2926.
106. Kuppuswamy D, Kerr C, Narishige T, *et al.* Association of tyrosine phosphorylated c-Src with the cytoskeleton of hypertrophying myocardium. *J Biol Chem* 1997; 272: 4500-8.
107. Willey CD, Balasubramanian S, Rodriguez Rosas MC, *et al.* Focal complex formation in adult cardiomyocytes is accompanied by the activation of β_3 integrin and c-Src. *J Mol Cell Cardiol* 2003; 35: 671-83.
108. Balasubramanian S, Kuppuswamy D. RGD-containing peptides activate S6K1 through β_3 integrin in adult cardiac muscle cells. *J Biol Chem* 2003; 278: 42214-24.

109. Franchini KG, Torsoni AS, Soares PHA, *et al.* Early activation of the multicomponent signaling complex associated with focal adhesion kinase induced by pressure overload in the rat heart. *Circ Res* 2000; 87: 558-65.
110. Domingos PP, Fonseca PM, Nadruz W, *et al.* Load-induced focal adhesion kinase activation in the myocardium: role of stretch and contractile activity. *Am J Physiol Heart Circ Physiol* 2002; 282: H556-H564.
111. Taylor JM, Rovin JD, Parsons JT. A role for focal adhesion kinase in phenylephrine-induced hypertrophy of rat ventricular cardiomyocytes. *J Biol Chem* 2000; 275: 19250-7.
112. Eble DM, Strait JB, Govindarajan G, *et al.* Endothelin-induced cardiac myocyte hypertrophy: role for focal adhesion kinase. *Am J Physiol Heart Circ Physiol* 2000; 278: H1695-H1707.
113. Kovacic-Milivojevic B, Roediger F, Almeida EAC, *et al.* Focal adhesion kinase and p130Cas mediate both sarcomeric organisation and activation of genes associated with cardiac myocyte hypertrophy. *Mol Biol Cell* 2001; 12: 2290-2307.
114. Torsoni AS, Constancio SS, Nadruz W jr, *et al.* Focal adhesion kinase is activated and mediates the early hypertrophic response to stretch in cardiac myocytes. *Circ Res* 2003; 93: 140-7.
115. Govindarajan G, Eble DM, Lucchesi PA, *et al.* Focal adhesion kinase is involved in angiotensin II-mediated protein synthesis in cultured vascular smooth muscle cells. *Circ Res* 2000; 87: 10-6.
116. Liang F, Atakilit A, Gardner DG. Integrin dependence of brain natriuretic peptide gene promoter activation by mechanical strain. *J Biol Chem* 2000; 275: 20355-60.
117. Sadoshima J-I, Takahashi T, Jahn L, *et al.* Roles of mechano-sensitive ion channels, cytoskeleton, and contractile activity in stretch-induced immediate-early gene expression and hypertrophy of cardiac myocytes. *Proc Natl Acad Sci USA* 1992; 89: 9905-9.
118. Sadoshima J-I, Jahn L, Takahashi T, *et al.* Molecular characterization of the stretch-induced adaptation of cultured cardiac cells: an in vitro model of load-induced cardiac hypertrophy. *J Biol Chem* 1992; 267: 10551-60.
119. Sadoshima J-I, Izumo S. Mechanical stretch rapidly activates multiple signal transduction pathways in cardiac myocytes: potential involvement of an autocrine/paracrine mechanism. *EMBO J* 1993; 12: 1681-92.
120. Yamazaki T, Komuro I, Kudoh S, *et al.* Mechanical stress activates protein kinase cascade of phosphorylation in neonatal rat cardiac myocytes. *J Clin Invest* 1995; 96: 438-46.
121. Seko Y, Seko Y, Takahashi N, *et al.* Pulsatile stretch activates mitogen-activated protein kinase (MAPK) family members and focal adhesion kinase (p125^{FAK}) in cultured rat cardiac myocytes. *Biochem Biophys Res Commun* 1999; 259: 8-14.
122. Yamazaki T, Tobe K, Hoh E, *et al.* Mechanical loading activates mitogen-activated protein kinase and S6 peptide kinase in cultured rat cardiac myocytes. *J Biol Chem* 1993; 268: 12069-76.
123. Takimoto E, Champion HC, Li M, *et al.* Oxidant stress from nitric oxide synthase-3 uncoupling stimulates cardiac pathologic remodeling from chronic pressure load. *J Clin Invest* 2005; 115: 1221-31.
124. Bayraktutan U, Yang Z-K, Shah AM. Selective dysregulation of nitric oxide synthase type 3 in cardiac myocytes but not coronary microvascular endothelial cells of spontaneously hypertensive rats. *Cardiovasc Res* 1998; 38: 719-26.
125. Sanada S, Node K, Minamino T, *et al.* Long-acting Ca²⁺ blockers prevent myocardial remodeling induced by chronic NO inhibition in rats. *Hypertension* 2003; 41: 963-7.
126. Wenzel S, Rohde C, Wingerning S, *et al.* Lack of endothelial nitric oxide synthase-derived nitric oxide formation favors hypertrophy in adult ventricular cardiomyocytes. *Hypertension* 2007; 49: 193-200.
127. Huang PL, Huang ZH, Mashimo H, *et al.* Hypertension in mice lacking the gene for endothelial nitric oxide synthase. *Nature* 1995; 377: 239-42.

128. Ichinose F, Bloch KD, Wu JC, *et al.* Pressure overload-induced hypertrophy and dysfunction in mice are exacerbated by congenital NOS3 deficiency. *Am J Physiol Heart Circ Physiol* 2004; 286: H1070-H1075.
129. Buys ES, Raheer MJ, Blake SL, *et al.* Cardiomyocyte-restricted restoration of nitric oxide synthase 3 attenuates left ventricular remodeling after chronic pressure overload. *Am J Physiol Heart Circ Physiol* 2007; 293: H620-H627.
130. Bubikat A, de Windt LJ, Zetsche B, *et al.* Local ANP signalling prevents hypertensive cardiac hypertrophy in endothelial NO synthase (eNOS)-deficient mice. *J Biol Chem* 2005; 280: 21594-9.
131. Ozaki M, Kawashima S, Yamashita T, *et al.* Overexpression of endothelial nitric oxide synthase attenuates cardiac hypertrophy induced by chronic isoproterenol infusion. *Circ J* 2002; 66: 851-6.
132. Janssens S, Pokreisz P, Schoonjams L, *et al.* Cardiomyocyte-specific overexpression of nitric oxide synthase 3 improves left ventricular performance and reduces compensatory hypertrophy after myocardial infarction. *Circ Res* 2004; 94: 1256-62.
133. Massion PB, Feron O, Dessy C, *et al.* Nitric oxide and cardiac function: ten years after, and continuing. *Circ Res* 2003; 93: 388-98.
134. Zhang P, Xu X, Hu X, *et al.* Inducible nitric oxide synthase deficiency protects the heart from systolic overload-induced ventricular hypertrophy and congestive heart failure. *Circ Res* 2007; 100: 1089-98.
135. Lorell BH, Carabello BA. Left ventricular hypertrophy: pathogenesis, detection, and prognosis. *Circulation* 2000; 102: 470-9.
136. Hasenfuss G, Meyer M, Schillinger W, *et al.* Calcium handling proteins in the failing human heart. *Basic Res Cardiol* 1997; 92: 87-93.
137. Hessel MHM, Bleeker GB, Bax JJ, *et al.* Reverse ventricular remodeling after cardiac resynchronization therapy is associated with a reduction in serum tenascin-C and plasma matrix metalloproteinase-9 levels. *Eur J Heart Fail* 2007; 9: 1058-63.
138. Schroen B, Heymans S, Sharma U, *et al.* Thrombospondin-2 is essential for myocardial matrix integrity. Increased expression identifies failure-prone cardiac hypertrophy. *Circ Res* 2004; 95: 515-22.
139. Rysä J, Leskinen H, Ilves M, *et al.* Distinct upregulation of extracellular matrix genes in transition from hypertrophy to hypertensive heart failure. *Hypertension* 2005; 45: 927-33.
140. Iwanaga Y, Aoyama T, Kihara Y, *et al.* Excessive activation of matrix metalloproteinases coincides with left ventricular remodeling during transition from hypertrophy to heart failure in hypertensive rats. *J Am Coll Cardiol* 2002; 39: 1384-91.
141. Wehrens XH, Marks AR. Altered function and regulation of cardiac ryanodine receptors in cardiac disease. *Trends Biochem Sci* 2003; 28: 671-8.
142. Marx SO, Reiken S, Hisamatsu Y, *et al.* PKA phosphorylation dissociates FKBP12.6 from the calcium release channel (ryanodine receptor): Defective regulation in failing hearts. *Cell* 2000; 101: 365-76.
143. Swan JS, Dibb K, Negretti N, *et al.* Effects of eicosapentaenoic acid on cardiac SR Ca²⁺-release and ryanodine receptor function. *Cardiovasc Res* 2003; 60: 337-46.
144. Thomas NL, George CH, Lai FA. Functional heterogeneity of ryanodine receptor mutations associated with sudden cardiac death. *Cardiovasc Res* 2004; 64: 52-60.
145. Deschamps AM, Spinale FG. Pathways of matrix metalloproteinase induction in heart failure: Bioactive molecules and transcriptional regulation. *Cardiovasc Res* 2006; 69: 666-76.
146. Li YY, Feldman AM, Sun Y, *et al.* Differential expression of tissue inhibitors of metalloproteinases in the failing human heart. *Circulation* 1998; 98: 1728-34.
147. Tyagi SC, Kumar S, Voelker DJ, *et al.* Differential gene expression of extracellular matrix components in dilated cardiomyopathy. *J Cell Biochem* 1996; 63: 185-98.
148. Altieri P, Brunelli C, Garibaldi S, *et al.* Metalloproteinases 2 and 9 are increased in plasma of patients with heart failure. *Eur J Clin Invest* 2003; 33: 648-56.

149. Thomas CV, Coker ML, Zellner JL, *et al.* Increased matrix metalloproteinase activity and selective upregulation in LV myocardium from patients with end-stage dilated cardiomyopathy. *Circulation* 1998; 97: 1708-15.
150. Spinale FG, Coker ML, Heung LJ, *et al.* A matrix metalloproteinase induction/activation system exists in the human left ventricular myocardium and is upregulated in heart failure. *Circulation* 2000; 102: 1944-9.
151. Spinale FG. Matrix metalloproteinases: regulation and dysregulation in the failing heart. *Circ Res* 2002; 90: 520-30.
152. Yokoseki O, Yazaki Y, Suzuki J, *et al.* Association of matrix metalloproteinase expression and left ventricular function in idiopathic dilated cardiomyopathy. *Jpn Circ J* 2000; 64: 352-7.
153. Barton PJ, Birks EJ, Felkin LE, *et al.* Increased expression of extracellular matrix regulators TIMP1 and MMP1 in deteriorating heart failure. *J Heart Lung Transplant* 2003; 22: 738-44.
154. Lindsay MM, Maxwell P, Dunn FG. TIMP-1: a marker of left ventricular diastolic dysfunction and fibrosis in hypertension. *Hypertension* 2002; 40: 136-41.
155. Torre-Amione G, Kapadia S, Benedict C, *et al.* Proinflammatory cytokine levels in patients with depressed left ventricular ejection fraction: A report from the Studies of Left Ventricular Dysfunction (SOLVD). *J Am Coll Cardiol* 1996; 27: 1201-6.
156. Siwik DA, Chang DL, Colucci WS. Interleukin-1 β and tumor necrosis factor- α decrease collagen synthesis and increase matrix metalloproteinase activity in cardiac fibroblasts in vitro. *Circ Res* 2000; 86: 1259-65.
157. Li YY, McTiernan CF, Feldman AM. Proinflammatory cytokines regulate tissue inhibitors of metalloproteinases and disintegrin metalloproteinase in cardiac cells. *Cardiovasc Res* 1999; 42: 162-72.
158. Gurjar MV, Deleon J, Sharma RV, *et al.* Mechanism of inhibition of matrix metalloproteinase-9 induction by NO in vascular smooth muscle cells. *J Appl Physiol* 2001; 91: 1380-6.
159. Fedak PW, Moravec CS, McCarthy PM, *et al.* Altered expression of disintegrin metalloproteinases and their inhibitor in human dilated cardiomyopathy. *Circulation* 2006; 113: 238-45.
160. Fielitz J, Leuschner M, Zurbrügg HR, *et al.* Regulation of matrix metalloproteinases and their inhibitors in the left ventricular myocardium of patients with aortic stenosis. *J Mol Med* 2004; 82: 809-20.
161. Wilson EM, Gunasinghe HR, Coker ML, *et al.* Plasma matrix metalloproteinase and inhibitor profiles in patients with heart failure. *J Card Fail* 2002; 8: 390-8.
162. Yamazaki T, Lee JD, Shimizu H, *et al.* Circulating matrix metalloproteinase-2 is elevated in patients with congestive heart failure. *Eur J Heart Fail* 2004; 6: 41-5.
163. Rohde LE, Ducharme A, Arroyo LH, *et al.* Matrix metalloproteinase inhibition attenuates early left ventricular enlargement after experimental myocardial infarction in mice. *Circulation* 1999; 99: 3063-70.
164. Chancey AL, Brower GL, Peterson JT, *et al.* Effects of matrix metalloproteinase inhibition on ventricular remodeling due to volume overload. *Circulation* 2002; 105: 1983-8.
165. Peterson JT, Hallak H, Johnson L, *et al.* Matrix metalloproteinase inhibition attenuates left ventricular remodeling and dysfunction in a rat model of progressive heart failure. *Circulation* 2001; 103: 2303-9.
166. Janicki JS, Brower GL, Gardner JD, *et al.* The dynamic interaction between matrix metalloproteinase activity and adverse myocardial remodeling. *Heart Fail Rev* 2004; 9: 33-42.
167. Spinale FG, Coker ML, Thomas CV, *et al.* Time-dependent changes in matrix metalloproteinase activity and expression during the progression of congestive heart failure. Relation to ventricular and myocyte function. *Circ Res* 1998; 82: 482-95.

168. Rossi A, Cicoira M, Golia G, *et al.* Amino-terminal propeptide of type III procollagen is associated with restrictive mitral filling pattern in patients with dilated cardiomyopathy: a possible link between diastolic dysfunction and prognosis. *Heart* 2004; 90: 650-4.
169. Klappacher G, Franzen P, Haab D, *et al.* Measuring extracellular matrix turnover in the serum of patients with idiopathic or ischemic dilated cardiomyopathy and impact on diagnosis and prognosis. *Am J Cardiol* 1995; 75: 913-8.
170. Zannad F, Alla F, Dousset B, *et al.* Limitation of excessive extracellular matrix turnover may contribute to survival benefit of spironolactone therapy to patients with congestive heart failure. *Circulation* 2000; 102: 2700-6.
171. Cicoira M, Rossi A, Bonapace S, *et al.* Independent and additional prognostic value of aminoterminal propeptide of type III procollagen circulating levels in patients with chronic heart failure. *J Card Failure* 2004; 10: 403-11.
172. Wang TL, Yang YH, Chang H, *et al.* Angiotensin II signals mechanical stretch-induced cardiac matrix metalloproteinase expression via JAK-STAT pathway. *J Mol Cell Cardiol* 2004; 37: 785-94.
173. Liang F, Atakilit A, Gardner DG. Integrin dependence of brain natriuretic peptide gene promoter activation by mechanical strain. *J Biol Chem* 2000; 275: 20355-60.
174. MacKenna D, Summerour SR, Villarreal FJ. Role of mechanical factors in modulating cardiac fibroblast function and extracellular matrix synthesis. *Cardiovasc Res* 2000; 46: 257-63.
175. Shai SY, Harpf AE, Babbitt CJ, *et al.* Cardiac myocyte-specific excision of the $\beta 1$ integrin gene results in myocardial fibrosis and cardiac failure. *Circ Res* 2002; 90: 458-64.
176. Pfister R, Acksteiner C, Baumgarth J, *et al.* Loss of $\beta 1$ D-integrin function in human ischemic cardiomyopathy. *Basic Res Cardiol* 2007; 102: 257-64.
177. Pacher P, Schulz R, Liaudet L, *et al.* Nitrosative stress and pharmacological modulation of heart failure. *Trends Pharmacol Sci* 2005; 26: 302-10.
178. Takimoto E, Kass DA. Role of oxidative stress in cardiac hypertrophy and remodeling. *Hypertension* 2007; 49: 241-8.
179. Mollnau H, Wendt M, Szöcs K, *et al.* Effects of angiotensin II infusion on the expression and function of NAD(P)H oxidase and components of nitric oxide/cGMP signaling. *Circ Res* 2002; 90: e58-e65.
180. Turko IV, Murad F. Protein nitration in cardiovascular diseases. *Pharmacol Rev* 2002; 54: 619-34.
181. Mihm MJ, Coyle CM, Schanbacher BL, *et al.* Peroxynitrite induced nitration and inactivation of myofibrillar creatine kinase in experimental heart failure. *Cardiovasc Res* 2001; 49: 798-807.
182. Kuzkaya N, Weissmann N, Harrison DG, *et al.* Interactions of peroxynitrite, tetrahydrobiopterin, ascorbic acid, and thiols: implications for uncoupling endothelial nitric oxide synthase. *J Biol Chem* 2003 ;278 :22546-54.
183. Xia Y, Dawson VL, Dawson TM, *et al.* Nitric oxide synthase generates superoxide and nitric oxide in arginine-depleted cells leading to peroxynitrite-mediated cellular injury. *Proc Natl Acad Sci USA* 1996;93:6770-4.
184. Rosen GM, Tsai P, Weaver J, *et al.* The role of tetrahydrobiopterin in the regulation of neuronal nitric-oxide synthase-generated superoxide. *J Biol Chem* 2002; 277: 40275-80.
185. Ferdinandy P, Danial H, Ambrus I, *et al.* Peroxynitrite is a major contributor to cytokine-induced myocardial contractile failure. *Circ Res* 2000; 87: 241-7.
186. Vaziri ND, Ni Z, Oveisi F, *et al.* Enhanced nitric oxide inactivation and protein nitration by reactive oxygen species in renal insufficiency. *Hypertension* 2002; 39: 135-41.
187. Szabo C. Multiple pathways of peroxynitrite cytotoxicity. *Toxicol Lett* 2003; 140-141: 105-12.
188. Wang W, Sawicki G, Schulz R. Peroxynitrite-induced myocardial injury is mediated through matrix metalloproteinase-2. *Cardiovasc Res* 2002a; 53: 165-74.

189. Shiomi T, Tsutsui H, Matsusaka H, *et al.* Overexpression of glutathione peroxidase prevents left ventricular remodeling and failure after myocardial infarction in mice. *Circulation* 2004; 109: 544-9.
190. Feng Q, Fortin AJ, Lu X, *et al.* Effects of L-arginine on endothelial and cardiac function in rats with heart failure. *Eur J Pharmacol* 1999; 376: 37-44.
191. Piech A, Massart PE, Dessy C, *et al.* Decreased expression of myocardial eNOS and caveolin in dogs with hypertrophic cardiomyopathy. *Am J Physiol Heart Circ Physiol* 2002; 282: H219-H231.
192. Drexler H, Kästner S, Strobel A, *et al.* Expression, activity and functional significance of inducible nitric oxide synthase in the failing human heart. *J Am Coll Cardiol* 1998 ;32: 955-63.
193. Damy T, Ratajczak P, Shah AM, *et al.* Increased neuronal nitric oxide synthase-derived NO production in the failing human heart. *Lancet* 2004; 363: 1365-7.
194. Stein B, Eschenhagen T, Rüdiger J, *et al.* Increased expression of constitutive nitric oxide synthase III, but not inducible nitric oxide synthase II, in human heart failure. *J Am Coll Cardiol* 1998; 32: 1179-86.
195. Fukuchi M, Hussain SNA, Giaid A. Heterogeneous expression and activity of endothelial and inducible nitric oxide synthases in end-stage human heart failure. Their relation to lesion site and β -adrenergic receptor therapy. *Circulation* 1998; 98: 132-9.
196. Gealekman O, Abassi Z, Rubinstein I, *et al.* Role of myocardial inducible nitric oxide synthase in contractile dysfunction and β -adrenergic hyporesponsiveness in rats with experimental volume-overload heart failure. *Circulation* 2002; 105: 236-43.
197. Smith RS jr, Agata J, Xia C-F, *et al.* Human endothelial nitric oxide synthase gene delivery protects against cardiac remodeling and reduces oxidative stress after myocardial infarction. *Life Sci* 2005; 76: 2457-71.
198. Jones SP, Greer JJM, van Haperen R, *et al.* Endothelial nitric oxide synthase overexpression attenuates congestive heart failure in mice. *Proc Natl Acad Sci USA* 2003; 100: 4891-6.
199. Scherrer-Crosbie M, Ullrich R, Bloch KD, *et al.* Endothelial nitric oxide synthase limits left ventricular remodeling after myocardial infarction in mice. *Circulation* 2001; 104: 1286-91.
200. Liu Y-H, Xu J, Yang X-P, *et al.* Effect of ACE inhibitors and angiotensin II type 1 receptor antagonists on endothelial NO synthase knockout mice with heart failure. *Hypertension* 2002; 39: 375-81.
201. Haywood GA, Tsao PS, von der Leyen HE, *et al.* Expression of inducible nitric oxide synthase in human heart failure. *Circulation* 1996; 93: 1087-94.
202. Vejlsstrup NG, Bouloumie A, Boesgaard S, *et al.* Inducible nitric oxide synthase (iNOS) in the human heart: expression and localization in congestive heart failure. *J Mol Cell Cardiol* 1998; 30: 1215-23.
203. Chen Y, Traverse JH, Du R, *et al.* Nitric oxide modulates myocardial oxygen consumption in the failing heart. *Circulation* 2002; 106: 273-9.
204. Thoenes M, Förstermann U, Tracey WR, *et al.* Expression of inducible nitric oxide synthase in failing and non-failing human heart. *J Mol Cell Cardiol* 1996; 28: 165-9.
205. Heymes C, Vanderheyden M, Bronzwaer JGF, *et al.* Endomyocardial nitric oxide synthase and left ventricular preload reserve in dilated cardiomyopathy. *Circulation* 1999; 99: 3009-16.
206. Feng Q, Lu X, Jones DL, *et al.* Increased inducible nitric oxide synthase expression contributes to myocardial dysfunction and higher mortality after myocardial infarction in mice. *Circulation* 2001; 104: 700-4.
207. Sam F, Sawyer DB, Xie Z, *et al.* Mice lacking inducible nitric oxide synthase have improved left ventricular contractile function and reduced apoptotic cell death late after myocardial infarction. *Circ Res* 2001; 89: 351-6.

208. Jones SP, Greer JJ, Ware PD, *et al.* Deficiency of iNOS does not attenuate severe congestive heart failure in mice. *Am J Physiol Heart Circ Physiol* 2005; 288: H365-H370.
209. Liu Y-H, Carretero OA, Cingolani OH, *et al.* Role of inducible nitric oxide synthase in cardiac function and remodeling in mice with heart failure due to myocardial infarction. *Am J Physiol Heart Circ Physiol* 2005; 289: H2616-H2623.
210. Narula J, Haider N, Virmani R, *et al.* Apoptosis in myocytes in end-stage heart failure. *N Engl J Med* 1996; 335: 1182-9.
211. Olivetti G, Abbi R, Quaini F, *et al.* Apoptosis in the failing human heart. *N Engl J Med* 1997; 336: 1131-41.
212. Damy T, Ratajczak P, Robidel E, *et al.* Up-regulation of cardiac nitric oxide synthase 1-derived nitric oxide after myocardial infarction in senescent rats. *FASEB J* 2003; 17: 1934-6.
213. Bendall JK, Damy T, Ratajczak P, *et al.* Role of myocardial neuronal nitric oxide synthase-derived nitric oxide in β -adrenergic hyporesponsiveness after myocardial infarction-induced heart failure in rat. *Circulation* 2004; 110: 2368-75.
214. Kawakami M, Okabe E. Superoxide anion radical-triggered Ca^{2+} release from cardiac sarcoplasmic reticulum through ryanodine receptor Ca^{2+} channel. *Mol Pharmacol* 1998; 53: 497-503.
215. Seddon M, Looi YH, Shah AM. Oxidative stress and redox signalling in cardiac hypertrophy and heart failure. *Heart* 2007; 93: 903-7.
216. Keith M, Geranmayegan A, Sole MJ, *et al.* Increased oxidative stress in patients with congestive heart failure. *J Am Coll Cardiol* 1998; 31: 1352-6.
217. Belch JFF, Bridges AB, Scott N, *et al.* Oxygen free radicals and congestive heart failure. *Br Heart J* 1991; 65: 245-8.
218. Saraiva RM, Minhas KM, Raju SVY, *et al.* Deficiency of neuronal nitric oxide synthase increases mortality and cardiac remodeling after myocardial infarction. Role of nitroso-redox equilibrium. *Circulation* 2005; 112: 3415-22.
219. Casadei B. The emerging role of neuronal nitric oxide synthase in the regulation of myocardial infarction. *Exp Physiol* 2006; 91.6: 943-55.
220. Kinugawa S, Huang H, Wang Z, *et al.* A defect of neuronal nitric oxide synthase increases xanthine oxidase-derived superoxide anion and attenuates the control of myocardial oxygen consumption by nitric oxide derived from endothelial nitric oxide synthase. *Circ Res* 2005; 96: 355-62.
221. Sun J, Picht E, Ginsburg KS, *et al.* Hypercontractile female hearts exhibit increased S-nitrosylation of the L-type Ca^{2+} channel $\alpha 1$ subunit and reduced ischemia-reperfusion injury. *Circ Res* 2006; 98: 403-11.
222. Gonzalez DR, Beigi F, Treuer AV, *et al.* Deficient ryanodine receptor S-nitrosylation increases sarcoplasmic reticulum calcium leak and arrhythmogenesis in cardiomyocytes. *Proc Natl Acad Sci USA* 2007; 104: 20612-7.
223. Saraiva RM, Hare JM. Nitric oxide signaling in the cardiovascular system: implications for heart failure. *Curr Opin Cardiol* 2006; 21: 221-8.
224. Barouch LA, Cappola TP, Harrison RW, *et al.* Combined loss of neuronal and endothelial nitric oxide synthase causes premature mortality and age-related hypertrophic cardiac remodeling in mice. *J Mol Cell Cardiol* 2003; 35: 637-44.
225. Loyer X, Gómez AM, Milliez P, *et al.* Cardiomyocyte overexpression of neuronal nitric oxide synthase delays transition toward heart failure in response to pressure overload by preserving calcium cycling. *Circulation* 2008; 117: 3187-98.
226. Henrich CJ, Simpson PC. Differential acute and chronic response of protein kinase C in cultured neonatal rat heart myocytes to alpha 1-adrenergic and phorbol ester stimulation. *J Mol Cell Cardiol* 1988; 20: 1081-5.
227. Kariya K, Karns LR, Simpson PC. Expression of a constitutively activated mutant of the beta-isozyme of protein kinase C in cardiac myocytes stimulates the promoter of the beta-myosin heavy chain isogene. *J Biol Chem* 1991; 266: 10023-6.

228. Kariya K, Farrance IK, Simpson PC. Transcriptional enhancer factor-1 in cardiac myocytes interacts with an alpha 1-adrenergic- and beta-protein kinase C-inducible element in the rat beta-myosin heavy chain promoter. *J Biol Chem* 1993; 268: 26658-62.
229. Kariya K, Karns LR, Simpson PC. An enhancer core element mediates stimulation of the rat beta-myosin heavy chain promoter by an alpha 1-adrenergic agonist and activated beta-protein kinase C in hypertrophy of cardiac myocytes. *J Biol Chem* 1994; 269: 3775-82.
230. Yamazaki T, Komuro I, Kudoh S, *et al.* Endothelin-1 is involved in mechanical stress-induced cardiomyocyte hypertrophy. *J Biol Chem* 1996; 271: 3221-8.
231. Sadoshima J-I, Xu Y, Slayter HS, *et al.* Autocrine release of angiotensin II mediates stretch-induced hypertrophy of cardiac myocytes in vitro. *Cell* 1993; 75: 977-84.
232. Tamura K, Umemura S, Nyui N, *et al.* Activation of angiotensinogen gene in cardiac myocytes by angiotensin II and mechanical stretch. *Am J Physiol Regul Integrat Comp Physiol* 1998; 275: R1-R9.
233. Sen S, Kundu G, Mekhail N, *et al.* Myotrophin: Purification of a novel peptide from spontaneously hypertensive rat heart that influences myocardial growth. *J Biol Chem* 1990; 265: 16635-43.
234. Vandenburgh HH, Solerssi R, Shansky J, *et al.* Response of neonatal rat cardiomyocytes to repetitive mechanical stimulation in vitro. *Ann NY Acad Sci* 1995; 752: 19-29.
235. Komuro I, Kaida T, Shibazaki Y, *et al.* Stretching cardiac myocytes stimulates protooncogene expression. *J Biol Chem* 1990; 265: 3595-8.
236. Kira Y, Nakaoka T, Hashimoto E, *et al.* Effect of long-term cyclic mechanical load on protein synthesis and morphological changes in cultured myocardial cells from neonatal rat. *Cardiovasc Drugs Ther* 1994; 8: 251-62.
237. Vliegen HW, van der Laarse A, Huysman JAN, *et al.* Morphometric quantification of myocyte dimensions validated in normal growing rat hearts and applied to hypertrophic human hearts. *Cardiovasc Res* 1987; 21: 352-7.
238. van der Laarse A, Vliegen HW, van der Nat KH, *et al.* Comparison of myocardial changes between pressure induced hypertrophy and normal growth in the rat heart. *Cardiovasc Res* 1989; 23: 308-14.
239. van der Laarse A, Bloys van Treslong CHF, Vliegen HW, *et al.* Relation between ventricular DNA content and number of myocytes and non-myocytes in hearts of normotensive and spontaneously hypertensive rats. *Cardiovasc Res* 1987; 21: 223-9.
240. Schwartz K, Boheler KR, De La Bastie D, *et al.* Switches in cardiac muscle gene expression as a result of pressure and volume overload. *Am J Physiol Regul Integrat Comp Physiol* 1992; 262: R364-R369.
241. Long CS, Kariya K, Karns L, *et al.* Sympathetic modulation of the cardiac myocyte phenotype: studies with a cell-culture model of myocardial hypertrophy. *Basic Res Cardiol* 1992; 87(suppl 2): 19-31.
242. Hasenfuss G, Just H. Myocardial phenotype changes in heart failure: cellular and subcellular adaptations and their functional significance. *Br Heart J* 1994; 72(suppl): S10-S17.
243. Yue P, Long CS, Austin R, *et al.* Post-infarction heart failure in the rat is associated with distinct alterations in cardiac myocyte molecular phenotype. *J Mol Cell Cardiol* 1998; 30: 1615-30.
244. Boluyt MO, Bing OH, Lakatta EG. The ageing spontaneously hypertensive rat as a model of the transition from stable compensated hypertrophy to heart failure. *Eur Heart J* 1995; 16(suppl N): 19-30.
245. Butler WH, Mattocks AR, Barnes JM. Lesions in the liver and lungs of rats given pyrrole derivatives of pyrrolizidine alkaloids. *J Pathol* 1970; 100: 169-75.

246. Lafranconi WM, Huxtable RJ. Hepatic metabolism and pulmonary toxicity of monocrotaline using isolated perfused liver and lung. *Biochem Pharmacol* 1984; 33: 2479-84.
247. Wilson DW, Segall HJ, Pan LC, *et al.* Mechanisms and pathology of monocrotaline pulmonary toxicity. *Crit Rev Toxicol* 1992; 22: 307-25.
248. Lamé MW, Jones AD, Morin D, *et al.* Association of dehydromonocrotaline with rat red blood cells. *Chem Res Toxicol* 1997; 10: 694-701.
249. Reindel JF, Hoorn CM, Wagner JG, *et al.* Comparison of response of bovine and porcine pulmonary arterial endothelial cells to monocrotaline pyrrole. *Am J Physiol Lung Cell Mol Physiol* 1991; 261: L406-L414.
250. Reindel JF, Roth RA. The effects of monocrotaline pyrrole on cultured bovine pulmonary artery endothelial and smooth muscle cells. *Am J Pathol* 1991; 138: 707-19.
251. Ghodsi F, Will JA. Changes in pulmonary structure and function induced by monocrotaline intoxication. *Am J Physiol Heart Circ Physiol* 1981; 240: H149-H155.
252. Hessel MH, Steendijk P, den Adel B, *et al.* Characterization of right ventricular function after monocrotaline-induced pulmonary hypertension in the intact rat. *Am J Physiol Heart Circ Physiol* 2006; 291: H2424-H2430.
253. Henkens IR, Mouchaers KTB, Vliegen HW, *et al.* Early changes in rat hearts with developing pulmonary arterial hypertension can be detected with three-dimensional electrocardiography. *Am J Physiol Heart Circ Physiol* 2007; 293: H1300–H1307.

CHAPTER 2

Integrin stimulation-induced hypertrophy in neonatal rat cardiomyocytes is NO-dependent

S. Umar
E.J.M. van der Valk
M.J. Schaliij
E.E. van der Wall
D.E. Atsma
A. van der Laarse

Molecular and Cellular Biochemistry 2009;320:75-84

Abstract

Background: Prolonged myocardial stretch typically leads to hypertrophy of cardiomyocytes. As integrins are cellular receptors of stretch, we hypothesize that integrin stimulation induces cardiomyocyte hypertrophy.

Methods: Integrins of neonatal rat cardiomyocytes (NRCMs) were stimulated with a peptide containing the Arg-Gly-Asp (RGD) sequence for 24 h. For comparison, α_1 -adrenergic stimulation by phenylephrine (PE) for 24 h was applied. Saline-treated NRCMs were used as control. The hypertrophic response was quantified by measuring cell surface area (CSA). Phosphorylation of NO-synthase-1 (NOS1) was assessed by immunocytochemistry.

Results: CSA was increased by 38% (IQR 31-44%) with RGD and by 68% (IQR 64-84%) with PE vs. control (both $p < 0.001$). NOS-1 phosphorylation was increased by 61% with RGD and by 21% with PE vs. control (both $p < 0.01$). A general NOS inhibitor (L-NAME) inhibited RGD-induced hypertrophy completely, but had no significant effect on PE-induced hypertrophy. Administration of NO-donor to NRCMs co-incubated with RGD + L-NAME partly restored hypertrophy (to 62% of the hypertrophic effect of RGD alone), but had no effect if incubated with PE + L-NAME. Ryanodine and BAPTA-AM inhibited RGD-induced hypertrophy completely, but not that induced by PE.

Conclusions: Integrin stimulation of NRCMs by RGD leads to hypertrophy, likely by activation of NOS-1. Abrogation of RGD-induced hypertrophic response upon NOS-inhibition and rescue of this hypertrophic effect by NO-donor suggest that integrin stimulation-induced hypertrophy of NRCMs is NO-dependent.

Key words: cardiomyocytes, hypertrophy, integrin, α_1 -adrenergic receptor, phenylephrine, nitric oxide synthase-1

Abbreviations: FAK, focal adhesion kinase; nNOS, neuronal nitric oxide synthase; NOS1, neuronal nitric oxide synthase; NO, nitric oxide; PBS, phosphate-buffered saline; ERK, extracellular signal-regulated kinase; MAP kinase, mitogen-activated protein kinase; MEK, mitogen-activated protein kinase kinase, also indicated by MAPK/ERK kinase; NRCM, neonatal rat cardiomyocyte; PE, phenylephrine; RGD, -Arg-Gly-Asp- sequence; L-NAME, N ω -nitro-L-arginine methyl ester; SMTC, S-methyl-L-thiocitrulline; PKC, protein kinase C; BAPTA-AM, 1,2-bis(2-aminophenoxy)ethane-N,N,N',N'-tetraacetic acid tetrakis-acetoxymethyl ester;

Introduction

The primary stimulus for cardiac hypertrophy in response to hemodynamic overload is mechanical stretch itself. Upon mechanical stretch *in vitro*, protein synthesis in cardiomyocytes is stimulated associated with expression of “immediate-early” (IE) genes and re-expression of fetal genes [1-6]. As to the mechanosensors involved in stretch-induced protein synthesis of cardiomyocytes, the integrins are likely candidates as they take a central position between the extracellular matrix (ECM) of the tissue on which the stretch is applied and the cellular cytoskeleton through which the cell becomes deformed in response to stretch [7,8]. When ECM proteins interact with integrins, signals are transmitted by integrins to the cell cytoplasm through “outside-in signaling” [7]. Transmission of intracellular signals after integrin ligation is carried by, among others, focal adhesion kinase (FAK), a key cytoplasmic tyrosine kinase [9,10]. FAK associates with several different signaling proteins such as Src-family protein-tyrosine kinases, p130^{Cas}, Shc, Grb2, and paxillin [11-14].

Earlier we have shown that short-term integrin stimulation of neonatal rat cardiomyocytes (NRCMs) using a pentapeptide containing the Arg-Gly-Asp (RGD) sequence resulted in elevations of intracellular Ca²⁺ and NO concentrations [15]. The latter was considered the result of an increased concentration of the phosphorylated form of NO-synthase-1 (NOS1) [15].

In the present study we compared integrin stimulation-induced cardiomyocyte hypertrophy with a well-established cell model of hypertrophy, PE-induced cardiomyocyte hypertrophy [16], with respect to components of the intracellular signaling cascade [17]. Specifically, NRCMs were exposed to integrin stimulation by RGD or PE for 24 h, followed by assessment of the state of phosphorylation of several candidate signaling molecules, and quantification of the hypertrophic response. The specific roles in the hypertrophic process of NOS1, NO, Ca²⁺, ryanodine receptor, protein kinase C, and ERK1/2 were studied using inhibitors and an NO donor, sodium nitroprusside.

Materials and Methods

Cardiomyocyte cultures

Neonatal (2-day-old) rat ventricular cardiomyocytes (NRCMs) were prepared as described before [18]. Briefly, ventricular myocardium was dissociated with collagenase (Worthington, USA) and preplated in plastic dishes (Falcon Primaria, Becton-Dickinson, USA) to allow preferential attachment of non-cardiomyocytes. Then, 1 h later, non-adherent cells were transferred to Petri dishes (ø 35 mm), each containing a glass cover-slip (ø 25 mm) coated with rat-tail collagen (20 µg/mL; Sigma, USA). The culture medium consisted of Ham's F10 supplemented with 10% heat-inactivated fetal bovine serum (FBS), 10% heat-inactivated horse serum (HS), 100 U/mL penicillin and 0.1 g/L streptomycin, all from Invitrogen (the Netherlands). The culture medium was replaced 24 h after seeding by a medium containing Ham's F10 and DMEM (Invitrogen)(1:1, v/v), 5% HS, antibiotics, and

100 $\mu\text{mol/L}$ 5-bromo-2'-deoxyuridine (Sigma) to inhibit cardiac fibroblast proliferation. The cultures of NRCMs were grown in a humidified incubator at 37°C and 5% CO_2 . The medium was replaced 48 h after seeding by a medium containing Ham's F10 and DMEM (1:1, $\frac{v}{v}$), 2.5% HS and antibiotics. The experiments had the approval of the Animal Experiments Committee of the Leiden University Medical Center.

Experimental protocol

Seventy-two hours after seeding the NRCMs, PE (100 $\mu\text{mol/L}$, Sigma), the pentapeptide Gly-Arg-Gly-Asp-Ser (RGD, 300 $\mu\text{g/mL}$, Sigma), or PBS (control) were added to the culture medium. Twenty-four hours later, spontaneously beating NRCMs were lysed with ice-cold lysis buffer containing 0.1 mol/L Tris-HCl, 0.1% Tween-20 and 0.5 mmol/L sodium orthovanadate (Sigma), pH 7.5. After freezing and thawing for three times, the cell extracts were sonified two times for 30 s each, at 60% output using the microtip (Branson Ultrasonics, USA). Cell extracts were stored at -20°C before assay.

In separate series of experiments, spontaneously beating NRCMs were incubated with several drugs and agents, added to the culture medium 30 min before adding RGD, PE or PBS for a total duration of 24 h. These drugs and agents were (*i*) the general NOS-inhibitor N ω -nitro-L-arginine methyl ester (L-NAME, 100 $\mu\text{mol/L}$, Sigma); (*ii*) the specific NOS1-inhibitor S-methyl-L-thiocitrulline (SMTC, 0.1 $\mu\text{mol/L}$, Sigma); (*iii*) the MAP kinase inhibitors apigenin (10 $\mu\text{mol/L}$, Calbiochem, USA) and PD98059 (100 $\mu\text{mol/L}$, Calbiochem); (*iv*) the protein kinase C inhibitors chelerythrine (10 $\mu\text{mol/L}$, Sigma) and bisindolylmaleimide (50 $\mu\text{mol/L}$, Sigma); (*v*) an NO-donor (sodium nitroprusside (SNP), 10 $\mu\text{g/mL}$, pharmacy of LUMC); (*vi*) an inhibitor of the Ca^{2+} release channel of the sarcoplasmic reticulum ryanodine (100 $\mu\text{mol/L}$, Sigma); (*vii*) the intracellular Ca^{2+} chelator BAPTA-AM (50 $\mu\text{mol/L}$, Invitrogen); (*viii*), and the sarcolemmal L-type Ca^{2+} channel blocker verapamil (100 $\mu\text{mol/L}$, Sigma).

Protein assay

Protein concentration was determined by the bicinchoninic acid (BCA) protein assay (Pierce, USA) using bovine serum albumin (2 mg/mL, Pierce) as a standard.

Western blotting

Ten μg of protein was loaded per well and run on SDS-PAGE, using NuPage 12% Bis-Tris gels (Invitrogen) and electro-transferred to polyvinylidene difluoride filter (PVDF) membrane (Hybond-P, GE Healthcare, the Netherlands). To reduce non-specific binding, the PVDF membrane was blocked for 1 h at room temperature with blocking buffer (ECL Advance blocking agent, GE Healthcare) in TBST solution composed of 10 mmol/L Tris-HCl, 0.05% Tween-20, 150 mmol/L NaCl, pH 8.0. Thereafter, the PVDF membrane was incubated with primary antibodies diluted 1:50,000 in blocking buffer at room temperature for 60 min, washed four times in TBST solution, and incubated with horseradish peroxidase-conjugated secondary antibodies diluted 1:35,000 in blocking buffer at room temperature for 60 min.

For ANP and GAPDH, the PVDF membrane was incubated with both anti-ANP and anti-GAPDH primary antibodies at the same time. For ERK1-P/ERK1 and ERK2-P/ERK2, the PVDF membrane was incubated with anti-phospho ERK1 and anti-phospho ERK2 antibody followed by incubation with anti-ERK1 or anti-ERK2 antibody, respectively, after stripping the membrane.

Bands were visualized with the enhanced chemiluminescence detection system (ECL Advance western blotting detection kit, GE Healthcare), exposed to X-ray film (GE Healthcare), and analysed using a densitometer (Ultrascan XL, LKB, Sweden).

Primary antibodies used were: rabbit polyclonal anti-ANP antibody (Chemicon), mouse monoclonal anti-GAPDH antibody (Chemicon), and mouse monoclonal anti-phospho ERK1 and anti-phospho ERK2 antibodies (Cell Signaling Technology, USA). Secondary antibodies used were goat anti-mouse IgG conjugated to HRP (Santa Cruz Biotechnology, USA) and goat anti-rabbit IgG conjugated to HRP (Santa Cruz Biotechnology).

Immunofluorescence microscopy

Cultures of NRCMs were processed as described earlier [15]. Primary antibodies used were: mouse monoclonal anti-sarcomeric α -actinin antibody (Sigma), rabbit anti-phospho (Tyr397) FAK antibody (Upstate, USA), and rabbit anti-phospho NOS1 antibody (Upstate). The primary antibodies were diluted 1:200 in PBS containing 1% FBS. Secondary antibodies were goat anti-rabbit IgG conjugated to FITC (Sigma), goat anti-mouse IgG conjugated to FITC (Sigma), goat anti-rabbit IgG conjugated to Alexa-568 (Molecular Probes, USA) and rabbit anti-mouse IgG conjugated to Alexa-568 (Molecular Probes, USA). The secondary antibodies were diluted 1:150 in PBS containing 1% FBS. Immunofluorescence images were produced using a fluorescence microscope (Eclipse, Nikon, Japan) equipped with a digital camera (DXM1200, Nikon). Images were analysed quantitatively using Image Pro Plus software (Media Cybernetics, USA) providing pixel intensity distributions of blue, green and red fluorescence.

Cell surface areas were measured by morphometric analysis of α -actinin stained NRCMs using Image Pro Plus software (Media Cybernetics). Surface areas of five cells per field and a total of 60-80 cells per glass cover-slip were determined.

Statistics

Results are expressed as median with interquartile range (IQR), unless stated otherwise. The significance of differences between means was calculated by Student's t-test and one-way analysis of variance (ANOVA) followed by Bonferroni's *post hoc* test wherever appropriate. Correlations were determined using a parametric test (Pearson). Differences were considered significant at $p < 0.05$. SPSS12 for Windows (SPSS Inc., USA) was used for statistical analysis. Experimental data were always compared with data collected in control experiments performed at the same day.

Results

Effects of RGD and PE on hypertrophy

Cardiomyocytes incubated with RGD-peptide (300 $\mu\text{g}/\text{mL}$) or PE (100 $\mu\text{mol}/\text{L}$) for 24 h showed a median increase in cell surface area by 38% (IQR 31-44%; $p < 0.001$ vs. control) or by 68% (IQR 64-84%; $p < 0.001$ vs. control) compared with the cells treated with PBS (Fig.1a). The left panel of fig.1a shows the medians, interquartile ranges and ranges of the cell areas in the three groups of one representative experiment, indicating that the large variability of cell surface area data per group represents a true variation in cell surface area within a particular NRCM culture. In the right panel of fig.1a the medians, interquartile ranges and ranges of 8 median values of cell areas obtained from 8 independent experiments are presented. Unlike the large variation of cell areas within a treatment group of one experiment (variation coefficient of $\approx 30\%$), the between-experiment variation in the groups with the same treatment is much lower (variation coefficient of $\approx 10\%$).

After treatment with RGD for 24 h we found an increase in average ($\pm\text{SD}$) ANP/GAPDH ratio by $49 \pm 9\%$ compared with PBS ($p < 0.05$) (Fig. 1b). After treatment with PE for 24 h we found an increase in average ($\pm\text{SD}$) ANP/GAPDH ratio by $111 \pm 27\%$ compared with PBS ($p < 0.05$) (Fig. 1b).

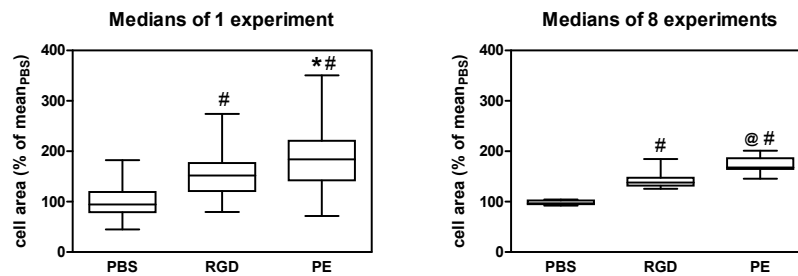


Figure 1A. LEFT Box and whisker plots of cell areas of three groups of NRCMs grown in the presence of phenylephrine (PE, 100 $\mu\text{mol}/\text{L}$), RGD-containing pentapeptide (RGD, 300 $\mu\text{g}/\text{mL}$), or control (PBS) for 24 h. Cell areas are expressed as percentage of the mean value of cell areas of the control culture. The boxes show median, 1st and 3rd quartiles, and the whiskers show the range. Data shown originate from one representative experiment. Per group $n=77$. **RIGHT** Box and whisker plots of median values of cell areas obtained from 8 independent experiments with NRCMs grown in the presence of phenylephrine (PE, 100 $\mu\text{mol}/\text{L}$), RGD-containing pentapeptide (RGD, 300 $\mu\text{g}/\text{mL}$), or control (PBS) for 24 h.

$p < 0.001$ vs. control (PBS), by ANOVA and Bonferroni correction

* $p < 0.001$ PE vs. RGD, by ANOVA and Bonferroni correction

@ $p < 0.01$ PE vs. RGD, by ANOVA and Bonferroni correction

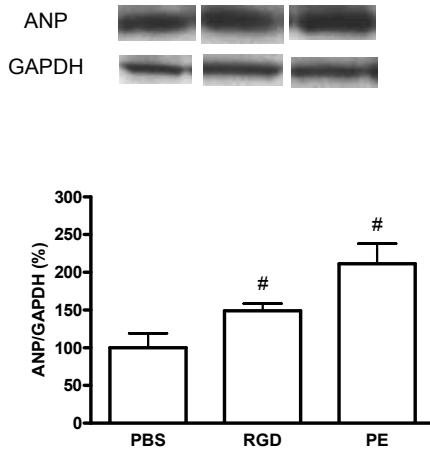


Figure 1B. ANP/GAPDH protein ratio in NRCMs treated with PBS (control), RGD (300 $\mu\text{g/mL}$), and PE (100 $\mu\text{mol/L}$) for 24 h. Values are mean \pm SD. $n=3$ cultures per bar. Representative blotting results are presented ([#] $p<0.05$ vs. PBS).

Effects of RGD and PE on activation of FAK, NOS1, ERK1/2 and PKC

After 24 h incubation, RGD had caused an average (\pm SD) increase in FAK phosphorylation by $34\pm 27\%$ compared with PBS ($p<0.05$). Incubation with PE for 24 h had caused an average (\pm SD) increase in FAK phosphorylation by $111\pm 17\%$ compared with PBS ($p<0.001$) (Table).

NOS1 phosphorylation was increased by $61\pm 29\%$ (mean \pm SD) by incubation with RGD for 24 h compared to PBS ($p<0.01$), whereas PE had caused an increase in NOS1 phosphorylation by $21\pm 11\%$ (mean \pm SD; $p<0.01$) (Table).

Signaling molecule	Control	+RGD	+PE	<i>P</i> (RGD vs. PE)
FAK-P	100±46	134±27 [#]	211±17 ^{###}	<0.001
NOS1-P	100±29	161±29 ^{###}	121±11	<0.01
ERK1-P	100±9	163±18 ^{##}	74±14	<0.001
ERK2-P	100±5	152±4 [#]	101±40	<0.05

[#] *p*<0.05 vs. Control ^{##} *p*<0.01 vs. Control ^{###} *p*<0.001 vs. Control

Table. Quantification of phosphorylated forms of signaling molecules such as focal adhesion kinase (FAK), nitric oxide synthase-1 (NOS1), and extracellular related kinases-1 and -2 (ERK1 and ERK2, respectively) after 24 h incubation of NRCMs in control medium (Control), medium containing RGD peptide (+RGD, 300 µg/mL), phenylephrine (+PE, 100 µmol/L). Phosphorylated forms of FAK and NOS1 were quantified by immunofluorescence microscopy. Number of independent observations is 5 per group. Phosphorylated forms of ERK1 and ERK2 were quantified by western blot. Number of independent observations is 3 per group.

Figure 2 shows representative immunofluorescent images of NRCMs stained for phosphorylated FAK and NOS1 before and after stimulation with PE (100 µmol/L) or RGD (300 µg/mL).

In NRCMs incubated with RGD for 24 h phosphorylated forms of ERK1 and ERK2 had increased by, on average (±SD), 63±18% and 52±4%, compared with PBS, respectively (both *p*<0.05). Incubation with PE for 24 h had no significant effects on ERK1/2 phosphorylation (Table). However, phosphorylation of ERK1/2 had already peaked during the first hour of incubation with PE, whereas their phosphorylation was still rising at the end of first hour incubation with RGD (data not shown).



Figure 2a. Immunofluorescence images of phosphorylated FAK in NRCMs treated with PBS (control, **A**), RGD (300 µg/mL, **B**) and PE (100 µmol/L, **C**).

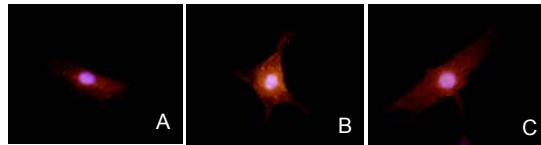


Figure 2b. Immunofluorescence images of phosphorylated NOS1 in NRCMs treated with PBS (control, **A**), RGD (300 µg/mL, **B**) PE (100 µmol/L, **C**). In panels A, B, and C the secondary antibody used was goat anti-rabbit IgG conjugated to Alexa-568 (red). All images were taken at 100x magnification.

Cells pre-treated with MAP kinase inhibitor apigenin in the presence of RGD showed a complete inhibition of hypertrophy ($p < 0.001$ vs. RGD). Cells pre-treated with MAP kinase inhibitor PD98059 or with the combination of apigenin and PD98059 also showed complete inhibition of RGD-induced hypertrophy ($p < 0.001$ vs. RGD)(Fig. 3a). Cells pre-treated with apigenin in the presence of PE showed no significant change in CSA compared with cells treated with the “PE only” group. Likewise, cells pre-treated with PD98059 or with the combination of apigenin and PD98059 did not show a significant change in CSA compared with the “PE only” group (Fig. 3a).

Addition of the protein kinase C inhibitors bisindolylmaleimide (50 µmol/L) and chelerythrine (10 µmol/L) reduced the PE-induced hypertrophy by 41% ($p < 0.001$ vs. “PE only”), whereas the RGD-induced hypertrophy was not significantly influenced by these agents compared to “RGD only” (Fig. 3b).

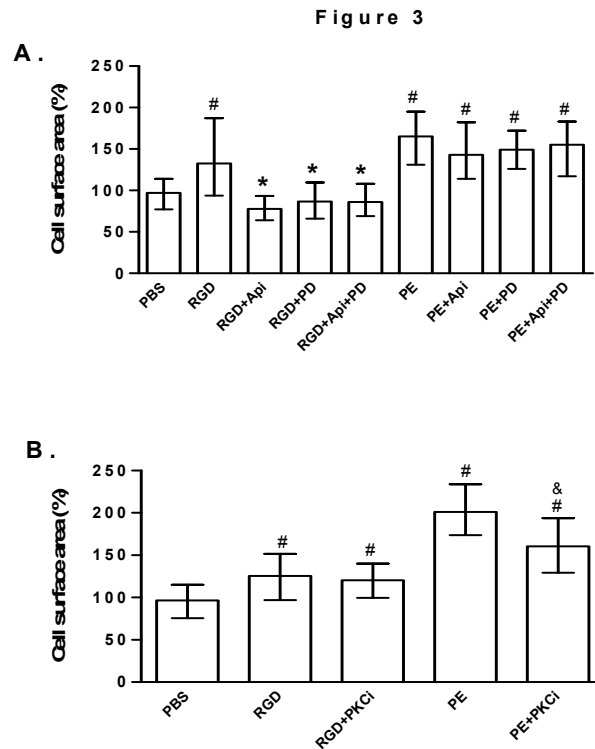


Figure 3

A. Effect of RGD (300 $\mu\text{g}/\text{mL}$) on cell surface area without and with pre-treatment with the MAP kinase inhibitors apigenin (Api, 10 $\mu\text{mol}/\text{L}$), PD98059 (PD, 100 $\mu\text{mol}/\text{L}$), and the combination of these two inhibitors and the effect of PE (100 $\mu\text{mol}/\text{L}$) on cell surface area without and with pre-treatment of apigenin (10 $\mu\text{mol}/\text{L}$), PD98059 (100 $\mu\text{mol}/\text{L}$), and the combination of these two inhibitors.

In all series of experiments, the incubations lasted 24 h.

Columns show median values with 1st and 3rd quartiles. N= 36-83 cells per bar.

$p < 0.05$ vs. PBS

* $p < 0.05$ vs. "RGD only"

B. Effect of RGD (300 $\mu\text{g}/\text{mL}$) on cell surface area without and with pre-treatment with protein kinase C inhibitors (PKCi, being 50 $\mu\text{mol}/\text{L}$ bisindolylmaleimide and 10 $\mu\text{mol}/\text{L}$ chelerythrine) and the effect of PE (100 $\mu\text{mol}/\text{L}$) on cell surface area without and with pre-treatment with these protein kinase C inhibitors.

In all series of experiments, the incubations lasted 24 h. Columns show median values with 1st and 3rd quartiles. N= 20-59 cells per bar.

$p < 0.05$ vs. PBS

§ $p < 0.05$ vs. "PE only"

Effect of intracellular NO on RGD- and PE-induced hypertrophy

NRCMs pre-treated with a general NOS-inhibitor L-NAME (100 $\mu\text{mol/L}$) in the presence of RGD showed a complete inhibition of hypertrophy ($p < 0.001$ vs. RGD) (Fig. 4a). Cells pre-treated with the specific NOS1-inhibitor SMTC (0.1 $\mu\text{mol/L}$) in the presence of RGD also showed a complete inhibition of hypertrophy ($p < 0.001$ vs. RGD)(data not shown).

Cells pre-treated with L-NAME (100 $\mu\text{mol/L}$) in the presence of PE showed no significant change in CSA compared with the "PE only" group (Fig. 4a). Cells pre-treated with SMTC (0.1 $\mu\text{mol/L}$) in the presence of PE showed a 55% inhibition of hypertrophy compared with the "PE only" group ($p < 0.05$ vs. PE)(data not shown). Addition of SNP (10 $\mu\text{g/mL}$) to NRCMs incubated with RGD + L-NAME for 24 h partially restored the hypertrophic capacity of RGD to 132% ($p < 0.001$ vs. RGD+L-NAME) which is 62% of the full effect by "RGD only". SNP added to NRCMs incubated with PE + L-NAME had no significant effect (Fig. 4a).

Effect of intracellular Ca^{2+} on RGD- and PE-induced hypertrophy

Pretreatment of NRCMs by BAPTA (50 $\mu\text{mol/L}$) inhibited the hypertrophic effect of RGD completely ($p < 0.001$ vs "RGD only"). Likewise, blockade of the ryanodine receptor by ryanodine (100 $\mu\text{mol/L}$) caused a complete inhibition of RGD-induced hypertrophy. Verapamil (100 $\mu\text{mol/L}$) had no significant effect on RGD-induced hypertrophy (Fig. 4b). So, Ca^{2+} release from the sarcoplasmic reticulum appears to be a prerequisite for the hypertrophic capacity of RGD.

In PE-incubated NRCMs, BAPTA, nor ryanodine, nor verapamil had any effect on the hypertrophic effect of PE (Fig. 4b).

Figure 4

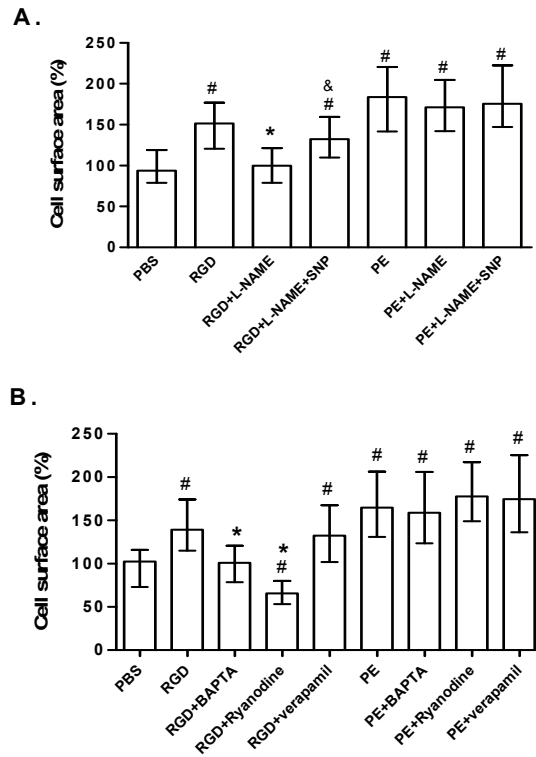


Figure 4 A. Effect of RGD (300 $\mu\text{g}/\text{mL}$) on cell surface area without and with pre-treatment with L-NAME (100 $\mu\text{mol}/\text{L}$) and L-NAME + SNP (10 $\mu\text{g}/\text{mL}$) and the effect of PE (100 $\mu\text{mol}/\text{L}$) on cell surface area without and with pre-treatment with L-NAME (100 $\mu\text{mol}/\text{L}$) and L-NAME + SNP (10 $\mu\text{g}/\text{mL}$). Columns show median values with 1st and 3rd quartiles. N= 72-80 cells per bar.

$p < 0.05$ vs. PBS

* $p < 0.05$ vs. "RGD only"

& $p < 0.05$ vs. RGD + L-NAME

B. Effect of RGD (300 $\mu\text{g}/\text{mL}$) on cell surface area without and with pre-treatment with BAPTA (50 $\mu\text{mol}/\text{L}$), ryanodine (100 $\mu\text{mol}/\text{L}$) and verapamil (100 $\mu\text{mol}/\text{L}$), and the effect of PE (100 $\mu\text{mol}/\text{L}$) on cell surface area without and with pre-treatment with BAPTA (50 $\mu\text{mol}/\text{L}$), ryanodine (100 $\mu\text{mol}/\text{L}$) and verapamil (100 $\mu\text{mol}/\text{L}$). In all series of experiments, the incubations lasted 24 h. Columns show median values with 1st and 3rd quartiles. N= 48-90 cells per bar.

$p < 0.05$ vs. PBS

* $p < 0.05$ vs. "RGD only"

Discussion

The present study shows that integrin stimulation with a pentapeptide containing the Arg-Gly-Asp (RGD) sequence for 24 h leads to NRCM hypertrophy *in vitro* via an NO-dependent mechanism. In comparison to the frequently used model of cellular hypertrophy by α_1 -adrenergic stimulation using PE, the intracellular signaling cascades of the two models differed in a number of aspects including dependence upon NO, intracellular Ca^{2+} , and protein kinase C.

Cardiac hypertrophy is a fundamental process of adaptation to an increased workload. During development of cardiac hypertrophy, cardiomyocytes undergo specific changes, such as rapid induction of immediate-early genes, quantitative and qualitative changes in gene expression and increased rate of protein synthesis [6]. The primary stimulus for cardiac hypertrophy is mechanical stress and/or an accompanying increase in neurohumoral factors [1-5]. Mechanical stretch of cardiomyocytes *in vitro* produces effects that are generally similar to those observed in the heart exposed to hemodynamic overload [1-5], including activation of MAP kinases [3,19,20].

The cardiomyocyte's mechanosensors are the integrins, being transmembrane proteins that link the extracellular matrix (ECM) to the cellular cytoskeleton at places called focal adhesion sites [21]. The cytoplasmic domain forms links with cytoskeletal proteins and intracellular signaling molecules such as focal adhesion kinase (FAK) [21,22]. Integrins can function as signal transducers that regulate gene expression and cellular growth [7,23]. Integrins also influence the hypertrophic response in cardiomyocytes [24]. Overexpression of β_1 -integrin in the cardiomyocyte increases ANP expression and protein synthesis without affecting DNA synthesis [24]. In addition, Kuppuswamy *et al.* have shown an association of β_3 -integrin and two non-receptor kinases, FAK and c-Src, with the cytoskeleton in hypertrophic cat hearts [25]. Upon integrin-induced phosphorylation of these kinases, they become activated, may recruit Grb2/Sos and then initiate the Ras/ERK signal transduction pathway [11,26-30]. We found an increase in FAK phosphorylation in both integrin-stimulated as well as PE-stimulated NRCMs after 24 h, although significantly more with PE than with integrin stimulation. Pham *et al.* have shown that α_1 -adrenergic receptor stimulation induced a rapid and sustained phosphorylation of FAK, which appeared to be a prerequisite for a hypertrophic response of α_1 -adrenoceptor agonists, as FAK-mutants had a blunted α_1 -adrenoceptor-induced hypertrophic response [31].

PE, like several other agonists of G-protein coupled receptors, stimulates sarcomeric organization, induces ANP and produces hypertrophy in NRCMs. Moreover, PE stimulates a rapid increase in tyrosine phosphorylation of focal adhesion proteins including FAK, paxillin, and p130Crk-associated substrate and subsequent formation of peripheral focal complexes [32]. α_1 -adrenergic receptor-stimulated signaling implies phosphorylation of p90RSK [33]. Eukaryotic elongation factor 2 kinase (eEF2K) is a known p90RSK target. eEF2K phosphorylation was significantly reduced by the protein kinase C inhibitor bisindolylmaleimide [34]. In the nucleus p90RSK phosphorylates transcription factors, including c-Fos, Nur77 and CREB [35,36]. In the present study, inhibition

of protein kinase C reduced PE-induced hypertrophy by 41%, but had no effect on RGD-induced hypertrophy.

Although ERK signaling has been shown to be involved in effective PE-induced cardiomyocyte hypertrophy [37-39], other studies including the present study have shown that the MEK1 inhibitor PD98059 did not block PE-induced cardiomyocyte hypertrophy to a significant extent [40-42]. In the present study, the MAP kinase inhibitors apigenin and PD98059 inhibited hypertrophy considerably in RGD-treated NRCMs, and hardly in PE-treated NRCMs.

The present study has been conducted with NRCMs that upon stimulation of integrins with RGD-peptide revealed increased intracellular concentrations of NO and Ca^{2+} , in combination with markedly increased concentrations of phosphorylated NOS1 [15]. Accordingly, the NOS inhibitors L-NAME and SMTC prevented the RGD-induced hypertrophy of NRCMs, but had little effect on PE-induced hypertrophy of NRCMs. However, the pro-hypertrophic effect of NO and the anti-hypertrophic effect of NO inhibitors have to be considered in association with integrin stimulation. In the literature we can find studies reporting that NO has pro-hypertrophic effects [43-46] and studies reporting that NO has anti-hypertrophic effects [47-49]. These apparently contradictory observations are explained by taking into account the fact that in the cardiomyocyte NOS3 and NOS1 are localized at sarcolemma and sarcoplasmic reticulum, respectively, leading to NO formation that is confined to particular compartments with different consequences. This is illustrated by the finding that in NOS3-deficient mice, blood pressure is $\approx 30\%$ higher than in wild-type mice and associated with LV hypertrophy [49], whereas in NOS1-deficient mice blood pressure is similar to that in wild-type mice when awake, and hypotensive under anaesthesia [50,51]. Other factors that may explain why NO may have pro- and anti-hypertrophic effects are (i) the formation of other vasoactive compounds, such as ANP and angiotensin-II, (ii) the formation of superoxide anion due to “uncoupling” of the NOS isoenzyme, thereby causing oxidative stress, (iii) the reaction of NO with superoxide anion to form peroxynitrite, and (iv) direct effects of NO on proteins by means of S-nitrosylation, or indirect effects via stimulation of guanylate cyclase and cGMP formation.

The present study has clearly demonstrated the calcium dependence of the integrin stimulation-induced hypertrophy. This dependence was demonstrated particularly by inhibiting RyR function and by chelating intracellular Ca^{2+} ions, whereas blockade of Ca^{2+} influx via L-type Ca^{2+} channels by verapamil was without any effect. Ca^{2+} release from the SR appears necessary for integrin stimulation-induced hypertrophy. NO controls RyR2 function probably by NO-induced nitrosylation of RyR2, leading to increased conductance of RyR2 and increased Ca^{2+} concentration [52-55].

As to the limitations of our study, we note (i) the use of collagen as an ECM substrate to culture the NRCMs; we did not investigate the effects of other ECM components such as fibronectin, laminin and gelatin on NRCM hypertrophy; (ii) the use of neonatal rat cardiomyocytes in vitro; we did not investigate whether adult rat cardiomyocytes were behaving similarly, as in our hands adult rat cardiomyocytes loose vitality within 24 h; (iii) the time window of 24 h which represents acute rather than chronic events.

Conclusions

The present study demonstrates that although integrin stimulation and α_1 -adrenergic receptor stimulation both lead to hypertrophy of NRCMs *in vitro*, intracellular signaling cascades differ between the two models. In Fig. 5 a hypothetical scheme of both signal transduction pathways is presented, showing that the PE-stimulated signaling cascade is protein kinase C-dependent and that the RGD-stimulated signaling cascade contains both release of Ca^{2+} ions from the SR and production of NO. In the latter pathway, we have clearly demonstrated that exogenous NO (donated by nitroprusside) was able to bypass the L-NAME-induced blockade of the signaling pathway. Absence of a hypertrophic response by NOS-inhibition suggests that integrin stimulation-induced hypertrophy is NO-dependent, whereas stimulation by PE appears largely NO-independent.

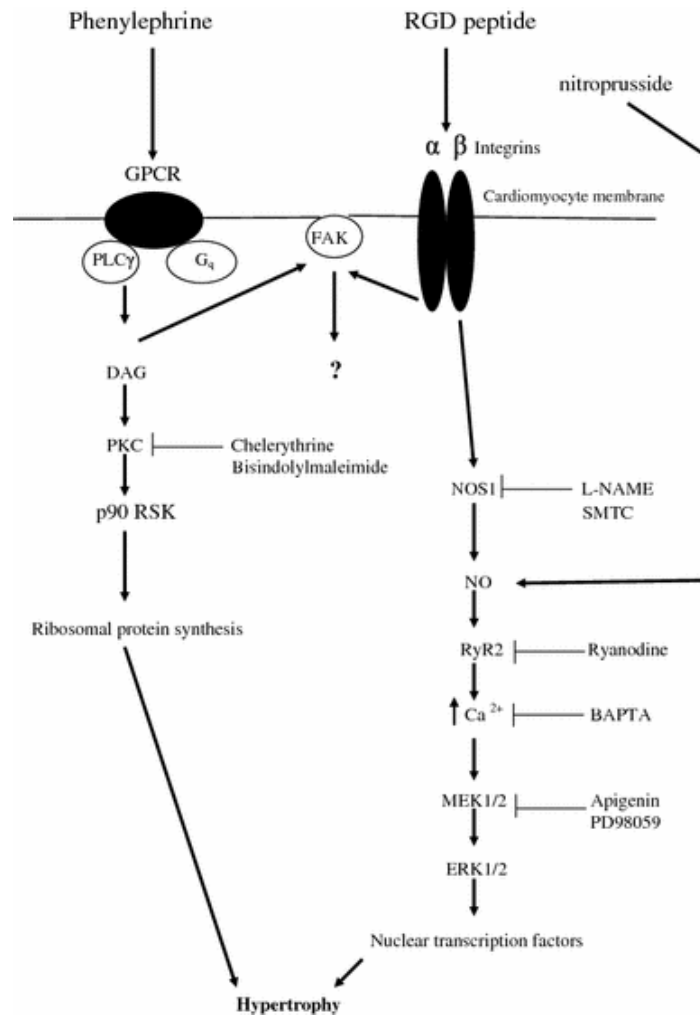


Figure 5

A hypothetical scheme of signaling events leading to hypertrophy induced by α_1 -adrenergic receptor stimulation using phenylephrine and by integrin stimulation using RGD peptide.

Abbreviations: GPCR, G-protein coupled receptor; PLC γ , phospholipase- γ ; G $_q$, G-protein q; DAG, diacylglycerol; PKC, protein kinase C; p90RSK, p90 ribosomal S6 kinase; FAK, focal adhesion kinase; NOS1, nitric oxide synthase-1; L-NAME, N ω -nitro-L-arginine methyl ester; SMTC, S-methyl-L-thiocitrulline; NO, nitric oxide; RyR2, ryanodine receptor-2; BAPTA-AM, 1,2-bis(2-aminophenoxy)ethane-N,N,N',N'-tetraacetic acid tetrakis-acetoxymethyl ester; MEK1/2, MAP kinase kinase 1/2; ERK1/2, p44 and p42 MAP kinase

References

1. Mann DL, Kent RL, Cooper IV G (1989) Load regulation of the properties of adult feline cardiomyocytes: growth induction by cellular deformation. *Circ Res* 64: 1079-1090.
2. Komuro I, Kaida T, Shibasaki Y *et al* (1990) Stretching cardiac myocytes stimulates protooncogene expression. *J Biol Chem* 265: 3595-3598.
3. Sadoshima J, Jahn L, Takahashi T *et al* (1992) Molecular characterization of the stretch-induced adaptation of cultured cardiac cells. An *in vitro* model of load-induced cardiac hypertrophy. *J Biol Chem* 267: 10551-10560.
4. Kira Y, Nakaoka T, Hashimoto E *et al* (1994) Effect of long-term cyclic mechanical load on protein synthesis and morphological changes in cultured myocardial cells from neonatal rat. *Cardiovasc Drugs Ther* 8: 251-262.
5. Vandenburg HH, Solerssi R, Shansky J *et al* (1995) Response of neonatal rat cardiomyocytes to repetitive mechanical stimulation *in vitro*. *Ann NY Acad Sci* 752: 19-29.
6. Ruwhof C, van der Laarse A (2000) Mechanical stress-induced cardiac hypertrophy: Mechanisms and signal transduction pathways. *Cardiovasc Res* 47: 23-37.
7. Ingber DE (2002) Mechanical signaling and the cellular response to extracellular matrix in angiogenesis and cardiovascular physiology. *Circ Res* 91: 877-887.
8. Ross RS (2002) The extracellular connections: the role of integrins in myocardial remodeling. *J Card Fail* 8 (suppl): S326-S331.
9. Schlaepfer DD, Hauck CR, Sieg DJ (1999) Signaling through focal adhesion kinase. *Progr Biophys Mol Biol* 71: 435-478.
10. Schaller MD (2001) Biochemical signals and biological responses elicited by the focal adhesion kinase. *Biochim Biophys Acta* 1540: 1-21.
11. Franchini KG, Torsoni AS, Soares PHA *et al* (2000) Early activation of the multicomponent signaling complex associated with focal adhesion kinase induced by pressure overload in the rat heart. *Circ Res* 87: 558-565.
12. Laser M, Willey CD, Jiang W *et al* (2000) Integrin activation and focal complex formation in cardiac hypertrophy. *J Biol Chem* 275: 35624-35630.
13. Kovacic-Milivojevic B, Roediger F, Almeida EA *et al* (2001) Focal adhesion kinase and p130Cas mediate both sarcomeric organization and activation of genes associated with cardiac myocyte hypertrophy. *Mol Biol Cell* 12: 2290-2307.
14. Domingos PP, Fonseca PM, Nadruz W Jr *et al* (2002) Load-induced focal adhesion kinase activation in the myocardium: role of stretch and contractile activity. *Am J Physiol Heart Circ Physiol* 282: H556-H564.
15. van der Wees CGC, Bax WH, van der Valk EJM *et al* (2006) Integrin stimulation induces calcium signalling in rat cardiomyocytes by a NO-dependent mechanism. *Pflügers Arch - Eur J Physiol* 451: 588-595.
16. Shubeita HE, McDonough PM, Harris AN *et al* (1990) Endothelin induction of inositol phospholipid hydrolysis, sarcomere assembly, and cardiac gene expression in ventricular myocytes. A paracrine mechanism for myocardial cell hypertrophy. *J Biol Chem* 265: 20555-20562.
17. Simpson PC, Kariya K, Karns LR *et al* (1991) Adrenergic hormones and control of cardiac myocyte growth. *Mol Cell Biochem* 104: 35-43.
18. Li L, Hessel M, van der Valk L, *et al* (2004) Partial and delayed release of troponin-I compared with the release of lactate dehydrogenase from necrotic cardiomyocytes. *Pflügers Arch – Eur J Physiol* 448: 146-152.
19. Sadoshima J, Izumo S (1993) Mechanical stretch rapidly activates multiple signal transduction pathways in cardiac myocytes: potential involvement of an autocrine/paracrine mechanism. *EMBO J* 12: 1681-1692.
20. Yamazaki T, Tobe K, Hoh E *et al* (1993) Mechanical loading activated mitogen-

- activated protein kinase and S6 peptide kinase in cultured rat cardiac myocytes. *J Biol Chem* 268: 12069-12076.
21. Hynes RO (1992) Integrins: versatility, modulation and signaling in cell adhesion. *Cell* 69: 11–25.
 22. Lewis JM, Schwartz AM (1995) Mapping *in vivo* associations of cytoplasmic proteins with integrin $\beta 1$ cytoplasmic domain mutants. *Mol Biol Cell* 6: 151–160.
 23. Chen CS, Mrksich M, Huang S *et al* (1997) Geometric control of cell life and death. *Science* 276: 1425–1428.
 24. Ross RS, Pham C, Shai S *et al* (1998) $\beta 1$ Integrins participate in the hypertrophic response of rat ventricular myocytes. *Circ Res* 82: 1160–1172.
 25. Kuppuswamy D, Kerr C, Narishige T *et al* (1997) Association of tyrosine-phosphorylated c-Src with the cyto-skeleton of hypertrophying myocardium. *J Biol Chem* 272: 4500–4508.
 26. Juliano RL, Haskill S. Signal transduction from the extracellular matrix (1993) *J Cell Biol* 120: 577–585.
 27. Clark EA, Brugge JS (1995) Integrins and signal transduction pathways: The road taken. *Science* 268: 233–239.
 28. Parsons JT, Parsons SJ (1997) Src family protein tyrosine kinases: cooperating with growth factor and adhesion signaling pathways. *Curr Opin Cell Biol* 9: 187–192.
 29. Shyy JY, Chien S (1997) Role of integrins in cellular responses to mechanical stress and adhesion. *Curr Opin Cell Biol* 9: 707–713.
 30. Miyamoto S, Teramoto H, Coso OA *et al* (1995) Integrin function: angiotensin II mediates stretch-induced hypertrophy of cardiac Molecular hierarchies of cytoskeletal and signaling molecules. *J Cell Biol* 131: 791–805.
 31. Pham CG, Harpf AE, Keller RS *et al* (2000) Striated muscle-specific $\beta 1 D$ -integrin and FAK are involved in cardiac myocyte hypertrophic response pathway. *Am J Physiol Heart Circ Physiol* 279: H2916-H2926.
 32. Taylor JM, Rovin JD, Parsons JT (2000) A role for focal adhesion kinase in phenylephrine-induced hypertrophy of rat ventricular cardiomyocytes. *J Biol Chem* 275: 19250-19257.
 33. Kuster GM, Pimentel DR, Adachi T *et al* (2005) $\alpha 1$ -adrenergic receptor-stimulated hypertrophy in adult rat ventricular myocytes is mediated via thioredoxin-1-sensitive oxidative modification of thiols on Ras. *Circulation* 111: 1192-1198.
 34. Roberts NA, Haworth RS, Avkiran M (2005) Effects of bisindolylmaleimide PKC inhibitors on p90^{RSK} activity *in vitro* and in adult ventricular myocytes. *Br J Pharmacol* 145: 477-489.
 35. Frödin M, Gammeltoft S (1999) Role and regulation of 90 kDa ribosomal S6 kinase (RSK) in signal transduction. *Mol Cell Endocrinol* 151: 65-77.
 36. Abe J-I, Okuda M, Huang Q *et al* (2000) Reactive oxygen species activate p90 ribosomal S6 kinase via Fyn and Ras. *J Biol Chem* 275: 1739-1748.
 37. Glennon PE, Kaddoura S, Sale EM *et al* (1996) Depletion of mitogen-activated protein kinase using an antisense oligodeoxynucleotide approach downregulates the phenylephrine-induced hypertrophic response in rat cardiac myocytes. *Circ Res* 78: 954-961.
 38. Yue T-L, Gu J-L, Wang C *et al* (2000) Extracellular signal-regulated kinase plays an essential role in hypertrophic agonists, endothelin-1 and phenylephrine-induced cardiomyocyte hypertrophy. *J Biol Chem* 275: 37895-37901.
 39. Ueyama T, Kawashima S, Sakoda T *et al* (2000) Requirement of activation of the extracellular signal-regulated kinase cascade in myocardial cell hypertrophy. *J Mol Cell Cardiol* 32: 947-960.
 40. Thorburn J, Carlson JM, Mansour SJ *et al* (1995) Inhibition of a signaling pathway in cardiac muscle cells by active mitogen-activated protein kinase kinase. *Mol Biol Cell* 6: 1479-1490.

41. Choukroun G, Hajjar R, Kyriakis JM *et al* (1998) Role of the stress-activated protein kinases in endothelin-induced cardiomyocyte hypertrophy. *J Clin Invest* 102: 1311-1320.
42. Post GR, Goldstein D, Thuerlauf DJ *et al* (1996) Dissociation of p44 and p42 mitogen-activated protein kinase activation from receptor-induced hypertrophy in neonatal rat ventricular myocytes. *J Biol Chem* 271: 8452-8457.
43. Gödecke A, Molojavyi A, Heger J *et al* (2003) Myoglobin protects the heart from inducible nitric-oxide synthase (iNOS)-mediated nitrosative stress. *J Biol Chem* 278:21761-21766.
44. Mungrue IN, Gros R, You X *et al* (2002) Cardiomyocyte overexpression of iNOS in mice results in peroxynitrite generation, heart block, and sudden death. *J Clin Invest* 109:735-743.
45. Wunderlich C, Schober K, Lange SA *et al* (2006) Disruption of caveolin-1 leads to enhanced nitrosative stress and severe systolic and diastolic heart failure. *Biochem Biophys Res Commun* 340: 702-708.
46. de Oliveira CF, Cintra KA, Teixeira SA *et al* (2000) Development of cardiomyocyte hypertrophy in rats under prolonged treatment with a low dose of a nitric oxide synthesis inhibitor. *Eur J Pharmacol* 391: 121-126.
47. Booz GW (2005) Putting the brakes on cardiac hypertrophy. Exploiting the NO-cGMP counter-regulatory system. *Hypertension* 45:341-346.
48. Barouch LA, Cappola TP, Harrison RW *et al* (2003) Combined loss of neuronal and endothelial nitric oxide synthase causes premature mortality and age-related hypertrophic cardiac remodeling in mice. *J Mol Cell Cardiol* 35:637-644.
49. Huang PL, Huang Z, Mashimo H *et al* (1995) Hypertension in mice lacking the gene for endothelial nitric oxide synthase. *Nature* 377:239-242.
50. Irikura K, Huang PL, Ma J *et al* (1995) Cerebrovascular alterations in mice lacking neuronal nitric oxide synthase gene expression. *Proc Natl Acad Sci USA* 92:6823-6827.
51. Snyder SH (1995) Nitric oxide. No endothelial NO. *Nature* 377:196-197.
52. Stoyanovski D, Murphy T, Anno PR *et al* (1997) Nitric oxide activates skeletal and cardiac ryanodine receptors. *Cell Calcium* 21: 19–29.
53. Sun J, Xin C, Eu JP *et al* (2001) Cysteine-3635 is responsible for skeletal muscle ryanodine receptor modulation by NO. *Proc Natl Acad Sci USA* 98: 11158–11162.
54. Vila Petroff MG, Kim SH, Pepe S *et al* (2001) Endogenous nitric oxide mechanisms mediate the stretch dependence of Ca²⁺ release in cardiomyocytes. *Nat Cell Biol* 3: 867–873.
55. Xu L, Eu JP, Meissner G *et al* (1998) Activation of the cardiac calcium release channel (ryanodine receptor) by poly-S-nitrosylation. *Science* 279: 234–237.

CHAPTER 3

Myocardial collagen metabolism in failing hearts before and during cardiac resynchronisation therapy

S. Umar
J. J. Bax
M. Klok
R. J. Van Bommel
M. H. Hessel
B. den Adel
G. B. Bleeker
M. M. Henneman
D. E. Atsma
E. E. van der Wall
M. J. Schalij
A. van der Laarse

European Journal of Heart Failure 2008;10:878-883

Abstract

Background: In patients with heart failure cardiac resynchronization therapy (CRT) leads to reverse ventricular remodelling.

Aim: To evaluate whether myocardial collagen metabolism in patients with heart failure is implicated in adverse ventricular remodelling and response to CRT.

Methods: Collagen synthesis and degradation were assessed from the concentrations of aminoterminal propeptides of type I and type III collagen (PINP and PIIINP) and carboxyterminal telopeptide of type I collagen (ICTP), respectively, in serum of 64 patients with heart failure before and after 6 months of CRT. The pro-form of matrix metalloproteinase-1 (proMMP1) and tissue inhibitor of metalloproteinase-1 (TIMP1) were also assayed at these time points. Forty-six patients (72%) showed a >10% reduction in LV end-systolic volume at follow-up and were classified as responders to CRT, the other 18 patients (28%) were classified as non-responders.

Results: Responders demonstrated a mean (\pm SEM) increase of serum PINP and PIIINP during follow-up, from 32.9 ± 2.2 to 46.7 ± 4.0 $\mu\text{g/L}$ ($p<0.001$) and from 4.59 ± 0.24 to 5.13 ± 0.36 $\mu\text{g/L}$ ($p<0.05$), respectively. In non-responders, serum PINP and PIIINP remained unchanged during follow-up. At baseline, responders had significantly lower serum PINP than non-responders (32.9 ± 2.2 vs. 41.8 ± 4.3 $\mu\text{g/L}$; $p<0.05$). ICTP levels of responders at baseline tended to be higher than in non-responders (3.54 ± 0.56 vs. 2.08 ± 0.37 $\mu\text{g/L}$, $p=\text{ns}$), and in both groups ICTP levels did not change upon CRT.

Conclusion: Reverse LV remodelling following CRT is associated with increased collagen synthesis rate in the first 6 months of follow-up.

Key words: Heart failure, cardiac resynchronisation therapy, PINP, PIIINP, ICTP

Introduction

In addition to myocardial hypertrophy, overloaded hearts frequently demonstrate a reactive fibrosis due to alterations in collagen synthesis and degradation. Accumulation of interstitial collagen type I and type III increases myocardial stiffness resulting in changes in diastolic properties of the left ventricle (LV) [1].

Collagen type I and type III are secreted by interstitial fibroblasts as procollagens followed by splitting off of propeptides by endopeptidases and the release of their aminoterminal propeptides, PINP and PIIINP, and carboxyterminal propeptides, PICP and PIIICP, into the circulation. During degradation of type I collagen fibrils the carboxyterminal telopeptide of type I collagen (ICTP) is formed, which is a 12 kD peptide [2].

Extracellular matrix components, like collagen type I and type III, are continuously synthesized and degraded. With respect to degradation, matrix metalloproteinase-1 (MMP1), a collagenase, and MMP2 and MMP9, two gelatinases, can be upregulated at the mRNA level [3], can be activated at the protein level, for instance by MT₁-MMP (or MMP14)[4], and can be stimulated by lowered concentrations of MMP inhibitors like tissue inhibitor of metalloproteinases (TIMPs) [5].

The myocardial extracellular matrix is implicated in a number of conditions and diseases, such as hypertensive heart disease, dilated cardiomyopathy, and cardiac remodelling. In failing hearts myocardial MMP1 and MMP2 concentrations have been shown to be elevated, while TIMP1 levels were depressed or unchanged [6]. Rapid myocardial collagen synthesis rate and slow collagen degradation rate impair diastolic function and promote LV adverse remodelling, probably due to cardiomyocyte slippage secondary to increased LV diastolic pressures [7].

In the present study, the biochemical markers of collagen synthesis rate (PINP and PIIINP) and collagen degradation rate (ICTP), including proMMP1 and TIMP1, were assayed in patients with heart failure before and after 6 months of cardiac resynchronisation therapy (CRT), to evaluate whether responders and non-responders to CRT differ with regard to serum markers of collagen metabolism at those two time points and whether serum markers of collagen metabolism can predict response to CRT.

Methods

Patients

Sixty-four patients with heart failure, scheduled for implantation of a CRT device, were included in the study. Baseline characteristics of these patients have been reported in an earlier study evaluating the levels of circulating biomarkers of extracellular matrix metabolism [8]. The group had a mean age 64 ± 1.2 years and consisted of 52 men (81%) and 12 women (19%). Ischaemic aetiology of heart failure was present in 45 patients (70%) and non-ischaemic aetiology in 19 patients (30%). Selection criteria for CRT were New York Heart Association (NYHA) functional class III-IV, LV ejection fraction $\leq 35\%$, and QRS duration > 120 ms. Patients with decompensated heart failure and patients with a recent myocardial infarction (< 3 months) were excluded. LV dyssynchrony was quantified at baseline. Clinical status was assessed before CRT implantation (baseline) and at 6 months follow-up. At both time points, 2-dimensional echocardiography was performed to determine LV volumes and LV ejection fraction.

Clinical evaluation

At baseline and at 6 months follow-up clinical status was evaluated by (i) assessment of NYHA functional class, (ii) determination of quality-of-life score using the Minnesota Living with Heart Failure questionnaire, and (iii) assessment of exercise capacity using the distance of a 6-minute hall walk test.

Echocardiography

Echocardiography was performed as described previously [8,9]. A commercially available system (Vingmed system Seven, General Electric-Vingmed, Milwaukee, Wisconsin, USA) was used to acquire conventional apical 2- and 4-chamber images, which allow calculation of LV end-systolic and end-diastolic volumes (LVESV and LVEDV) and LV ejection fraction, using the biplane Simpson's technique [10] and commercial software (Echopac version 5.0.1, General Electric – Vingmed). Echocardiographic data were analyzed by two independent observers who were blinded to all other patient data. Inter- and intra-observer variabilities for assessment of LV ejection fraction and LV volumes were 90% and 96%, respectively [11]. Based on recent data [12], patients with a reduction of $> 10\%$ in LVESV at 6 months follow-up were classified as responders to CRT, whereas patients with a reduction of $\leq 10\%$ in LVESV or an increased LVESV at 6 months follow-up, were classified as non-responders. For the assessment of LV dyssynchrony, two regions of interest were selected in the basal portions of the septum and the LV lateral wall allowing calculation of the septal-to-lateral delay in time-to-peak systolic myocardial velocity [9]. A septal-to-lateral delay of ≥ 65 ms was considered to represent significant LV dyssynchrony [13]. Additionally, wall motion score index (WMSI) was assessed in all subjects. The LV was divided into 16 segments. A semi quantitative scoring system (1, normal; 2, hypokinesia; 3, akinesia; 4, dyskinesia) was used to analyze each study. Global WMSI was

calculated by the standard formula: sum of the segment scores divided by the number of segments scored [14].

Pacemaker implantation

The LV pacing lead was inserted via the subclavian vein. After a coronary sinus venogram was obtained, the LV pacing lead was introduced into the coronary sinus and placed as far as possible in the venous system, preferably in a (postero-) lateral vein. The right atrial and right ventricular leads were positioned according to standard procedures. Implantation of leads and CRT device was accomplished in all patients without major complications.

Biochemical analysis

Blood samples were obtained before CRT and after 6 months follow-up. Serum and EDTA-plasma samples were stored at -80°C prior to assay.

Serum levels of carboxyterminal cross-linked telopeptide of type I collagen (ICTP) were assayed by a competitive ELISA (Orion Diagnostica, Espoo, Finland) which has a measurement range of 1.0-50 µg/L [15]. Inter-assay variations were 6% both at high (28 µg/L) and low (3 µg/L) ICTP concentrations. Detection limit of the assay was 0.3 µg/L. Intra-assay variability was 11% at low ICTP concentrations, and 7% at high ICTP concentrations. Reference ranges of human serum ICTP concentrations were 1.6-4.2 µg/L for women and 1.5-4.3 µg/L for men.

To measure of rates of synthesis of collagen type I and type III, we chose to use serum levels of aminoterminal propeptides of type I collagen (PINP) and of type III collagen (PIIINP). We acknowledge that there is ample experience with the use of the carboxyterminal propeptide of collagen I (PICP) (see for instance [16]); however, the commercial availability of assays for both PINP and PIIINP and the fact that there is a 1:1:1 stoichiometric relationship between the aminoterminal propeptide, the carboxyterminal propeptide and the collagen molecule formed for either collagen type, influenced our decision to use the assays to quantify PINP and PIIINP. Serum levels of PINP were assayed by radioimmunoassay (Orion Diagnostica) which has a measurement range of 5-250 µg/L [17]. Inter-assay variations were 6% both at high (167 µg/L) and 9.8% at low (12 µg/L) PINP concentrations. Detection limit of the assay was 2 µg/L. Intra-assay variability was 9.8% at low PINP concentrations (12 µg/L) and 10.2% at high (173 µg/L) PINP concentrations. Reference ranges of human serum PINP concentrations were 19-83 µg/L for women and 22-87 µg/L for men.

Serum levels of PIIINP were assayed by radioimmunoassay (Orion Diagnostica) which has a measurement range of 1.0-50 µg/L [18]. Inter-assay variations were 7.2 % at high (12.2 µg/L) and 6.5 % at low (2.7 µg/L) PIIINP concentrations. Detection limit of the assay was 0.3 µg/L. Intra-assay variability was 3.0 % at low PIIINP concentrations (2.8 µg/L) and 4.1% at high (11.9 µg/L) PIIINP concentrations. Reference ranges of adult human serum PIIINP concentrations were 2.3-6.4 µg/L.

The tissue inhibitor of metalloproteinases-1 (TIMP1) was assayed in EDTA-plasma by ELISA (GE Healthcare, Little Chalfont, Buckinghamshire, UK) which has a measurement range of 3-50 µg/L. Inter-assay variations were 15% at low (12.5 µg/L) and 13% at high (47.3 µg/L) TIMP1 concentrations. Intra-assay

variability was 11% at low (10.3 µg/L) and 9% at high (39.4 µg/L) TIMP1 concentrations. Reference range of adult human EDTA-plasma TIMP1 concentrations was 49 – 183 µg/L [19].

Serum levels of pro-matrix metalloproteinase-1 (proMMP-1) were assayed by ELISA (Quantikine, R&D Systems, Abingdon Science Park, Abingdon, UK) which has a measurement range of 0.15 – 10 µg/L. Inter-assay variations were 10.4% at low (0.74 µg/L) and 6.7% at high (4.66 µg/L) proMMP-1 concentrations. Intra-assay variability was 5.6% at low (0.70 µg/L) and 5.4% at high (4.43 µg/L) proMMP-1 concentrations. Detection limit of the assay was 0.02 µg/L. According to the manufacturer, average value of healthy adult human serum proMMP-1 concentration was 3.45 µg/L, with a range of 0.91 – 9.34 µg/L. Mean reference values (\pm SD) reported in literature are 8.5 ± 5.2 µg/L [20] and 2.43 ± 0.37 µg/L [21].

Statistical analysis

Data were expressed as mean \pm SEM unless stated otherwise. Differences between the two groups (responders and non-responders) were tested with two-tailed Student's t-test for paired or unpaired data when appropriate. Univariable and multivariable logistic regression analyses were performed to characterize predictors of good response to CRT. Continuous variables included baseline values of NYHA functional class, quality-of-life score, 6-minute hall walk distance, LVESV, LVEDV, LV ejection fraction, NT-proBNP, PINP, PIIINP, ICTP, TIMP1 and proMMP1. All variables with $p < 0.25$ entered the multivariable regression analysis that was performed by stepwise backward deletion. All variables with $p < 0.25$ remained in the final model. All statistical tests were performed with SPSS 12.1 software (SPSS Inc, Chicago, IL, USA). For all tests, a probability value < 0.05 was considered statistically significant.

Results

None of the patients died during the 6 months follow-up period. CRT was successful in reducing LVESV by $>10\%$ in the first 6 months in 46 (72%) patients (responders), whereas in 18 (28%) patients LVESV was reduced by $<10\%$ or was even increased (non-responders). The clinical and echocardiographic variables at baseline and after 6 months of CRT in responders and non-responders have been presented previously [8]. At baseline, responders (**1**) were older (65.5 ± 1.4 yrs vs. 59.5 ± 2.6 yrs, $p = 0.03$), (**2**) had more dyssynchrony (100 ± 8 ms vs. 71 ± 11 ms, $p = 0.05$), and (**3**) had longer QRS duration (165 ± 3 ms vs. 135 ± 8 ms, $p < 0.001$), compared to non-responders. There was no difference in baseline WMSI between responders and non-responders (2.30 ± 0.27 vs. 2.18 ± 0.20 , n.s.). In responders, NYHA class improved from 3.1 ± 0.1 to 2.0 ± 0.1 ($p < 0.001$), the 6-minute hall walk distance improved from 333 ± 18 m to 427 ± 17 m ($p < 0.001$), and quality-of-life score improved from 35 ± 3 to 17 ± 3 ($p < 0.001$).

Responders had a lower serum PINP level at baseline (32.9 ± 2.2 $\mu\text{g/L}$ vs. 41.9 ± 4.3 $\mu\text{g/L}$, $p=0.04$) than non-responders. During follow-up, responders demonstrated an increase in serum PINP level from 32.9 ± 2.2 $\mu\text{g/L}$ to 46.7 ± 4.0 $\mu\text{g/L}$ ($p<0.001$), whereas non-responders demonstrated no significant change (see Figure). At baseline, plasma levels of PIIINP in responders did not differ from those of nonresponders. In responders, plasma PIIINP levels increased during follow-up (from 4.59 ± 0.24 to 5.13 ± 0.36 $\mu\text{g/L}$, $p<0.05$), whereas in non-responders plasma PIIINP levels remained unchanged (see Figure).

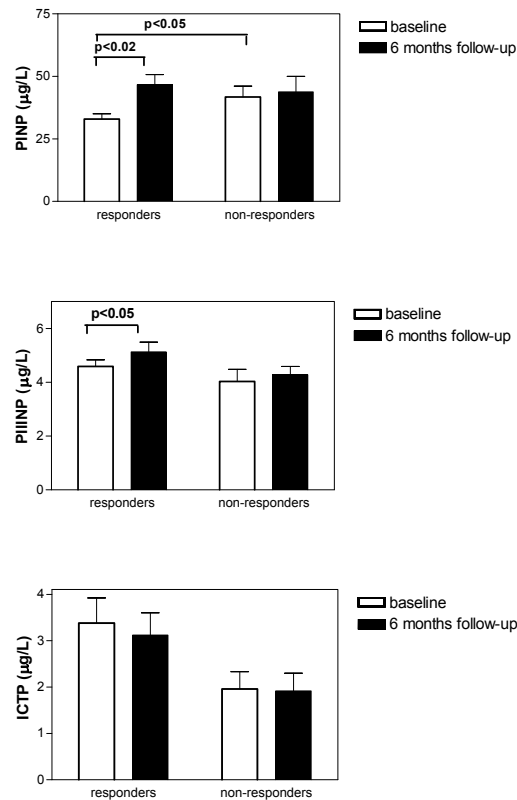


Figure 1. Levels of aminoterminal propeptide of type I procollagen (PINP), aminoterminal propeptide of type III procollagen (PIIINP), and carboxyterminal cross-linked telopeptide of type I collagen (ICTP) measured in serum of 64 patients with congestive heart failure at baseline (\square) and at 6 months follow-up (\blacksquare), divided in a group of patients who were successfully treated by CRT (responders) and a group of patients who responded poorly to CRT (non-responders).

Serum ICTP levels tended to be higher in responders at baseline and at 6 months follow-up than in non-responders at corresponding time points (see Figure). Plasma levels of proMMP1, TIMP1 and proMMP1/TIMP1 did not differ between responders and non-responders at baseline, nor during follow-up (see Table 1).

Table 1. TIMP1 and proMMP1 concentrations in plasma of 64 patients with heart failure determined before CRT (baseline) and at 6 months follow-up, divided according to response to CRT. (mean values \pm SEM).

	Responders n=46	Non-responders n=18	p-value
TIMP1 (baseline) ($\mu\text{g/L}$)	124 \pm 5.2	111 \pm 7.1	0.16
TIMP1 (6 months follow-up) ($\mu\text{g/L}$)	129 \pm 5.8	112 \pm 7.7	0.11
proMMP1 (baseline) ($\mu\text{g/L}$)	7.55 \pm 0.72	8.04 \pm 1.12	0.71
proMMP1 (6 mo follow-up) ($\mu\text{g/L}$)	7.89 \pm 0.85	8.08 \pm 1.11	0.90
proMMP1/TIMP1 (baseline)	0.063 \pm 0.006	0.080 \pm 0.015	0.20
proMMP1/TIMP1 (6 mo f-u)	0.064 \pm 0.007	0.083 \pm 0.017	0.21

Abbreviations: CRT, cardiac resynchronisation therapy; TIMP1, tissue inhibitor of metalloproteinases-1; proMMP1, pro-matrix metalloproteinase-1.

Univariable correlation of the following baseline parameters, NYHA functional class, quality-of-life score, 6-minute hall walk distance, LVESV, LVEDV, LV ejection fraction, NT-proBNP, PINP, ICTP, PIIINP, TIMP1 and proMMP1, with good response to CRT demonstrated that PINP scored best (Table 2). Multivariable correlation of all variables that had an univariable probability value <0.25 demonstrated that PINP, PIIINP and LVEDV at baseline were correlated with good response to CRT, but only PINP to a significant extent (Table 2).

Table 2. Univariable and multivariable correlation of baseline parameters with good response to CRT (reduction of LVESV by >10%).

	Univariable analysis			Multivariable analysis		
	OR	CI	p-value	OR	CI	p-value
NYHA functional class	0.74	0.28-1.96	0.55			
Quality-of-life score	0.99	0.96-1.01	0.45			
6-min hall walk distance	1.00	0.99-1.00	0.76			
LVESV	1.00	0.99-1.01	0.15			
LVEDV	1.00	0.99-1.01	0.20	1.00	0.99-1.01	0.14
LV ejection fraction	0.94	0.88-1.02	0.15			
NT-proBNP	1.00	1.00-1.00	0.22			
PINP	0.99	0.93-1.00	0.05	0.96	0.93-0.99	0.03
ICTP	1.24	0.93-1.66	0.13			
PIIINP	1.23	0.86-1.76	0.23	1.35	0.94-1.93	0.10
TIMP1	1.01	0.99-1.03	0.16			
proMMP1	0.97	0.87-1.09	0.71			

Abbreviations: OR, odds ratio; CI, 95% confidence limits; CRT, cardiac resynchronisation therapy; NYHA, New York Heart Association; LVESV, left ventricular end-systolic volume; LVEDV, left ventricular end-diastolic volume; NT-proBNP, N-terminal pro B-type natriuretic peptide; PINP, aminoterminal propeptide of type I procollagen; ICTP, carboxyterminal cross-linked telopeptide of type I collagen; PIIINP, aminoterminal propeptide of type III procollagen; TIMP1, tissue inhibitor of metalloproteinases-1; proMMP1, pro-matrix metalloproteinase-1.

Discussion

The present study demonstrated that patients with heart failure who were successfully treated with CRT had relatively low serum levels of PINP at baseline, a measure of collagen synthesis rate, and relatively high serum levels of ICTP at baseline, a measure of collagen degradation rate. After 6 months of CRT, serum PINP and PIIINP levels had increased significantly, whereas serum ICTP had hardly changed. Accordingly, a high serum level of PINP at baseline is associated with failure to respond to CRT, which is in line with reports showing that high levels of markers of collagen synthesis in serum of patients with heart failure are associated with poor outcome [16, 22-24].

In patients with hypertension and LV hypertrophy, elevated PINP levels in serum at baseline are associated with an increased myocardial collagen volume fraction (a measure of myocardial fibrosis) [25], low plasma levels of total and free MMP1, and high plasma levels of total and free TIMP1 [26]. Myocardial fibrosis is often associated with abnormal myocardial stiffness [27], diastolic abnormalities, and a decline in myocardial elastance during contraction, a measure of systolic dysfunction [28]. Perivascular accumulation of collagen may impair the vasodilator capacity of intramyocardial coronary arteries and contribute to the decrease in coronary reserve [29]. In patients with hypertrophic cardiomyopathy, high serum levels of PINP were associated with reduced diastolic function [30]. In patients with essential hypertension, serum levels of PINP and PIIINP were elevated compared to normotensives. In hypertensives, serum PIIINP levels were inversely correlated to diastolic (dys)function, whereas serum PINP levels were correlated positively to LV mass index [24]. In patients with dilated cardiomyopathy, the presence of a restrictive mitral pattern was associated with highest serum levels of PIIINP and high serum levels of PIIINP were related to poor outcome [31]. In patients with dilated cardiomyopathy, serum PIIINP levels were significantly elevated compared to corresponding levels in controls, these serum PIIINP levels were correlated to NYHA functional class, daily diuretics dosage, and mean right atrial pressure, and were inversely correlated to cardiac output [24].

In the present study, the responders to CRT tended to have higher serum ICTP levels than non-responders. Six months therapy with CRT had no significant effect on serum ICTP in responders, nor in non-responders. However, serum levels of proMMP1, a collagenase, did not differ between baseline and follow-up, nor did they differ between responders and non-responders at these two time points.

Previously it has been demonstrated that patients with dilated cardiomyopathy had higher serum levels of MMP1 than controls, which was associated with higher MMP1/TIMP1 ratio, and serum free MMP1 as well as MMP1/TIMP1 ratio which correlated positively with LV end-diastolic volume and negatively with cardiac index [21]. In failing hearts supported by a LV assist device myocardial MMP1 levels decreased, whereas TIMP1 and TIMP3 levels increased [32].

High serum levels of ICTP have also been observed in patients with dilated cardiomyopathy [21] and in patients with hypertrophic cardiomyopathy [30]. Klappacher et al. found that serum ICTP levels beyond a cut-off level of 7.6 µg/L

in patients with dilated cardiomyopathy were associated with increased risk of advanced clinical stage, increased risk of poor haemodynamic condition, increased risk of hyponatraemia (<138 mmol/L), and increased risk of heart transplantation [24].

The increase of serum PINP in responders to CRT (the patients demonstrating reverse LV remodelling) in the present study, is interpreted as an increased myocardial collagen synthesis in responders to CRT during 6 months follow-up. This increased myocardial collagen synthesis in responders may be a reaction of the myocardium induced by improved loading conditions (due to improved synchronicity of segmental wall motion); and thus LVESV and LVEDV were decreased by biochemical forces within the tissue that provide “passive tissue contraction”.

The responders were the group of patients with the lowest collagen synthesis at baseline, which according to the above explanation, associates with adverse LV remodelling by weakening the myocardial structure, thereby allowing progressive LV dilatation. In a study using myocardial biopsies from patients with end-stage heart failure taken before and after 100-600 days of left ventricular assist device (LVAD) implantation, Bruggink and co-workers observed an increase in ECM volume in the first 200 days after LVAD implantation, followed by a gradual decrease of ECM volume in the following 200 days to a level that was still higher than that observed pre-LVAD [33]. Plasma PINP levels increased considerably (≈ 3 -fold) in the first month after LVAD implantation, and remained increased in the first 6 months after LVAD implantation. Thus, reverse LV remodelling induced by LV unloading was associated with increased collagen synthesis and expanded ECM space. Although in our study the tertiles of plasma PINP levels at baseline showed a tendency to associate with response to CRT (lowest tertile: 17/21 responders, 81%; middle tertile: 16/22 responders, 73%; highest tertile 13/21 responders, 62%), our study population was probably too small to find a significant association.

One or more patients with systemic diseases that would induce abnormalities in collagen metabolism may have been included in the study; however, signs and symptoms of such diseases were absent. Furthermore, echocardiography-derived backscatter data indicative of myocardial fibrosis were not available in this study.

In conclusion, elevated collagen synthesis rate at baseline is unfavourable in terms of therapeutic success of CRT. Reverse LV remodelling upon CRT is associated with increased collagen synthesis rate in the first 6 months of follow-up.

Acknowledgements

This study was supported by the Netherlands Heart Foundation (Grant nr 2001B124 and 2002B109).

References

1. Weber KT, Brilla CG. Pathological hypertrophy and cardiac interstitium. Fibrosis and the renin-angiotensin-aldosterone system. *Circulation* 1991;83:1849-65.
2. Laurent GJ. Dynamic state of collagen: pathways of collagen degradation in vivo and their possible role in regulation of collagen mass. *Am J Physiol* 1987;252:C1-C9.
3. Fini ME, Cook JR, Mohan R, Brinckerhoff CE. Regulation of matrix metalloproteinase gene expression. In: Parks WC, Mecham RP (editors). *Matrix Metalloproteinases*. San Diego, Academic Press, 1998; pp. 299-362.
4. Sato H, Takino T, Kinoshita T, *et al*. Cell surface binding and activation of gelatinase A induced by expression of membrane-type-1- matrix metalloproteinase (MT1-MMP). *FEBS Lett* 1996;385:238-40.
5. Gomez DE, Alonso DF, Yoshiji H, Thorgeirsson UP. Tissue inhibitors of metalloproteinases: structure, regulation and biological functions. *Eur J Cell Biol* 1997;74:111-22.
6. Sakata Y, Yamamoto K, Mano T, *et al*. Activation of matrix metalloproteinases precedes left ventricular remodeling in hypertensive heart failure rats. *Circulation* 2004;109:2143-9.
7. Burlew BS, Weber KT. Cardiac fibrosis as a cause of diastolic dysfunction. *Herz* 2002;27:92-8.
8. Hessel MHM, Bleeker GB, Bax JJ, *et al*. Reverse ventricular remodelling after cardiac resynchronisation therapy is associated with a reduction in serum tenascin-C and plasma matrix metalloproteinase-9 levels. *Eur J Heart Fail* 2007;9:1058-63.
9. Bax JJ, Bleeker GB, Marwick TH, *et al*. Left ventricular dyssynchrony predicts response and prognosis after cardiac resynchronization therapy. *J Am Coll Cardiol* 2004;44:1834-40.
10. Schiller NB, Shah PM, Crawford M, *et al*. Recommendations for quantitation of the left ventricle by two-dimensional echocardiography. American Society of Echocardiography Committee on Standards, Subcommittee on Quantitation of Two-Dimensional Echocardiograms. *J Am Soc Echocardiogr* 1989;2:358-67.
11. Ypenburg C, Roes SD, Bleeker GB, *et al*. Effect of total scar burden on contrast-enhanced magnetic resonance imaging on response to cardiac resynchronisation therapy. *Am J Cardiol* 2007;99:657-60.
12. Yu CM, Bleeker GB, Fung JW, *et al*. Left ventricular reverse remodeling but not clinical improvement predicts long-term survival after cardiac resynchronization therapy. *Circulation* 2005;112:1580-6.
13. Bax JJ, Marwick TH, Molhoek SG, *et al*. Left ventricular dyssynchrony predicts benefit of cardiac resynchronization therapy in patients with end-stage heart failure before pacemaker implantation. *Am J Cardiol* 2003;92:1238-40.
14. Lang RM, Bierig M, Devereux RB, *et al*. Recommendations for chamber quantification. *Eur J Echocardiography* 2006;7:79-108.
15. Risteli J, Elomaa I, Niemi S, Novamo A, Risteli L. Radioimmunoassay for the pyridinoline cross-linked carboxy-terminal telopeptide of type I collagen: A new serum marker of bone collagen degradation. *Clin Chem* 1993;39:635-40.
16. Garcia-Bolao I, Macias A, Lopez B, *et al*. A biomarker of myocardial fibrosis predicts long-term response to cardiac resynchronization therapy. *J Am Coll Cardiol* 2006;47:23335-7.
17. Melkko J, Kauppila S, Niemi S, *et al*. Immunoassay for intact amino-terminal propeptide of human type I procollagen. *Clin Chem* 1996;42:947-54.
18. Risteli J, Niemi S, Trivedi P, Mäentausta O, Mowat AP, Risteli L. Rapid equilibrium radioimmunoassay for the amino-terminal propeptide of human type III procollagen. *Clin Chem* 1988;34:715-8.
19. Plumpton TA, Clark IM, Plumpton C, Calvin J, Cawston TE. Development of an enzyme-linked immunosorbent assay to measure total TIMP-1 (free TIMP-1 and TIMP-1 in

- combination with matrix-metalloproteinases) and measurement of TIMP-1 and CRP in serum. *Clin Chim Acta* 1995;240:137-54.
20. Zhang J, Fujimoto N, Iwata K, Sakai T, Okada Y, Hayakawa T. A one-step sandwich enzyme immunoassay for human matrix metalloproteinase 1 (interstitial collagenase) using monoclonal antibodies. *Clin Chim Acta* 1993;219:1-14.
21. Schwartzkopff B, Fassbach M, Pelzer B, Brehm M, Strauer BE. Elevated serum markers of collagen degradation in patients with mild to moderate dilated cardiomyopathy. *Eur J Heart Fail* 2002;4:439-44.
22. Zannad F, Alla F, Dousset B, Perez A, Pitt B, on behalf of the RALES Investigators. Limitation of excessive extracellular matrix turnover may contribute to survival benefit of spironolactone therapy to patients with congestive heart failure. *Circulation* 2000;102:2700-6.
23. Cicoira M, Rossi A, Bonapace S, *et al.* Independent and additional prognostic value of aminoterminal propeptide of type III procollagen circulating levels in patients with chronic heart failure. *J Card Failure* 2004;10:403-11.
24. Klappacher G, Franzen P, Haab D, *et al.* Measuring extracellular matrix turnover in the serum of patients with idiopathic or ischemic dilated cardiomyopathy and impact on diagnosis and prognosis. *Am J Cardiol* 1995;75:913-8.
25. Querejeta R, Varo N, Lopez B, *et al.* Serum carboxy-terminal propeptide of procollagen type I is a marker of myocardial fibrosis in hypertensive heart disease. *Circulation* 2000;101:1729-35.
26. Laviades C, Varo N, Fernandez J, *et al.* Abnormalities of the extracellular degradation of collagen type I in essential hypertension. *Circulation* 1998;98:535-40.
27. Zannad F, Dousset B, Alla F. Treatment of congestive heart failure. Interfering the aldosterone-cardiac extracellular matrix relationship. *Hypertension* 2001;38:1227-32.
28. Maceira AM, Barba J, Varo N, Beloqui O, Diez J. Ultrasonic backscatter and serum marker of cardiac fibrosis in hypertensives. *Hypertension* 2002;39:923-8.
29. Lopez B, Gonzalez A, Varo N, Laviades C, Querejeta R, Diez J. Biochemical assessment of myocardial fibrosis in hypertensive heart disease. *Hypertension* 2001;38:1222-6.
30. Lombardi R, Betocchi S, Losi MA, *et al.* Myocardial collagen turnover in hypertrophic cardiomyopathy. *Circulation* 2003;108:1455-60.
31. Rossi A, Cicoira M, Golia G, *et al.* Amino-terminal propeptide of type III procollagen is associated with restrictive mitral filling pattern in patients with dilated cardiomyopathy : a possible link between diastolic dysfunction and prognosis. *Heart* 2004;90:650-4.
32. Li YY, Feng Y, McTiernan CF, *et al.* Downregulation of matrix metalloproteinases and reduction in collagen damage in the failing human heart after support with left ventricular assist devices. *Circulation* 2001;104:1147-52.
33. Bruggink AH, van Oosterhout MFM, de Jonge N, *et al.* Reverse remodeling of the myocardial extracellular matrix after prolonged left ventricular assist device support follows a biphasic pattern. *J Heart Lung Transplant* 2006;25:1091-8.

Chapter 4

Activation of signaling molecules and matrix metalloproteinases in right ventricular myocardium of rats with pulmonary hypertension

S. Umar
M. H. M. Hessel
P. Steendijk
W. H. Bax
C. I. Schutte
M. J. Schalij
E. E. Van der Wall
D.E. Atsma
A. van der Laarse

Pathology – Research and Practice 2007;203:863-872

Abstract

Background: Pulmonary hypertension induces right ventricular (RV) overload that is transmitted to cardiomyocytes via integrins that activate intracellular messengers, including focal adhesion kinase (FAK) and neuronal nitric oxide synthase (NOS1). We investigated whether RV hypertrophy (RVH) and RV failure (RVF) were associated with activation of FAK, NOS1 and matrix metalloproteinases (MMPs).

Methods: Rats were treated without (RVC) or with monocrotaline in low dose (30 mg/kg) to induce RVH and in high dose (80 mg/kg) to induce RVF. After \approx 30 days, RV function was determined using combined pressure-conductance catheter. After sacrifice, FAK, NOS1, their phosphorylated forms (FAK-P and NOS1-P), MMP-2 and MMP-9 were quantified in RV myocardium by immunohistochemistry.

Results: In RVH and RVF, RV weight/ body weight increased by 36% and 109%, whereas RV ejection fraction decreased by 23% and 57% vs. RVC, respectively. FAK-P and FAK-P/FAK were highest in RVH (2.87 ± 0.12 and 2.52 ± 0.23 fold compared to RVC, respectively) and slightly elevated in RVF (1.76 ± 0.17 and 1.15 ± 0.13 fold compared to RVC, resp.). NOS1-P and NOS1-P/NOS1 were increased in RVH (1.63 ± 0.12 and 3.06 ± 0.80 fold compared to RVC, resp.) and RVF (2.16 ± 0.03 and 3.30 ± 0.38 fold compared to RVC, resp.). MMP-2 was highest in RVH and intermediate in RVF (3.50 ± 0.12 and 1.84 ± 0.22 fold compared to RVC, resp.). MMP-9 was elevated in RVH and RVF (2.39 ± 0.35 and 2.92 ± 0.68 fold compared to RVC, resp.).

Conclusions: Activation of FAK in RVH points to an integrin-dependent hypertrophic response of the myocardium. Activation of NOS1 in failing RV suggests a role of excessive NO in development of failure and activation of MMPs leading to ventricular remodeling.

Key words:

Hypertrophy; heart failure; focal adhesion kinase; neuronal nitric oxide synthase; matrix metalloproteinase

Abbreviations: FAK, focal adhesion kinase; nNOS, neuronal nitric oxide synthase; NOS1, neuronal nitric oxide synthase; NO, nitric oxide; MMP, matrix metalloproteinase; ECM, extracellular matrix; SR, sarcoplasmic reticulum; RyR, ryanodine receptor; MCT, monocrotaline; ROS, reactive oxygen species; CHF, congestive heart failure; RV, right ventricle; LV, left ventricle; IVS, interventricular septum; RVC, right ventricular control; RVH, right ventricular hypertrophy; RVF, right ventricular failure; PBS, phosphate-buffered saline; LVH, left ventricular hypertrophy; LVEF, left ventricular ejection fraction; LVESV, left ventricular end systolic volume; SNP, Sodium nitroprusside.

Introduction

Pulmonary hypertension is a condition that causes overloading of the right ventricle (RV). The forces of overload are transferred to the cardiomyocytes via integrins, a family of transmembrane adhesion receptors. Integrin signaling occurs via a large array of intracellular messenger systems, including focal adhesion kinase (FAK) [25, 26]. FAK is a cytoplasmic tyrosine kinase that discretely localizes to membrane regions that attach to the extracellular matrix (ECM), called focal adhesions. FAK transmits signals from the ECM via integrins to the cytoskeleton and particular cytoplasmic proteins. Stimulation of integrins and FAK leads to a hypertrophic response in cardiomyocytes [17].

Earlier we have shown that integrin stimulation was associated with immediate FAK phosphorylation and delayed phosphorylation of neuronal nitric oxide synthase (nNOS, NOS1) [32, 33]. NOS1 is located on the sarcoplasmic reticulum (SR) of cardiomyocytes, and is considered to modify SR function via nitrosylation of the ryanodine receptor (RyR) which is the calcium release site of the SR [3, 19, 29, 34, 38]. NO and reactive oxygen species (ROS) produce peroxynitrite, known to activate matrix metalloproteinases (MMPs) [20, 35] that are involved in ventricular remodeling [27]. The exact role of the NO formed in the failing myocardium is not yet fully elucidated. We hypothesize that signaling pathways involved in myocardial hypertrophy and failure are NO-dependent, including NO-dependent MMP activation leading to ventricular remodeling.

A frequently used model to study functional, structural and molecular changes associated with compensated RV hypertrophy (RVH) and RV failure (RVF) is the rat treated with monocrotaline (MCT), a pyrrolizidine alkaloid [13, 16]. MCT selectively injures the vascular endothelium of the lung and induces pulmonary vasculitis [37]. Muscularization and hypertrophy of media of pulmonary arteries lead to increased vascular resistance and increased pulmonary arterial pressure [8, 22]. MCT-induced pulmonary hypertension is associated with the development of compensated RVH progressing to RVF within weeks, depending on the dose of MCT and the age of the rats [7, 15, 36]. Previous studies have shown selective induction of either RVH or RVF after 4 weeks of treatment with a low dose (30 mg/kg body weight) or a high dose (80 mg/kg body weight) of MCT, respectively [7, 14].

In the rat model of MCT-induced pulmonary hypertension, we determined activation of FAK, NOS1, immunoreactive MMP-2 and MMP-9 in RV myocardium to compare differences with respect to their activation patterns between controls, RVH and RVF. To test whether NO stimulates expression of MMP-2 and MMP-9, neonatal rat ventricular cardiomyocyte cultures were treated without and with the NO-donor sodium-nitroprusside for 24 h, followed by quantitative determination of immunoreactive MMP-2 and MMP-9.

Materials and Methods

Animal model

All animals were treated in accordance with the national guidelines and with the approval of the Animals Experiments Committee of the Leiden University Medical Center. A total of 14 male Wistar rats (Harlan, Zeist, the Netherlands) weighing 200-250 g were randomly assigned to three groups. Animals received a single subcutaneous injection of MCT (Sigma-Aldrich, Zwijndrecht, the Netherlands) diluted in phosphate-buffered saline (PBS) in a low dose (30 mg/kg body weight, n=5; RVH group) or in a high dose (80 mg/kg body weight, n=5, RVF group). Control rats (RVC, n=4) were injected with an equal volume of PBS.

Hemodynamics

After 4 weeks of MCT administration RV pressure and volume signals were recorded by combined pressure-conductance catheter. To that purpose rats were sedated by inhalation of a mixture of isoflurane (4%) and oxygen. General anesthesia was administered by intraperitoneal (i.p.) injection of a fentanyl-fluanison-midazolam mixture in a dose of 0.25 mL/100 g body weight. The mixture consisted of 2 parts Hypnorm[®] (0.315 mg/mL fentanyl + 10 mg/mL fluanison, VitalPharma, Maarheeze, the Netherlands), 1 part Dormicum[®] (5 mg/mL midazolam, Roche, Mijdrecht, the Netherlands) and 1 part saline. After tracheotomy the animals were ventilated mechanically using a pressure-controlled respirator and a mixture of air and oxygen.

After midsternal thoracotomy a combined pressure-conductance catheter (SPR-878, Millar Instruments, Houston, TX, USA) was introduced via the apex into the RV and positioned along the long axis of the RV. The catheter was connected to a Sigma-SA signal processor (CD Leycom, Zoetermeer, the Netherlands) and RV pressures and volumes were recorded digitally. All data were acquired using Conduct-NT software (CD Leycom) at a sample rate of 2000 Hz and analysed off-line by custom-made software. The volume signal was calibrated using an ultrasonic flow probe (Transonic Systems, Maastricht, the Netherlands) around the ascending aorta, essentially as described by Hessel et al. [14].

Heart rate, RV stroke volume, cardiac output, RV end-diastolic volume, RV end-systolic volume, RV ejection fraction, RV end-diastolic pressure, RV peak systolic pressure and RV end-systolic pressure were determined from pressure-volume loops.

Tissue preparation

Immediately after hemodynamic measurements, hearts were rapidly dissected and weighed. The RV, left ventricle (LV) and interventricular septum (IVS) were cut free, weighed, fixed in 4% formaline for more than 24 h, and embedded in paraffin. Subsequently, 4 µm thick sections of the RV tissue were cut and deparaffinized in Ultraclear[®] (Klinipath, Duiven, the Netherlands) for 5 min. Sections were rehydrated in decreasing graded alcohols (100-25%) followed by two 5-min washes in distilled water and TBS (10 mmol/L Tris-HCl, 150 mmol/L NaCl, pH 8.0).

Immunohistochemistry

Sections cut from RV myocardium of RVC, RVH and RVF groups were stained for FAK, FAK-P, NOS1, NOS1-P, MMP-2 and MMP-9. Rabbit anti-FAK and anti-FAK-P antibodies were from Santa Cruz Biotechnology (Santa Cruz, CA, USA). Rabbit anti-NOS1 and anti-NOS1-P antibodies were from Upstate (Charlottesville, VA, USA). Mouse anti-MMP-2 antibody and mouse anti-MMP-9 antibody were from Chemicon International (Temecula, CA, USA).

Secondary antibodies used were donkey anti-rabbit IgG conjugated to Texas Red (Santa Cruz), goat anti-rabbit IgG conjugated to FITC (Sigma-Aldrich), goat anti-mouse IgG conjugated to FITC (Sigma-Aldrich), and donkey anti-mouse IgG conjugated to Cy3 (Jackson Immuno Research Labs, West Grove, PA, USA).

Sections were incubated in a solution of 0.1% sodium citrate and 0.5% Triton X-100 at room temperature for 3 min. After washing with distilled water and TBS solution, sections were incubated for 20 min in 10% serum derived from the same animal species in which the secondary antibody was raised, in TBSB (TBS containing 0.05 mg/mL bovine serum albumin). After removal of blocking serum, the sections were incubated overnight at 4°C with the primary antibody diluted in TBSB. After removal of the primary antibody and washing three times with TBS, sections were incubated with secondary antibody diluted in TBSB for 1 h at room temperature in the dark. Subsequently, sections were washed three times with TBS, and counterstained with 0.01 mg/mL Hoechst 33342 (Molecular Probes, Eugene, OR, USA) for 10 min at room temperature in the dark. Sections were washed three times with TBS and mounted on microscope glass using Vectashield (Vector Laboratories, Burlingame, CA, USA). Sections were photographed in a fluorescence microscope (Nikon Eclipse, Nikon Europe, Badhoevedorp, the Netherlands) equipped with a 100x oil-immersion objective and a digital camera (Nikon DXM 1800). Images were analyzed using Image-Pro Plus software (Media Cybernetics, Silver Spring, MD, USA) that allows quantification of blue, green and red separately. Per section 5 images were acquired and analyzed to compensate for variations within a section.

Preparation of neonatal rat ventricular cardiomyocytes and immunocytochemistry of cellular MMP2 and MMP9

Neonatal (2-day-old) rat ventricular cardiomyocytes were prepared as described before [24]. Cells were plated in 6-well plates containing per well a collagen-coated glass cover-slip and were grown in growth medium consisting of DMEM and Ham's F10 (1:1, v/v), 2.5% horse serum, 100 U/mL penicillin and 100 µg/mL streptomycin (all from Invitrogen, Breda, the Netherlands). Three days after isolation, the cardiomyocytes were used for experiments. At termination of the experiment, the cover-slips were prepared for immunofluorescence microscopy according to a protocol described before [33]. Briefly the cover-slip was washed, incubated with PBS containing 1% formalin for 30 min, washed, incubated with PBS containing 0.1% Triton X-100 for 10 min, washed, and incubated overnight with first antibody (200x diluted in PBS + 1% FBS) at 4°C. Primary antibodies raised against MMP2 and MMP9 were the same as used with the myocardial tissue sections. After washing, the cells were incubated with secondary rabbit anti-mouse Alexa568-conjugated antibody (Molecular Probes; 400x diluted in

PBS + 1% FBS) for 1 h. After washing, the cultures were incubated with 10 µg/mL Hoechst 33342 for 10 min. After washing, cells were mounted on microscope slides using Vectashield. Microscope and camera were the same as used with the myocardial tissue sections.

Statistics

Data are expressed as mean \pm SD. The effect of treatment (RVC, RVH and RVF) was evaluated by one-way analysis of variance (ANOVA) followed by Bonferroni's *post hoc* test. Correlations were determined using a parametric test (Pearson). Differences were considered significant at $p < 0.05$. SPSS12 for Windows (SPSS Inc, Chicago, IL, USA) was used for statistical analysis.

Results

Body and heart weights

Table 1 summarizes characteristics of the animals at the day they were sacrificed. Immediately after hemodynamic measurements, hearts were rapidly dissected and weighed. Body weight of RVF rats was significantly lower than that of RVC and RVH rats ($p < 0.05$ vs. RVC and RVH). RV weight of RVF animals was significantly higher than that of RVC and RVH rats ($p < 0.05$ vs. RVC and RVH). The degree of RV hypertrophy was determined as the ratio of RV weight over the body weight. This hypertrophy parameter was increased (by +36%) in RVH ($p < 0.05$ vs. RVC) and was significantly higher in RVF (+109% compared to RVC, +53% compared to RVH, both $p < 0.05$). Furthermore, weight of RV as a fraction of total ventricular weight was significantly increased in RVH (+27% compared to RVC) and in RVF (+54% compared to RVC, +21% compared to RVH, both $p < 0.05$) confirming RV hypertrophy in both MCT-treated groups. Conversely, there was no significant increase in the ratios of (LV+IVS) weight over body weight and (LV+IVS) weight over total ventricular weight in RVH and RVF compared with RVC (Table 1).

Table 1. General and cardiac characteristics of RVC, RVH and RVF animals

	RVC (n=4)	RVH (n=5)	RVF (n=5)
Body weight (g)	370 ± 24.71	365.2 ± 26.52	319.8 ± 24.04 ^{*#}
RV weight (g)	0.24 ± 0.03	0.33 ± 0.03 [*]	0.44 ± 0.08 ^{*#}
(LV+IVS) weight (g)	0.85±0.1	0.84±0.08	0.85±0.06
VW (RV+LV+IVS) (g)	1.09 ± 0.12	1.17 ± 0.11	1.29 ± 0.12 [*]
RV/BW (mg.g ⁻¹)	0.66±0.08	0.90±0.05 [*]	1.38±0.3 [*]
RV/VW	0.22±0.02	0.28±0.01 [*]	0.34±0.03 ^{*#}
VW/BW (mg.g ⁻¹)	2.94 ± 0.13	3.2 ± 0.16 [*]	4.05 ± 0.47 ^{*#}
(LV+IVS)/BW (mg.g ⁻¹)	2.28± 0.12	2.3± 0.13	2.67± 0.19
(LV+IVS)/VW	0.77±0.02	0.72±0.01	0.66±0.04

* $p < 0.05$ vs. RVC

$p < 0.05$ vs. RVH

abbreviations: RVC, RV control; RVH, RV hypertrophy; RVF, RV failure; RV, right ventricle; VW, Ventricular weight; BW, body weight; LV, left ventricle; IVS, interventricular septum

Right ventricular function

Results of combined pressure-conductance catheter measurements are summarized in Table 2.

RV ejection fraction (RVEF) was 53.2 ± 5.7 % in RVC, 40.9 ± 9.6 % in RVH and 22.7 ± 6.9 % in RVF ($p < 0.05$ vs. RVC) while RV end-diastolic pressure was 1.4 ± 0.4 mmHg in RVC, 3.6 ± 0.4 mmHg in RVH and 8.0 ± 1.5 mmHg in RVF ($p < 0.05$ vs. RVC and RVH) confirming RV failure in the RVF group. Furthermore, in RVH rats, cardiac output (CO) and stroke volume (SV) were maintained, indicating a compensatory state at the expense of increased RV end-diastolic and end-systolic volumes and increased RV filling pressure (all $p < 0.05$ vs. RVC).

Table 2. Cardiac and right ventricular function of RVC, RVH and RVF animals

	RVC (n=4)	RVH (n=5)	RVF (n=5)
Heart rate (min^{-1})	407 ± 24	397 ± 22	259 ± 77
Stroke volume (μL)	145 ± 11.4	162 ± 13.1	177 ± 26.5
Cardiac output ($\text{mL} \cdot \text{min}^{-1}$)	58.3 ± 1.2	64.0 ± 5.3	41.8 ± 7.3
RV end-systolic volume (μL)	134 ± 29.2	265 ± 52.1	$690 \pm 186^*$
RV end-diastolic volume (μL)	276 ± 40.7	409 ± 47.2	$833 \pm 197^*$
RV ejection fraction (%)	53.2 ± 5.7	40.9 ± 9.6	$22.7 \pm 6.9^*$
RV end-systolic pressure (mmHg)	25.9 ± 4.1	28.6 ± 3.7	46.7 ± 10.9
RV end-diastolic pressure (mmHg)	1.4 ± 0.4	3.6 ± 0.4	$8.0 \pm 1.5^{*\#}$

* $p < 0.05$ vs. RVC

$p < 0.05$ vs. RVH

abbreviations: RVC, RV control; RVH, RV hypertrophy; RVF, RV failure; RV, right ventricle

FAK phosphorylation

FAK is involved in the hypertrophic response of cardiomyocytes and undergoes autophosphorylation on integrin stimulation. To assess the activation of FAK in our RV hypertrophy and failure model, we quantified its phosphorylation and FAK-P/FAK ratio by immunohistochemical techniques (Fig. 1). Myocardial FAK-P concentration was highest in RVH (2.87 ± 0.12 fold higher than the corresponding value in RVC, $p < 0.05$ vs. RVC) and less elevated in RVF (1.76 ± 0.17 fold higher than the corresponding value in RVC, $p < 0.05$ vs. RVC) (Fig. 1b). The ratio of FAK-P/FAK was also found to be the highest in RVH (2.52 ± 0.23 fold higher than the corresponding value in RVC, $p < 0.05$ vs. RVC) and hardly elevated in RVF group (1.15 ± 0.13 fold higher than the corresponding value in RVC) (Fig. 1c). Hence there was an increase in phosphorylation of FAK as well as FAK-P/FAK ratio in RV hypertrophy group.

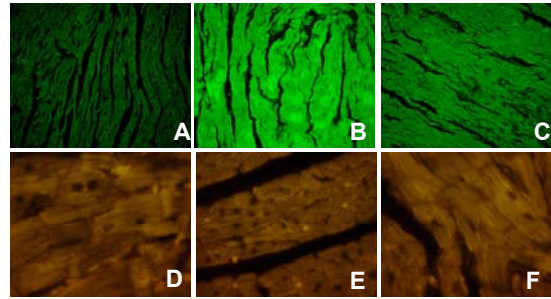


Figure 1a. Immunofluorescence images of phosphorylated FAK in RVC (A), RVH (B) and RVF (C) using an FITC labeled secondary antibody. All images were taken at 20x magnification. . Immunofluorescence images of total FAK in RVC (D), RVH (E) and RVF (F) are also shown. Images were taken at 100x magnification.

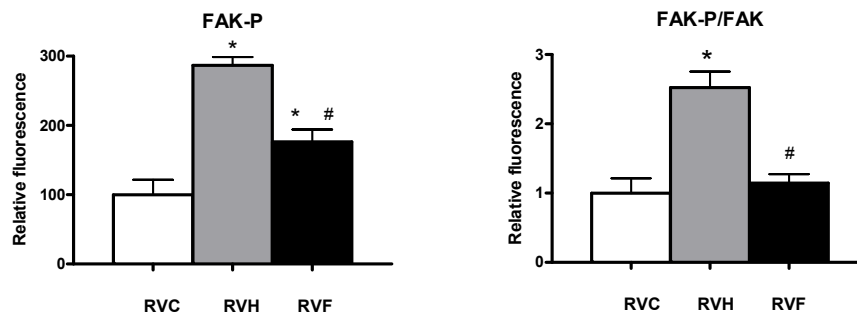


Figure 1b. Relative fluorescence of FAK-P in RVC, RVH and RVF. (* $p < 0.05$ vs. RVC; # $p < 0.05$ vs. RVH)

Figure 1c. Ratios of the relative fluorescence of phosphorylated FAK/ total FAK (FAK-P/FAK) in RVC, RVH and RVF. (* $p < 0.05$ vs. RVC; # $p < 0.05$ vs. RVH)

NOS1 phosphorylation

NOS1 is another signaling protein thought to be involved in integrin stimulation. We assessed NOS1 phosphorylation by quantification of immunofluorescence (Fig. 2a). Myocardial NOS1-P concentration was found to be increased in RVH (1.63 ± 0.21 fold higher than the the corresponding value in RVC, $p < 0.05$ vs. RVC) and RVF (2.16 ± 0.03 fold higher than the corresponding value in RVC, $p < 0.05$ vs. RVC and RVH) (Fig. 2b). The ratio of NOS1-P/NOS1 was markedly elevated in RVH (3.06 ± 0.80 fold higher than the corresponding value in RVC, $p < 0.05$ vs. RVC) and RVF (3.30 ± 0.38 fold higher than the corresponding value in RVC, $p < 0.05$ vs. RVC) (Fig. 2c), showing elevated NOS1 phosphorylation state with RV hypertrophy and failure.

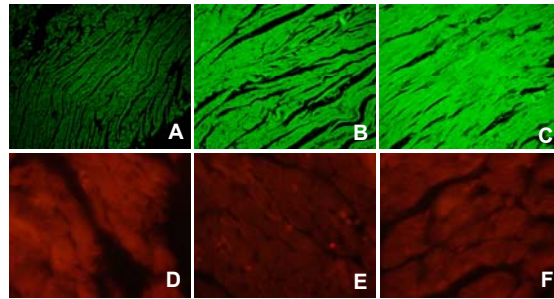


Figure 2a. Immunofluorescence images of phosphorylated NOS1 in RVC (A), RVH (B) and RVF (C) using an FITC labeled secondary antibody. All images were taken at 20x magnification. Immunofluorescence images of total NOS1 in RVC (D), RVH (E) and RVF (F) are also shown. Images were taken at 100x magnification.

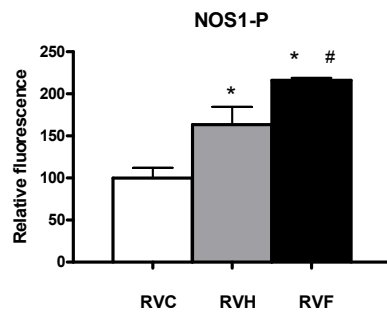


Figure 2b. Relative fluorescence of NOS1-P in RVC, RVH and RVF. (* $p < 0.05$ vs. RVC; # $p < 0.05$ vs. RVH)

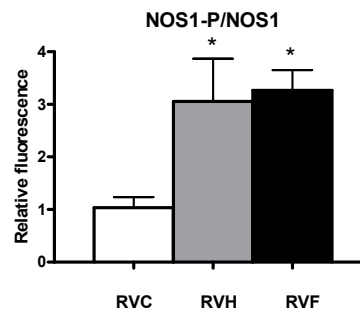


Figure 2c. Ratios of the relative fluorescence of phosphorylated NOS1/ total NOS1 (NOS1-P/NOS1) in RVC, RVH and RVF. (* $p < 0.05$ vs. RVC)

Activation of MMP-2 and MMP-9 by exogenous NO

Neonatal rat ventricular cardiomyocytes were incubated with 10 $\mu\text{g}/\text{mL}$ sodium-nitroprusside (SNP) for 24 h and subsequently analysed for cellular MMP2 and MMP9 immunoreactivity by immunofluorescence microscopy. This dose of NO-donor caused an increase of MMP2 by 222% ($p < 0.001$) and an increase of MMP9 by 72% ($p < 0.001$) in 24 h (Figure 3), indicating that NO stimulates MMP2 and MMP9 expression.

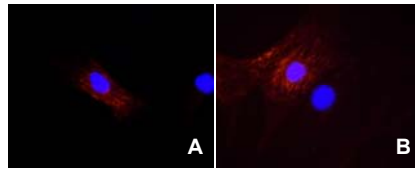


Figure 3a. Immunofluorescence images of MMP2 in rat ventricular cardiomyocytes incubated without (SNP 0, A) and with 10 µg/mL sodium-nitroprusside (SNP 10, B) for 24 h. Quantitative analysis of signal intensities is presented. (# $p < 0.001$ vs. SNP0)

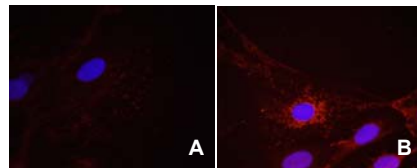
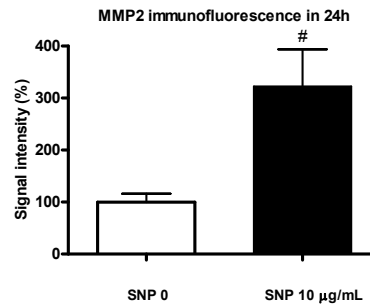
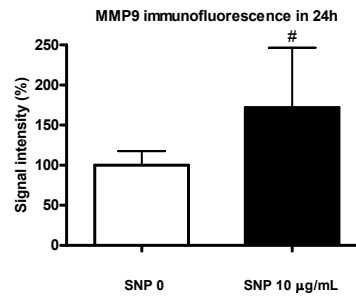


Figure 3b. Immunofluorescence images of MMP9 in rat ventricular cardiomyocytes incubated without (SNP 0, A) and with 10 µg/mL sodium-nitroprusside (SNP 10, B) for 24 h. Quantitative analysis of signal intensities is presented. (# $p < 0.001$ vs. SNP0)



Activation of MMP-2 and MMP-9 in hypertrophied and failing RV

MMP-2 and MMP-9 are the most commonly implied MMPs in ventricular failure and remodeling. We assessed the activation of RV myocardial immunoreactive MMP-2 and MMP-9 in our rat model of heart failure by immunohistochemical methods. We found that myocardial MMP-2 concentration (Fig. 4b) was the highest in RVH (3.50 ± 0.12 fold higher than the corresponding value in RVC, $p < 0.05$ vs. RVC) and intermediate in RVF (1.84 ± 0.22 fold higher than the corresponding value in RVC, $p < 0.05$ vs. RVC).

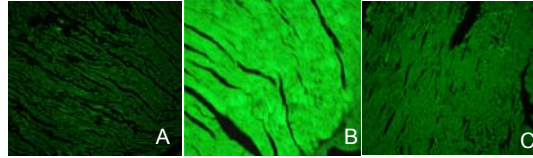


Figure 4a. Immunofluorescence images of immunoreactive MMP-2 in RVC (A), RVH (B) and RVF (C) using an FITC labeled secondary antibody. All images were taken at 20x magnification.

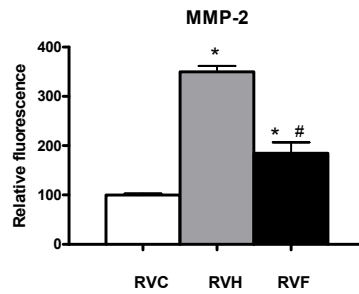


Figure 4b. Relative fluorescence of MMP-2 in RVC, RVH and RVF. (* $p < 0.05$ vs. RVC; # $p < 0.05$ vs. RVH)

Myocardial MMP-9 concentration was significantly increased both in RVH and RVF (2.39 ± 0.35 and 2.92 ± 0.68 fold higher than the corresponding values in RVC, respectively, both $p < 0.05$ vs. RVC) (Fig 5b). Hence we found an activation of both MMP-2 and MMP-9 in the remodeling RV myocardium.

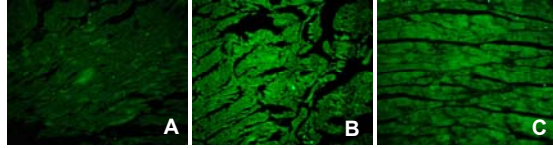


Figure 5a. Immunofluorescence images of immunoreactive MMP-9 in RVC (A), RVH (B) and RVF (C) using an FITC labeled secondary antibody. All images were taken at 20x magnification.

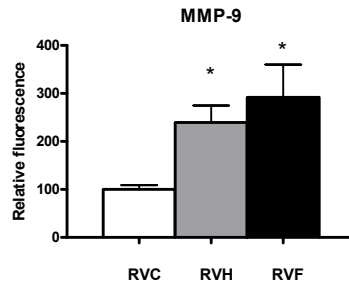


Figure 5b. Relative fluorescence of MMP-9 in RVC, RVH and RVF. (* $p < 0.05$ vs. RVC)

Discussion

In the present study we showed that in a rat model of pulmonary hypertension, there is an activation of signaling proteins FAK and NOS1 with concurrent activation of matrix metalloproteinases MMP-2 and MMP-9 in the RV myocardium. In rat cardiomyocyte cultures, exogenous NO was found to activate cellular MMP-2 and MMP-9. In the rat model of pulmonary hypertension, we found a dose-dependent effect of the toxin, monocrotaline, on the pulmonary vasculature, leading to compensated RV hypertrophy in RVH group and RV failure in RVF group.

For the RV, pulmonary hypertension means increased afterload. The forces associated with increased afterload are transferred to the cardiomyocytes of the RV myocardium via integrins, a family of transmembrane adhesion receptors. Integrins couple the proteins of the extracellular matrix to the cellular cytoskeleton and other specific proteins, like FAK. Stimulation of integrins elicits cellular signaling pathways via a large array of cellular messenger systems, including autophosphorylation of FAK. Stimulation of integrins and FAK leads to a hypertrophic response in cardiomyocytes [17]. Integrin-mediated signaling activates protein tyrosine kinases such as FAK and Src, and results in the activation of the ERK2 and JNK1 pathways which in turn activate transcription factors relevant to MMP transcriptional regulation [23, 18].

Bayer *et al.* [4] have shown that FAK levels increased during established phase of compensatory left ventricular hypertrophy (LVH) and the transition from compensated LVH to heart failure in a rat model of LVF induced by abdominal aortic coarctation. Furthermore, phosphorylated FAK levels also increased during established phase of compensatory LVH and transition from compensated LVH to heart failure. FAK undergoes tyrosine phosphorylation in response to growth factor stimulation in both cardiomyocytes and smooth muscle cells, and FAK phosphorylation is necessary for activation of downstream signaling cascades leading to cytoskeletal reorganization and cellular growth. Increased FAK expression occurred in both cardiomyocytes and cardiac fibroblast [4].

Earlier we have shown selective induction of either RVH or RVF after 4 weeks of treatment with a low dose (30 mg/kg body weight) or a high dose (80 mg/kg body weight) of MCT, respectively [14]. Here we show that phosphorylation of FAK is significantly increased in MCT-induced RV hypertrophy (RVH) and failure groups (RVF) compared with the control RVC ($p < 0.05$ vs. RVC), while the ratio of phosphorylated FAK to total FAK is significantly increased in RVH only ($p < 0.05$ vs. RVC).

NO synthase (NOS) is expressed constitutively as two isoforms: endothelial (eNOS) and neuronal (nNOS, NOS1) [30]. Earlier we showed that neuronal nitric oxide synthase (NOS1) is activated by integrin stimulation [32, 33]. NOS1 is located on the SR of cardiomyocytes, and is considered to modify SR function via nitrosylation of the ryanodine receptor which is the calcium release site of the SR [3, 19, 29, 34, 38].

The protein level and the activity of NOS1 have been shown to be enhanced in the LV myocardium of chronically infarcted animals and in failing human hearts [5, 9, 11], suggesting that NOS1 may play a part in the myocardial response to

stress. Furthermore, under these conditions, NOS1 seems to be preferentially localized to the sarcolemmal membrane (rather than to the SR), where it colocalizes with caveolin-3. Bendall *et al.* [5] have shed some light on the functional significance of these findings by showing that under basal conditions NOS1 inhibition increased basal LV inotropy and prolonged the time constant of isovolumic relaxation in sham operated rat hearts, whereas in failing hearts these effects were significantly reduced. In contrast, inhibition of NOS1 enhanced the inotropic and lusitropic response to β -adrenergic stimulation in failing hearts but had no significant effect in sham-operated rats.

In the present study we show that phosphorylated NOS1 as well as the ratio of phosphorylated NOS1 to total NOS1 are significantly increased in MCT-induced RV hypertrophy (RVH) and failure groups (RVF) compared with the control RVC ($p < 0.05$ vs. RVC).

Nitric oxide (NO) and reactive oxygen species produce peroxynitrite, known to activate matrix metalloproteinases (MMPs) [20, 35] that are involved in ventricular remodeling [27]. The stimulating effect of NO on expression of MMP2 and MMP9 has been confirmed in neonatal rat ventricular cardiomyocytes, suggesting that NOS1 activation may be responsible for increased immunoreactivity of MMP-2 and MMP-9. MMPs comprise a family of endopeptidases encompassing more than 25 members able to degrade numerous extracellular matrix components and several intracellular proteins. MMPs are involved in many pathological conditions, including inflammation and different stages of heart failure [6, 28]. In the present study we analysed whether pulmonary hypertension-induced RV failure in rats is associated with an activation of MMP-2 and MMP-9 in RV myocardium.

The structural basis for the development of congestive heart failure (CHF) is a maladaptive myocardial remodeling process which occurs secondarily to post-myocardial infarction (MI), hypertension-induced LV hypertrophy, or cardiomyopathy. Both cellular and extracellular factors are involved in the remodeling process and it is the combined action of these factors giving rise to changes in myocardial structure which eventually affects function. One component in this remodeling process is the MMPs. Many bioactive molecules such as cytokines/chemokines, bioactive peptides, and neurohormones which are operative in CHF likely contribute to the induction of MMPs. For example, a specific cassette of transcription factors is likely induced with extracellular stimuli in the context of CHF which in turn induces MMPs and contributes to the maladaptive remodeling process [12].

MMP-2 and MMP-9 have been shown to be increased in the plasma of patients with heart failure [1]. A study conducted by Banfi *et al.* [2] also demonstrated that plasma levels of both MMP-2 and MMP-9 were elevated in patients with idiopathic and ischemic dilated cardiomyopathy. In another recently conducted study, elevated plasma MMP-9 levels correlated with lower LVEF and higher LVESV [39]. These findings suggest that monitoring of plasma markers of myocardial remodeling may provide important prognostic information with respect to ongoing adverse LV remodeling in patients with heart failure. A study by Tyagi *et al.* [31] also showed an induction of MMP-2 and MMP-9 in ventricular tissues from human heart end-stage failure secondary to ischemic cardiomyopathy. Focusing on the RV myocardium, we found an activation of immunoreactive MMP-2 and MMP-9 in the remodeled RV myocardium of rats with pulmonary hypertension induced RV

failure, suggesting that these MMPs are implicated in RV remodeling. The lower value of MMP-2 immunoreactivity in RV myocardium of rats with RV failure compared to RV myocardium of rats with RV hypertrophy may be due to the release of MMP-2 from the tissue into the circulation, as was reported for MMP-2 concentration in serum of patients with CHF [1,2].

A recent study by Morita *et al.* [21] has shown that selective MMP inhibition attenuates progression of LV dysfunction and remodeling in dogs with CHF.

In conclusion, tyrosine phosphorylation of FAK was most pronounced in hypertrophic RV myocardium whereas phosphorylation of NOS1 was most pronounced in failing RV myocardium, which may point to a role of excessive NO formation in development of failure and an activation of MMPs leading to ventricular remodeling. The exact role of the NO formed in the failing myocardium is not yet fully elucidated.

Acknowledgements

We would like to thank Prof. D.L. Ypey (Dept. of Cardiology, LUMC) for his valuable suggestions regarding the preparation of this manuscript.

References

1. P. Altieri, C. Brunelli, S. Garibaldi, A. Nicolino, S. Ubaldi, P. Spallarossa, L. Olivotti, P. Rossettin, A. Barsotti, G. Ghigliotti. Metalloproteinases 2 and 9 are increased in plasma of patients with heart failure. *Eur. J. Clin. Invest.* 33 (2003) 648-656.
2. C. Banfi, V. Cavalca, F. Veglia, M. Brioschi, S. Barcella, L. Mussoni, L. Boccotti, E. Tremoli, P. Biglioli, P. Agostoni. Neurohormonal activation is associated with increased levels of plasma matrix metalloproteinase-2 in human heart failure. *Eur. Heart J.* 26 (2005) 481-488.
3. L.A. Barouch, R.W. Harrison, M.W. Skaf, G.O. Rosas, T.P. Cappola, Z.A. Kobeissi, I.A. Hobai, C.A. Lemmon, A.L. Burnett, B. O'Rourke, E.R. Rodriguez, P.L. Huang, J.A.C. Lima, D.E. Berkowitz, J.M. Hare. Nitric oxide regulates the heart by spatial confinement of nitric oxide synthase isoforms. *Nature* 416 (2002) 337-340.
4. A.L. Bayer, M.C. Heidkamp, N. Patel, M.J. Porter, S.J. Engman, A.M. Samarel. PYK2 expression and phosphorylation increases in pressure overload-induced left ventricular hypertrophy. *Am. J. Physiol. Heart Circ. Physiol.* 283 (2002) H695-H706.
5. J.K. Bendall, T. Damy, P. Ratajczak, X. Loyer, V. Monceau, I. Marty, P. Milliez, E. Robidel, F. Marotte, J.L. Samuel, C. Heymes. Role of myocardial neuronal nitric oxide synthase derived nitric oxide in β -adrenergic hyporesponsiveness after myocardial infarction-induced heart failure in rat. *Circulation* 110 (2004) 2368-2375.
6. H. Birkedal-Hansen. Proteolytic remodeling of extracellular matrix. *Curr. Opin. Cell Biol.* 7 (1995) 728-735.
7. H.P. Buermans, E.M. Redout, A.E. Schiel, R.J. Musters, M. Zuidwijk, P.P. Eijk, C. van Hardeveld, S. Kasanmoentalib, F.C. Visser, S. Ylstra, W.S. Simonides. Microarray analysis reveals pivotal divergent mRNA expression profiles early in the development of either compensated hypertrophy or heart failure. *Physiol. Genomics* 21 (2005) 314-323.
8. K.N. Cowan, A. Heilbut, T. Humpl, C. Lam, S. Ito, M. Rabinovitch. Complete reversal of fatal pulmonary hypertension in rats by a serine elastase inhibitor. *Nat. Med.* 6 (2000) 698-702.
9. T. Damy, P. Ratajczak, E. Robidel, J.K. Bendall, P. Olivero, J. Boczkowski, T. Ebrahimian, F. Marotte, J.L. Samuel, C. Heymes. Up-regulation of cardiac nitric oxide synthase 1-derived nitric oxide after myocardial infarction in senescent rats. *FASEB J.* 17 (2003) 1934-1936.
10. T. Damy, P. Ratajczak, A.M. Shah, E. Camors, I. Marty, G. Hasenfuss, F. Marotte, J.L. Samuel, C. Heymes. Increased neuronal nitric oxide synthase-derived NO production in the failing human heart. *Lancet* 363 (2004) 1365-1367.
11. D. Dawson, C.A. Lygate, M.H. Zhang, K. Hulbert, S. Neubauer, B. Casadei. nNOS gene deletion exacerbates pathological left ventricular remodeling and functional deterioration after myocardial infarction. *Circulation* 112 (2005) 3729-3737.
12. A.M. Deschamps, F.G. Spinale. Pathways of matrix metalloproteinase induction in heart failure: Bioactive molecules and transcriptional regulation. *Cardiovasc. Res.* 59 (2006) 666-676.
13. F. Ghodsi, J.A. Will. Changes in pulmonary structure and function induced by monocrotaline intoxication. *Am. J. Physiol.* 240 (1981) H149-H155.
14. M.H.M. Hessel, P. Steendijk, B. den Adel, C.I. Schutte, A. van der Laarse. Characterization of right ventricular function after monocrotaline-induced pulmonary hypertension in the intact rat. *Am. J. Physiol. Heart Circ. Physiol.* 291 (2006) H2424-H2430.
15. A. Hislop, L. Reid. Arterial changes in *Crotalaria spectabilis*-induced pulmonary hypertension in rats. *Br. J. Exp. Pathol.* 55 (1974) 153-163.

16. K.M. Ito, M. Sato, K. Ushijima, M. Nakai, K. Ito. Alterations of endothelium and smooth muscle function in monocrotaline-induced pulmonary hypertensive arteries. *Am. J. Physiol. Heart Circ. Physiol.* 279 (2000) H1786-H1795.
17. M. Laser, C.D. Willey, W. Jiang, G. Cooper IV, D.R. Menick, M.R. Zile, D. Kuppaswamy. Integrin activation and focal complex formation in cardiac hypertrophy. *J. Biol. Chem.* 275 (2000) 275: 35624-35630.
18. D.A. MacKenna, F. Dolfi, K. Vuori, E. Ruoslahti. Extracellular signal regulated kinase and c-Jun NH2-terminal kinase activation by mechanical stretch is integrin-dependent and matrix-specific in rat cardiac fibroblasts. *J. Clin. Invest.* 101 (1998) 301-310.
19. A. Martinez-Ruiz, S. Lamas. S-nitrosylation: a potential new paradigm in signal transduction. *Cardiovasc. Res.* 62 (2004) 43-52.
20. K. Migita, Y. Maeda, S. Abiru, A. Komori, T. Yokoyama, Y. Takii, M. Nakamura, H. Yatsuhashi, K. Eguchi, H. Ishibashi. Peroxynitrite-mediated matrix metalloproteinase-2 activation in human hepatic stellate cells. *FEBS Lett.* 579 (2005) 3119-3125.
21. H. Morita, S. Khanal, S. Rastogi, G. Suzuki, M. Imai, A. Todor, V.G. Sharov, S. Goldstein, T.P. O'Neill, H.N. Sabbah. Selective matrix metalloproteinase inhibition attenuates progression of left ventricular dysfunction and remodeling in dogs with chronic heart failure. *Am. J. Physiol. Heart Circ. Physiol.* 290 (2006) H2522-H2527.
22. H.C. Rosenberg, M. Rabinovitch. Endothelial injury and vascular reactivity in monocrotaline pulmonary hypertension. *Am. J. Physiol.* 255 (1988) H1484-H1491.
23. R.S. Ross, T.K. Borg. Integrins and the myocardium. *Circ. Res.* 88 (2001) 1112-1119.
24. C. Ruwhof, A.E.T. van Wamel, J.M. Egas, A. van der Laarse. Cyclic stretch induces the release of growth promoting factors from cultured neonatal cardiomyocytes and cardiac fibroblasts. *Mol. Cell. Biochem.* 208 (2000) 89-98.
25. J.Y.J. Shyy, S. Chien. Role of integrins in cellular responses to mechanical stress and adhesion. *Curr. Opin. Cell Biol.* 9 (1997) 707-713.
26. M.D. Sjaastad, R.S. Lewis, W.J. Nelson. Mechanisms of integrin-mediated calcium signaling in MDCK cells: regulation of adhesion by IP₃- and stress-independent calcium influx. *Mol. Biol. Cell.* 7 (1996) 1025-1041.
27. F.G. Spinale, M.L. Coker, C.V. Thomas, J.D. Walker, R. Mukherjee, L. Hebbard. Time-dependent changes in matrix metalloproteinase activity and expression during the progression of congestive heart failure. *Circ. Res.* 82 (1998) 482-495.
28. F.G. Spinale. Matrix metalloproteinases: regulation and dysregulation in the failing heart. *Circ. Res.* 90 (2002) 520-530.
29. D. Stoyanovski, T. Murphy, P.R. Anno, Y.M. Kim, G. Salama. Nitric oxide activates skeletal and cardiac ryanodine receptors. *Cell Calcium* 21 (1997) 19-29.
30. M.S. Sumeray, D.D. Rees, D.M. Yellon. Infarct size and nitric oxide synthase in murine myocardium. *J. Mol. Cell. Cardiol.* 32 (2000) 35-42.
31. S.C. Tyagi, S.G. Kumar, S.J. Haas, H.K. Reddy, D.J. Voelker, M.R. Hayden, T.L. Demmy, R.A. Schmalz, J.J. Curtis. Post-transcriptional regulation of extracellular matrix metalloproteinase in human heart end-stage failure secondary to ischemic cardiomyopathy. *J. Mol. Cell. Cardiol.* 28(1996) 1415-1428.
32. A. van der Laarse, C.C. van der Wees, E.J. van der Valk, W.H. Bax. Integrin stimulation induced signaling includes phosphorylation of focal adhesion kinase and nitric oxide synthase-1 leading to elevation of intracellular NO and calcium concentrations in cardiomyocytes. *Circulation* 112 (Abstract 2005) II-1114.
33. C.G.C. van der Wees, W.H. Bax, E.J.M. van der Valk, A. van der Laarse. Integrin stimulation induces calcium signalling in rat cardiomyocytes by a NO-dependent mechanism. *Pflügers Arch. – Eur. J. Physiol.* 451 (2006) 588-595.
34. M.G. Vila Petroff, S.H. Kim, S. Pepe, C. Dessy, E. Marban, J.L. Balligand, S.J. Sollott. Endogenous nitric oxide mechanisms mediate the stretch dependence of Ca²⁺ release in cardiomyocytes. *Nat. Cell Biol.* 3 (2001) 867-873.

35. W. Wang, G. Sawicki, R. Schulz. Peroxynitrite-induced myocardial injury is mediated through matrix metalloproteinase-2. *Cardiovasc. Res.* 53 (2002) 165-174.
36. P.M. Werchan, W.R. Summer, A.M. Gerdes, K.H. McDonough. Right ventricular performance after monocrotaline-induced pulmonary hypertension. *Am. J. Physiol.* 256(1989) H1328-H1336.
37. D.W. Wilson, H.J. Segall, L.C. Pan, M.W. Lame, J.E. Estep, D. Morin. Mechanisms and pathology of monocrotaline pulmonary toxicity. *Crit. Rev. Toxicol.* 22 (1992) 307-325.
38. L. Xu, J.P. Eu, G. Meissner, J.S. Stamler. Activation of the cardiac calcium release channel (ryanodine receptor) by poly-S-nitrosylation. *Science* 279 (1998) 234-237.
39. A.T. Yan, R.T. Yan, F.G. Spinale, R. Afzal, H.R. Gunasinghe, M. Arnold, C. Demers, R.S. Mckelvie, P.P. Liu. Plasma matrix metalloproteinase-9 level is correlated with left ventricular volumes and ejection fraction in patients with heart failure. *J. Card. Fail.* 12 (2006) 514-519.

Chapter 5

Novel approaches to treat pulmonary arterial hypertension

S. Umar
P. Steendijk
D.L. Ypey
D.E. Atsma
E.E. Van der Wall
M. J. Schalij
A. van der Laarse

Submitted for publication

Abstract

Objective: Pulmonary arterial hypertension (PAH) is a life-threatening disease characterized by an increase in pulmonary artery pressure leading to right ventricular (RV) hypertrophy, RV failure and, ultimately, (sudden) cardiac death. Current treatments can improve symptoms and reduce the severity of the hemodynamic disorder in patients with PAH but frequently gradual deterioration in the patient's condition necessitates a lung transplant. In this review we discuss the treatment options tested so far in experimental models of PAH.

Data sources: PubMed.

Study selection: These treatment options include a spectrum of pharmacologic agents ranging from elastase inhibitors, endothelin receptor antagonists, phosphodiesterase inhibitors and phytoestrogens to Rho-kinase inhibitors, serotonin receptor antagonists and statins. In addition, we discuss the emerging trends of using gene and cell therapy for the treatment of PAH. Finally, we discuss the possible applications of experimentally tested interventions for therapeutic purposes in humans with PAH.

Conclusions: Several of these therapeutic options have been shown to be effective also in PAH patients leading to improved life expectations and a better quality of life. However, many patients remain symptomatic despite therapy. Cell therapy is a novel treatment option, but more animal data should be collected to investigate optimal cell type, *in vitro* cell transduction, route of cell administration, and number of cells to inject. Autologous MSC therapy is expected to be a safe and efficacious option to treat patients with PAH.

Pulmonary Arterial Hypertension

Pulmonary arterial hypertension (PAH) is a progressive condition characterized by elevated pulmonary arterial pressures leading to RV failure. PAH is primarily a lung disorder which is associated with increased pulmonary vascular resistance, pulmonary vascular pathology, medial hypertrophy of arterioles, and inflammation of the lungs. Causes of PAH are many fold, including idiopathic PAH, familial PAH, chronic hypoxia-induced PAH, congenital heart disease associated PAH, infections and HIV-associated PAH, PAH due to inflammation and collagen vascular disease, and drugs- and toxins-induced PAH.

Current therapeutic strategies may improve symptoms and reduce the severity of the hemodynamic abnormality, but deterioration of pulmonary and cardiac functions in many cases ultimately necessitates a lung transplant. Novel approaches in treating PAH include reversing the advanced occlusive structural changes in the pulmonary circulation causing PAH and regeneration of damaged pulmonary tissue using stem cells. These approaches have been tested using (i) pharmacotherapy, (ii) gene therapy, and (iii) cell therapy.

Animal Models of Pulmonary Arterial Hypertension

Various experimental models have been proposed for induction of PAH in animals. These models include:

1. Monocrotaline-induced pulmonary hypertension with or without aortocaval shunt
2. Pulmonary artery banding-induced pulmonary hypertension
3. Chronic hypoxia-induced pulmonary hypertension
4. Chronic embolism-induced pulmonary hypertension
5. Ligation of ductus arteriosus
6. Genetically modified animal models

In the past 10 years most experimental studies on therapy of PAH have employed the monocrotaline-induced PAH model.

Monocrotaline-induced Pulmonary Arterial Hypertension Mechanism and Pathology of Pulmonary Toxicity of Monocrotaline

Monocrotaline (MCT), a pyrrolizidine alkaloid derived from *Crotalaria spectabilis*, causes a pulmonary vascular syndrome in rats characterized by proliferative pulmonary vasculitis, pulmonary artery hypertension (PAH), and cor pulmonale. Current lines of evidence of the pathogenesis of MCT-induced pneumotoxicity indicate that MCT is activated to one or more reactive metabolites in the liver, particularly a MCT pyrrole called dehydromonocrotaline [1-3], and is then transported by red blood cells to the lung [4], where it initiates endothelial injury [5, 6]. The endothelial injury does not appear to be acute cell death but rather a delayed functional alteration that leads to smooth muscle cell (SMC) proliferation

in the media of pulmonary arteriolar walls by unknown mechanisms. The role of inflammation in the progression of MCT-induced pulmonary vascular disease is uncertain. Both perivascular inflammation and platelet activation have been proposed as processes contributing to the response of the vascular media [3]. MCT and dehydroMCT are known to be toxic to a variety of domestic and laboratory animals and to humans. Major pathological effects induced by MCT poisoning include hepatic cirrhosis and megalocytosis, venoocclusive disease, PAH, and RV hypertrophy. There is a positive correlation between progressive PAH, thickening of the medial wall of small pulmonary arteries and arterioles, and RV hypertrophy as a function of time [7].

Treatment Options for Experimental Pulmonary Arterial Hypertension

1. Pharmacological interventions

Several pharmacologic agents have been used either alone or in combination to treat MCT-induced pulmonary hypertension. These agents are discussed below.

1.1 Serine elastase inhibitors

Progression of PAH is associated with increased serine elastase activity and the proteinase-dependent deposition of the extracellular matrix protein tenascin-C. Tenascin-C amplifies the response SMCs to growth factors, which are also liberated through matrix proteolysis. Recent organ culture studies using hypertrophied rat pulmonary arteries have shown that elastase inhibitors suppress tenascin-C and induce apoptosis of SMCs [8, 9]. This initiates complete regression of the hypertrophied vessel wall by a coordinated loss of cellularity and extracellular matrix. Elastase inhibitors can reverse advanced pulmonary vascular disease produced in rats by injecting MCT. If the peptidyl trifluoromethylketone serine elastase inhibitors M249314 or ZD0892 were orally administered from 21 days after injection of MCT onwards, survival after 1 week was 92%, compared with only 39% survival in untreated or vehicle-treated rats. Pulmonary artery pressure and muscularization were reduced by cardiomyocyte apoptosis and loss of extracellular matrix, specifically elastin and tenascin-C. After 2 weeks, pulmonary artery pressure and structure normalized, and survival was 86%, compared with 0% in untreated or vehicle-treated rats [10].

1.2 Platelet-derived growth factor inhibition

Progression of PAH is associated with increased proliferation and migration of pulmonary vascular SMCs. Platelet-derived growth factor (PDGF) is a potent mitogen and is involved in this process. It was reported that the PDGF receptor antagonist STI571 (imatinib) reversed advanced pulmonary vascular disease in two animal models of PAH. If in rats with MCT-induced PAH daily administration of STI571 was started 28 days after induction of the disease, there was 100% survival in the first 2 weeks, compared with only 50% in sham-treated rats. PAH and RV hypertrophy were reversed to near-normal levels. Similar results were

obtained in chronically hypoxic mice, which were treated with STI571 after full establishment of PAH. Moreover, expression of the PDGF receptor was found to be significantly increased in lung tissue from patients with PAH compared with healthy donor lung tissue. In conclusion, STI571 reversed vascular remodeling and cor pulmonale in severe experimental PAH regardless of the initiating stimulus. This regimen offers a unique novel approach for anti-remodeling therapy in progressed PAH [11].

1.3 Prostacyclin therapy

Male Wistar rats with flow-associated PAH due to an aortocaval shunt, in addition to MCT-induced PAH, were treated with low-dose aspirin (25 mg/kg/day) or iloprost (72 µg/kg/day), a prostacyclin analogue. Ninety % of the untreated rats with PAH developed dyspnea and pleural fluid, whereas this was seen in 50% and 10% of the aspirin and iloprost-treated rats, respectively. This could not be attributed to changes in pulmonary artery pressure, wall to lumen ratio of the pulmonary arterioles, or RV hypertrophy. However, both therapies restored the reduced RV capillary to cardiomyocyte ratio in rats with PAH (0.95 ± 0.10 in MCT-treated rats vs. 1.38 ± 0.18 in healthy rats, 1.32 ± 0.11 in aspirin-treated MCT rats and 1.29 ± 0.90 in iloprost-treated MCT rats) which was associated with improved RV contractility. Thus, interventions in the prostacyclin–thromboxane metabolism improve outcome in rats with flow-associated PAH. However, these effects may be attributed to effects on cardiac rather than on pulmonary vascular remodeling [12].

Subcutaneous administration of a novel prostacyclin agonist (ONO-1301) markedly attenuated MCT-induced PAH and improved survival in rats. The beneficial effects of ONO-1301 occurred through its long-lasting stimulation of cAMP and inhibition of thromboxane synthase [13].

Although prostacyclin is recognized as a therapeutic breakthrough for pulmonary hypertension, it needs continuous infusion because of its short half-life in plasma. Therefore, Obata *et al.* developed a new drug delivery system for prostacyclin by preparing ONO-1301MS, a novel sustained-release prostacyclin analogue polymerized with poly(D,L-lactic-co-glycolic acid) (PLGA) microspheres. A single injection of ONO-1301MS resulted in sustained activity for 3 weeks, and attenuated PAH, partly through its antiproliferative effect on vascular SMCs via inhibition of ERK phosphorylation [14]. The inhalation of iloprost has been shown to reverse PAH and vascular structural remodeling in MCT-treated rats. This regimen demonstrated the feasibility of a reverse remodeling therapy in PAH [15].

1.4 Combined prostacyclin and phosphodiesterase inhibition

Combination therapy with oral sildenafil, a phosphodiesterase inhibitor, and beraprost, an oral prostacyclin analogue, attenuated the development of MCT-induced PAH compared with treatment with either drug alone [16]. The combined administration of iloprost, a long-acting prostacyclin analogue, and a dual-selective phosphodiesterase 3/4 inhibitor, tolafentrine, reversed the development of PAH and cor pulmonale in response to MCT in rats [17].

1.5 Rho-kinase inhibition

Long-term treatment with a Rho-kinase inhibitor fasudil improved the mortality rate of MCT-induced PAH in rats [18], as well as ameliorated hypoxia-induced PAH in mice, partially by activation of endothelial nitric oxide synthase (eNOS) [19]. Fasudil exerts effective and selective vasodilatation of pulmonary arteries in rats with MCT-induced PAH, which explains its usefulness for the treatment of this fatal disorder [20]. Nagaoka *et al.* found in chronically hypoxic rats that inhalation of Rho-kinase inhibitors nearly normalized PAH, but had no pulmonary vascular selectivity [21].

1.6 Combined Rho-kinase inhibitor and prostacyclin therapy

Combination therapy has been advocated based on the potential for additive or synergistic effects. Long-term inhibition of Rho-kinase, an effector of the small GTPase Rho, ameliorated MCT-induced PAH in rats and hypoxia-induced PAH in mice. It was reported that prostacyclin and its oral analogue beraprost may lack direct inhibitory effect on Rho-kinase *in vitro*, suggesting that combination therapy with a Rho-kinase inhibitor and beraprost is effective for the treatment of PAH. Male Sprague-Dawley rats were given a subcutaneous injection of MCT (60 mg/kg), and subsequently treated without or with a Rho-kinase inhibitor (fasudil, 30 mg/kg/day), beraprost (200 mg/kg/day), or a combination of both drugs for 3 weeks. The combination therapy, when compared with each monotherapy, showed significantly more improvement in PAH, RV hypertrophy, and pulmonary medial thickness without any adverse effects. Plasma concentrations of fasudil were not affected by beraprost. These results demonstrated that combination therapy with a Rho-kinase inhibitor and a prostacyclin analogue exerts further beneficial effects on PAH [22].

1.7 Endothelin receptor antagonists

Endothelin-1 (ET-1), a potent vasoactive and mitogenic peptide, has been implicated in the pathogenesis of several forms of PAH. Hill *et al.* have shown that a nonspecific endothelin-receptor antagonist, bosentan, blunts MCT-induced PAH in rats [23].

The antagonism of the ET_A receptor was shown to be essential for the protection from MCT-induced PAH, irrespective of the presence of the ET_B receptors, although a protective role of ET_B receptor-mediated action in the pathogenesis of this disease model could not be ruled out [24].

Furthermore, in another study from the same group, the functional roles of endothelin ET_A and ET_B receptors in the development of MCT-induced PAH were investigated using MCT-treated rats in the absence or presence of a daily administration of A-192621, a selective ET_B receptor antagonist, ABT-627, a selective ET_A receptor antagonist, or a combination of both drugs. The results demonstrated that ET_A receptor-mediated action contributed exclusively to the pathogenesis of MCT-induced PAH [25].

1.8 Combined endothelin-A receptor antagonist and prostacyclin therapy

Rats with MCT-induced PAH were treated with oral ET_A receptor antagonist TA-0201 and/or the oral prostacyclin analogue beraprost for 19 days. The PAH-associated RV systolic pressure elevation was significantly depressed by TA-0201 and beraprost, and most strongly by TA-0201+beraprost. The indexes of RV hypertrophy showed the same tendency as the increase in RV systolic pressure in the groups MCT, MCT+TA-0201, MCT+beraprost and MCT+TA-0201+beraprost. The expression of the “fetal” gene β -myosin heavy chain was markedly upregulated in the “MCT only” group, and less upregulated in the MCT+TA-0201 and MCT+beraprost groups, and least upregulated in the MCT+TA-0201+beraprost groups. The same was true for medial wall thickness of the pulmonary artery, being most pronounced in “MCT only” group and least increased in the MCT+TA-0201+beraprost group. The combination of an oral ET_A receptor antagonist and an oral prostacyclin analogue appeared to be superior to the use of each drug alone in inhibiting the progression of PAH and its consequences to RV myocardium [26].

1.9 Serotonin transporter inhibition

Progression of PAH is associated with increased pulmonary expression of the serotonin transporter (5-HTT), which leads to hyperplasia of the pulmonary artery smooth muscle cells (PA-SMCs). Given the fact that overexpression of the 5-HTT gene in PA-SMCs leads to PAH [27], it was investigated whether the highly selective 5-HTT inhibitor fluoxetine prevented and/or reversed PAH in MCT-treated rats. Selective antagonists to the 5-HT_{1B/1D} receptor, 5-HT_{2A} receptor and 5-HT_{2B} receptor were used for comparative testing. MCT injection (60 mg/kg s.c.) was followed by an early peak in lung 5-HTT expression on day 1, which preceded the onset of PAH. Established PAH on day 15 was associated with a sustained 5-HTT increase. Continued fluoxetine treatment completely prevented PA-SMC proliferation and PAH development, and also suppressed the late 5-HTT increase, without affecting the early peak. The 5-HT receptor antagonists did not affect PAH. Oral fluoxetine (10 mg/kg/day) started 3 weeks after MCT injection completely reversed established PAH, normalizing pulmonary artery pressure and structure. MCT-induced PAH was also associated with increased expression of various cytokines, but only interleukin-1 β and monocyte chemoattractant protein-1 increased at the early phase and stimulated 5-HTT expression by cultured PA-SMCs. Complete reversal of established PAH by inhibiting 5-HTT provides a rationale for new therapeutic strategies in human PAH [28].

Furthermore, a selective serotonin re-uptake inhibitor (SSRI), sertraline, protects against MCT-induced PAH by decreasing pulmonary artery pressure, RV index, and pulmonary artery remodeling, probably related to a reduction in serotonin transporter mRNA [29].

A serotonin receptor antagonist, MCI-9042, attenuated the development of MCT-induced PAH, suggesting a pivotal role of serotonin in the development of PAH induced by MCT [30].

Specific 5-HT_{2A} receptor blockade with sarpogrelate, a 5-HT_{2A} receptor antagonist, immediately after MCT administration, inhibited PAH and prolonged survival in rats. These effects were accompanied by anti-inflammatory and anti-

proliferative effects in the lung tissue and marked improvement of pulmonary vascular endothelial dysfunction and activation [31].

1.10 Phosphodiesterase inhibition

Phosphodiesterase (PDE) inhibitors for treatment of PAH have been studied extensively. Oral sildenafil prevented (in a study in which sildenafil was given 1 day after MCT) and reversed (in a study in which sildenafil was given 3 weeks after MCT) the development of PAH in MCT-treated rats, associated with a reduction in the ET_A-receptor density in SMCs of pulmonary small arteries (diameter < 100 μm) [32]. The effects of oral pumafentrine, a mixed-selective PDE3/4 inhibitor, have been investigated in rats with MCT-induced PAH. When chronically administered in weeks 4 to 6 after a single injection of MCT (60 mg/kg), pumafentrine (10 mg/kg daily) partially reversed PAH and RV hypertrophy in rats [33]. In addition, small pulmonary arterial muscularization, medial hypertrophy and decrease in lumen area were largely reversed. Inhibition of PA-SMC proliferation by pumafentrine was demonstrated *in vivo*. Pumafentrine also had a pro-apoptotic effect on vascular cells *in vitro*. Moreover, pumafentrine dose-dependently increased cAMP levels and inhibited proliferation of cultured PA-SMCs. Thus, oral pumafentrine partially reverses MCT-induced PAH, pulmonary vascular remodeling, and RV hypertrophy in rats [33].

Schermuly *et al.* investigated chronic effects of sildenafil, a PDE5 inhibitor, in MCT-induced PAH in rats. Four weeks after a single subcutaneous injection of MCT, the animals displayed nearly threefold elevated pulmonary artery pressure and vascular resistance values, with a concomitant decline in central venous oxygen saturation and arterial oxygenation. Marked RV hypertrophy was evident, and massive thickening of the arteriolar SMC layer was histologically apparent. Sildenafil, administered from day 14 to day 28, significantly increased plasma cGMP and inhibited the development of PAH and RV hypertrophy, with improvement of central venous oxygen saturation and arterial oxygenation. A corresponding efficacy profile was also noted for treatment with sildenafil started at day 28 till day 42. Moreover, the death rate significantly decreased in those animals treated with sildenafil [34].

Pullamsetti *et al.* demonstrated for the first time that inhalation of combined PDE3/4 inhibitor tolafentrine reversed PAH that occurred in response to MCT in rats. This "reverse remodeling" effect included structural changes in the lung vascular wall and key molecular pathways of matrix regulation, concomitant with 60% normalization of hemodynamics [35].

1.11 Combination of phosphodiesterase and endothelin receptor inhibition

Clozel *et al.* evaluated the effects of bosentan, a nonspecific endothelin receptor antagonist, sildenafil, and their combination in rats with MCT-induced PAH [36]. A first group consisted of control rats without MCT injection. Four other groups of rats received MCT subcutaneously and were assigned to receive no treatment, 300 mg/kg/day bosentan in the food, 100 mg/kg/day sildenafil in drinking water, or their combination for 4 weeks. The doses of bosentan and sildenafil were the maximally effective doses based on a dose-range-finding study. Mortality was

0%, 53%, 11%, 11%, and 0%, respectively, in the five different groups. Bosentan and sildenafil significantly attenuated the increase in mean pulmonary arterial pressure, and the combination had an additional effect [36].

1.12 Caveolin-1 peptide

Caveolins, the principal structural proteins of caveolar microdomains, have been implicated in the development of PAH. Mice with homozygous deletion of the caveolin-1 (Cav-1) gene develop PAH and RV hypertrophy. In several animal models of PAH and in patients with severe PAH, reductions in pulmonary Cav-1 expression were apparent.

Whether in vivo modulation of Cav-1 expression could affect the development of PAH and RV hypertrophy was studied by Jasmin *et al.* [37]. Thirty minutes after injection of saline or MCT, rats were assigned to receive a daily injection of saline, a peptide corresponding to the homeodomain of the *Drosophila* transcription factor antennapedia (AP; 2.5 mg/kg/day), or a peptide consisting of the Cav-1–scaffolding domain coupled to AP (AP-Cav; 2.5 mg/kg/day) for 2 weeks. MCT and MCT+AP rats developed PAH with RV systolic pressures of 40.2 ± 1.5 and 39.6 ± 1.5 mmHg, respectively. Administration of AP-Cav to MCT rats significantly reduced the RV systolic pressure to 30.1 ± 1.3 mm Hg. MCT and MCT+AP rats also developed pulmonary artery medial hypertrophy and RV hypertrophy, which was normalized by administration of AP-Cav. Mechanistically, the development of PAH was associated with reduced expression of pulmonary Cav-1 and Cav-2, hyperactivation of the STAT3 signaling cascade, and upregulation of cyclin D1 and D3 protein levels, all of which were prevented by administration of AP-Cav. Thus, short-term administration of a Cav-based cell-permeable peptide to MCT rats prevented the development of pulmonary artery medial hypertrophy, PAH, and RV hypertrophy [37].

1.13 Estradiol

Daily supplementation of genistein, a phytoestrogen, potently attenuated MCT-induced PAH, RV hypertrophy, and pulmonary vascular remodeling in rats [38]. Also 2-methoxyestradiol (2ME), a non-estrogenic estradiol metabolite, prevented the development and retarded the progression of MCT-induced PAH [39]. 2ME significantly attenuated RV hypertrophy and pulmonary arterial medial hypertrophy, and reduced proliferative and inflammatory responses in the lungs. Furthermore, in diseased animals, 2ME (given from day 14 to 28) significantly decreased RV peak systolic pressure and RV hypertrophy, and reduced mortality. Thus, 2ME, a major non-estrogenic, non-carcinogenic metabolite of estradiol, prevented the development and retarded the progression of MCT-induced PAH [39, 40].

Recently, Tofovic *et al.* provided the first evidence that 2-ethoxyestradiol strongly inhibited vascular remodeling in PAH and suggested that anti-proliferative agents, including synthetic analogues of estradiol metabolites may be protective in PAH [41].

1.14 Statins

Various statins have been shown to be effective in treating experimental PAH. Simvastatin attenuated MCT-induced pulmonary vascular remodeling, PAH, and RV hypertrophy in rats [42]. Pravastatin reduced the development of MCT-induced PAH and improved endothelium-dependent pulmonary artery relaxation through reduced apoptosis and a restored eNOS expression of endothelial cells [43]. Rosuvastatin provided protection against the development of PAH and RV hypertrophy [44]. These studies demonstrate that the targeted preservation of coronary endothelial function and vasoactivity provides a novel approach to protect against cardiac remodeling.

1.15 Miscellaneous therapeutic agents

1.15.1 Amlodipine, a third-generation calcium channel blocker, inhibited the development of PAH and improved survival in rats independent of its effect on lowering blood pressure. These effects were associated with marked inhibition of the downregulation of eNOS and improvement of pulmonary vascular endothelial activation, as well as anti-inflammatory, antiproliferative and antifibrotic effects in the lung tissue. However, amlodipine failed to reverse established PAH [45].

1.15.2 Nicorandil, an ATP-sensitive potassium (K_{ATP}) channel opener with a nitrate-like action, inhibited development of MCT-induced PAH but failed to reverse it. These effects were associated with marked up-regulation of diminished lung eNOS concentration along with improvement of pulmonary vascular endothelial activation and anti-inflammatory and anti-proliferative effects in the lung tissue [46].

1.15.3 Infusion of **C-type natriuretic peptide (CNP)**, the third member of the natriuretic peptide family, attenuated MCT-induced PAH and improved survival. The beneficial effects were mediated by regeneration of pulmonary endothelium, inhibition of endothelial cell apoptosis, prevention of monocyte/macrophage infiltration, and restoration of fibrinolytic activity [47].

1.15.4 Repeated inhalation of **adrenomedullin**, a potent vasodilator peptide that was originally isolated from human pheochromocytoma, has been shown to inhibit MCT-induced PAH without systemic hypotension, and thereby improving survival in MCT rats [48].

1.15.5 Zhou *et al.* have shown that heme oxygenase-1 was critical for the antiproliferative and vascular protective effects of **rapamycin**, an immunosuppressive agent with antiproliferative activity not only against lymphocytes but also against vascular cells, *in vitro* and *in vivo* in MCT-induced PAH [49].

1.15.6 Granulocyte colony-stimulating factor (G-CSF) inhibited the progression of PAH in a rat model, possibly by stimulating pulmonary endothelial cells to proliferate at sites of impaired lung vasculature [50].

1.15.7 The NF- κ B nuclear localization and vascular cell adhesion molecule (VCAM-1) expression are temporally and spatially associated with the development of MCT-induced PAH in rats. Administration of a **NF- κ B inhibitor**, pyrrolidine dithiocarbamate (PDTTC), reversed the MCT-induced development of PAH in rats [51].

1.15.8 In rats with MCT-induced PAH treatment with an **interleukin-1 receptor antagonist** started at the same time as MCT administration and continued for the first 2 weeks prevented the development of PAH and RV hypertrophy as assessed 3 weeks after MCT injection [52].

1.15.9 In rats with MCT-induced PAH treatment with **antibodies to monocyte chemotactic and activating factor/monocyte chemoattractant protein-1** started at the same time as MCT administration, or at day 3.5, 7 or 14 after MCT administration. Antibody therapy started together with MCT administration was the most effective in alleviating RV hypertrophy, as compared to later starts [53]. Antibody therapy started together with MCT administration did not prevent development of pulmonary hypertension, but right ventricular peak systolic pressure was significantly lower than observed in rats treated with MCT only (≈ 50 mmHg and ≈ 70 mmHg, respectively).

1.15.10 Rats were, 1 day after MCT administration (60 mg/kg), treated without or with a specific **inhibitor of p38 mitogen-activated protein kinase**, FR167653, for 27 days. Four weeks after MCT administration pulmonary artery pressure and RV weight had hardly increased, compared to rats that received only MCT. The beneficial effects of FR167653 were ascribed to attenuated expression of inflammatory cytokines, thereby preventing the progression of pulmonary hypertension [54].

1.15.11 PAH is associated with endothelial injury [55] and with NO-dependent endothelial dysfunction [56]. Rats treated with daily i.p. doses of **L-arginine** (500 mg/kg), started 3 days before MCT administration, and continuing till sacrifice of the animals at day 17 after MCT injection, prevented the development of PAH, RVH, and pulmonary vascular disease [57].

1.15.12 Rats were, 2 day before MCT administration (60 mg/kg), treated without or with an **inhibitor of lipoxygenase pathways**, diethylcarbamazine, for 23 days. Three weeks after MCT administration, therapy with diethylcarbamazine appeared to have blocked the development of pulmonary hypertension and RVH, associated with inhibition of influx of polymorphonuclear cells and alveolar macrophages into the alveoli and the activation of these cells by lipoxygenase-related products [58].

2. Gene therapy

2.1 There is ample evidence that oxidative stress contributes to the pathogenesis and/or development of PAH. Intratracheal gene transfer of **human extracellular superoxide dismutase (EC-SOD)** was studied in rats with MCT-induced PAH [59]. MCT-injected rats were intratracheally administered either vehicle (MCT group) or an adenovirus encoding β -galactosidase (Ad β gal group), or human EC-SOD (AdEC-SOD group). After intratracheal gene transfer, EC-SOD was successfully expressed in lung tissue, bronchoalveolar lavage fluid, and plasma. Twenty-eight days after MCT injection, RV systolic pressure and the weight ratio of the RV to the LV plus septum were significantly lower in the AdEC-SOD group (42.5 ± 1.4 mmHg and 0.45 ± 0.02 , respectively) than in the MCT group (59.8 ± 1.6 mmHg and 0.63 ± 0.02 , respectively) and the Ad β gal group (61.5 ± 2.1 mmHg and 0.65 ± 0.03 , respectively). Moreover, vascular remodeling and proliferation of vascular smooth muscle cells in pulmonary arteries were markedly suppressed in the AdEC-SOD group [59]. Thus EC-SOD acts as an antioxidant in PAH, and apparently increased oxidative stress plays an important role in the pathogenesis of MCT-induced PAH.

2.2 Ikeda *et al.* have suggested that **monocyte/macrophage chemoattractant protein-1 (MCP-1)**, a potent chemoattractant chemokine and an activator for mononuclear cells, may play a role in the initiation and/or progression of PAH [60]. They found that anti-MCP-1 gene therapy attenuated PAH in rats. Hence an anti-inflammatory strategy via blockade of the MCP-1 signal pathway may be an alternative approach to treat subjects with PAH.

2.3 Prostacyclin is a potent vasodilator that also inhibits platelet adhesion and cell growth. Intratracheal transfer of the **human prostacyclin synthase (PGIS)** gene to rats with MCT-induced PAH augmented pulmonary prostacyclin synthesis, ameliorated MCT-induced PAH, and improved survival in MCT rats [61]. An intramuscular injection of adeno-associated virus (AAV) vector harboring the PGIS gene (AAV-PGIS) also prevented MCT-induced PAH in rats. This approach provides an attractive therapeutic alternative for preventing PAH in humans [62].

2.4 Cell-based gene transfer with **angiopoietin-1 (Ang-1)**, a newly discovered ligand of the endothelial-specific tyrosine kinase receptor Tie-2, has been shown to improve survival and pulmonary hemodynamics in experimental PAH by a mechanism involving the inhibition of apoptosis and protection of the pulmonary microvasculature [63].

2.5 In another study, Zhao *et al.* demonstrated that cell-based **endothelial NO synthase (eNOS)** gene transfer was more effective than vascular endothelial growth factor A (VEGF) in reversing established PAH, associated with evidence of regeneration of pulmonary microcirculation [64].

2.6 **Interleukin (IL)-10** is a pleiotropic anti-inflammatory cytokine with vasculoprotective properties. After rats were injected intramuscularly with an AAV serotype 1 vector expressing IL-10, followed by MCT injection, it was demonstrated that IL-10 expression prevented MCT-induced PAH in rats [65].

3. Cell therapy

3.1 Intratracheal mesenchymal stem cell therapy

Baber *et al.* studied the effect of intratracheal administration of rat bone marrow derived mesenchymal stem cells (rMSCs) on MCT-induced PAH and impaired endothelium-dependent responses in the rat [66]. rMSCs had been transfected with the lacZ gene before intratracheal administration. The intratracheal administration of 3×10^6 rMSCs 2 weeks after administration of MCT attenuated the rise in pulmonary arterial pressure and pulmonary vascular resistance, and restored pulmonary responses to acetylcholine toward values measured in control rats. Treatment with rMSCs decreased RV hypertrophy induced by PAH. Immunohistochemical studies showed widespread distribution of lacZ-labeled rMSCs in lung parenchym surrounding airways in MCT-treated rats. These rMSCs retained expression of von Willebrand factor and α -smooth muscle-actin, being markers specific for endothelial cell and SMC phenotypes, respectively. However, lacZ expressing rMSCs were not detected in the wall of pulmonary vessels. These data suggest that the decrease in pulmonary vascular resistance and improved responses to acetylcholine in PAH rats treated with MSCs were the result of paracrine effects of transplanted rMSCs in lung parenchym on vascular endothelial function in the injured lungs [66].

3.2 Intravenous administration of pulmonary artery smooth muscle cells

Primary cultures of PA-SMCs from Fisher 344 rats were labeled with a fluorescent, membrane-impermeable dye chloromethyl-trimethyl-rhodamine or transfected with the β -galactosidase (β Gal) reporter gene under the control of the cytomegalovirus (CMV) promoter (pCMV- β) [67]. Transfected or labeled SMCs (5×10^5 cells/animal) were delivered to syngeneic recipient rats by injection into the jugular vein. The animals were killed at intervals between 15 min and 2 weeks, and the lungs, spleen, kidneys, and skeletal muscle were excised and examined. At 15 min after transplantation, injected cells were detected mainly in the lumen of small pulmonary arteries and arterioles, often in groups of three or more cells. After 24 h, labeled SMCs were found incorporated into the vascular wall of pulmonary arterioles, and transgene expression persisted *in situ* for 14 d with no evidence of any immune response. Approximately $57 \pm 5\%$ of the labeled cells injected into the venous circulation were recovered in the lungs after 15 min, $34 \pm 7\%$ at 48 h, $16 \pm 3\%$ at 1 week, and $15 \pm 5\%$ at 2 weeks. Similar results were observed using cells transfected with the LacZ gene. To determine whether this method of gene transfer is effective in inhibiting the development of pulmonary vascular disease, PA-SMCs were transfected *in vitro* with either the full-length coding sequence of the eNOS gene or with the control vector (pcDNA3.1) and injected simultaneously with MCT. At 28 d after injection the RV systolic pressure was 50 ± 4 mmHg in animals injected with the null-transfected SMCs, and 33 ± 3 mmHg in animals injected with the eNOS-transfected SMCs ($p < 0.01$). These results indicate that a cell-based strategy of *ex vivo* transfection provides an effective nonviral approach for the selective delivery of foreign transgenes to pulmonary microvessels in the treatment of pulmonary vascular disease [67].

Campbell *et al.* prepared primary cultures of PA-SMCs and transfected these cells with vascular endothelial growth factor (VEGF)-A [68]. These cells were administered i.v. into Fisher 344 rats with MCT-induced PAH. Four weeks after MCT and i.v. SMC administration, PAH, RV hypertrophy and medial hypertrophy of pulmonary arterioles were significantly less in the VEGF-treated animals compared to MCT-treated animals that did not receive cell therapy. Four weeks after gene transfer, the VEGF mRNA was still detectable in the pulmonary tissue of animals injected with VEGF-transfected cells, demonstrating survival of transfected cells and persistent transgene expression. If cell-based gene transfer using VEGF-expressing PA-SMCs was delayed till PAH had developed, also a significant decrease in the progression of PAH and RV hypertrophy was documented [68]. These results indicate that cell-based VEGF gene transfer is effective in preventing the development and progression of PAH in the MCT model. Thus, a therapeutic role for angiogenic factors in the therapy of PAH is very likely.

3.3 Intravenous administration of endothelial progenitor cells

PAH is characterized by a progressive increase in pulmonary vascular resistance caused by narrowing and loss of pulmonary microvasculature, which in its late stages becomes refractory to traditional therapies. Zhao *et al.* isolated bone marrow–derived endothelial progenitor cells (EPCs) from Fisher-344 rats, cultured them for 7 to 10 days in endothelial growth medium and injected them intravenously in syngeneic MCT-treated rats [69]. The EPCs engrafted at the level of the distal pulmonary arterioles and incorporated into the endothelial lining of the MCT-injured lung. The administration of EPCs 3 days after MCT administration nearly completely prevented the increase in RV systolic pressure observed at 3 weeks with MCT alone (31 ± 1 versus 48 ± 3 mmHg, respectively; $p<0.001$), whereas i.v. administration of skin fibroblasts had no protective effect (51 ± 5 mmHg). Delayed administration of EPCs 3 weeks after MCT prevented the further progression of PAH 2 weeks later, whereas animals receiving EPCs transfected with the human eNOS gene exhibited significant regression of established disease at day 35 (31 ± 2 mmHg, $p<0.005$) compared with day 21 (50 ± 3 mmHg). Fluorescent microangiography revealed widespread occlusion of pulmonary arterioles 3 weeks after MCT, whereas arteriolar-capillary continuity and microvascular architecture were preserved if syngeneic EPCs had been administered. Moreover, the delivery of EPCs to rats with established PAH resulted in marked improvement in survival, which was greatest in the group receiving eNOS-transduced EPCs [69]. Thus bone marrow–derived EPCs can engraft and repair the MCT-damaged lung, restoring structure and function of pulmonary microvasculature. Therefore, the regeneration of lung vascular endothelium by injection of EPCs, and in particular eNOS-transduced EPCs, may represent a novel treatment for patients with PAH.

3.4 Intravenous administration of bone marrow-derived cells

Recent evidence suggests that bone marrow–derived cells may differentiate into vascular cells that participate in arterial repair and/or lesion formation [70]. However, it remains uncertain whether bone marrow-derived cells can also participate in vascular remodeling associated with PAH. The bone marrow of

Sprague-Dawley rats was reconstituted with that of green fluorescent protein (GFP)-transgenic rats. The bone marrow-chimeric rats were injected intraperitoneally with 60 mg/kg MCT after unilateral pneumonectomy, and concurrently underwent wire-mediated endovascular injury in one femoral artery. After 28 days, they had elevated RV systolic pressure (58.8 ± 5.4 versus 20.4 ± 2.4 mmHg in sham-control; $p < 0.01$) [71]. The pulmonary arterioles were markedly thickened, with an infiltration of GFP-positive macrophages into the perivascular areas. The endothelium of pulmonary arterioles contained only a few GFP-positive cells, and GFP-positive cells were seldomly detected in the media of thickened pulmonary arterioles. In contrast, bone marrow-derived smooth muscle-like cells could be readily detected in the thickened neointima and media of the wire-injured femoral artery. Moreover, intravenous injection of 10^8 unfractionated bone marrow-derived cells from young rats had no beneficial effects on PAH, pulmonary arterial remodeling, and survival in the aged rats treated with MCT plus unilateral pneumonectomy. No injected bone marrow-derived cell was identified as an endothelial cell or a vascular SMC [71]. These results suggest that bone marrow-derived cells can participate in arterial neointimal formation after mechanical injury, whereas they do not contribute substantially to pulmonary arterial remodeling associated with MCT-induced PAH in pneumonectomized rats.

Raoul *et al.* investigated the effect of bone marrow-derived cells on PAH induced by either MCT or exposure to chronic hypoxia in mice [72]. Intravenous administration of the active MCT metabolite (monocrotaline pyrrole, MCTp) to C57BL/6 mice induced PAH within 15 days, due to remodeling of small pulmonary arterioles. Three days after MCTp injection, the mice were injected with bone marrow-derived cells harvested from femurs and tibias of donor mice treated with 5-fluorouracil (3.5 mg i.p./animal) to deplete mature cells and to allow proliferation of progenitor cells. Bone marrow-derived cells significantly attenuated PAH as assessed by reductions in RV systolic pressure (20 ± 1 mmHg vs. 27 ± 1 mmHg, $p \leq 0.01$), weight ratio of RV to the LV plus septum (0.29 ± 0.02 vs. 0.36 ± 0.01 , $p \leq 0.03$), and percentage of muscularized pulmonary arterioles (26.4% vs. 33.5%, $p \leq 0.05$), compared to irradiated bone marrow-derived cells administered to MCTp-treated animals. Tracking cells from constitutive GFP-expressing male donor mice with anti-GFP antibodies or chromosome Y quantification by real-time PCR demonstrated the presence of bone marrow-derived cells in the lung. In contrast, chronically hypoxic mice subjected to the same procedure failed to show improvement in PAH [72]. These results demonstrate bone marrow-derived cells limit pulmonary vascular remodeling induced by vascular injury but not pulmonary vascular remodeling induced by hypoxia.

3.5 Intravenous administration of mesenchymal stem cells overexpressing endothelial nitric oxide synthase (eNOS)

Bone marrow-derived cell transplantation is reported to reduce the development of PAH by increasing or repairing vascular beds in the pulmonary circulation, and upregulated eNOS expression enforces this therapeutic effect. Kanki-Horimoto *et al.* have studied the efficacy of intravenous administration of eNOS-transfected, bone marrow-derived MSCs (MSCs/eNOS) in rats with MCT-induced PAH [73]. One week after MCT administration, the rats received 3 different treatments:

MSCs (MSC group), MSCs/eNOS, (MSC/eNOS group), or no treatment (PAH group). As the negative control, rats received saline instead of MCT (control group). RV systolic pressures in the MSC and MSC/eNOS groups were significantly lower than in the PAH group, and RV systolic pressure in the MSC/eNOS group was significantly lower than in the MSC group. Similar results were obtained with regard to RV hypertrophy in the 3 groups. The survival time of rats receiving MSCs/eNOS was significantly longer than survival time of PAH rats without treatment [73]. Hence, intravenous administration of MSCs/eNOS offers therapeutic effects on MCT-induced PAH, RV hypertrophy, and mortality.

3.6 Transplantation of endothelial progenitor cells into the lung

EPCs have been shown to promote neovascularization. Takahashi *et al.* have examined the effects of EPC transplantation into the lungs of dogs with dehydromonocrotaline-induced PAH [74]. The lung parenchyma of dogs with PAH was injected with *ex vivo*-expanded, autologous EPCs using a bronchoscope. EPC transplantation resulted in significant improvements in mean pulmonary artery pressure, pulmonary vascular resistance and cardiac output. Histological evaluation revealed improvement in the medial thickness of the small pulmonary arteries and neovascularization of lung tissue [74]. These results indicate that EPC transplantation into the lung is effective at preventing the progression of dehydromonocrotaline-induced PAH in dogs, and may provide a new therapeutic option for patients with PAH.

3.7 Intravenous administration of MSCs from rats suffering with PAH

Recently, we completed a study in which rats with MCT-induced PAH were, 14 days after MCT injection, treated with a single i.v. MSC injection (10^6 cells/rat) obtained from bone marrow of rats with MCT-induced PAH, or a single injection with PBS. Another 2 weeks later RV pressures were measured, the rats were sacrificed and heart and lungs were dissected. The PBS-treated MCT rats developed PAH as expected. In the MSC-treated MCT rats the RV pressures were significantly lower compared to the PBS-treated MCT rats. Accordingly, RV hypertrophy in the MSC-treated MCT rats was significantly lower compared to the PBS-treated MCT rats. In this study we have demonstrated that bone marrow-derived MSCs obtained from donor rats suffering from PAH when administered to acceptor rats with PAH reduce RV pressure overload and RV hypertrophy (unpublished results).

Cell Therapy for PAH: from Experimental Models to Clinical Disease

Cell therapy is a promising novel therapeutic option, and several cell types have been tested in experimental models of PAH. Endothelial progenitor cells have recently been explored as a potential source for neovascularization of the diseased pulmonary circulation in patients with PAH. A randomized trial by Wang *et al.* has indicated that intravenous infusion of autologous EPCs to patients with idiopathic PAH appears to be feasible and safe, and has beneficial effects on

exercise capacity and pulmonary hemodynamics in patients with idiopathic PAH [75].

Also MSC is a cell type that can improve the pulmonary pathology of PAH by either differentiating into other cell types leading to regeneration of the diseased vasculature or secreting an array of substances, the “pro-survival factors” including various growth factors and cytokines, leading to improvement in lung pathology by paracrine mechanisms. Autologous bone marrow-derived MSC therapy has a practical advantage over other types of cell therapies, as the mode of administration is rather simple and has proven to be safe.

Conclusions

In conclusion, a wealth of therapeutic modalities including pharmacotherapy, gene therapy and cell therapy has been tested in several animal models of PAH including MCT-induced PAH. Several of these therapeutic options have been shown to be effective also in PAH patients leading to improved life expectations and a better quality of life. However, many patients remain symptomatic despite therapy. Cell therapy is a novel treatment option, but more animal data should be collected to investigate optimal cell type, *in vitro* cell transduction, route of cell administration, and number of cells to inject. Autologous MSC therapy is expected to be a safe and efficacious option to treat patients with PAH.

Table. Classification of published therapies of experimental pulmonary hypertension

Anti-mitogenic (particularly towards PA-SMCs)	(ref)
PDGF inhibitors	(11)
Endothelin receptor blockers	(23-26,36)
Prostacyclin	(12-17,22,26)
Serotonin transporter inhibitors	(28)
Serotonin receptor blockers	(30,31)
Serotonin re-uptake inhibitor	(29)
PDE 4/5 and 3/4 inhibitors	(16,17,32-36)
Caveolin-1 blockers	(37)
Estradiol (derivatives)	(38-41)
Amlodipine	(45)
Rapamycin	(49)
Endothelial NO synthase gene	(64)
Prostacyclin synthase gene	(61,62)
NF- κ B inhibitor	(51)
Pro-endothelial function, vasodilatation and pro-angiogenesis	
Rho-kinase inhibitors	(18-22)
Statins	(43,44)
Nicorandil	(46)
Granulocyte-colony stimulating factor	(50)
L-arginine	(57)
Prostacyclin	(12-17,22,26)
Endothelin receptor blockers	(23-26,36)
PDE 4/5 and 3/4 inhibitors	(16,17,32-36)
Adrenomedullin	(48)
Prostacyclin synthase gene	(61,62)
Angiopoietin-1 gene	(63)
Cell therapy using EPCs and MSCs	(66,69,73-75)
Cell therapy using differentiated cells transduced with eNOS gene	(67,69,73)
Cell therapy using differentiated cells transduced with VEGF gene	(68)
Anti-inflammatory and anti-oxidative	
Serotonin receptor blockers	(30,31)
Amlodipine	(45)
Nicorandil	(46)
Statins	(43,44)
C-type natriuretic factor	(47)
Interleukin-1 receptor antagonist	(52)
Antibodies to monocyte chemoattractant and activating factor/MCP1	(53)
Inhibitor of p38 mitogen-activated protein kinase	(54)
Inhibitor of lipoxygenase pathways	(58)
Anti-monocyte chemoattractant protein-1 gene	(60)
Interleukin-10 gene	(65)
Extracellular superoxide dismutase gene	(59)
Pro-apoptosis of PA-SMCs	
Serine-elastase inhibitors	(10)
PDE 4/5 and 3/4 inhibitors	(16,17,32-36)

Abbreviations: PA-SMCs, pulmonary artery-derived smooth muscle cells; PDGF, platelet-derived growth factor; PDE, phosphodiesterase; NO, nitric oxide; EPC, endothelial progenitor cells; MSC, mesenchymal stem cells; eNOS, endothelial NO-synthase; VEGF, vascular endothelial growth factor; MCP1, monocyte chemoattractant protein-1.

References

1. Butler WH, Mattocks AR, Barnes JM. Lesions in the liver and lungs of rats given pyrrole derivatives of pyrrolizidine alkaloids. *J Pathol* 1970; 100: 169-175
2. Lafranconi WM, Huxtable RJ. Hepatic metabolism and pulmonary toxicity of monocrotaline using isolated perfused liver and lung. *Biochem Pharmacol* 1984; 33: 2479-2484
3. Wilson DW, Segall HJ, Pan LC, *et al.* Mechanisms and pathology of monocrotaline pulmonary toxicity. *Crit Rev Toxicol* 1992; 22: 307-325
4. Lamé MW, Jones AD, Morin D, *et al.* Association of dehydromonocrotaline with rat red blood cells. *Chem Res Toxicol* 1997; 10: 694-701
5. Reindel JF, Hoorn CM, Wagner JG, *et al.* Comparison of response of bovine and porcine pulmonary arterial endothelial cells to monocrotaline pyrrole. *Am J Physiol Lung Cell Mol Physiol* 1991; 261: L406-L414
6. Reindel JF, Roth RA. The effects of monocrotaline pyrrole on cultured bovine pulmonary artery endothelial and smooth muscle cells. *Am J Pathol* 1991; 138: 707-719
7. Ghodsi F, Will JA. Changes in pulmonary structure and function induced by monocrotaline intoxication. *Am J Physiol Heart Circ Physiol* 1981; 240: H149-H155
8. Cowan KN, Jones PL, Rabinovitch M. Regression of hypertrophied rat pulmonary arteries in organ culture is associated with suppression of proteolytic activity, inhibition of tenascin-C, and smooth muscle cell apoptosis. *Circ Res* 1999; 84: 1223-1233
9. Cowan KN, Jones PL, Rabinovitch M. Elastase and matrix metalloproteinase inhibitors induce regression and tenascin-C antisense prevents progressive vascular disease. *J Clin Invest* 2000; 105: 21-34
10. Cowan KN, Heilbut A, Humpl T, *et al.* Complete reversal of fatal pulmonary hypertension in rats by a serine elastase inhibitor. *Nat Med* 2000; 6: 698-702
11. Schermuly RT, Dony E, Ghofrani HA, *et al.* Reversal of experimental pulmonary hypertension by PDGF inhibition. *J Clin Invest* 2005 a; 115: 2811-2821
12. van Albada ME, Berger RMF, Niggebrugge M, *et al.* Prostacyclin therapy increases right ventricular capillarisation in a model for flow-associated pulmonary hypertension. *Eur J Pharmacol* 2006; 549: 107-116
13. Kataoka M, Nagaya N, Satoh T, *et al.* A long-acting prostacyclin agonist with thromboxane inhibitory activity for pulmonary hypertension. *Am J Respir Crit Care Med* 2005; 172:1575-1580
14. Obata H, Sakai Y, Ohnishi S, *et al.* Single injection of a sustained-release prostacyclin analog improves pulmonary hypertension in rats. *Am J Respir Crit Care Med* 2008; 177:195-201
15. Schermuly RT, Yilmaz H, Ghofrani HA, *et al.* Inhaled iloprost reverses vascular remodeling in chronic experimental pulmonary hypertension. *Am J Respir Crit Care Med* 2005 b; 172:358-363
16. Itoh T, Nagaya N, Fujii T, *et al.* A combination of oral sildenafil and beraprost ameliorates pulmonary hypertension in rats. *Am J Respir Crit Care Med* 2004; 169:34-38
17. Schermuly RT, Kreisselmeier KP, Ghofrani HA, *et al.* Antiremodeling effects of iloprost and the dual-selective phosphodiesterase 3/4 inhibitor tolafentrine in chronic experimental pulmonary hypertension. *Circ Res* 2004; 94:1101-1108
18. Abe K, Shimokawa H, Morikawa K, *et al.* Long-term treatment with a Rho-kinase inhibitor improves monocrotaline-induced fatal pulmonary hypertension in rats. *Circ Res* 2004; 94:385-393
19. Abe K, Tawara S, Oi K, *et al.* Long-term inhibition of Rho-kinase ameliorates hypoxia-induced pulmonary hypertension in mice. *J Cardiovasc Pharmacol* 2006; 48:280-285

20. Jiang BH, Tawara S, Abe K, *et al.* Acute vasodilator effect of fasudil, a Rho-kinase inhibitor, in monocrotaline-induced pulmonary hypertension in rats. *J Cardiovasc Pharmacol* 2007; 49:85-89
21. Nagaoka T, Fagan KA, Gebb SA, *et al.* Inhaled Rho kinase inhibitors are potent and selective vasodilators in rat pulmonary hypertension. *Am J Respir Crit Care Med* 2005; 171:494-499
22. Tawara S, Fukumoto Y, Shimokawa H. Effects of combined therapy with a Rho-Kinase inhibitor and prostacyclin on monocrotaline-induced pulmonary hypertension in rats. *J Cardiovasc Pharmacol* 2007; 50: 195-200
23. Hill NS, Warburton RR, Pietras L, *et al.* Nonspecific endothelin-receptor antagonist blunts monocrotaline-induced pulmonary hypertension in rats. *J Appl Physiol* 1997; 83:1209-1215
24. Nishida M, Okada Y, Akiyoshia K, *et al.* Role of endothelin ET_B receptor in the pathogenesis of monocrotaline-induced pulmonary hypertension in rats. *Eur J Pharmacol* 2004 a; 496:159- 165
25. Nishida M, Eshiro K, Okada Y, *et al.* Roles of endothelin ET_A and ET_B receptors in the pathogenesis of monocrotaline-induced pulmonary hypertension. *J Cardiovasc Pharmacol* 2004 b; 44:187-191
26. Ueno M, Miyauchi T, Sakai S, *et al.* A combination of oral endothelin-A receptor antagonist and oral prostacyclin analogue is superior to each drug alone in ameliorating pulmonary hypertension in rats. *J Am Coll Cardiol* 2002; 40: 175- 181
27. Guignabert C, Izikki M, Tu LI, *et al.* Transgenic mice overexpressing the 5-hydroxytryptamine transporter gene in smooth muscle develop pulmonary hypertension. *Circ Res* 2006; 98:1323-1330
28. Guignabert C, Raffestin B, Benferhat R, *et al.* Serotonin transporter inhibition prevents and reverses monocrotaline-induced pulmonary hypertension in rats. *Circulation* 2005; 111: 2812-2819
29. Li X, Hong Y, Wang Y, *et al.* Sertraline protects against monocrotaline-induced pulmonary hypertension in rats. *Clin Exp Pharmacol Physiol* 2006; 33:1047-1051
30. Miyata M, Ito M, Sasajima T, *et al.* Development of monocrotaline-induced pulmonary hypertension is attenuated by a serotonin receptor antagonist. *Lung* 2000; 178:63-73
31. Hironaka E, Hongo M, Sakai A, *et al.* Serotonin receptor antagonist inhibits monocrotaline-induced pulmonary hypertension and prolongs survival in rats. *Cardiovasc Res* 2003; 60:692-699
32. Liu H, Liu ZY, Guan Q. Oral sildenafil prevents and reverses the development of pulmonary hypertension in monocrotaline-treated rats. *Interactive CardioVasc Thorac Surg* 2007; 6:608-613
33. Dony E, Lai Y, Dumitrascu R, *et al.* Partial reversal of experimental pulmonary hypertension by phosphodiesterase 3/4 inhibition. *Eur Respir J* 2008;31:599-610
34. Schermuly RT, Kreisselmeier KP, Ghofrani HA, *et al.* Chronic sildenafil treatment inhibits monocrotaline-induced pulmonary hypertension in rats. *Am J Respir Crit Care Med* 2004; 169: 39-45
35. Pullamsetti S, Krick S, Yilmaz H, *et al.* Inhaled tolafentrine reverses pulmonary vascular remodeling via inhibition of smooth muscle cell migration. *Respir Res* 2005; 6:128.
36. Clozel M, Hess P, Rey M, *et al.* Bosentan, sildenafil, and their combination in the monocrotaline model of pulmonary hypertension in rats. *Exp Biol Med* 2006; 231: 967-973
37. Jasmin J, Mercier I, Dupuis J, *et al.* Short-term administration of a cell-permeable Caveolin-1 peptide prevents the development of monocrotaline-induced pulmonary hypertension and right ventricular hypertrophy. *Circulation* 2006; 114: 912-920
38. Homma N, Morio Y, Takahashi H, *et al.* Genistein, a phytoestrogen, attenuates monocrotaline-induced pulmonary hypertension. *Respiration* 2006; 73:105-112

39. Tofovic SP, Salah EM, Mady HH, *et al.* Estradiol metabolites attenuate monocrotaline-induced pulmonary hypertension in rats. *J Cardiovasc Pharmacol* 2005; 46:430-437
40. Tofovic SP, Zhang X, Jackson EK, *et al.* 2-Methoxyestradiol mediates the protective effects of estradiol in monocrotaline-induced pulmonary hypertension. *Vascul Pharmacol* 2006; 45:358-367
41. Tofovic SP, Zhang X, Zhu H, *et al.* 2-Ethoxyestradiol is antimitogenic and attenuates monocrotaline-induced pulmonary hypertension and vascular. *Vascul Pharmacol* 2008; 48:174-183
42. Nishimura T, Faul JL, Berry GJ, *et al.* Simvastatin attenuates smooth muscle neointimal proliferation and pulmonary hypertension in rats. *Am J Respir Crit Care Med* 2002; 166:1403-1408
43. Guerard P, Rakotoniaina Z, Goirand F, *et al.* The HMG-CoA reductase inhibitor, pravastatin, prevents the development of monocrotaline-induced pulmonary hypertension in the rat through reduction of endothelial cell apoptosis and overexpression of eNOS. *Naunyn Schmiedebergs Arch Pharmacol* 2006; 373:401-414
44. Sun X, Ku DD. Rosuvastatin provides pleiotropic protection against pulmonary hypertension, right ventricular hypertrophy, and coronary endothelial dysfunction in rats. *Am J Physiol Heart Circ Physiol* 2008; 294:H801-809
45. Mawatari E, Hongo M, Sakai A, *et al.* Amlodipine prevents monocrotaline-induced pulmonary arterial hypertension and prolongs survival in rats independent of blood pressure lowering. *Clin Exp Pharmacol Physiol* 2007; 34:594-600
46. Hongo M, Mawatari E, Sakai A, *et al.* Effects of nicorandil on monocrotaline-induced pulmonary arterial hypertension in rats. *J Cardiovasc Pharmacol* 2005; 46:452-458
47. Itoh T, Nagaya N, Murakami S, *et al.* C-type natriuretic peptide ameliorates monocrotaline-induced pulmonary hypertension in rats. *Am J Respir Crit Care Med* 2004;170:1204-1211
48. Nagaya N, Okumura H, Uematsu M, *et al.* Repeated inhalation of adrenomedullin ameliorates pulmonary hypertension and survival in monocrotaline rats. *Am J Physiol Heart Circ Physiol* 2003; 285:H2125-2131
49. Zhou H, Liu H, Porvasnik SL, *et al.* Heme oxygenase-1 mediates the protective effects of rapamycin in monocrotaline-induced pulmonary hypertension. *Lab Invest* 2006; 86:62-71
50. Maruyama H, Watanabe S, Kimura T, *et al.* Granulocyte colony-stimulating factor prevents progression of monocrotaline-induced pulmonary arterial hypertension in rats. *Circ J* 2007; 71: 138 -143
51. Sawada H, Mitani Y, Maruyama J, *et al.* A nuclear factor-KB inhibitor pyrrolidine dithiocarbamate ameliorates pulmonary hypertension in rats. *Chest* 2007; 132:1265-1274
52. Voelkel NF, Tuder RM, Bridges J, Arend WP. Interleukin-1 receptor antagonist treatment reduces pulmonary hypertension generated in rats by monocrotaline. *Am J Respir Cell Mol Biol* 1994; 11: 664-675
53. Kimura H, Kasahara Y, Kurosu K, *et al.* Alleviation of monocrotaline-induced pulmonary hypertension by antibodies to monocyte chemotactic and activating factor/monocyte chemoattractant protein-1. *Lab Invest* 1998; 78: 571-581
54. Lu J, Shimpo H, Shimamoto A, *et al.* Specific inhibition of p38 mitogen-activated protein kinase with FR167653 attenuates vascular proliferation in monocrotaline-induced pulmonary hypertension in rats. *J Thorac Cardiovasc Surg* 2004;128: 850-859
55. Rosenberg HC, Rabinovitch M. Endothelial injury and vascular reactivity in monocrotaline pulmonary hypertension. *Am J Physiol Heart Circ Physiol* 1988; 255: H1484-H1491
56. Maruyama J, Maruyama K. Impaired nitric oxide-dependent responses and their recovery in hypertensive pulmonary arteries of rats. *Am J Physiol Heart Circ Physiol* 1994; 266: H2476-H2488

57. Mitani Y, Maruyama K, Sakurai M. Prolonged administration of L-arginine ameliorates chronic pulmonary hypertension and pulmonary vascular remodeling in rats. *Circulation* 1997; 96: 689-697
58. Stenmark KR, Morganroth ML, Remigio LK, et al. Alveolar inflammation and arachidonate metabolism in monocrotaline-induced pulmonary hypertension. *Am J Physiol Heart Circ Physiol* 1985; 248: H859-H866
59. Kamezaki F, Tasaki H, Yamashita K, et al. Gene transfer of extracellular superoxide dismutase ameliorates pulmonary hypertension in rats. *Am J Respir Crit Care Med* 2008; 177: 219-226
60. Ikeda Y, Yonemitsu Y, Kataoka C, et al. Anti-monocyte chemoattractant protein-1 gene therapy attenuates pulmonary hypertension in rats. *Am J Physiol Heart Circ Physiol* 2002; 283: H2021-H2028
61. Nagaya N, Yokoyama C, Kyotani S, et al. Gene transfer of human prostacyclin synthase ameliorates monocrotaline-induced pulmonary hypertension in rats. *Circulation* 2000; 102:2005-2010
62. Ito T, Okada T, Mimuro J, et al. Adenoassociated virus-mediated prostacyclin synthase expression prevents pulmonary arterial hypertension in rats. *Hypertension* 2007 a; 50:531-536
63. Zhao YD, Campbell AI, Robb M, et al. Protective role of angiotensin-1 in experimental pulmonary hypertension. *Circ Res* 2003; 92:984-991
64. Zhao YD, Courtman DW, Ng DS, et al. Microvascular regeneration in established pulmonary hypertension by angiogenic gene transfer. *Am J Respir Cell Mol Biol* 2006; 35:182-189
65. Ito T, Okada T, Miyashita H, et al. Interleukin-10 expression mediated by an adeno-associated virus vector prevents monocrotaline-induced pulmonary arterial hypertension in rats. *Circ Res* 2007 b; 101:734-741
66. Baber SR, Deng, Master RG, et al. Intratracheal mesenchymal stem cell administration attenuates monocrotaline induced pulmonary hypertension and endothelial dysfunction. *Am J Physiol Heart Circ Physiol* 2007; 292: H1120-H1128
67. Campbell AIM, Kuliszewski MA, Stewart DJ. Cell-based gene transfer to the pulmonary vasculature. Endothelial nitric oxide synthase overexpression inhibits monocrotaline-induced pulmonary hypertension. *Am J Respir Cell Mol Biol* 1999; 21: 567-575
68. Campbell AIM, Zhao Y, Sandhu R, et al. Cell-based gene transfer of vascular endothelial growth factor attenuates monocrotaline-induced pulmonary hypertension. *Circulation* 2001; 104: 2242-2248
69. Zhao YD, Courtman DW, Deng Y, et al. Rescue of monocrotaline-induced pulmonary arterial hypertension using bone marrow-derived endothelial-like progenitor cells: efficacy of combined cell and eNOS gene therapy in established disease. *Circ Res* 2005; 96: 442-450
70. Asahara T, Kawamoto A. Endothelial progenitor cells for postnatal vasculogenesis. *Am J Physiol Cell Physiol* 2004; 287: C572-C579
71. Sahara M, Sata M, Morita T, et al. Diverse contribution of bone marrow-derived cells to vascular remodeling associated with pulmonary arterial hypertension and arterial neointimal formation. *Circulation* 2007; 115: 509-517
72. Raoul W, Wagner-Ballon O, Saber G, et al. Effects of bone marrow-derived cells on monocrotaline- and hypoxia-induced pulmonary hypertension in mice. *Respir Res* 2007; 8: 8
73. Kanki-Horimoto S, Horimoto H, Mieno S, et al. Implantation of mesenchymal stem cells overexpressing endothelial nitric oxide synthase improves right ventricular impairments caused by pulmonary hypertension. *Circulation* 2006; 114(suppl I); I-181-I-185
74. Takahashi M, Nakamura T, Toba T, et al. Transplantation of endothelial progenitor cells into the lung to alleviate pulmonary hypertension in dogs. *Tissue Eng* 2004; 10: 771-779

75. Wang X, Zhang F, Shang Y, *et al.* Transplantation of autologous endothelial progenitor cells may be beneficial in patients with idiopathic pulmonary arterial hypertension. *J Am Coll Cardiol* 2007; 49:1566–1571.

Chapter 6

Stem cells from rats with pulmonary hypertension reduce pulmonary parenchymal damage, medial hypertrophy of pulmonary arterioles, and right ventricular hypertrophy in rats with pulmonary hypertension

S. Umar
Y. P. de Visser
P. Steendijk
C. I. Schutte
E.H. Laghmani
G. T. M. Wagenaar
W. H. Bax
D. A. Pijnappels
D. E. Atsma
M. J. Schalijs
E. E. van der Wall
A. van der Laarse

Submitted for publication

Abstract

Background: Pulmonary arterial hypertension (PAH) is a chronic lung disease characterized by increased pulmonary artery pressure, pulmonary vascular damage and medial hypertrophy of pulmonary arterioles. Stem cell therapy may improve pulmonary damage in patients with PAH.

Purpose: To test the effects of treatment with bone marrow-derived mesenchymal stem cells (MSCs) obtained from donor rats with monocrotaline (MCT)-induced PAH to recipient rats with MCT-induced PAH on (i) pulmonary artery pressure, (ii) lung histology, (iii) pulmonary arteriolar diameters, and (iv) right ventricular (RV) hypertrophy. This model was chosen to mimic autologous stem cell therapy.

Methods: Female Wistar rats were divided in 4 groups, receiving either PBS (control, n=10), MCT (60 mg/kg, n=10), MCT (60 mg/kg) 14 days later followed by administration of 10^6 MSCs per rat i.v. (n=10), or 10^6 skin fibroblasts (SFs) per rat i.v. (n=10). MSCs were obtained from bone-marrow of PAH rats treated with MCT (60 mg/kg) for 28 days. SFs were obtained from healthy rats. At 28 days after MCT (or PBS) administration, the animal was sacrificed, lungs and heart were excised, weighed, fixed and examined by histology.

Results: At 28 days after MCT-treatment, rats had PAH (RV peak systolic pressure of 42 ± 17 vs. 27 ± 5 mmHg in control; $p<0.02$), and increased lung weight (1.66 ± 0.32 vs. 0.96 ± 0.15 g in control; $p<0.05$). Lung histology demonstrated severe narrowing of precapillary arterioles, thickening of arteriolar walls (3.4 times increased vs. control; $p<0.001$), thickening of alveolar septa (3.5 times increased vs. control; $p<0.001$), and increased RV mass (by 63%; $p<0.01$). Treatment with MSCs for 14 days attenuated PAH (31 ± 4 mmHg; n.s. vs. MCT60; n.s. vs. control), and almost normalized lung weight (1.16 ± 0.24 g; $p<0.05$ vs. MCT60), wall thickness of arterioles ($p<0.01$ vs. MCT60), thickness of alveolar septa ($p<0.01$ vs. MCT60), and RV hypertrophy ($p<0.01$ vs. MCT60). In MCT-treated rats i.v. therapy with SFs from healthy rats had less beneficial effects than i.v. therapy with MSCs from PAH rats.

Conclusions: Intravenous administration of MSCs from donor rats with PAH to recipient rats with PAH decreased RV peak systolic pressure, pulmonary arteriolar narrowing, alveolar septum thickening, and RV hypertrophy. These results suggest that autologous stem cell therapy may help to alleviate cardiac and pulmonary symptoms in patients with PAH.

Introduction

Pulmonary arterial hypertension (PAH) is a chronic lung disease characterized by increased pulmonary artery pressure, pulmonary vascular damage and medial hypertrophy of pulmonary arterioles. In the current study we use a well-established model of experimental PAH induction in rats by a single injection of monocrotaline (MCT). MCT, a pyrrolizidine alkaloid derived from *Crotalaria spectabilis*, causes a pulmonary vascular syndrome in rats characterized by proliferative pulmonary vasculitis, PAH, and cor pulmonale. Current lines of evidence of the pathogenesis of MCT-induced pneumotoxicity indicate that MCT is activated to one or more reactive metabolites in the liver, particularly a MCT pyrrole called dehydromonocrotaline [1-3], and is then transported by red blood cells to the lung [4], where it initiates endothelial injury [5,6]. The endothelial injury does not appear to be acute cell death but rather a pathological condition that leads to smooth muscle cell proliferation in the media of pulmonary arteriolar walls by unknown mechanisms. The role of inflammation in the progression of MCT-induced pulmonary vascular disease is uncertain. Both perivascular inflammation and platelet activation have been proposed as processes contributing to the response of the vascular media [3]. The resulting lung lesions mimic the changes observed in lungs of the patients with PAH. There is a positive correlation between progressive PAH, thickening of the medial wall of small pulmonary arteries and arterioles, and RV hypertrophy as a function of time [7].

PAH is a difficult disease to treat and has been shown to be refractory to most of the conventional therapies. Many treatment modalities have been employed for treating PAH ranging from calcium channel blockers [8], phosphodiesterase inhibitors [9], endothelin receptor antagonists [10] to prostacyclin analogues [11], but still a standard treatment is lacking. Combination therapy has also been employed more recently [12], but still no definitive results have been obtained.

Stem cell therapy may constitute a new treatment modality for patients with PAH. Different modes of administration of stem cells including intravenous [13], intratracheal [14], and direct implantation of cells into the lungs [15] have been used. We have used the intravenous route of administration being a safe and feasible method of cell injection.

We hypothesize that when administered intravenously, the mesenchymal stem cells (MSCs) filter through the lungs and have a chance to engraft at the sites of lung parenchymal or vascular damage. Once these cells reside in damaged tissue, they start secreting 'pro-survival factors' such as growth factors or cytokines, hence helping improve the tissue's condition by paracrine mechanisms [16] or possibly by differentiating into endothelial or smooth muscle cells [17] and help to ameliorate pulmonary damage.

Although i.v. administration of bone marrow-derived MSCs to treat PAH has been studied already [13], our purpose was to treat recipient rats with MCT-induced PAH with bone marrow-derived MSCs obtained from donor rats with MCT-induced PAH, to mimic autologous stem cell transplantation. In this study we demonstrate that treatment of rats with PAH with MSCs from donor rats with PAH results in (i) lower pulmonary artery pressure, (ii) lower lung weight, (iii) less

abnormalities of pulmonary architecture, and (*iv*) less RV hypertrophy, compared to rats with PAH that were not treated with MSCs.

Materials and Methods

Animals

All animals were treated in accordance with the national guidelines and with permission of the Animal Experiments Committee of the Leiden University Medical Center. Eight-week-old female Wistar rats weighing 200-250 g (Harlan, Zeist, The Netherlands) were treated with MCT (Sigma-Aldrich, Zwijndrecht, The Netherlands) to produce pulmonary hypertension. Rats were randomly assigned to four groups. The animals received a single subcutaneous injection of MCT diluted in phosphate-buffered saline (PBS) (MCT60, 60 mg/kg body wt, $n = 10$) or the same dose of MCT followed 14 days later by intravenous injection into the jugular vein of 10^6 Dil-labeled mesenchymal stem cells (MCT+MSC, $n = 10$), or 10^6 Dil-labeled skin fibroblasts (MCT+SF, $n = 10$). Control (Cont) rats ($n = 10$) were injected with an equal volume of PBS. The animals were housed, two animals per cage, with a 12:12-h light-dark cycle and an unrestricted food and water supply. After 4 wk, RV pressure was measured, and the rats were sacrificed.

Haemodynamic measurements

At day 28 after MCT (or PBS) administration, RV pressure was measured as published previously [18]. Briefly, the rats were sedated by inhalation of a mixture of isoflurane (4%) and oxygen. Subsequently, general anesthesia was induced by intraperitoneal (i.p.) injection of a fentanyl-fluanison-midazolam mixture in a dose of 0.25 mL/100 g body weight. The mixture consisted of two parts Hypnorm (0.315 mg/mL fentanyl+10 mg/mL fluanison; Vital-Pharma, Maarheeze, the Netherlands): one part Dormicum (5 mg/mL midazolam; Roche, Mijdrecht, the Netherlands) and one part saline. The animals were placed on a controlled warming pad to keep body temperature constant. After a tracheotomy was performed, a cannula (18G, Biovalve, Vygon, Ecoen, France) was inserted, and the animals were mechanically ventilated using a pressure-controlled respirator and a mixture of air and oxygen. The animals were placed under a stereomicroscope (Zeiss, Hamburg, Germany). After a midsternal thoracotomy was performed, a combined pressure-conductance catheter (model FT212, SciSense, London, Ontario, Canada) was introduced via the apex into the RV and positioned towards the pulmonary valve. The catheter connected to a signal processor (FV898 Control Box, SciSense) and RV pressures were recorded digitally. All data were acquired at a sample rate of 2,000 Hz and analyzed off-line by dedicated software (SciSense).

Cell isolation

Mesenchymal stem cell isolation and culture

Four weeks after MCT treatment (60 mg/kg, $n=10$) adult donor rats were anesthetized with isoflurane and killed by i.v. injection of KCl (100 mmol/L). Femurs and tibiae were removed and cleaned of all connective tissue and attached muscles. The proximal ends were clipped and bones placed in microfuge tubes supported by plastic inserts cut from 200 μ L pipette tips. Microfuge tubes were briefly centrifuged at 13,000 rpm for 1 min. The marrow pellets were resuspended in 10 mL of growth medium [Dulbecco's modified Eagle's medium (DMEM; Invitrogen, Breda, the Netherlands), supplemented with 15% fetal bovine serum (FBS; Invitrogen), penicillin (50 U/L), streptomycin (50 μ g/L), and amphotericin B solution (0.25 μ g/mL; Sigma-Aldrich)] supplemented with 6% heparin (400 IE/mL). This suspension was centrifuged again at 1000 rpm for 10 min. Next, the pellet was resuspended in 7 mL of growth medium supplemented with 5.75 μ g/mL DNase I (Sigma-Aldrich). The cells were plated in 25-cm² culture flasks (Becton Dickinson, Franklin Lakes, NJ, USA) and the culture was kept in a humidified hypoxic incubator CO₂/O₂ (5%/5%) at 37°C. The non-adherent cells were replated after 6 h. Two days later, non-adherent cells were removed by changing the medium to 12 mL of fresh growth medium. The medium was refreshed twice a week until the primary cultures were confluent. The advantages of culturing MSCs in a hypoxic environment have been documented frequently [19-23].

Skin fibroblasts

Skin fibroblasts (SFs) were grown from pieces of skin of healthy rats anesthetized by excess CO₂ and killed by i.v. injection of KCl (100 mmol/L). Skin samples were transferred to porcine gelatin (Sigma-Aldrich)-coated flasks, and cultured in DMEM containing 100 U/mL penicillin, 100 μ g/mL streptomycin, and 10% fetal bovine serum (FBS, all from Invitrogen) in a normoxic incubator (20% O₂ and 5% CO₂) at 37°C. Outgrowth of cells was visible 2 days after culture initiation. Three days later the skin pieces were removed and the skin fibroblasts were detached with trypsin-EDTA solution (Invitrogen), and reseeded in new culture flasks. For intravenous infusion into rats which had had MCT administration 14 days earlier, we used passage 4-6.

Cell injection

Before injection, the cells were trypsinized and labelled with the viable fluorescent dye CM-Dil according to the manufacturer's recommendations (CellTracker™, Molecular Probes, Invitrogen). At day 14, each rat was fixed on its back, and anaesthetized with isoflurane. The jugular vein in the neck was prepared free. A venous catheter (20G, Biovalve) was introduced in the vein. Through this catheter 1 mL of cell suspension (10⁶ cells/mL) was injected slowly. This suspension contained MSCs from rats with MCT-induced PAH or SFs from healthy rats. After removal of the catheter, the vein was pressed for 5 min to allow closure of the puncture and the skin was closed. The control animals received i.v. injections of 1 mL of PBS.

Tissue preparations

After hemodynamic measurements, lungs and heart were removed, snap-frozen in liquid nitrogen, and stored at -80°C until isolation of RNA. For histology studies, the trachea was cannulated (18G, Biovalve), and the lungs were fixed *in situ* via the trachea cannula with buffered formaldehyde (4% paraformaldehyde in PBS, pH 7.4) at a pressure of 25 cm H_2O for 5 min. After removal of lungs and hearts, lungs were fixed (additionally) in formaldehyde for 24 h at 4°C , and embedded in paraffin after dehydration in a graded alcohol series and xylene.

Real-time RT-PCR

Total RNA was isolated from lung tissue homogenates using guanidium-phenol-chloroform extraction and isopropanol precipitation (RNA-Bee, Tel-Test Inc., Bio-Connect BV, Huissen, the Netherlands). The RNA sample was dissolved in RNase-free water and quantified spectrophotometrically. First-strand cDNA synthesis was performed with the SuperScript Choice System (Life Technologies, Breda, the Netherlands) by mixing 2 μg total RNA with 0.5 μg of oligo(dT)12-18 primer in a total volume of 12 μL . After the mixture was heated at 70°C for 10 min, a solution containing 50 mmol/L Tris-HCl (pH 8.3), 75 mmol/L KCl, 3 mmol/L MgCl_2 , 10 mmol/L DTT, 0.5 mmol/L dNTPs, 0.5 μL RNase inhibitor, and 200 U Superscript Reverse Transcriptase was added, resulting in a total volume of 20.5 μL . This mixture was incubated at 42°C for 1 h; total volume was adjusted to 100 μL with RNase-free water and stored at -80°C until further use. For *real-time* quantitative PCR, 1 μL of first-strand cDNA diluted 1:10 in RNase-free water was used in a total volume of 25 μL , containing 12.5 μL 2x SYBR Green PCR Master Mix (Applied Biosystems, Foster City, CA, USA) and 200 ng of each primer. Primers, designed with the Primer Express software package (Applied Biosystems), are:

Interleukin-6:	forward	5'-ATATGTTCTCAGGGAGATCTTGGAA-3'
	reverse	5'-TGCATCATCGCTGTTTCATACAA-3'
TNFα:	forward	5'-ACAAGGCTGCCCGACTAT-3'
	reverse	5'-CTCCTGGTATGAAGTGGCAAATC-3'
Endothelin-1:	forward	5'-TGTGCTCACCAAAAAGACAAGAA-3'
	reverse	5'-GGTACTTTGGGCTCGGAGTTC-3'
VEGF-A:	forward	5'-GCGGATCAAACCTCACCAA-3'
	reverse	5'-TTGGTCTGCATTCACATCTGCTA-3'
NOS-2:	forward	5'-GCTGCATGTGACTCCATCGA-3'
	reverse	5'-TCTCCATTGCCCGAGTTTTT-3'
NOS-3:	forward	5'-CCCTGCCAACGTGGAGAT-3'
	reverse	5'-ATCAAAGCGGCCATTTCT-3'
Tenascin-C:	forward	5'-TCACAGCTCTCGATGGTCCAT-3'
	reverse	5'-TGGCCAAGGCTTCTGAGTCT-3'
MMP2:	forward	5'-CCCACGAAGCCTTGTTTACC-3'
	reverse	5'-GAAGCGGAACGGGAAGTTG-3'
MMP9:	forward	5'-TCCGCAGTCCAAGAAGATTTTC-3'
	reverse	5'-GCACCGTCTGGCCTGTGTA-3'
β-actin:	forward	5'-GGCTCCTAGCACCATGAAGATC-3'
	reverse	5'-GAGCCACCAATCCACACAGA-3'

PCR reactions, consisting of 95°C for 10 min (1 cycle), 94°C for 15 s, and 60°C for 1 min (40 cycles), were performed on an ABI Prism 7900 HT Fast Real Time PCR system (Applied Biosystems) of the Leiden Genome Technology Center. Data were analyzed with the ABI Prism 7900 sequence detection system software (version 2.2) and quantified with the comparative threshold cycle method with β -actin as a housekeeping gene reference [24].

Histochemical analysis

Fixed lung tissue, embedded in paraffin, was cut into 4- μ m-thick sections and stained with hematoxylin-phloxin-saffron for determination of thickness of alveolar septa.

Tracing the Dil-labeled stem cells in the lungs

Four μ m thick sections of lung tissue were deparaffinised in Ultraclear (Klinipath, Duiven, the Netherlands) and rehydrated in decreasing series of graded alcohols (100-25%), followed by two 5-min washes in distilled water and TBS (150 mmol/L NaCl, 10 mmol/L Tris-HCl, pH 8.0). Subsequently, nuclei were stained with 10 μ g/mL Hoechst 33342 solution (Molecular Probes, Invitrogen) for 10 min at room temperature. Sections were washed three times with TBS and mounted with Vectashield (Vector Laboratories, Burlingame, CA, USA).

Antibodies

Primary antibodies used were mouse anti α -smooth muscle actin (ASMA) antibody (S2547, Sigma-Aldrich), mouse anti-ED1 antibody (gift from Dr. E. de Heer, Department of Pathology, LUMC) to stain for interstitial monocytes/macrophages, mouse anti-myeloperoxidase (MPO) antibody (Thermo Fisher Scientific, Waltham, MA, USA) for neutrophil identification, and rabbit anti-CC10 antibody (C5828-03, United States Biological, Swampscott, MA, USA) to identify Clara cells.

Secondary HRP conjugated antibody were goat anti-mouse-IgG conjugated to HRP (sc2005, Santa Cruz Biotechnology, Santa Cruz, CA, USA), or goat anti-rabbit-IgG conjugated to HRP (sc2004, Santa Cruz Biotechnology). Substrate was 3,3'-diaminobenzidine (DAB)(Pierce, Perbio Science, Etten-leur, the Netherlands) or NovaRed (Vector Laboratories).

Immunoperoxidase staining protocol

Tissue was deparaffinized in Ultraclear two times for 10 min each, followed by 100% ethanol 2 times for 5 min each. The sections were rehydrated in decreasing graded alcohols (from 96% to 50%) for 3 min each and washed twice for 5 min each in distilled water and PBS. To inhibit endogenous peroxidase activity, the sections were incubated with 0.3% H₂O₂ in PBS for 20 min at room temperature. Next, the sections were boiled in 1.8% citrate buffer in a microwave for 12 min at 98°C. The next step was incubation in blocking solution, consisting of 5% bovine serum albumin (BSA) in PBS, for 1 hour at room temperature. Subsequently, sections were incubated with primary antibody diluted in PBS containing 1% BSA

and 0.05% Tween (100 μ L per sample), in a dilution of 1:100, overnight at room temperature. The sections were washed in PBS 3 times for 5 min each. Next, the sections were incubated with secondary antibody diluted in PBS containing 1% BSA and 0.05% Tween (100 μ L per sample), in a dilution of 1:200, for 60 min at room temperature. After washing, 100 μ L DAB was added to the sections (250 μ L of 10x DAB solution and 2250 μ L buffer (Pierce)) for 5 min, and washed again. Sections were stained in 1% hematoxylin for 1 min, and rinsed under running tap water for 10 min. In the end, to dehydrate the slides, sections were incubated in 50%, 70% and 96% ethanol for 3 min each, in 100% ethanol 2 times for 5 min, and in Ultraclear 2 times for 10 min each. Next, sections were mounted with D.P.X (BDH, Brunschwig Chemie, Amsterdam, the Netherlands), and examined under the microscope with light microscopy.

Microscopy

Stained slides were photographed using a microscope (Nikon Eclipse, Nikon Europe, Badhoevedorp, the Netherlands) equipped with 10x, 20x, 40x and 100x objectives and a digital camera (model DXM1800, Nikon). This microscope performed both light microscopy and fluorescence microscopy.

Quantitative image analysis

Quantitative image analysis was performed with Image-Pro Plus software (Media Cybernetics, Silver Spring, MD, USA). For determination of alveolar septum thickness hematoxylin-phloxin-saffron stained lung tissue was photographed at high magnification (100x). At locations distant from branch points and arterioles alveolar septum thickness was measured with calipers in Image-Pro Plus. For determination of precapillary arteriolar wall thickness, ASMA-stained lung tissue was photographed at high magnification (100x). Wall thickness of arterioles localized at branch points of alveolar septa was measured with calipers in Image-Pro Plus.

Assessment of RV hypertrophy

To quantify the degree of right ventricular hypertrophy hearts were harvested, followed by the removal of the left and right atrium. Hereafter the right ventricular free wall (RV) was dissected, weighted separately from the left ventricle (LV), including the interventricular septum (IVS), and frozen immediately in liquid nitrogen and stored at -80°C . RV mass is used as an indicator of right ventricular hypertrophy.

Statistical analysis

The effect of treatment (cell therapy with MSCs, cell therapy with SFs) was evaluated by one-way ANOVA followed by Bonferroni's *post-hoc* test. SPSS12 for Windows (SPSS Inc., Chicago, IL, USA) was used for statistical analysis. Differences were considered significant at $p < 0.05$. Values are represented by means \pm SD, unless stated otherwise.

Results

RV peak systolic pressure

At the end of the experimental period, RV peak systolic pressures were significantly higher in MCT60 group than in the control group, indicating the development of PAH (42 ± 17 vs. 27 ± 5 mmHg in control; $p < 0.02$). In MCT-treated rats that had been given cell therapy with MSCs, mean RV peak systolic pressure was attenuated (31 ± 4 mmHg) although not significantly different from MCT60, nor from control. In the MCT+SF group, the RV peak systolic pressure was 32 ± 6 mmHg, which was not significantly different from MCT60 nor from control (Figure 1).

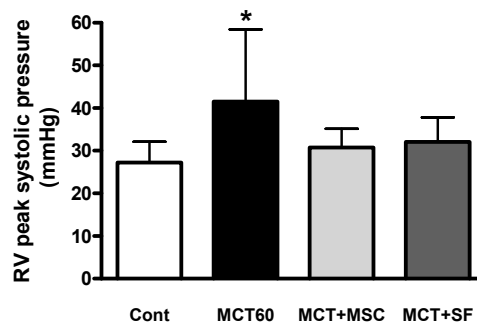


Figure 1. RV peak systolic pressures (mmHg) of Control, MCT60, MCT+MSC and MCT+SF groups are shown. Values are expressed as mean \pm SD (* $p < 0.05$ vs. Control).

Lung weights

Lung weight was 0.96 ± 0.15 g in control animals. Lung weight was significantly increased in the MCT60 group to 1.66 ± 0.32 g ($p < 0.05$ vs. control). With stem cell therapy, lung weight had decreased to 1.16 ± 0.24 g ($p < 0.05$ vs. MCT60). Lung weight in the MCT+SF group was 1.52 ± 0.20 g ($p < 0.05$ vs. control), which was not different from MCT60 (Figure 2). The increase in lung weight observed in the MCT60 and MCT+SF groups is symptomatic for an increased remodeling of lung tissue in these groups, rather than to pulmonary edema [18].

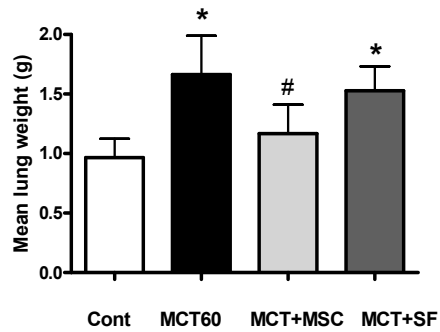


Figure 2. Lung weights (g) of Control, MCT60, MCT+MSC and MCT+SF groups are shown. Values are expressed as mean \pm SD (* $p < 0.05$ vs. Control, # $p < 0.05$ vs. MCT60).

RV hypertrophy

In MCT-treated rats RV mass had increased from 143 ± 26 mg to 233 ± 53 mg ($p < 0.05$). RV mass of MCT-treated rats that had received MSCs was 162 ± 25 mg ($p < 0.01$ vs. MCT60) which was not different from Control. In MCT-treated rats that had received SFs RV mass was 183 ± 33 mg ($p < 0.05$ vs. MCT60) which was not different from Control rats (Figure 3)..

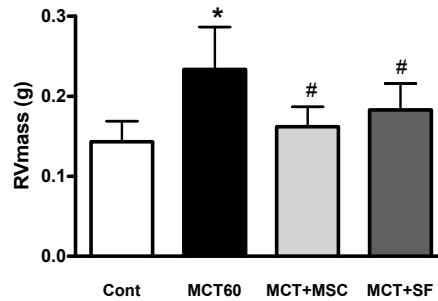


Figure 3. Right ventricular weight (RV mass) of Control, MCT60, MCT+MSC and MCT+SF groups are shown. Values are expressed as mean \pm SD (* $p < 0.05$ vs. Control, # $p < 0.05$ vs. MCT60).

mRNA in pulmonary tissue

Relative concentrations of mRNA encoding IL6, TNF α and MMP2 have increased in lungs of rats with MCT-induced PAH, although only significant for IL6 and MMP2 (Figure 4). However, mRNA encoding ET1 and VEGF-A had decreased significantly in lungs of rats treated with MCT. In the lungs of rats receiving cell therapy relative concentrations of mRNA did not differ, or only slightly, from those in rats of the MCT60 group. mRNA encoding NOS2 and NOS3 did not show changes between the experimental groups of rats (Figure 4).

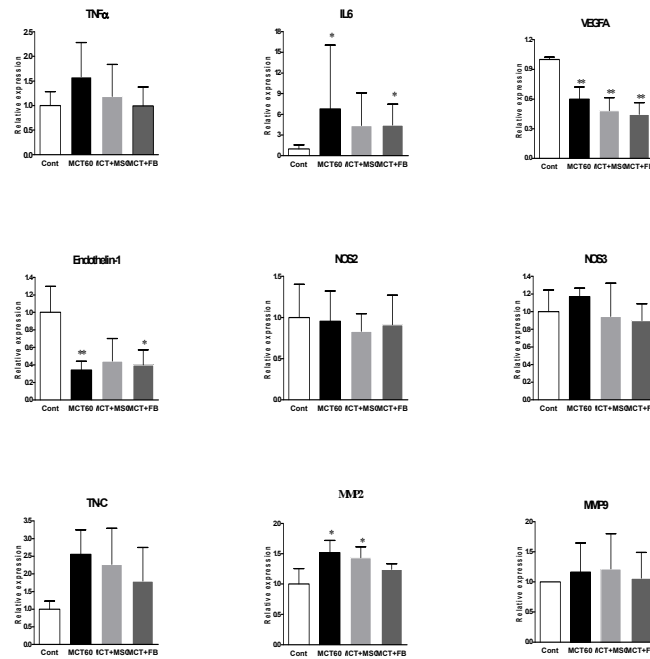


Figure 4. Right ventricular concentrations of mRNA encoding tumor necrosis factor- α (TNF α), interleukin-6 (IL-6), vascular endothelial growth factor-A (VEGFA), endothelin-1 (ET-1), nitric oxide synthase-2 (NOS2), nitric oxide synthase-3 (NOS3), tenascin-C (TN-C), matrix metalloproteinase-2 (MMP2) and matrix metalloproteinase-9 (MMP9). For each mRNA, myocardial concentration is normalized for the concentration found in hearts of PBS-treated rats (controls, Cont). * $p < 0.05$ vs. Cont (control), ** $p < 0.01$ vs. Cont (control)

Mean pulmonary arteriolar wall thickness

Mean pulmonary arteriolar wall thickness was significantly increased in MCT60 group to 343 ± 60 % ($p < 0.05$ vs. control). With MSC therapy, the arteriolar wall thickness had decreased to 120 ± 28 % ($p < 0.05$ vs. MCT60). The wall thickness in the MCT+SF group was 296 ± 35 % ($p < 0.05$ vs. control), which was not different from MCT60 (Figure 5). The increase in pulmonary arteriolar wall thickness observed in the MCT60 and MCT+SF groups represents arteriolar medial hypertrophy in these rats, which is apparently prevented largely by treatment with MSCs.

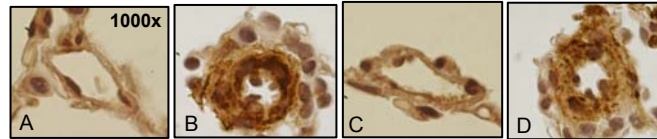


Figure 5a. Immunoperoxidase images of paraffin sections of lung tissue stained with anti α -smooth muscle actin antibody. Representative pulmonary arterioles of Control (panel A), MCT60 (panel B), MCT+MSC (panel C) and MCT+SF (panel D) are shown.

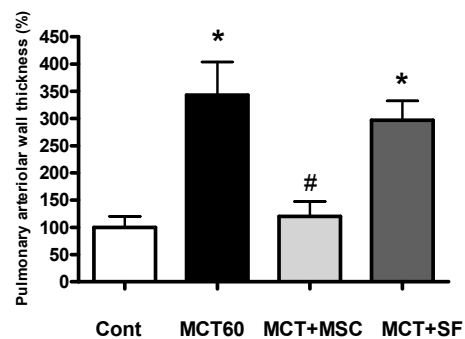


Figure 5b. Pulmonary arteriolar wall thickness (%) of Control, MCT60, MCT+MSC and MCT+SF groups are shown. Values are expressed as mean \pm SD (* $p < 0.05$ vs. Control, # $p < 0.05$ vs. MCT60).

Mean pulmonary alveolar septum thickness

Mean pulmonary alveolar septum thickness was significantly increased in the MCT60 group to 353 ± 56 % ($p < 0.05$ vs. control). With stem cell therapy, the alveolar septum thickness was only 109 ± 20 % ($p < 0.05$ vs. MCT60). Alveolar septum thickness in the MCT+SF group was 309 ± 28 % ($p < 0.05$ vs. control), which was not different from MCT60 (Figure 6). The increase in the mean pulmonary alveolar septum thickness observed in MCT60 and MCT+SF groups is prevented largely by treatment with MSCs.

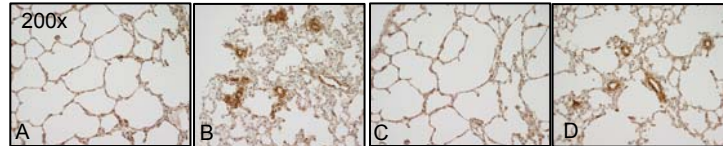


Figure 6a. Immunoperoxidase images of paraffin sections of lung tissue stained with anti α -smooth muscle actin antibody. Lung histology of Control (panel A), MCT60 (panel B), MCT+MSC (panel C) and MCT+SF (panel D) are shown.

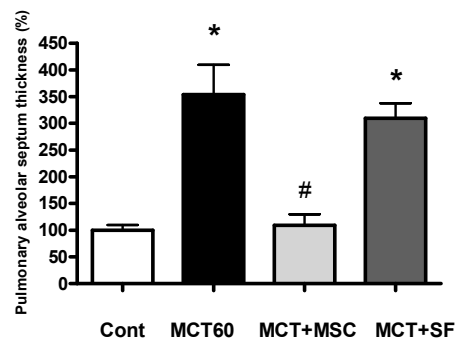


Figure 6b. Pulmonary alveolar septum thickness (%) of Control, MCT60, MCT+MSC and MCT+SF groups are shown. Values are expressed as mean \pm SD (* $p < 0.05$ vs. Control, # $p < 0.05$ vs. MCT60).

Recovery of Dil-labeled MSCs in the lung

In each rat that received cell therapy with MSCs (at day 14) the lungs were found to contain Dil-labeled MSCs at day 28 (Figure 7). Labeled MSCs were located in or near the pulmonary arterioles. They were not positive for CC10, thereby excluding the possibility that injected MSCs had differentiated into Clara cells.

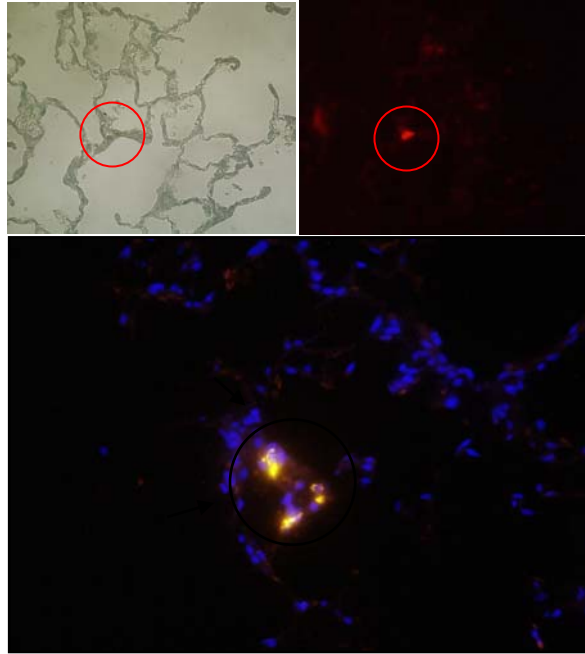


Figure 7. Fluorescence images of Dil-labeled MSCs in lungs acquired using 200x (top panels) and 400x (bottom panel) objectives. Dil-labelled MSCs are stained red, whereas nuclei are stained blue.

Abundance of ED1-positive and MPO-positive cells in lung tissue

Numbers of MPO-positive cells in lung tissue, nor numbers of ED1-positive cells in lung tissue differed between the experimental groups of rats (Figure 8).

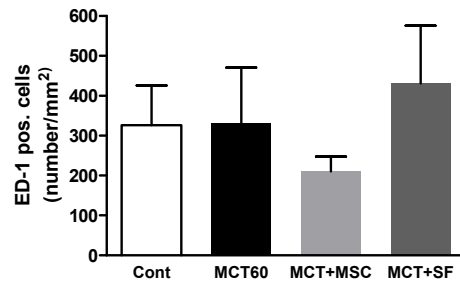


Figure 8a. Number of myeloperoxidase (MPO)-positive cells per image (0.34 mm²) of lung tissue from rats in 4 experimental groups. Per bar, 5 images have been scored. Indicated are mean values and SD.

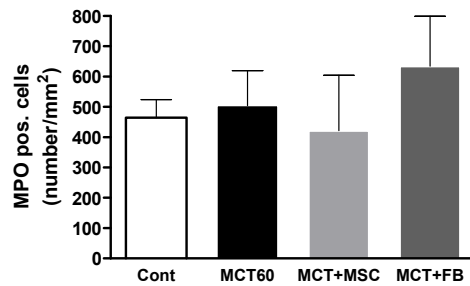


Figure 8b. Number of ED1-positive cells per image (0.34 mm²) of lung tissue from rats in 4 experimental groups. Per bar, 5 images have been scored. Indicated are mean values and SD.

Discussion

In the present study we have shown that i.v. injection of MSCs obtained from donor rats suffering from PAH into recipient rats with PAH has beneficial effects on lungs and heart, such as decreased RV peak systolic pressure, reduced pulmonary arteriolar narrowing and alveolar septum thickening, and less RV hypertrophy, compared to rats not receiving cell therapy.

MCT, a plant-derived toxin, causes endothelial cell injury, as observed in reduced expression of VEGF and endothelin-1, and subsequently an infiltration of mononuclear cells into the perivascular regions of arterioles and muscular arteries when injected i.v. in rats. These animals develop severe PAH after exposure to MCT [25]. Although typical plexiform lesions are not normally found in MCT-induced PAH, it is used as a standard model for PAH and primary pulmonary hypertension.

The important role of inflammation in this model has led to several studies focusing on immunosuppressive and anti-cytokine treatment, and, therefore, raises the question of how inflammation is involved in the installation and evolution of PAH lesions in humans.

Pathological changes in lungs of patients with PAH do not involve the whole pulmonary arterial tree, but remain restricted to certain vessel types. The concentric obliterative arteriopathy concerns muscular arteries of $\leq 500 \mu\text{m}$ in diameter, corresponding to the smaller arteries and their down-stream arterioles. Different and characteristic lesions, such as medial hypertrophy, intimal fibrosis, and typical plexiform lesions, as well as perivascular lymphocytic infiltrates are found [27,27]. Also Dorfmueller and coworkers reported that inflammatory mechanisms play a significant role in MCT-induced PAH in rats and pulmonary arterial hypertension of various origins in humans [28]. As for the MCT-model in the rat, typical plexiform lesions of smaller arteries are usually not found, but the primary importance of inflammation is illustrated by successful therapies using an interleukin-1 receptor antagonist [29] and antibodies to monocyte chemoattractant protein-1 [30]. In the present study we found significantly increased pulmonary expression of IL-6 in rats with MCT-induced PAH, which remained unaffected by cell therapy with SFs and with MSCs, although pulmonary IL6 mRNA concentration in MCT-treated rats that received MSCs was not significantly different from that in control lungs (Fig 4). MCT-induced endothelial cell dysfunction is associated with deregulated expression of vasoactive, mitogenic and proinflammatory mediators that may cause these changes [31,32]. Although we have stained the lung tissue for ED1 and MPO, we did not find ample evidence for interstitial accumulation of monocytes/macrophages and neutrophils in the lung, respectively. In the lungs of patients with pulmonary hypertension there is medial hypertrophy of arteries and increased pulmonary vascular resistance. In contrast to the lungs of control subjects, NOS was hardly expressed in the vascular endothelium of all type of vessels in the lungs of patients with pulmonary hypertension [33]. The arterial expression of NOS correlated inversely with the severity of histologic changes. The lack of NOS3-derived NO is responsible for proliferation of medial smooth muscle cells [34], which explains the simultaneous presence of, and interrelation between, lack of endothelial NOS

and arterial/arteriolar wall thickening. In the present study we found no indications of a downregulation of NOS3 induced by MCT without or with cell therapy.

In the lungs of patients with pulmonary hypertension endothelial expression of endothelin-1 (ET1) was abundant, predominantly in endothelial cells of pulmonary arteries with medial thickening and intimal fibrosis. At sites of increased ET1 immunoreactivity the ET1 mRNA concentration was high [35]. High levels of ET1 may induce proliferation of fibroblasts and increase the production of fibrous tissue *in vitro* [36]. In the present study, expression of ET1 in lung tissue of rats with MCT-induced PAH is markedly depressed, is unaffected by cell therapy with SFs, but has improved somewhat by cell therapy with MSCs.

In our study, we have observed remodeling of lung tissue in MCT-induced PAH as depicted by an increase in lung weights in MCT60 and MCT+SF groups (Fig. 2). The increase in lung weights observed in these groups is indicative for an increased ECM deposition in lung tissue in these groups, rather than pulmonary edema [18]. In addition, there was an increase in the mean alveolar septal thickness along with a higher incidence of discontinuous alveolar septa leading to larger alveolar spaces (Fig. 6). On further histological analysis, the mean pulmonary arteriolar wall thickness was significantly increased in MCT60 and MCT+SF groups (Fig. 5). With regard to the expression of MMPs in lung tissue, we found that MMP9 expression did not differ significantly between the groups, while MMP2 expression was significantly increased in MCT60 and MCT+MSC groups. Although TNC expression was increased in MCT60 group (1.6 times vs. control), the increase was not significant (Fig. 4). Increased expression of TNC has been shown to be associated with progression of clinical and experimental pulmonary hypertension [37,38]. Furthermore, MMP expression and activity are increased in experimental PAH [39]. Cell proliferation and ECM accumulation are also prominent features of idiopathic PAH. An important component of these changes is ECM remodeling, which results from a complex interplay between the synthesis and proteolysis of ECM constituents [40]. Hence any therapy having anti-remodeling effects may also be effective in treating PAH in the patients.

Many treatment options for PAH have been tested so far, but an effective therapy is lacking. Cell therapy constitutes a novel therapeutic option for PAH patients. Several groups have tested several cell types to treat experimental PAH, including endothelial progenitor cells [41], unfractionated bone marrow-derived cells [42,43], and mesenchymal stem cells (MSCs)[13]. MSCs are unique in possessing (*i*) a potential to differentiate into other cell types, and (*ii*) an ability to secrete paracrine factors leading to improvements in tissue injury [44]. Stem cell therapy using bone marrow-derived MSCs may actively replace differentiated cells that were damaged by MCT and/or contribute to tissue repair by secreting a wide variety of cytokines and growth factors. Generally the highest levels of engraftment are observed in tissues that are severely injured. Nagaya and coworkers recovered i.v. administered endothelial progenitor cells (EPCs) engrafted in pulmonary arterioles and capillaries of rats with MCT-induced PAH and differentiated endothelial cells [45]. With stem cell therapy we found anti-remodeling effects in the MCT+MSC group including a decrease in lung weights (Fig. 2), alveolar septal thickness (Fig. 6) and arteriolar wall thickness (Fig. 5), combined with an improvement in pulmonary architecture.

In the lungs we found most Dil-labeled MSCs engrafted in or near the arterioles (Fig. 7). Their therapeutic effect is, therefore, interpreted to originate from their paracrine effect, *i.e.* the production of cytokines and growth factors. These factors promote angiogenesis and may stop the proliferative thickening of arteriolar medial layers. I.v. administration of pulmonary artery-derived smooth muscle cells that were *in vitro* transduced with the VEGF-A gene was shown to have a substantial therapeutic effect in rats with MCT-induced PAH, whereas the use of the same cell type without gene transduction was without effect [46].

Apparently, the paracrine effects of intrapulmonary engrafted MSCs are more important than the differentiation of engrafted MSCs into vascular smooth muscle cells, endothelial cells, and/or Clara cells. With the anti-CC10 antibody we were unable to find any Dil-labeled MSC in the lung tissue that was CC10 positive. In contrast to the marked benefits of the therapy with i.v. MSCs, the effects obtained after injection with SFs were small, if present at all. Earlier Campbell and coworkers have used pulmonary artery-derived smooth muscle cells (PA-SMCs) injected i.v. together with MCT and found no therapeutic effect on pulmonary artery pressure [47]. If PA-SMCs were injected 2 weeks after MCT administration, cell therapy had no effect [46]. I.v. injected skin fibroblasts 3 days after MCT administration had no therapeutic effect as assessed 3 weeks later [41]. Using skin fibroblasts from healthy rats, injected i.v. in rats 2 weeks after MCT administration, we found no significant therapy effect on lung weight, arteriolar wall thickness, and alveolar septum thickness, although an unexplained therapy effect on RV mass is observed. Compared to injected MSCs, the injected SFs had slight therapeutic effects that may be ascribed to their inability to secrete large quantities of cytokines and growth factors.

Conclusion

In conclusion, i.v. administration of bone marrow-derived MSCs obtained from donor rats suffering from PAH into recipient rats with PAH decreases RV peak systolic pressure, pulmonary arteriolar narrowing, alveolar septum thickening, and RV hypertrophy. Based on these results, the use of autologous bone marrow-derived MSCs to treat PAH in humans is recommended.

Acknowledgements

Dr. J.W.A. van der Hoorn (TNO-Prevention & Health, Leiden) is gratefully acknowledged for staining lung tissue. The anti-ED1 antibody was a kind gift from Dr. E. de Heer (Department of Pathology, Leiden University Medical Center).

References

1. Butler WH, Mattocks AR, Barnes JM. Lesions in the liver and lungs of rats given pyrrole derivatives of pyrrolizidine alkaloids. *J Pathol* 1970; 100: 169-75.
2. Lafranconi WM, Huxtable RJ. Hepatic metabolism and pulmonary toxicity of monocrotaline using isolated perfused liver and lung. *Biochem Pharmacol* 1984; 33: 2479-84.
3. Wilson DW, Segall HJ, Pan LC, Lame MW, Estep JE, Morin D. Mechanisms and pathology of monocrotaline pulmonary toxicity. *Crit Rev Toxicol* 1992; 22: 307-25.
4. Lamé MW, Jones AD, Morin D, Wilson DW, Segall HJ. Association of dehydromonocrotaline with rat red blood cells. *Chem Res Toxicol* 1997; 10: 694-701.
5. Reindel JF, Hoorn CM, Wagner JG, Roth RA. Comparison of response of bovine and porcine pulmonary arterial endothelial cells to monocrotaline pyrrole. *Am J Physiol Lung Cell Mol Physiol* 1991; 261: L406-L414.
6. Reindel JF, Roth RA. The effects of monocrotaline pyrrole on cultured bovine pulmonary artery endothelial and smooth muscle cells. *Am J Pathol* 1991; 138: 707-19.
7. Ghodsi F, Will JA. Changes in pulmonary structure and function induced by monocrotaline intoxication. *Am J Physiol Heart Circ Physiol* 1981; 240: H149-H155.
8. Mawatari E, Hongo M, Sakai A, Terasawa F, Takahashi M, Yazaki Y, Kinoshita O, Ikeda U. Amlodipine prevents monocrotaline-induced pulmonary arterial hypertension and prolongs survival in rats independent of blood pressure lowering. *Clin Exp Pharmacol Physiol* 2007; 34:594-600.
9. Dony E, Lai Y, Dumitrascu R, Pullamsetti SS, Savai R, Ghofrani HA, Weissmann N, Schudt C, Flockerzi D, Seeger W, Grimminger F, Schermuly RT. Partial reversal of experimental pulmonary hypertension by phosphodiesterase 3/4 inhibition. *Eur Respir J* 2008;31:599-610.
10. Nishida M, Eshiro K, Okada Y, Takaoka M, Matsumura Y. Roles of endothelin ET_A and ET_B receptors in the pathogenesis of monocrotaline-induced pulmonary hypertension. *J Cardiovasc Pharmacol* 2004; 44:187-91.
11. Obata H, Sakai Y, Ohnishi S, Takeshita S, Mori H, Kodama M, Kangawa K, Aizawa Y, Nagaya N. Single injection of a sustained-release prostacyclin analog improves pulmonary hypertension in rats. *Am J Respir Crit Care Med* 2008; 177:195–201.
12. Clozel M, Hess P, Rey M, Iglarz M, Binkert C, Qiu C. Bosentan, sildenafil, and their combination in the monocrotaline model of pulmonary hypertension in rats. *Exp Biol Med* 2006; 231: 967–73.
13. Kanki-Horimoto S, Horimoto H, Mieno S, Kishida K, Watanabe F, Furuya E, Katsumata T. Implantation of mesenchymal stem cells overexpressing endothelial nitric oxide synthase improves right ventricular impairments caused by pulmonary hypertension. *Circulation* 2006; 114(suppl I); I-181-I-185.
14. Baber SR, Deng, Master RG, Bunnell BA, Taylor BK, Murthy SN, Hyman AL, Kadowitz PJ. Intratracheal mesenchymal stem cell administration attenuates monocrotaline induced pulmonary hypertension and endothelial dysfunction. *Am J Physiol Heart Circ Physiol* 2007; 292: H1120-H1128.
15. Takahashi M, Nakamura T, Toba T, Kajiwara N, Kato H, Shimizu Y. Transplantation of endothelial progenitor cells into the lung to alleviate pulmonary hypertension in dogs. *Tissue Eng* 2004; 10: 771-9.
16. Kinnaird T, Stabile E, Burnett MS, Shou M, Lee CW, Barr S, Fuchs S, Epstein SE. Local delivery of marrow-derived stromal cells augments collateral perfusion through paracrine mechanisms. *Circulation* 2004;109:1543-9.
17. Al-Khaldi A, Al-Sabti H, Galipeau J, Lachapelle K. Therapeutic angiogenesis using autologous bone marrow stromal cells: Improved blood flow in a chronic limb ischemia model. *Ann Thorac Surg* 2003;75:204-9.

18. Hessel MH, Steendijk P, den Adel B, Schutte CI, van der Laarse A. Characterization of right ventricular function after monocrotaline-induced pulmonary hypertension in the intact rat. *Am J Physiol Heart Circ Physiol* 2006; 291: H2424-H2430.
19. Lennon DP, Edmison JM, Caplan AI. Cultivation of rat marrow-derived mesenchymal stem cells in reduced oxygen tension: Effects of in vitro and in vivo osteochondrogenesis. *J Cell Physiol* 2001;187:345-55.
20. Grayson WL, Zhao F, Bunnell B, Ma T. Hypoxia enhances proliferation and tissue formation of human mesenchymal stem cells. *Biochem Biophys Res Comm* 2007;358:948-53.
21. Buravkova LB, Anokhina EB. Effect of hypoxia on stromal precursors from rat bone marrow at the early stage of culturing. *Bull Exp Biol Med* 2007; 143: 411-3.
22. Rosova I, Dao M, Capoccia B, Link D, Nolte JA. Hypoxic preconditioning results in increased motility and improved therapeutic potential of human mesenchymal stem cells. *Stem Cells* 2008;26:2173-82.
23. Hu X, Yu SP, Fraser JL, Lu Z, Ogle ME, Wang J-A, Wei L. Transplantation of hypoxia-preconditioned mesenchymal stem cells improves infarcted heart function via enhanced survival of implanted cells and angiogenesis. *J Thorac Cardiovasc Surg* 2008;135:799-808.
24. Pfaffl MW. A new mathematical model for relative quantification in real-time RT-PCR. *Nucleic Acids Res* 2001; 29: e45.
25. Nishimura T, Faul JL, Berry GJ, Veve I, Pearl RG, Kao PN. 40-O-(2-Hydroxyethyl)-rapamycin attenuates pulmonary arterial hypertension and neointimal formation in rats. *Am J Resp Crit Care Med* 2001; 163: 498-502.
26. Tuder RM, Groves B, Badesch DB, Voelkel NF. Exuberant endothelial cell growth and element of inflammation are present in plexiform lesions of pulmonary hypertension. *Am J Pathol* 1994; 144: 275-85.
27. Pietra GG. The pathology of primary pulmonary hypertension. In: Rubin L, Rich S, eds. *Primary pulmonary hypertension*. New York, Marcel Dekker, 1997; pp. 19-61.
28. Dorfmueller P, Perros F, Balabanian K, Humbert M. Inflammation in pulmonary arterial hypertension. *Eur Respir J* 2003; 22: 358-63.
29. Voelkel NF, Tuder RM, Bridges J, Arend WP. Interleukin-1 receptor antagonist treatment reduces pulmonary hypertension generated in rats by monocrotaline. *Am J Respir Cell Mol Biol* 1994;11:664-75.
30. Kimura H, Kasahara Y, Kurosu K, Sugito K, Takiguchi Y, Terai M, Mikata A, Natsume M, Mukaida N, Matsushima K, Kuriyama T. Alleviation of monocrotaline-induced pulmonary hypertension by antibodies to monocyte chemoattractant and activating factor/monocyte chemoattractant protein-1. *Lab Invest* 1998;78:571-81.
31. Loscalzo J. Endothelial dysfunction in pulmonary hypertension. *N Engl J Med* 1992; 327: 117-9.
32. Lopes AA, Maeda NY, Goncalves RC, Bydlowski SP. Endothelial cell dysfunction correlates differentially with survival in primary and secondary pulmonary hypertension. *Am Heart J* 2000; 139: 618-23.
33. Giaid A, Saleh D. Reduced expression of endothelial nitric oxide synthase in the lungs of patients with pulmonary hypertension. *N Engl J Med* 1995;333:214-21.
34. Cornwell TL, Arnold E, Boerth NJ, Lincoln TM. Inhibition of smooth muscle cell growth by nitric oxide and activation of cAMP-dependent protein kinase by cGMP. *Am J Physiol Cell Physiol* 1994;267:C1405-C1413.
35. Giaid A, Yanagisawa M, Langleben D, Michel RP, Levy R, Shennib H, Kimura S, Masaki T, Duguid WP, Stewart DJ. Expression of endothelin-1 in the lungs of patients with pulmonary hypertension. *N Engl J Med* 1993;328:1732-9.
36. Kahaleh MB. Endothelin, an endothelial-dependent vasoconstrictor in scleroderma. Enhanced production and profibrotic action. *Arthritis Rheum* 1991;34:978-83.

37. Jones PL, Cowan K, Rabinovitch M. Tenascin-C, proliferation and subendothelial accumulation of fibronectin in progressive pulmonary vascular disease. *Am J Pathol* 1997; 150:1349-60.
38. Jones PL, Rabinovitch M. Tenascin-C is induced with progressive pulmonary vascular disease in rats and is functionally related to increased smooth muscle cell proliferation. *Circ Res* 1996;79:1131-42.
39. Frisdal E, Gest V, Vieillard-Baron A, Levame M, Lepetit H, Eddahibi S, Lafuma C, Harf A, Adnot S, d'Ortho M. Gelatinase expression in pulmonary arteries during experimental pulmonary hypertension. *Eur Respir J* 2001;18:838-45.
40. Archer S, Rich S. Primary pulmonary hypertension: a vascular biology and translational research "Work in progress". *Circulation* 2000;102:2781-91.
41. Zhao YD, Courtman DW, Deng Y, Kugathasan L, Zhang Q, Stewart DJ. Rescue of monocrotaline-induced pulmonary arterial hypertension using bone marrow-derived endothelial-like progenitor cells. Efficacy of combined cell and eNOS gene therapy in established disease. *Circ Res* 2005; 96: 442-50.
42. Sahara M, Sata M, Morita T, Nakamura K, Hirata Y, Nagai R. Diverse contribution of bone marrow-derived cells to vascular remodeling associated with pulmonary arterial hypertension and arterial neointimal formation. *Circulation* 2007;115:509-17.
43. Raoul W, Wagner-Ballon O, Saber G, Hulin A, Marcos E, Giraudier S, Vainchenker W, Adnot S, Eddahibi S, Maitre B. Effects of bone marrow-derived cells on monocrotaline- and hypoxia-induced pulmonary hypertension in mice. *Resp Res* 2007;8:8.
44. Passier R, Mummery C. Origin and use of embryonic and adult stem cells in differentiation and tissue repair. *Cardiovasc Res* 2003; 58: 324-35.
45. Nagaya N, Kangawa K, Kanda M, Uematsu M, Horio T, Fukuyama N, Hino J, Harada-Shiba M, Okumura H, Tabata Y, Mochizuki N, Chiba Y, Nishioka K, Miyatake K, Asahara T, Hara H, Mori H. Hybrid cell-gene therapy for pulmonary hypertension based on phagocytosing action of endothelial progenitor cells. *Circulation* 2003;108:889-95.
46. Campbell AIM, Zhao Y, Sandhu R, Stewart DJ. Cell-based gene transfer of vascular endothelial growth factor attenuates monocrotaline-induced pulmonary hypertension. *Circulation* 2001;104:2242-8.
47. Campbell AIM, Kuliszewski MA, Stewart DJ. Cell-based gene transfer to the pulmonary vasculature. Endothelial nitric oxide synthase overexpression inhibits monocrotaline-induced pulmonary hypertension. *Am J Respir Cell Mol Biol* 1999;21:567-75.

Chapter 7

Intravenous cell therapy with mesenchymal stem cells from donor rats with pulmonary hypertension reduces right ventricular pressure overload and reverses right ventricular hypertrophy in recipient rats with pulmonary artery hypertension

S. Umar
P. Steendijk
Y. P. de Visser
G. T. M. Wagenaar
C. I. Schutte
W. H. Bax
E. Mantikou
D. A. Pijnappels
D. E. Atsma
M. J. Schalijs
E. E. Van der Wall
A. van der Laarse

Submitted for publication

Abstract

Background: Pulmonary artery hypertension (PAH) is characterized by progressive increase in pulmonary artery pressure leading to right ventricular (RV) hypertrophy, RV failure and sudden cardiac death. Standard treatment is still inadequate for PAH. Stem cell therapy may constitute a new treatment modality for PAH patients.

Purpose of the study: To test whether administration of bone marrow-derived mesenchymal stem cells (MSCs) obtained from donor rats with monocrotaline (MCT)-induced PAH to rats with MCT-induced PAH resulted in (i) decreased pulmonary artery pressure, (ii) reversal of RV hypertrophy (RVH), and (iii) improvement of RV function.

Methods: At day 1, healthy female Wistar rats received PBS (group 1, n=10) or 60 mg/kg subcutaneous MCT (groups 2-4, each n=10) to induce PAH. At day 14, group 1 (Control) and group 2 (untreated PAH) received intravenous injection of PBS, group 3 (MSC-treated PAH) received 10^6 MSCs (group 3), and group 4 (SF-treated PAH) received 10^6 skin fibroblasts. MSCs were obtained from donor rats which received MCT (60 mg/kg) 28 days prior to bone-marrow harvesting. SFs were obtained from healthy rats. At day 28 the rats were instrumented to assess, RV function by combined pressure-conductance catheter. Subsequently, rats were sacrificed. RVH was quantified by weighing the RV free wall relative to the LV including the interventricular septum (IVS). Immunohistochemistry was performed to assess changes in the extracellular matrix of the RV.

Results: Comparing group 2 vs 1 indicated that MCT induced PAH (42 ± 17 vs. 27 ± 5 mmHg, $p < 0.05$), RVH (RV/(IVS+LV) weight ratio of 0.47 ± 0.12 vs. 0.25 ± 0.04 , $p < 0.001$) and depressed LV ejection fraction ($43 \pm 6\%$ vs. $56 \pm 11\%$, $p < 0.005$). MSC treatment (group 3) limited PAH (31 ± 4 mmHg; $p = 0.08$ vs. group 2), RVH (0.32 ± 0.07 ; $p < 0.005$ vs. group 2), and normalized RV ejection fraction ($52 \pm 5\%$; $p < 0.005$ vs. group 2). In group 4, treatment effects on RV pressure, RVH and RV function were less pronounced than in group 3.

Conclusion: Treatment with intravenous administration of MSCs obtained from donor rats with PAH reduced pressure overload, hypertrophy and RV dysfunction in rats with MCT-induced PAH. These results suggest that patients with PAH may be treated successfully using autologous MSCs.

Introduction

Pulmonary arterial hypertension (PAH), which refers to a progressive increase in pulmonary artery pressure, is a chronic debilitating disease leading to right ventricular (RV) hypertrophy, RV failure and eventually to death [1]. PAH is characterized by a progressively severe symptomatology of dyspnea, fatigue, chest pain, syncope, and right heart failure.

In a study on novel therapeutic options for patients with PAH, we have employed the monocrotaline (MCT)-induced rat model of PAH, a model which is widely used in experimental studies [2,3]. The consequences of two doses of MCT (30 and 80 mg/kg) on RV function at 28 days after MCT administration were dose-dependent (*i*) RV hypertrophy, (*ii*) RV dilatation, and (*iii*) impairment of systolic function, without marked effects on RV diastolic function [4]. Earlier, we demonstrated that tenascin-C, an extracellular matrix protein that is absent in normal myocardium, is abundantly expressed in RV myocardium of rat hearts with MCT-induced PAH [5]. In the heart, extracellular matrix proteins are predominantly secreted by fibroblasts, whereas the matrix degrading enzymes are produced by many cell types, such as fibroblasts, cardiomyocytes and macrophages. In patients with severe heart failure myocardial expression of collagenases, like matrix metalloproteinase-1 (MMP1) mRNA, was increased [6], and decreased after implantation of a left ventricular assist device (LVAD) [7]. In analogy, in the failing heart supported by LVAD also other myocardial collagenases, such as cathepsin K, demonstrated decreased concentrations [8].

The model of MCT-induced PAH is extremely useful to test new drugs to treat PAH and to study their mechanisms of action [9]. Many treatment options for PAH have been tested so far, but an effective therapy is lacking. Cell therapy constitutes a novel therapeutic option for PAH patients. Several groups have tested various cell types to treat experimental PAH, including mesenchymal stem cells (MSCs). MSCs are unique in possessing (*i*) a potential to differentiate into other cell types, and (*ii*) an ability to secrete paracrine factors leading to improvements in tissue injury [10].

Intravenous (i.v.) infusion of autologous endothelial progenitor cells (EPCs) to patients with idiopathic PAH was shown to be safe and to have beneficial effects on exercise capacity and pulmonary hemodynamics [11]. I.v. infusion of bone marrow-derived EPCs from Fisher-344 rats, cultured in endothelial growth medium for 7-10 days, to syngeneic rats 3 days after MCT administration nearly completely prevented the increase in RV systolic pressure. EPCs were recovered in the distal pulmonary arterioles and incorporated into the endothelial lining of the MCT-injured lung. Delayed i.v. injection of EPCs 3 weeks after MCT administration prevented the further progression of PAH in the following 2 weeks [12]. However, i.v. injection of unfractionated bone marrow-derived cells from donor rats to rats with MCT-induced PAH plus unilateral pneumonectomy had no beneficial effect on PAH, pulmonary arterial remodeling, and survival [13]. I.v. injection of rat bone marrow-derived mesenchymal stem cells (MSCs) to rats that had received MCT one week earlier caused lower peak pulmonary pressure and less RV hypertrophy [14]. Even if EPCs were injected into the lungs of dogs with

MCT-induced PAH, pulmonary artery pressure and pulmonary vascular resistance decreased and cardiac output increased [15].

To develop a therapeutic strategy in which a patient with developed PAH will be treated by i.v. administration of autologous bone marrow-derived MSCs, we investigated whether rats with MCT-induced PAH are treated successfully after i.v. administration of bone marrow-derived MSCs isolated from rats with MCT-induced PAH. As a reference cell type we chose skin fibroblasts (SFs) of healthy rats, used by Zhao *et al.* [12] to distinguish between stem cells and differentiated cells in terms of therapeutic effect of rats with PAH.

To analyse the effects of MCT-induced PAH and cell therapy in this model, we measured (i) RV pressures, (ii) RV volumes and RV ejection fraction, (iii) RV hypertrophy, (iv) expression of genes associated with myocardial hypertrophy, such as β -myosin heavy chain, pro-atrial natriuretic peptide and pro-B-type natriuretic peptide, (v) RV myocardial expression of tenascin-C and collagens I and III, and (vi) RV myocardial concentrations of collagenolytic enzymes, such as matrix metalloproteinase-1 (MMP1), cathepsin K and cathepsin S, in normal rat hearts and in hearts of rats with MCT-induced PAH without and with cell therapy.

Materials and Methods

Animal model

All animals were treated in accordance with the national guidelines and with permission of the Animal Experiments Committee of the Leiden University Medical Center. Healthy, adult, female Wistar rats (200-250 g body weight; Harlan, Zeist, the Netherlands) were randomly assigned to four experimental groups. At day 1, group 1 received subcutaneous (s.c.) PBS (Control, n=10), the other groups received a single s.c. injection of MCT (Sigma-Aldrich, Zwijndrecht, the Netherlands; 60 mg/kg, n=10 each group). At day 14, group 1 and 2 received 1 ml PBS intravenously (i.v.), rats from group 3 were treated by i.v. administration of 10^6 MSCs, whereas rats from group 4 received 10^6 skin fibroblasts (SFs). The animals were housed, two animals per cage, with a 12h/12h light/dark cycle and an unrestricted food supply. The rats were weighed three times per week.

Mesenchymal stem cell isolation and culture

To obtain MSCs, donor rats were injected s.c. with MCT (60 mg/kg, n=5) and anaesthetized with isoflurane and killed by i.v. injection of KCl (100 mmol/L) after 28 days. Femurs and tibiae were removed and cleaned of all connective tissue and attached muscle. The proximal ends were clipped and bones placed in microfuge tubes supported by plastic inserts cut from pipette tips. Microfuge tubes were briefly centrifugated at 13,000 rpm for 1 min. The marrow pellets were resuspended in 10 mL of growth medium [Dulbecco Minimal Essential Medium (DMEM) supplemented with 15% fetal bovine serum (FBS; Invitrogen, Breda, the Netherlands), penicillin (50 U/L), streptomycin (50 μ g/L), and amphotericin B solution (0.25 μ g/mL, Sigma-Aldrich)] supplemented with 6% heparin (400 IE/ml). This suspension was centrifuged again at 1000 rpm for 10 min. Next, the pellet

was resuspended in 7 mL of growth medium supplemented with 5.75 µg/mL DNase I (Sigma-Aldrich). The cells were plated in a 25-cm² culture flasks (Becton Dickinson, Franklin Lakes, NJ, USA) and the culture was kept in a humidified hypoxic incubator CO₂/O₂ (5%/5%) at 37°C. The non-adherent cells were replated after 6 h. Two days later, non-adherent cells were removed by changing the medium to 12 mL of fresh growth medium. The medium was refreshed twice a week until the primary cultures were confluent. Previously it was reported that MSCs cultured in 2%-5% O₂ have increased proliferation rate and upregulated VEGF expression compared to MSCs cultured in ambient air, while maintaining their multi-lineage potential [16-20]. As far as differentiation capacity of MSCs is concerned, hypoxia was shown to have positive [16] as well as negative effects on osteogenic differentiation [19,21-23].

Before injection, the cells were trypsinized and labelled with the viable fluorescent dye CM-Dil according to the manufacturer's recommendations (CellTracker™, Molecular Probes, Invitrogen).

In vitro assays of MSCs

MSCs from MCT-treated rats and healthy rats, grown in hypoxic or normoxic incubator were tested for (*i*) proliferation rate, (*ii*) membrane protein repertoire by FACS, (*iii*) production and secretion of VEGF, and (*iv*) capacity of adipogenic and osteogenic differentiation. In addition, it was tested what effects the major metabolite of MCT, dehydromonocrotaline (dhMCT), has on proliferation and VEGF production/secretion by MSCs, by incubation of MSCs with dhMCT *in vitro*.

Proliferation rate of MSCs

MSCs isolated from bone marrow of healthy rats and bone marrow of rats with MCT-induced PAH were grown at 5% oxygen and at 20% oxygen in 96-well plates. At two moments in time, spaced 4 days, media were poured off, and cells were analysed with the XTT assay (Roche, Almere, the Netherlands). The assay is based on the cleavage of the tetrazolium salt XTT in the presence of an electron-coupling reagent, producing a soluble formazan salt. This conversion only occurs in viable cells. The measured absorbance directly correlates to the cell number.

Flow cytometry of MSCs

MSCs isolated from bone marrow of healthy rats and bone marrow of rats with MCT-induced PAH were grown in 5% oxygen and 20% oxygen incubators, and analysed for surface marker expression by flow cytometry. The MSCs were detached using trypsin/EDTA (Bio-Whittaker Europe, Verviers, Belgium) and resuspended in PBS containing 0.5% bovine serum albumine (Sigma-Aldrich), and divided in aliquots of 5x10⁴ cells. Cells were then incubated for 30 min at 4°C with fluorescein isothiocyanate (FITC)- or phycoerythrin (PE)-conjugated antibodies against rat CD34, CD29, CD44, CD45, CD106 (all from Becton Dickinson) and CD90 (Serotec, Kidlington, Oxford, UK). Labeled cells were washed and analyzed using a FACSort flow cytometer (BD Pharmingen, San Jose, CA, USA), equipped with a 488-nm argon ion laser and a 635-nm red diode laser. Isotype-matched control antibodies (BD Pharmingen) were used to

determine background fluorescence. At least 5000 cells per sample were acquired and data were processed using CellQuest software (BD Pharmingen). Generally, MSCs are found to be positive for CD29, CD44, CD90 CD105 and CD106, and negative for CD34 and CD45 (unpublished observations).

Production and secretion of VEGF by MSCs

MSCs isolated from bone marrow of healthy rats and bone marrow of rats with MCT-induced PAH were grown at 5% oxygen in 96-well plates. At two moments in time, spaced 4 days, media were poured off, and cells were analysed for protein content using the bicinchoninic acid (BCA) protein assay (Pierce, Etten-Leur, the Netherlands). The media were assayed for VEGF using a rat VEGF assay kit (rat base kit supplied with rat VEGF microparticle concentrate, R&D Systems Europe, Abingdon, UK). VEGF concentrations in the media were expressed as ng per mg of cellular protein.

Adipogenic and osteogenic differentiation of MSCs

MSCs isolated from bone marrow of healthy rats and bone marrow of rats with MCT-induced PAH grown in a 5% oxygen incubator were characterized using established differentiation assays [24]. Briefly, 5000 MSCs per well were plated in a 12-well culture plate, and exposed to adipogenic or osteogenic induction medium. Adipogenic differentiation medium consisted of a regular culture medium (DMEM supplemented with 15% FBS, 100 U/L penicillin and 100 µg/mL streptomycin, 1 µg/mL amphotericin B solution) supplemented with 5 µg/mL insulin, 1 µmol/L dexamethason, 50 µmol/L indomethacin and 0.5 µmol/L 3-isobutyl-1-methylxanthine (IBMX) (all from Sigma-Aldrich), and was refreshed every 3-4 days for a period of 3 weeks. Lipid accumulation was assessed by Oil Red O staining of the cultures (15 mg Oil Red O/mL of 60% isopropanol) and light microscopy. Osteogenic differentiation medium consisted of culture medium supplemented with 10 mmol/L β-glycerophosphate, 50 µg/mL ascorbic acid and 10 nmol/L dexamethason (all from Sigma-Aldrich), and was refreshed every 3-4 days for a period of 2 weeks. Afterwards, the cells were washed with phosphate-buffered saline (PBS), and calcium deposits were visualized by staining of the cells for 2-5 min with 2% Alizarine Red S in 0.5% NH₄OH (pH 5.5).

Effects of dehydroMCT on MSCs in vitro

Dehydromonocrotaline (dehydroMCT) was prepared from MCT by chemical oxidation using o-chloranil according to Mattocks *et al.* [25]. Mass spectrometric analyses have shown that 25-30% of the input MCT was converted to dehydroMCT by this method [26]. Proliferation of MSCs from healthy rats in the absence and presence of 50 µmol/L dehydroMCT was determined by XTT assay (Roche) over a 4-day interval.

Skin fibroblasts

Skin fibroblasts (SFs) were grown from pieces of skin of healthy rats anesthetized by CO₂ and killed by i.v. injection of KCl (100 mmol/L). Skin samples were transferred to porcine gelatin (Sigma-Aldrich)-coated flasks, and cultured in DMEM containing 100 U/mL penicillin, 100 µg/mL streptomycin, and 10% FBS (all

from Invitrogen) in a normoxic incubator (20% O₂ and 5% CO₂) at 37°C. Outgrowth of cells was visible 2 days after culture initiation. Three days later the skin pieces were removed and the skin fibroblasts were detached with trypsin-EDTA solution (Invitrogen), and reseeded in new culture flasks.

For intravenous infusion into rats which had had MCT administration 14 days earlier, we used passage 4-6. Prior to injection into the jugular vein, the SFs were labeled with a Dil derivative according to the recommendations of the supplier (CellTracker CM-Dil, Molecular Probes, Invitrogen). Per rat, 10⁶ SFs in 0.5 mL of PBS were injected in the jugular vein.

Cell injection

At day 14, the rats were anaesthetized with isoflurane, the left jugular vein was cannulated (20G, Biovalve, Vygon, Ecoen, France), and 1 mL of cell suspension (10⁶ cells/mL) or an equal amount of PBS (control animals) was injected slowly in approximately 30 s. The cell suspensions contained either MSCs from rats with MCT-induced PAH or SFs from healthy rats. Next, the canula was removed, the vein was pressed for 5 min to ensure closure of the puncture, and the skin was closed.

Hemodynamic measurements

RV function was measured as published previously [4]. Briefly, the rats were sedated by inhalation of a mixture of isoflurane (4%) and oxygen. Subsequently, general anesthesia was induced by intraperitoneal (i.p.) injection of a fentanyl—fluanison—midazolam mixture in a dose of 0.25 mL/100 g body weight. The mixture consisted of two parts Hypnorm (0.315 mg/mL fentanyl+10 mg/mL fluanison; Vital-Pharma, Maarheeze, the Netherlands): one part Dormicum (5 mg/mL midazolam; Roche, Mijdrecht, the Netherlands) and one part saline. The animals were placed on a controlled warming pad to keep body temperature constant. A tracheotomy was performed, a cannula (18G, Biovalve) was inserted, and the animals were mechanically ventilated using a pressure-controlled respirator and a mixture of air and oxygen. The animals were placed under a stereomicroscope (Zeiss, Hamburg, Germany), and the left jugular vein was cannulated for infusion of hypertonic saline (10%) to determine parallel conductance. A midsternal thoracotomy was performed, and a combined pressure-conductance catheter (model FT212, SciSense, London, Ontario, Canada) was introduced via the apex into the RV and positioned towards the pulmonary valve. The catheter was connected to a signal processor (FV898 Control Box, SciSense) and RV pressures and volumes were recorded digitally. All data were acquired at a sample rate of 2,000 Hz and analyzed off-line by dedicated software. The slope factor α was calculated as the cardiac output determined by the uncalibrated conductance catheter divided by the cardiac output determined by LV echocardiography (VisualSonics, Toronto, Ontario, Canada).

Hemodynamics

Heart rate, stroke volume, cardiac output, RV end-diastolic volume, RV end-systolic volume, RV ejection fraction, RV end-diastolic pressure, RV end-systolic

pressure, and RV peak-systolic pressure were determined from steady state pressure-volume loops. In addition, stroke work (SW) was obtained as the area of the pressure-volume loop, and the maximal rates of RV pressure upstroke and fall (dP/dt_{\max} and dP/dt_{\min} , respectively) were calculated. The relaxation time constant (τ) was assessed as the time constant of monoexponential decay of RV pressure during isovolumic relaxation [27]. Effective pulmonary arterial elastance (E_a), as a measure of RV afterload, was calculated as RV end-systolic pressure divided by RV stroke volume.

RV end-systolic and end-diastolic pressure-volume relations (ESPVR and EDPVR) and the preload recruitable stroke work relation (PRSW: RV-stroke work vs. RV end-diastolic volume) were determined from pressure-volume loops recorded during transient preload reduction by occlusion of the inferior vena cava. End-systolic elastance E_{es} , the linear slope of the ESPVR, and M_w , the slope of the PRSW, are load-independent measures of systolic ventricular function. Diastolic stiffness was determined as the slope of the EDPVR, E_{ed} [28].

Tissue preparations

After hemodynamic measurements heart and lungs were taken out. From each heart the ventricles were isolated, the RV was cut free, and the remainder was split into the intraventricular septum (IVS) and the left ventricle (LV). These three parts of ventricular tissue were weighed, and each was split in three parts for individual storage (*i*) at -80°C for RNA isolation, (*ii*) at -80°C to prepare homogenates, and (*iii*) in formaline (4%) to perform histochemical analysis.

Assessment of RV hypertrophy

As an indicator of right ventricular hypertrophy the weight ratio of RV/(LV + IVS) was calculated. Independently, we determined the length and width of 25-50 cardiomyocytes per group (control, MCT60, MCT+MSC and MCT+SF) isolated from the RV and LV of collagenase-dissociated hearts.

Real-time RT-PCR

Total RNA was isolated from heart tissue homogenates using guanidium-phenol-chloroform extraction and isopropanol precipitation (RNA-Bee, Tel-Test Inc., Bio-Connect BV, Huissen, the Netherlands). The RNA sample was dissolved in RNase-free water and quantified spectrophotometrically. The integrity of the RNA was studied by gel electrophoresis on a 1% agarose gel, containing ethidium bromide. Samples did not show degradation of ribosomal RNA by visual inspection under ultraviolet light. First-strand cDNA synthesis was performed with the SuperScript Choice System (Life Technologies, Breda, the Netherlands) by mixing 2 μg total RNA with 0.5 μg of oligo(dT)12-18 primer in a total volume of 12 μL . After the mixture was heated at 70°C for 10 min, a solution containing 50 mmol/L Tris-HCl (pH 8.3), 75 mmol/L KCl, 3 mmol/L MgCl_2 , 10 mmol/L DTT, 0.5 mmol/L dNTPs, 0.5 μL RNase inhibitor, and 200 U Superscript Reverse Transcriptase was added, resulting in a total volume of 20.5 μL . This mixture was incubated at 42°C for 1 h; total volume was adjusted to 100 μL with RNase-free water and stored at -80°C until further use. For real-time quantitative PCR, 1 μL

of first-strand cDNA diluted 1:10 in RNase-free water was used in a total volume of 25 μ L, containing 12.5 μ L 2x SYBR Green PCR Master Mix (Applied Biosystems, Foster City, CA, USA) and 200 ng of each primer.

Primers, designed with the Primer Express software package (Applied Biosystems), were:

Primers (orientation: 5'-3')

	Forward	reverse
proANP	CCAGGCCATATTGGAGCAAA	AGGTTCTTGAAATCCATCAGATCTG
proBNP	GAAGCTGCTGGAGCTGATAAGAG	TGTAGGGCCTTGGTCCTTTG
α -MHC	CTTCAAGCTCAAGAATGCCTATGA	TGCACATTTTTACCCCCTTCTC
β -MHC	AGGCCCAGAAACAAGTGAAGAG	GGCACGGACTGCGTCATC
β -actin	GGCTCCTAGCACCATGAAGATC	GAGCCACCAATCCACACAGA

PCR reactions, consisting of 95°C for 10 min (1 cycle), 94°C for 15 s, and 60°C for 1 min (40 cycles), were performed on an ABI Prism 7900 HT Fast Real Time PCR system (Applied Biosystems). Data were analyzed with the ABI Prism 7900 sequence detection system software (version 2.2) and quantified with the comparative threshold cycle method with β -actin as a housekeeping gene reference [29].

(Immuno)histochemistry

After fixation, heart tissue samples were embedded in paraffin. Blocks were embedded in upright position to distinguish the endocardium, the midwall, and the epicardium of the RV and LV free wall in cross-sections. Tissue was cut into 4- μ m thick sections and dried for at least 24 h at 37°C. After 10 min incubation at 60°C, sections were deparaffinized in Ultraclear (Klinipath, Duiven, the Netherlands) for 5 min and rehydrated in decreasing graded alcohols (100-25%) followed by two 5-min washes in distilled water and TBS (150 mmol/L NaCl, 10 mmol/L Tris-HCl, pH 8.0).

To study the distribution of myocardial collagen I, collagen III, and tenascin-C, sections were exposed to immunohistochemistry. Inhibition of endogenous peroxidase activity was obtained by 20 min incubation in 0.3% hydrogen peroxide in PBS. The sections were incubated in citrate buffer at 97°C for 10 min, to retrieve antigens and subsequently washed in PBS, 5 times for 3 min, and in PBS-Tween for 2 times. Sections were incubated for 3h at room temperature with (i) rabbit anti-collagen I antibody (1:200; ab24133, Abcam, Cambridge, UK), (ii) rabbit anti-collagen III antibody (1:200; ab7778, Abcam), and (iii) rabbit anti-tenascin-C antibody (1:200; sc20932, Santa Cruz Biotechnology, Santa Cruz, CA, USA), followed by goat anti-rabbit IgG conjugated to HRP (1:200, sc3837, Santa Cruz Biotechnology). After series of three washes in PBS and once in PBS-Tween, 1% BSA, and 0.05% Tween, the slides were developed with diaminobenzidine (DAB) solution (Pierce, Perbio Science, Etten-leur, the Netherlands). Nuclei were counterstained using hematoxylin for 2 min, followed by dehydration with graded alcohols and clearance in xylene. Finally, the sections were mounted with D.P.X. (BDH, VWR International, Lutterworth, Leicestershire, UK), covered with glass cover slips, and examined in a light microscope (Nikon

Eclipse, Nikon Europe, Badhoevedorp, the Netherlands) equipped with a digital camera (Nikon DXM 1800). Images were analyzed using Image-Pro Plus software (Media Cybernetics, Silver Spring, MD, USA). Per section, at least 16 images were acquired and analyzed to compensate for variations within a section.

Western blotting

Myocardial samples for biochemical analysis were freeze-dried, and homogenized in homogenising buffer (0.1 M Tris-HCl and 0.1% (v/v) Tween-20, pH 7.5), using a Potter tube (Kimble/Kontes, Vineland, NJ, USA). Homogenates (1 %, ^{w/v}) were stored in aliquots at -80°C. Protein concentrations were determined by bicinchoninic acid protein (BCA) assay (Pierce, Etten-Leur, the Netherlands).

For western blot analysis the heart homogenate were separated on a 12% Bis-Tris NuPage gel (Invitrogen) and blotted on a PVDF membrane (GE Healthcare, Diegem, Belgium). Non-specific binding sites were blocked by incubating the membranes in a blocking solution 20 g/L ECL Advance Blocking Agent (GE Healthcare) in TBS-Tween (10 mmol/L Tris-HCl, pH 8.0, 150 mmol/L NaCl, 0.05% Tween) for 1 h on an orbital shaker. Subsequently, membranes were incubated with (i) rabbit anti-MMP1 antibody conjugated to HRP (1:20,000, ab53142, Abcam), (ii) goat anti-cathepsin S antibody (1:20,000, sc6503, Santa Cruz Biotechnology) followed by donkey anti-goat IgG conjugated to HRP (1:10,000, sc2020, Santa Cruz Biotechnology), and (iii) rabbit anti-cathepsin K antibody (1:20,000, #3588-100, BioVision, Mountain View, CA, USA) followed by goat anti-rabbit IgG conjugated to HRP (1:10,000, sc3837, Santa Cruz Biotechnology). Subsequently, the membranes were washed four times in TBS-Tween, and incubated with a chemiluminescent reagent (ECL Advance kit, GE Healthcare) for 5 min. Light emission was detected by exposure to Hyperfilm ECL (GE Healthcare). The Western blot band intensities were quantified by the Molecular Imager ChemiDoc XRS system (Bio-Rad, Veenendaal, the Netherlands).

Cardiomyocyte isolation

A separate series of 20 rats were given the same experimental treatments (n=5 per group) as mentioned earlier. At day 28, the rats were anaesthetised and the thorax was opened. The heart was taken out quickly and immediately put into ice-cold, oxygenated Tyrode solution. The aorta was connected to the cannula of a Langendorff perfusion set-up (AD Instruments, Spechbach, Germany). The heart was perfused for 5 min with an oxygenated Tyrode solution at constant pressure (70 mmHg) at 37° C and resumed beating. The perfusion fluid was replaced by an oxygenated, low Ca²⁺ perfusion fluid. Contractions disappeared within 30 s. After 5 min of low calcium perfusion, the perfusion was continued in a recirculating manner at a perfusion pressure of ~60 mm Hg. At that time collagenase (0.06%, Worthington, Lakewood, NJ, USA) was added. Thirty min later, the flow rate was too high to maintain a perfusion pressure of 60 mm Hg. Then, the heart was removed, and the RV was separated from the LV (including IVS) using a scalpel. RV and LV were cut in small pieces, incubated in a fresh collagenase (0.06%) solution, and dissociated in a waterbath shaker at 37°C. Thereafter, sedimented cardiomyocytes were resuspended and stored at 37°C in fresh HEPES-buffered

salt solution containing (in mmol/L) NaCl 125, KCl 5, MgSO₄ 1, KH₂PO₄ 1, CaCl₂ 1.8, NaHCO₃ 10, HEPES 20, glucose 5.5, pH 7.4. The average fraction of rod-shaped cardiomyocytes was 80%. The percentage of rod-shaped cardiomyocytes decreased by about 10% during 6 h at 37° C. Per heart, roughly 50 intact, non-contracting, rod-shaped cardiomyocytes from RV as well as LV were photographed followed by measurement of length and width with calibrated ruler.

Statistical analysis

To assess the effect of treatment (cell therapy with MSCs, cell therapy with SFs vs. treatment by PBS) differences between groups were evaluated by one-way ANOVA followed by Bonferroni's *post-hoc* test (SPSS12 for Windows, SPSS Inc., Chicago, IL, USA). Differences were considered significant at $p < 0.05$. Values are represented by means \pm SD, unless stated otherwise.

Results

Proliferation rate of MSCs

MSCs from healthy rats proliferated roughly 2 times more rapidly than MSCs from MCT-treated rats if grown at 5% oxygen ($p=0.028$) but if grown at 21% oxygen this difference was absent ($p=0.576$). The use of an incubator with 5% oxygen was associated with higher proliferation rates of MSCs than in case using 21% oxygen, whether they originated from healthy rats or MCT-treated rats (≈ 3 -fold, $p=0.007$ and ≈ 2 -fold, $p=0.061$, respectively) (Figure 1, top left panel).

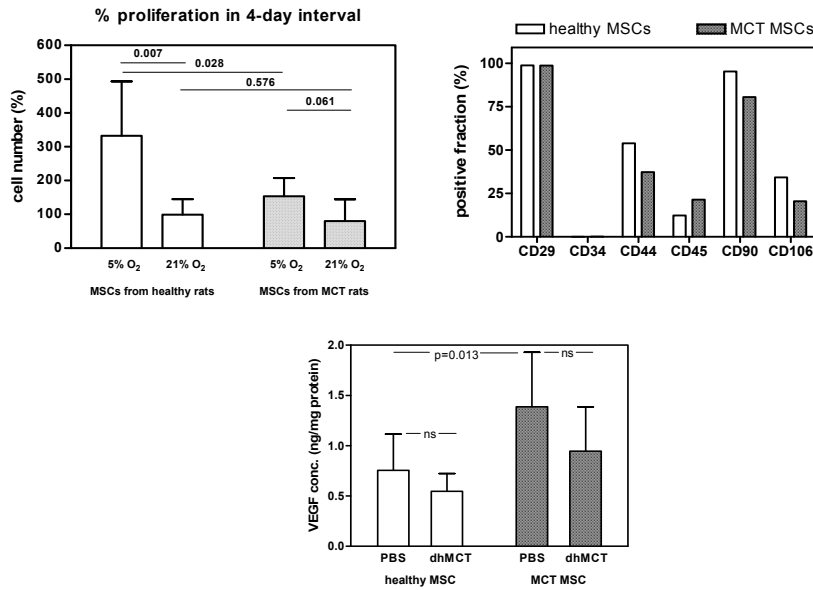


Figure 1. Top left panel. Proliferation of MSCs in 4-day intervals. MSCs from healthy rats and MSCs from rats with MCT-induced PAH were grown in an incubator with 5% oxygen, 5% CO₂ and 90% nitrogen (5% O₂) or in an incubator with 5% CO₂ and air (21% O₂). If grown in 5% oxygen, MSCs from healthy rats proliferated ≈ 2 times more rapidly than MSCs from rats with MCT-induced PAH ($p=0.028$), but if grown in 21% oxygen, proliferation rate did not differ between the two groups of MSCs ($p=0.576$).

Top right panel. Surface marker profile of MSCs from bone marrow of healthy rats and of MSCs from bone marrow of rats with MCT-induced PAH. Both types of MSCs were cultured in a 5% O₂/5% CO₂ incubator.

Bottom panel. VEGF concentration in the culture medium of MSCs isolated from healthy rats (healthy MSC) and isolated from rats with MCT-induced PAH. The stem cells were grown for 4 days in culture medium. After that time medium and cells were split, medium was analyzed for VEGF concentration, and cells were analyzed for protein content. Medium VEGF concentration is expressed as pg of VEGF in the medium per mg of cellular protein.

FACS analysis of MSCs

Comparison of FACS data obtained from MSCs isolated from rats with MCT-induced PAH with those obtained from MSCs from healthy rats, revealed minor differences in the repertoire of surface markers (Figure 1, top right). Both types of MSCs were cultured in a 5% O₂/5% CO₂ incubator.

VEGF production and secretion from MSCs

MSCs from healthy rats and MSCs of rats with MCT-induced PAH were grown in an 5% O₂/5% CO₂ incubator in 96-well plates for 4 days. At t=0 and t=4 days media were analysed for VEGF concentration, and cells were analysed for protein content. MSCs from rats with MCT-induced PAH had \approx 2-fold higher VEGF secretion than MSCs from healthy rats ($p < 0.02$) (Figure 1, bottom panel). Addition of 50 μ mol/L of dehydromCT, the toxic metabolite of MCT, slightly depressed VEGF secretion from both types of MSCs, but these decreases were not significant.

Differentiation potential of MSCs

MSCs from healthy rats and from rats with MCT-induced PAH, grown in a 5% O₂/5% CO₂ incubator, were investigated for adipogenic and osteogenic differentiation capacity. Adipogenic and osteogenic differentiation capacities, present in MSCs obtained from healthy rats, were well preserved in MSCs obtained from MCT-treated rats (Figure 2).

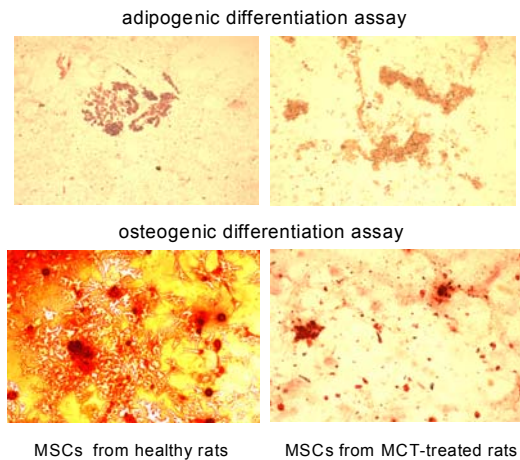


Figure 2. Differentiation into adipogenic phenotype (upper panels) and osteogenic phenotype (bottom panels) of MSCs isolated from healthy rats (left panels) and isolated from rats with MCT-induced PAH (right panels).

Body weights

The rats were weighed 3 times per week. The net body weight gain of rats with MCT-induced PAH in 4 weeks was less than that of control rats (18.1 ± 6.9 g vs. 28.1 ± 8.2 g, $p < 0.05$). The body weight gain in the MCT+MSC group was 20.6 ± 8.2 g, which was not significantly different from the MCT60 group, nor from the control group. The body weight gain in the MCT+SFB group was 17.9 ± 8.1 g (n.s. vs. MCT60; $p < 0.05$ vs. control) (Figure 3).

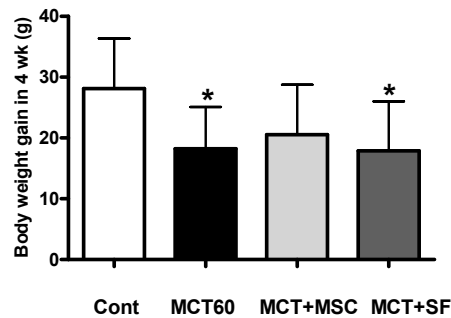


Figure 3. Increase in body weight in 4 weeks of the 4 groups of rats (control, MCT60, MCT+MSC and MCT+SFBs). Indicated are mean values \pm SD. (* $p < 0.05$ vs. Control, # $p < 0.05$ vs. MCT60).

RV peak systolic pressure

At the end of the experimental period, RV peak systolic pressures were significantly higher in MCT group than in the control group, indicating the development of PAH (41.5 ± 16.9 vs. 27.2 ± 4.9 mmHg in control; $p < 0.05$). If MCT-treated rats had been given cell therapy with MSCs, mean RV peak systolic pressure was attenuated (30.7 ± 4.4 mmHg) although not significantly ($p = 0.08$ vs. MCT60; n.s. vs. control). If MCT-treated rats had been given cell therapy with SFBs, mean RV peak systolic pressure was 32.1 ± 5.7 mmHg (n.s. vs. MCT60; n.s. vs. control) (Figure 4a).

RV function

Consistent with previous studies, MCT induced PAH and changes in RV volumes and ejection fraction. The hemodynamic effects are evident from the significant differences between the Control group and the MCT60 group: RV ejection fraction decreased, whereas RV peak pressure, RV end-systolic volume and RV end-diastolic pressure all increased (Table 2).

Table 2. Hemodynamic data of the rats that have been treated without or with MCT, and with and without additional cell therapy using MSCs or SFs. Data is collected at 28 days after MCT (or control) treatment.

		Control	MCT60	MCT+MSC	MCT+SF
Right Ventricle					
Heart rate	HR (bpm)	330±26	341±36	327±26	348±26
Stroke volume	SV (μL)	228±50	234±64	287±37	259±29
Cardiac output	CO (mL/min)	74±13	79±20	93±10*	90±9
Ejection fraction	EF (%)	56.2±11.2	42.8±6.2*	52.1±5.2	49.1±11.1
End-systolic volume	ESV (μL)	200±103	323±132	270±75	295±118
End-diastolic volume	EDV (μL)	427±150	556±183	557±99	554±143
End-systolic pressure	ESP (mmHg)	24±5	38±15*	28±4	30±5
End-diastolic pressure	EDP (mmHg)	1.3±1.2	3.9±1.8*	1.9±0.9	2.9±2.0
Peak pressure	Pmax (mmHg)	27.2±4.9	41.5±16.9*	30.7±4.4	32.1±5.7
dP/dt max	dPdtMax (mmHg/s)	1565±383	2215±1040	1832±455	1916±389
Negative dP/dt min	-dPdtMin (mmHg/s)	1334±385	1912±860	1675±493	1551±252
Stroke work	SW (mmHg.μL)	5071±1415	7044±2238	6682±1117	6239±1415
Relaxation time constant	Tau (ms)	13.7±3.8	14.0±2.9	12.9±4.7	13.5±4.7
Arterial elastance (afterload)	Ea (mmHg/μL)	0.11±0.04	0.19±0.12	0.10±0.03 [#]	0.12±0.03
End-systolic elastance	Ees (mmHg/μL)	0.19±0.17	0.17±0.20	0.10±0.07	0.12±0.07
End-diastolic elastance	Eed (mmHg/μL)	0.008±0.005	0.010±0.004	0.007±0.004	0.009±0.003
Preload recruitable stroke work	PRSW (mmHg)	21±7	25±15	19±5	23±7

* *p*-value < 0.05 vs. Cont

[#] *p*-value < 0.05 vs. MCT60

The animals that received MCT and were subsequently treated with MSCs showed much less pronounced differences in pressure and volume compared to the Control group. This indicates that MSC treatment substantially modified the effects of MCT. Compared to the MCT60 group, the MCT+MSC group showed

higher RV ejection fraction (Fig. 4b), higher stroke volume, and lower RV end-diastolic pressure, although these changes did not reach statistical significance. The MCT-induced changes in RV end-systolic and end-diastolic volumes, including the effects of i.v. therapy with MSCs and SFs are shown in Fig. 4c and d.

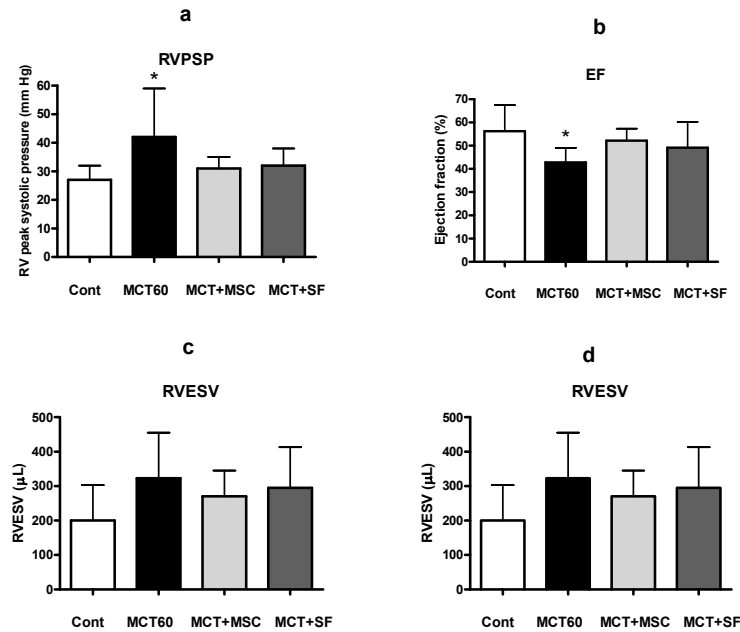


Figure 4a. RV peak systolic pressures, **b.** Ejection fraction (EF), **c.** RV end-systolic volumes (RVESV), and **d.** RV end-diastolic volumes (RVESV) of the 4 groups of rats (control, MCT60, MCT+MSC and MCT+SFB). Indicated are mean values ± SD (* $p < 0.05$ vs. Control).

Right ventricular hypertrophy

As a measure of RV hypertrophy we calculated the weight ratio of RV/ (LV+IVS). At 28 days after MCT, rats had developed RV hypertrophy with a RV/ (IVS+LV) weight ratio of 0.47 ± 0.12 vs. 0.25 ± 0.04 in control rats ($p < 0.001$). In PAH rats treated with MSCs, RV/ (IVS+LV) weight ratio was near normal (0.32 ± 0.07 ; $p < 0.005$ vs. MCT60; n.s. vs. control). In PAH rats treated with SFBs, RV/ (IVS+LV) weight ratio was 0.35 ± 0.06 ($p < 0.05$ vs. MCT60; n.s. vs. control (Figure 5)).

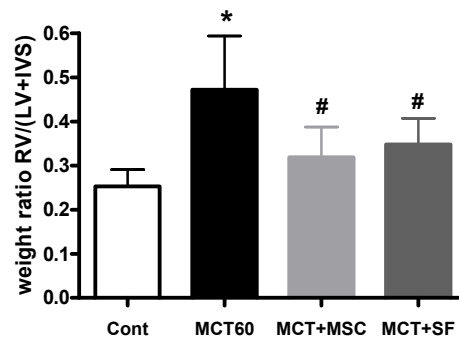


Figure 5. RV/ (LV+IVS) weight ratio of the hearts of the 4 group of rats (Control, MCT60, MCT+MSC, and MCT+SF). Indicated are mean values \pm SD.

Length and width of isolated RV cardiomyocytes were increased in rats that had received MCT compared to PBS-treated rats (Table 1). Although in control hearts RV cardiomyocyte dimensions are smaller than those of LV cardiomyocytes (significant difference for cardiomyocyte width only), in MCT-treated rats RV cardiomyocyte dimensions are larger than those of LV cardiomyocytes (significant differences for both width and length). Cell therapy with MSC reduces RV cardiomyocyte dimensions to levels that do not differ from dimensions of LV cardiomyocytes. Surprisingly, also the hearts of rats that had cell therapy with SFs showed equal dimensions of RV and LV cardiomyocytes (Table 1).

Table 1. Dimensions of cardiomyocytes isolated from hearts of rats treated without or with MCT, and with and without additional cell therapy using MSCs or SFs.

	RV cardiomyocytes mean \pm SD (n)	LV cardiomyocytes mean \pm SD (n)	P _{RV vs LV}
Cardiomyocyte length (μm)			
Control	99 \pm 19 (200)	102 \pm 20 (166)	0.087
MCT60	108 \pm 24 (221) *	100 \pm 18 (209)	<0.001
MCT+MSC	103 \pm 19 (201)	103 \pm 19 (232)	0.999
MCT+SFB	102 \pm 21 (204) #	103 \pm 18 (176)	0.618
Cardiomyocyte width (μm)			
Control	16.8 \pm 3.0 (200)	17.7 \pm 3.1 (166)	0.005
MCT60	18.2 \pm 3.0 (221) *	17.5 \pm 3.1 (209)	0.017
MCT+MSC	17.3 \pm 3.2 (201) #	17.8 \pm 3.2 (232)	0.106
MCT+SFB	16.9 \pm 3.2 (204) #	17.4 \pm 2.8 (176)	0.083

* $p < 0.05$ vs. Control

$p < 0.05$ vs. MCT60

mRNA in RV myocardium

RV myocardial concentrations of mRNAs encoding ANP and BNP were increased in rats with MCT-induced PAH compared to control rats, although not significantly (Figure 6). In RV myocardium of MCT-treated rats, mRNA of α MHC increased and mRNA of β MHC decreased, although not significantly, compared to PBS-treated rats. Cell therapy with MSCs or SFBs had no significant effects on these parameters.

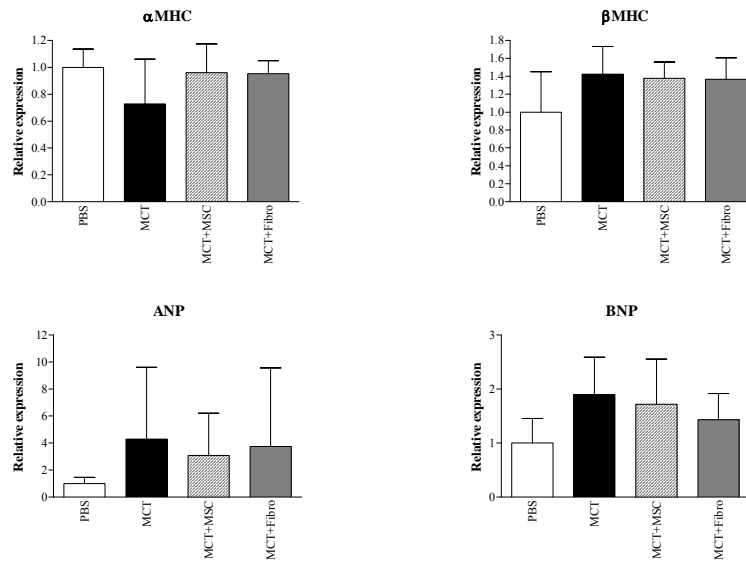


Figure 6

Right ventricular concentrations of mRNA encoding α - and β -myosin heavy chain (α MHC and β MHC, respectively), pro-atrial natriuretic peptide (ANP), and pro-B-type natriuretic peptide (BNP). Indicated are mean values \pm SD.

Extracellular matrix proteins

In normal RV and LV myocardium tenascin-C concentrations are very low (figure 7). However, in RV myocardium of rats of the MCT60 group tenascin-C concentration is increased considerably ($p < 0.005$ vs. control), whereas in the corresponding LV myocardium the tenascin-C concentrations remained low. In RV myocardium of rats from the MCT+MSC group the tenascin-C is as low as the tenascin-C concentration in the accompanying LV myocardium, which levels are not significantly different from corresponding values in control myocardium (Table 3). Myocardial collagen I and III concentrations were increased in RV myocardium of the MCT60 group, compared to the LV myocardium of the same hearts. Upon therapy with MSCs RV myocardial concentrations of collagen I and III remained elevated (both n.s. vs. MCT60), although comparison between RV and LV was only significant for collagen I.

Table 3. Myocardial concentrations of extracellular matrix proteins in RV and LV of rats that have been treated without or with MCT, and without or with additional therapy using MSCs

	Control	MCT60	MCT+MSC	P _{MCT60 vs Control}	P _{MCT60 vs. MCT+MSC}
Collagen I (pixels protein/total pixels)					
RV	0.072 ± 0.021	0.082 ± 0.018	0.078 ± 0.015	n.s.	n.s.
LV	0.050 ± 0.013	0.043 ± 0.020	0.034 ± 0.004	n.s.	n.s.
P _{RV vs. LV}	n.s.	0.003	0.006		
Collagen III (pixels protein/total pixels)					
RV	0.102 ± 0.026	0.131 ± 0.027	0.124 ± 0.026	0.006	n.s.
LV	0.081 ± 0.010	0.070 ± 0.021	0.095 ± 0.007	n.s.	n.s.
P _{RV vs. LV}	n.s.	<0.001	n.s.		
Tenascin-C (arbitrary units)					
RV	4475 ± 950	20138 ± 2469	6029 ± 875	<0.001	<0.001
LV	4540 ± 696	5877 ± 859	5221 ± 752		
P _{RV vs. LV}	n.s.	<0.001	n.s.		

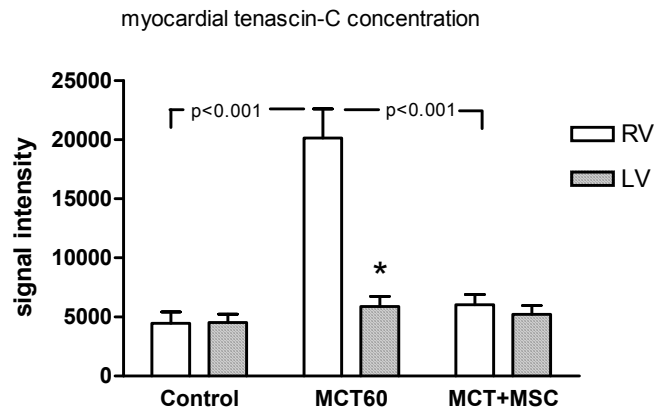
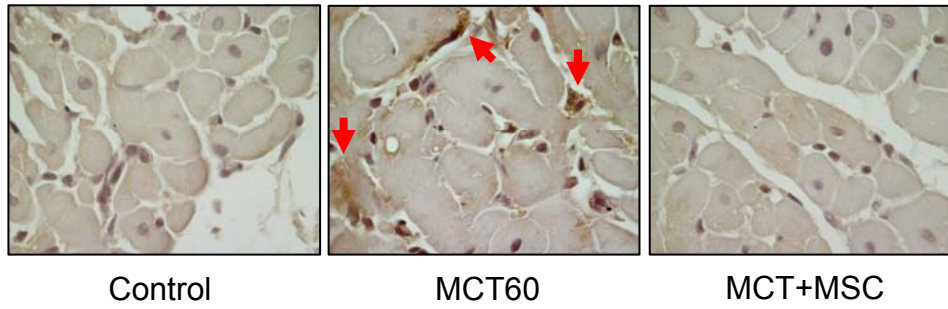


Figure 7
 Concentrations of tenascin-C in RV and LV myocardium of three groups of rats (Control, MCT60, and MCT+MSC) (lower panel). Upper panels present immunohistochemical images of myocardial tenascin-C in RV myocardium of control, MCT60 and MCT+MSC rats. Indicated are mean values \pm SEM of 16-64 analyzed images.
 * $p < 0.005$ vs. RV of the same group.

Collagenase activity

To answer the question whether RV failure is associated with increased myocardial collagenase activity that would allow RV dilatation, we analyzed myocardial concentrations of MMP1, cathepsin S and cathepsin K in RV myocardium of three groups of rats (control, MCT60, and MCT+MSC). These enzymes demonstrated no significant changes in RV myocardium between the groups (Table 4). In the MCT60 group myocardial concentrations in RV and LV did not differ significantly.

Table 4. Myocardial concentrations of three collagenolytic enzymes, matrix metalloproteinase-1 (MMP1), cathepsin S and cathepsin K in RV and LV of rats that have been treated without or with MCT, and without or with additional therapy using MSCs.

	Control	MCT60	MCT+MSC	P _{MCT60 vs Control}	P _{MCT60 vs MCT+MSC}
MMP1 (pixels protein/total pixels)					
RV	1.005±0.085(4)	1.122±0.141(4)	1.121±0.192(8)	n.s.	n.s.
LV	1.098±0.185(4)	1.200±0.230(4)	1.061±0.282(8)	n.s.	n.s.
P _{RV vs. LV}	n.s.	n.s.	n.s.		
Cathepsin S (pixels protein/total pixels)					
RV	0.924±0.344(5)	0.812±0.157(4)	0.717±0.222(8)	n.s.	n.s.
Cathepsin K (pixels protein/total pixels)					
RV	1.082±0.477(4)	1.430±0.676(3)	1.340±0.571(6)	n.s.	n.s.

Discussion

In this study we showed that i.v. administration of MSCs from donor rats with PAH to acceptor rats with MCT-induced PAH decreases RV peak systolic pressure, improves RV function, and prevents RV hypertrophy, at least to a great extent.

Pulmonary hypertension often occurs as a consequence of an isolated pulmonary arteriolar vasculopathy, and then is called pulmonary artery hypertension (PAH) [1]. Increased pulmonary vascular resistance imposes an overload to the RV, ultimately leading to RV failure. Although the distribution of ventilation/perfusion relationships in PAH patients is close to normal, arterial pO₂ is usually low, as is the venous oxygen saturation [30-32]. Although administration of 60 mg/kg MCT had resulted in a significant decrease of RV ejection fraction, several biochemical markers of RV overload were not conclusively positive. Expression of β MHC, proANP and proBNP mRNA in RV myocardium of rats in the MCT60 group was increased, but not significantly different from control. On the other hand, in overloaded RV myocardium several extracellular matrix proteins, such as tenascin-C, collagen I and collagen III, showed upregulated expression, whereas RV myocardial concentrations of three collagenolytic enzymes such as MMP1, cathepsin K and cathepsin S, were not significantly changed.

Current therapies of PAH include (i) prostacyclin analogues [33,34] such as epoprostenol [35,36], (ii) calcium channel blockers [37,38], (iii) angiotensin-converting enzyme [39], (iv) endothelin receptor antagonists such as bosentan [40,41], (v) phosphodiesterase-5 inhibitors such as sildenafil [32,42,43], and (vi) lung transplantation [44].

In experimental models of PAH several groups have shown that cell therapy using bone marrow-derived endothelial-like progenitor cells [12], bone marrow-derived MSCs [14], and umbilical cord blood mononuclear cells [45] given i.v. to rats with MCT-induced PAH resulted in lower pulmonary artery pressure, less RV hypertrophy, and improved survival. Bone marrow-derived cells obtained from rats injected with 5-fluorouracil 3 days earlier were able to reverse PAH, RV hypertrophy and medial hypertrophy in pulmonary arterioles [46]. The i.v. administration of MSCs *in vitro* transduced with the endothelial nitric oxide synthase (eNOS) gene into rats with MCT-induced PAH appeared more effective than i.v. administration of unmodified MSCs [14]. Similar results have been obtained with endothelial-like progenitor cells that after i.v. injection into MCT-treated rats were more effective in reversing PAH if transduced with the eNOS gene than if unmodified [12]. Likewise, pulmonary artery-derived smooth muscle cells that have been transduced *in vitro* with the eNOS gene, administered i.v. simultaneously with MCT, prevented the development of PAH, whereas pulmonary artery-derived smooth muscle cells transduced with a control vector did not [47]. The cell type carrying the eNOS gene is apparently not important, as even fibroblasts transfected with the eNOS gene were effective in reversing established PAH [48]. These results imply a major role for NO in vasodilation and regeneration of damaged lung tissue.

To date, the only clinical study reporting i.v. cell therapy in patients with PAH is a randomized study by Wang and coworkers who described a significant improvement of 6-minute hall walk distance after i.v. administration of autologous

endothelial progenitor cells in comparison with conventional therapy [11]. Other routes of administration of cells leading to successful therapeutic effects of cell therapy on PAH include intratracheal administration [49] and intra-parenchymal injection [15].

To mimic a therapeutic strategy in which a patient with PAH is treated by i.v. administration of autologous bone marrow-derived MSCs, we used MSCs that have been isolated from bone marrow of rats with MCT-induced PAH and injected i.v. to rats that had MCT treatment 14 days earlier. MSCs isolated from bone marrow of rats with MCT-induced PAH differed from MSCs isolated from bone marrow of healthy rats in several aspects. Proliferation rate was lower and VEGF secretion was higher, but potential of adipogenic and osteogenic differentiation and surface marker profile were not changed markedly in MSCs from rats with MCT-induced PAH, as compared to MSCs from healthy rats. In the present study we demonstrated that the therapy of rats with MCT-induced PAH with MSC from rats with MCT-induced PAH was successful, as RV systolic pressure was reduced, RV hypertrophy was reduced, and RV function was improved, compared to rats with MCT treatment without cell therapy.

The mechanism of action of i.v. cell therapy with MSCs is not yet elucidated. As to the localization of Dil-labeled MSCs in the lung, 14 days after i.v. injection of 10^6 MSCs per rat, no evidence of massive integration into arteries and bronchi have been obtained. Association and integration of MSCs with pulmonary arterioles have been noticed, but this can hardly explain the substantial therapeutic efficacy of MSCs in MCT-induced lung damage. The therapeutic actions of MSCs engrafted in injured lungs are considered to be the result of paracrine effects [50]. Particularly the secretion of cytokines and growth factors is the basis of angiogenic and reverse remodeling reactions. One important paracrine factor is VEGF that induces angiogenesis by inducing proliferation, differentiation and chemotaxis of endothelial cells [51,52]. In situations of vascular trauma cytokines and growth factors, such as VEGF, promote recruitment of endothelial (progenitor) cells to promote vascular healing and repair [53,54]. Administration of pulmonary artery-derived smooth muscle cells to rats with MCT-induced PAH had therapeutic effects only if transduced *in vitro* with the VEGF-A gene [55]. Likewise, i.v. administration of fibroblasts transfected with the VEGF-A gene were effective in reversing established PAH, whereas untransduced fibroblasts were not [48]. The relationship between pulmonary vascular remodeling and lack of VEGF is demonstrated by Fujita and coworkers who showed that in mice overexpressing TNF α development of PAH is associated with decreased VEGF mRNA in lung tissue [56]. Surprisingly, the stem cells used in the present study, the MSCs from bone-marrow of rats with MCT-induced PAH, produced even more VEGF *in vitro* than the MSCs from bone-marrow of healthy rats. This finding may explain the potent therapeutic effects of the MSCs from MCT-treated rats.

Several groups have shown that i.v. administration of pulmonary artery-derived smooth muscle cells [47], skin fibroblasts [12] or bone marrow-derived mononuclear cells [13] to rats with MCT-induced PAH had no appreciable effect on RV systolic pressure and pulmonary artery remodeling. As a reference cell type we chose skin fibroblasts (SFs) of healthy rats, also used by Zhao *et al.* [12] to illustrate their lack of effectivity to treat PAH in MCT-treated rats. However, we have observed some beneficial effects of injected SFs from healthy rats on RV

systolic pressure, RV hypertrophy, and RV function, although these effects were less pronounced than observed with MSCs from rats with MCT-induced PAH. We could not detect i.v. injected SFs trapped in the lung and/or the RV myocardium, but any therapeutic effect of injected SFs on PAH and RV hypertrophy should be explained by paracrine effects on the pulmonary arterioles, thereby decreasing the pulmonary vascular resistance.

Conclusions

In conclusion we have found that intravenous administration of MSCs from rats with PAH to acceptor rats with MCT-induced PAH decreased PAH, prevented RV hypertrophy, and improved RV function. These results suggest that patients with PAH may be treated successfully with autologous MSCs.

Acknowledgements

The technical support/assistance of Mrs. E. van Beelen (Department of Immunohematology & Blood Bank, LUMC) and Dr S. Knaan-Shanzer (Department of Molecular Cell Biology, LUMC) is gratefully acknowledged.

References

1. Farber HW, Loscalzo J. Pulmonary arterial hypertension. *N Engl J Med* 2004; 351:1655-65.
2. Lulich JJ, Merkow L. Pulmonary arteritis produced in rats by feeding *Crotalaria spectabilis*. *Lab Invest* 1961;10: 744-50.
3. Meyrick B, Gamble W, Reid L. Development of *Crotalaria* pulmonary hypertension: hemodynamic and structural study. *Am J Physiol Heart Circ Physiol* 1980; 239: H692-H702.
4. Hessel MHM, Steendijk P, den Adel B, Schutte CI, van der Laarse A. Characterization of right ventricular function after monocrotaline-induced pulmonary hypertension in the intact rat. *Am J Physiol Heart Circ Physiol* 2006; 291: 2424-30.
5. Hessel MHM, Steendijk P, den Adel B, Schutte CI, van der Laarse A. Pressure overload-induced right ventricular dilatation is associated with re-expression of myocardial tenascin-C and increased plasma levels of tenascin-C (abstract). *Circulation* 2006;114 (suppl II):II-133.
6. Barton PJR, Birks EJ, Felkin LE, Cullen ME, Koban MU, Yacoub MH. Increased expression of extracellular matrix regulators TIMP1 and MMP1 in deteriorating heart failure. *J Heart Lung Transplant* 2003;22:738-44.
7. Li YY, Feng Y, McTiernan CF, Pei W, Moravec CS, Wang P, Rosenblum W, Kormos RL, Feldman AM. Downregulation of matrix metalloproteinases and reduction in collagen damage in the failing human heart after support with left ventricular assist devices. *Circulation* 2001;104:1147-52.
8. Bruggink AH. Reverse remodeling of the extracellular matrix in heart failure after left ventricular mechanical support. PhD Thesis, University Utrecht, 2008.
9. Campian ME, Hardziyenka M, Michel MC, Tan HL. How valid are animal models to evaluate treatments for pulmonary hypertension? *Naunyn-Schmiedeberg's Arch Pharmacol* 2006; 373: 391-400.
10. Passier R, Mummery C. Origin and use of embryonic and adult stem cells in differentiation and tissue repair. *Cardiovasc Res* 2003; 58: 324-35.
11. Wang X-X, Zhang F-R, Shang Y-P, Zhu J-H, Xie X-D, Tao Q-M, Zhu J-H, Chen J-Z. Transplantation of autologous endothelial progenitor cells may be beneficial in patients with idiopathic pulmonary arterial hypertension. *J Am Coll Cardiol* 2007;49:1566-71.
12. Zhao YD, Courtman DW, Deng Y, Kugathasan L, Zhang Q, Stewart DJ. Rescue of monocrotaline-induced pulmonary arterial hypertension using bone marrow-derived endothelial-like progenitor cells. Efficacy of combined cell and eNOS gene therapy in established disease. *Circ Res* 2005; 96: 442-50.
13. Sahara M, Sata M, Morita T, Nakamura K, Hirata Y, Nagai R. Diverse contribution of bone marrow-derived cells to vascular remodeling associated with pulmonary arterial hypertension and arterial neointimal formation. *Circulation* 2007;115:509-17.
14. Kanki-Harimoto S, Horimoto H, Mieno S, Kishida K, Watanabe F, Furuya E, Katsumata T. Implantation of mesenchymal stem cells overexpressing endothelial nitric oxide synthase improves right ventricular impairments caused by pulmonary hypertension. *Circulation* 2006;114(suppl I):I-181-I-185.
15. Takahashi M, Nakamura T, Toba T, Kajiwara N, Kato H, Shimizu Y. Transplantation of endothelial progenitor cells into the lung to alleviate pulmonary hypertension in dogs. *Tissue Eng* 2004;10:771-9.
16. Lennon DP, Edmison JM, Caplan AI. Cultivation of rat marrow-derived mesenchymal stem cells in reduced oxygen tension: effects on in vitro and in vivo osteochondrogenesis. *J Cell Physiol* 2001;187:345-55.

17. Grayson WL, Zhao F, Izadpanah R, Bunnell B, Ma T. Effects of hypoxia on human mesenchymal stem cell expansion and plasticity in SD constructs. *J Cell Physiol* 2006; 207: 331-9.
18. Grayson WL, Zhao F, Bunnell B, Ma T. Hypoxia enhances proliferation and tissue formation of human mesenchymal stem cells. *Biochem Biophys Res Comm* 2007; 358: 948-53.
19. Potier E, Ferreira E, Andriamanalijaona R, Pujol J-P, Oudina K, Logeart-Avramoglou D, Petite H. Hypoxia affects mesenchymal stromal cell osteogenic differentiation and angiogenic factor expression. *Bone* 2007;40:1078-87.
20. Buravkova LB, Anokhina EB. Effect of hypoxia on stromal precursors from rat bone marrow at the early stage of culturing. *Bull Exp Biol Med* 2007; 143: 411-3.
21. Matsuda N, Morita N, Matsuda K, Watanabe M. Proliferation and differentiation of human osteoblastic cells associated with differential activation of MAP kinases in response to epidermal growth factor, hypoxia, and mechanical stress *in vitro*. *Biochem Biophys Res Comm* 1998;249:350-4.
22. Park JH, Park BH, Kim HK, Park TS, Baek HS. Hypoxia decreases Runx2/Cbfa1 expression in human osteoblast-like cells. *Mol Cell Endocrinol* 2002;192:197-203.
23. Tuncay OC, Ho D, Barker MK. Oxygen tension regulates osteoblast function. *Am J Orthod Dentofac Orthop* 1994;105:457-63.
24. Pittenger MF, Mackay AM, Beck SC, Jaiswal RK, Douglas R, Mosca JD, Moorman MA, Simonetti DW, Craig S, Marshak DR. Multilineage potential of adult human mesenchymal stem cells. *Science* 1999; 284: 143-7.
25. Mattocks AR, Jukes R, Brown J. Simple procedures for preparing putative toxic metabolites of pyrrolizidine alkaloids. *Toxicol* 1989; 27: 561-7.
26. Sehgal PB, Mukhopadhyay S, Xu F, Patel K, Shah M. Dysfunction of Golgi tethers, SNAREs, and SNAPs in monocrotaline-induced pulmonary hypertension. *Am J Physiol Lung Cell Mol Physiol* 2007; 292: L1526-L1542.
27. Leeuwenburgh BP, Steendijk P, Helbing WA, Baan J. Indexes of diastolic RV function: load dependence and changes after chronic RV pressure overload in lambs. *Am J Physiol Heart Circ Physiol* 2002;282:H1350-H1358.
28. Burkhoff D, Mirsky I, Suga H. Assessment of systolic and diastolic ventricular properties via pressure-volume analysis: a guide for clinical, translational, and basic researchers. *Am J Physiol Heart Circ Physiol* 2005; 289: H501-H512.
29. Pfaffl MW. A new mathematical model for relative quantification in real-time RT-PCR. *Nucleic Acids Res* 2001;29: e45.
30. Dantzker DR, Bower JS. Mechanisms of gas exchange abnormality in patients with chronic obliterative pulmonary vascular disease. *J Clin Invest* 1979;64:1050-5.
31. Melot C, Naeije R, Mols P, Vandembossche JL, Denolin H. Effects of nifedipine on ventilation/perfusion matching in primary pulmonary hypertension. *Chest* 1983;83:203-7.
32. Schermuly RT, Kreisselmeier KP, Ghofrani HA, Yilmaz H, Butrous G, Ermert L, Ermert M, Weissmann N, Rose F, Guenther A, Walmrath D, Seeger W, Grimminger F. Chronic sildenafil treatment inhibits monocrotaline-induced pulmonary hypertension in rats. *Am J Respir Crit Care Med*. 2004;169:39-45.
33. McLaughlin VV, Rich S. Pulmonary hypertension – advances in medical and surgical intervention. *J Heart Lung Transplant* 1998;17:739-43.
34. Wanstall JC, Jefferey TK. Recognition and management of pulmonary hypertension. *Drugs* 1998;56:989-1007.
35. Hinderliter AL, Willis PW, Barst RJ, Rich S, Rubin LJ, Badesch DB, Groves BM, McGoon MD, Tapson VF, Bourge RC, Brundage BH, Koerner SK, Langleben D, Keller CA, Murali S, Uretsky BF, Koch G, Li S, Clayton LM, Jöbsis MM, Blackburn SD jr, Crow JW, Long WA, for the Primary Pulmonary Hypertension Study Group. Effects of long-term infusion of prostacyclin (Epoprostenol) on echocardiographic measures of right ventricular structure and function in primary pulmonary hypertension. *Circulation* 1997;95:1479-86.

36. Oikawa M, Kagaya Y, Otani H, Sakuma M, Demachi J, Suzuki J, Takahashi T, Nawata J, Ido T, Watanabe J, Shirato K. Increased [¹⁸F]fluorodeoxyglucose accumulation in right ventricular free wall in patients with pulmonary hypertension and the effect of Epoprostenol. *J Am Coll Cardiol* 2005;45:1849-55.
37. Sitbon O, Humbert M, Jaïs X, Loos V, Hamid AM, Provencher S, Garcia G, Parent F, Hervé P, Simonneau G. Long-term response to calcium channel blockers in idiopathic pulmonary arterial hypertension. *Circulation* 2005;111:3105-11.
38. Mawatari E, Hongo M, Sakai A, Terasawa F, Takahashi M, Yazaki Y, Kinoshita O, Ikeda U. Amlodipine prevents monocrotaline-induced pulmonary arterial hypertension and prolongs survival in rats independent of blood pressure lowering. *Clin Exp Pharmacol Physiol* 2007;34:594-600.
39. Abraham WT, Reynolds MV, Gottschall B, Badesch DB, Wynne KM, Groves BM, Lowes BD, Bristow MR, Perryman MB, Voelkel NF. Importance of angiotensin-converting enzyme in pulmonary hypertension. *Cardiology* 1995;86(suppl 1):9-15.
40. Galiè N, Hinderliter AL, Torbicki A, Fourme T, Simonneau G, Pulido T, Espinola-Zavaleta N, Rocchi G, Manes A, Frantz R, Kurzyna M, Nagueh SF, Barst R, Channick R, Dujardin K, Kronenberg A, Leconte I, Rainisio M, Rubin L. Effects of the oral endothelin-receptor antagonist bosentan on echocardiographic and Doppler measures in patients with pulmonary arterial hypertension. *J Am Coll Cardiol* 2003;41:1380-6.
41. Dingemans J, van Giersbergen LM. Clinical pharmacology of bosentan, a dual endothelin receptor antagonist. *Clin Pharmacokinet* 2004;43(15):1089-1115.
42. Galiè N, Ghofrani HA, Torbicki A, Barst RJ, Rubin LJ, Badesch D, Fleming T, Parpia T, Burgess G, Branzi A, Grimminger F, Kurzyna M, Simonneau G, for the Sildenafil Use in Pulmonary Arterial Hypertension (SUPER) Study Group. Sildenafil citrate therapy for pulmonary arterial hypertension. *N Engl J Med* 2005;353:2148-57.
43. Wilkins MR, Paul GA, Strange JW, Tunariu N, Gin-Sing W, Banya WA, Westwood MA, Stefanidis A, Ng LL, Pennell DJ, Mohiaddin RH, Nihoyannopoulos P, Gibbs JSR. Sildenafil versus endothelin receptor antagonist for pulmonary hypertension (SERAPH) study. *Am J Respir Crit Care Med* 2005;171:1292-7.
44. Kasimir MT, Seebacher G, Jaksch P, Winkler G, Schmid K, Marta GM, Simon P, Klepetko W. Reverse cardiac remodelling in patients with primary pulmonary hypertension after isolated lung transplantation. *Eur J Cardiothorac Surg* 2004;26:776-81.
45. Nagaya N, Kangawa K, mKanda M, Uematsu M, Horio T, Fukuyama N, Hino J, Harada-Shiba M, Okumura H, Tabata Y, Mochizuki N, Chiba Y, Nishioka K, Miyatake K, Asahara T, Hara H, Mori H. Hybrid cell-gene therapy for pulmonary hypertension based on phagocytosing action of endothelial progenitor cells. *Circulation* 2003;108:889-95.
46. Raoul W, Wagner-Ballon O, Saber G, Hulin A, Marcos E, Giraudier S, Vainchenker W, Adnot S, Eddahibi S, Maitre B. Effects of bone marrow-derived cells on monocrotaline- and hypoxia-induced pulmonary hypertension in mice. *Resp Res* 2007;8:8.
47. Campbell AIM, Kuliszewski MA, Stewart DJ. Cell-based gene transfer to the pulmonary vasculature. Endothelial nitric oxide synthase overexpression inhibits monocrotaline-induced pulmonary hypertension. *Am J Respir Cell Mol Biol* 1999; 21: 567-75.
48. Zhao YD, Courtman DW, Ng DS, Robb MJ, Deng YP, Trogadis J, Han RN, Stewart DJ. Microvascular regeneration in established pulmonary hypertension by angiogenic gene transfer. *Am J Respir Cell Mol Biol* 2006;35:182-9.
49. Baber SR, Deng, Master RG, Bunnell BA, Taylor BK, Murthy SN, Hyman AL, Kadowitz PJ. Intratracheal mesenchymal stem cell administration attenuates monocrotaline induced pulmonary hypertension and endothelial dysfunction. *Am J Physiol Heart Circ Physiol* 2007; 292: H1120-H1128.
50. Patel KM, Crisostomo P, Lahm T, Markel T, Herring C, Wang M, Meldrum KK, Lillemoe KD, Meldrum DR. Mesenchymal stem cells attenuate hypoxic pulmonary vasoconstriction by a paracrine mechanism. *J Surg Res* 2007;143:281-5.

51. Leung DW, Cachianes G, Kuang WJ, Goeddel DV, Ferrara N. Vascular endothelial growth factor is a secreted angiogenic mitogen. *Science* 1989; 246: 1306-9.
52. Flamme I, Breier G, Risau W. Vascular endothelial growth factor (VEGF) and VEGF receptor 2 (flk-1) are expressed during vasculogenesis and vascular differentiation in the quail embryo. *Dev Biol* 1995; 169: 699-712.
53. Asahara T, Murohara T, Sullivan A, Silver M, van der Zee R, Li T, Witzenbichler B, Schatteman G, Isner JM. Isolation of putative progenitor endothelial cells for angiogenesis. *Science* 1997; 275: 964-7.
54. Takahashi T, Kalka C, Masuda H, Chen D, Silver M, Kearney M, Magner M, Isner JM, Asahara T. Ischemia- and cytokine-induced mobilization of bone marrow-derived endothelial progenitor cells for neovascularization. *Nat Med* 1999; 5: 434-8.
55. Campbell AIM, Zhao Y, Sandhu R, Stewart DJ. Cell-based gene transfer of vascular endothelial growth factor attenuates monocrotaline-induced pulmonary hypertension. *Circulation* 2001; 104: 2242-8.
56. Fujita M, Mason RJ, Cool C, Shannon JM, Hara N, Fagan KA. Pulmonary hypertension in TNF α -overexpressing mice is associated with decreased VEGF gene expression. *J Appl Physiol* 2002;93:2162-70.

Chapter 8

An exploration of the role of Kv channels in excitability of right ventricular cardiomyocytes from normal adult rats

S. Umar
W. P. M. van Meerwijk
D. A. Pijnappels
M. J. Schlij
A. van der Laarse
D. L. Ypey

Abstract

Purpose: In the present study we analyzed mechanisms of excitability of right ventricular myocytes (RVMCs) isolated from the adult rat heart, making use of the naturally occurring variability of excitability of these cells. We focused on the role of voltage-activated K^+ currents (I_{kv}) in shaping the current pulse-evoked action potential (AP) and in generating sustained depolarizing current-induced automaticity (DIA).

Methods: Membrane potentials and currents were measured with the whole-cell patch-clamp technique in current- and voltage-clamp configuration, respectively, with standard-normal intra- and extracellular solutions. Simulation experiments were carried out with a computer model describing the electrophysiology of the RVMC of the rat (Pandit *et al.*, 2001, 2003).

Results: The resting conditions were characterized by a resting membrane potential (RMP) of ~ -70 mV, a membrane resistance at RMP of ~ 111 M Ω , and a membrane capacitance (C_m) of ~ 173 pF (17-20 cells). Voltage-clamp experiments revealed the variable expression of voltage-activated Na^+ current (I_{nav}), inward rectifier K^+ current (I_{kir}) and voltage-activated K^+ current (I_{kv}), including the transient current I_t and sustained current I_{ss} (20 cells). L-type calcium current (I_{caL}) was recognized during inactivation of I_{nav} and I_{kv} by a holding potential of -40 mV. APs evoked by current-clamp pulses were variable in amplitude and duration, probably due to the variable (endo-, meso- and epicardial) origin of the myocytes. AP-properties are described for two example groups: (1) High-peak/Long-duration APs (HL-APs) with AP-peak amplitudes of 30-40 mV and AP-durations of 50-110 ms at half AP-height, and (2) Low-peak/Short-duration APs (LS-APs) with peaks of -10 to +10 mV and durations of 20-30 ms. AP-amplitude and duration in the whole population were negatively correlated with I_t expression, indicating that activation of I_t upon activation of I_{nav} lowers the degree of activation of I_{caL} during AP-generation. DIA was usually recorded as an after-effect of the first AP upon applying the sustained current, but it was always transient with 1-6 afterwaves within the first 1.6 s. DIA was critically dependent on the strength of the sustained current and occurred at membrane potentials > -40 mV, where all I_{na} and most I_{kv} are becoming inactivated. DIA was inhibited by 10 μ mol/L nifedipine ($n=4$) but was not clearly dependent on the size of I_t . This indicates that the automaticity mechanism of DIA largely depends on the properties of I_{caL} as an inward current. Model experiments reproduced the decrease of AP-duration with an increase in I_t and revealed a DIA-mechanism based on I_{caL} deinactivation and I_{ss} deactivation at depolarized potentials.

Conclusion: We discuss these results in terms of their implications for understanding normal RVMC excitability and for arrhythmogenic mechanisms in heart failure.

Introduction

While investigating in a recent study the effect of stem cell therapy on heart failure related changes in the electrophysiology of right ventricular myocytes (RVMCs) from hearts of rats with experimental pulmonary arterial hypertension, we were confronted with a much greater variability in excitability in these RVMCs, normal or diseased, than anticipated from the literature (Lee *et al.*, 1997 and Pandit *et al.*, 2001 & 2003). For example, one group of cells had a strongly reduced excitability as apparent from very low peak-height (at membrane potential $V_m < 0$ mV) and short-duration (~25 ms) action potentials (APs), while another group had normal peak-height (at $V_m \sim +40$ mV) and very long-duration (~100 ms) APs. This hampered comparison of the excitability properties of RVMCs from normal, diseased and stem cell-treated animals and required a preliminary electrophysiological study of RVMCs from normal rats to characterize and explain this variability.

One of the reasons why RVMCs are heterogeneous in their excitability properties is that they have a mixed histological endo-, meso- and epicardial origin (Clark *et al.*, 1993; Antzelevitch *et al.*, 2000). From a mechanistic point of view, variability may be a great source of information for understanding the functional consequences of electrophysiological differences between heart cells. This is of particular importance, as insights in mechanisms of normal and abnormal AP-shaping and of regular and irregular heart rhythm generation are still limited, despite intensive experimental and theoretical research on this subject (Pandit *et al.*, 2001, 2003; Pogwizd and Bers, 2004; Antoons *et al.*, 2007). Therefore, we have analyzed the variability in excitability of normal adult rat RVMCs by systematically comparing the current-clamp properties of the cells (excitability) with the voltage-clamp properties (ion channel expression) of the same cells under standard-normal conditions. Besides studying AP-shaping by the various ion channel types, we also studied the ionic mechanism of generating depolarizing current-induced automaticity (DIA), a mode of excitability of ventricular myocytes that has been studied before as a model for arrhythmogenesis 'from abnormal automaticity' mainly in other species of mammals than the rat (Katzung, 1975; Malecot *et al.*, 1985; Peters *et al.*, 2000). By contrasting the DIA-mode excitability under sustained current stimulation with that of current-pulse evoked APs in patch-clamp experiments and by theoretical modeling, we aimed to answer questions about the particular role of K_v -currents (I_{kv}) in pulse-evoked AP-shaping and in generating DIA.

Because we were primarily interested in the role of the electrical membrane properties in cardiomyocyte excitability, we excluded intracellular calcium dynamics by using the calcium buffer EGTA. This also prevented a significant role of the sodium/calcium-exchanger (NCX) in the measured myocyte excitability (cf. Pogwizd and Bers, 2004).

The model of Pandit *et al.* (2001, 2003) was used to explore mechanistic explanations of the observed excitability properties of rat RVMCs. A particular result was that the model simulations revealed that DIAs occurred as a result of the kinetic properties of I_{CaL} and I_{ss} .

The present results provide a basis for analyzing differences in excitability between ventricular myocytes from normal rats and from rats with experimental heart failure. They may also provide clues for a better understanding of mechanisms of heart failure-related ventricular arrhythmias.

Materials and Methods

Animals and ventricular myocyte isolation

Rats were treated in accordance with the national guidelines and with permission of the Animal Experiments Committee of the Leiden University Medical Center. The animals were housed, two animals per cage, with a 12:12-h light-dark cycle and an unrestricted food and water supply. Three-month old female Wistar rats weighing 200-250 g (Harlan, Zeist, the Netherlands) were used.

Cardiomyocyte isolation

The rat was anaesthetised, and the thorax was opened. The heart was taken out quickly and immediately transferred to ice-cold, oxygenated Tyrode solution. The heart was mounted to a Langendorff perfusion set-up and then perfused for 5 min with an oxygenated Tyrode solution at constant pressure (70 mmHg) at 37° C. The perfusion fluid was replaced by an oxygenated, low calcium (10 μ mol/L) perfusion fluid. Contractions disappeared within 30 s. After 5 min of low calcium perfusion, the perfusion was continued in a recirculating manner at a perfusion pressure of 60 mm Hg. At that time collagenase (0.06%) was added. Thirty min later, the flow rate was too high to maintain a perfusion pressure of 60 mm Hg. Then, the heart was removed and the right ventricle (RV) was separated from the left ventricle and the interventricular septum. RV was cut in small pieces, incubated in a fresh collagenase (0.06%) solution, and dissociated in a waterbath shaker at 37° C. After sedimentation of the myocytes, sedimented myocytes were resuspended and stored at 37° C in fresh HEPES-buffered salt solution containing (in mmol/L) NaCl 125, KCl 5, MgSO₄ 1, KH₂PO₄ 1, CaCl₂ 1.8, NaHCO₃ 10, HEPES 20, glucose 5.5, pH 7.4. The average fraction of rod-shaped myocytes was 80 %. The percentage of rod-shaped myocytes decreased by about 10 % during 6 h at 37° C.

Whole-cell patch-clamp experiments

Membrane potentials (V_m) and membrane currents (I_m) of right ventricular myocytes (RVMCs) from 22 cells from 5 rats were measured with the patch-clamp technique in the whole-cell current-clamp and voltage-clamp configuration, respectively. The recordings were performed at 21°C with an L/M-PC amplifier (List-Medical, Darmstadt, Germany), set at 3 KHz filtering. pClamp/Clampex8 software (Axon Instruments, Molecular Devices, Sunnyvale, CA, USA) was used for data acquisition and off-line analysis. The bath solution contained (in mmol/L) NaCl 137, KCl 5, MgCl₂ 1, CaCl₂ 1.8, HEPES 10, and glucose 11, pH 7.4, while the pipette solution contained (in mmol/L) Na₂ATP 6, KCl 115, MgCl₂ 1, EGTA 5 and HEPES 10, pH 7.4). Pipette resistance (R_{pip}) was 2.8 ± 0.4 M Ω (n=20), seal

resistance (R_{seal}) was $4.1 \pm 1.3 \text{ G}\Omega$ ($n=13$), and series resistance (R_{ser}) was $6.6 \pm 3.1 \text{ M}\Omega$ ($n=20$). Pipette potential offsets (V_{pips}) developing during the experiments were usually between +1 and -2.3 mV , and were not corrected for. Larger offsets were corrected in 3 cells.

In order to be able to check R_{ser} and C_m -measurements, R_{ser} was not compensated and the slow capacitive transients were not cancelled. R_{ser} -values apply to the immediately preceding or following voltage-clamp tests, because R_{ser} tended to increase during the experiment. Whole-cell recordings after gigasealing ($n=20$) were accepted for analysis if the membrane potential stabilized within a few minutes and if the membrane resistance measured in voltage-clamp at -60 mV ($R_m(-60)$) was $>100 \text{ M}\Omega$ (to avoid leaky membranes). Voltage-drop artifacts across R_{ser} during current-clamp stimulation (usually $<10 \text{ mV}$) were corrected for, except when they were $<2 \text{ mV}$. Voltage errors across R_{ser} during voltage-clamp were usually $<30 \text{ mV}$ ($<5 \text{ nA}$ times $6 \text{ M}\Omega$).

This was only considered acceptable for large driving forces, such as during I_{kv} recording at $+60 \text{ mV}$, where the ideal driving force ($V_m - E_k$) = 144 mV and the real driving force is $<20\%$ smaller because of the $<30\text{-mV}$ drop in voltage across R_{ser} . This kind of measurement error was confirmed in our model simulations (see below). We, therefore, realize that our R_{ser} -values are too large to reliably measure maximal values of I_{nav} , I_{kir} and I_{kv} . So, the average values of these currents presented in Table 1, measured at potentials where contamination with other currents is small, should still be considered as underestimates. Nevertheless, the R_{ser} values were good enough to allow identification of these currents and to detect the activation potentials of these currents for current detection levels within 0.5 nA ($<2\%$ voltage error). For a rough quantitative measurement of I_{kv} , its peak, I_{kvp} , was measured at $+60 \text{ mV}$, not only because its driving force is large at that potential, but also because I_{nav} and I_{caL} are minimal at that potential, since their reversal potentials are close to $+60 \text{ mV}$ (see Figs. 3 and 5). The amplitude of I_t was determined by subtracting the sustained I_{kv} (I_{ss}) at 60 mV , approximated by the current at $t=180 \text{ ms}$, from the peak I_{kv} (I_{kvp}). This procedure also included subtraction of leak current in the calculation of I_{tp} . To minimize disturbing effects of variability in I_{tp} -values related to a variability in cell size, I_{tp} values were corrected for cell size by dividing I_{tp} by C_m .

Modeling

We have used the computer model of the rat ventricular myocyte made by Pandit *et al.* (2001, 2003) to explore both the excitability mechanism of current-pulse evoked action potentials (pAPs) and that of depolarizing-current induced automaticity (DIA) in the RVMC of the adult rat.

The model of Pandit *et al.* (2001, 2003) is a Hodgkin-Huxley type membrane model coupled to an intracellular ion-dynamics model via the intracellular concentrations of Ca, Na and K. It can be used in a left-epicardial and left-endocardial myocyte version (Pandit *et al.*, 2001) and in a right-epicardial one (Pandit *et al.*, 2003).

The membrane model is largely based on published experimental work and contains the currents identified in the present experiments (I_{kir} , I_{nav} , I_{kv} (I_t and I_{ss}), I_{caL}) together with two other currents of smaller amplitude (I_f and background current I_b) and with the electrogenic currents of the ion transporters the sodium-calcium exchanger (NCX), the Na^+ , K^+ -ATPase and the plasma membrane calcium ATP-ase (PMCA). Dr. Pandit has kindly provided us with a list of misprint-corrections (including 5 obvious sign errors in exponentials) to allow us to make proper runs with the model (personal communication, 2008).

We have extended the model with the electrical connection of the pipette to the cell in order to be able to account for the non-ideal voltage- and current-clamp properties of the measurements (large series resistance R_{ser}). We have used the model as a plasma membrane model uncoupled from intracellular calcium signaling and ion changes by setting the intracellular concentrations of $[Ca^{2+}]_i=79$ nmol/L, $[Na]_i=10.7$ mmol/L, and $[K]_i=139.3$ mmol/L, which conditions approximate the conditions in our ruptured whole-cell experiments with EGTA in the pipette.

Statistics

Groups of observations are described as means \pm SD (n), unless mentioned otherwise. Correlation analysis is performed with nonparametric (Spearman) tests. We used the SPSS software (SPSS Inc., Chicago, IL, USA). A p -value <0.05 is considered to represent a significant test result.

Results

Basic electrical properties of adult rat RVMCs

Basic electrical membrane properties such as the RMP, R_m and C_m determine the excitability properties of an excitable cell. RMP determines the number of available Nav, Cav and Kv channels by controlling the degree of inactivation of these channels, while R_m and C_m determine the effectiveness of current stimuli to excite a cell. Therefore, we first consider those properties of our RVMCs under our standard-normal conditions, including the variabilities of these properties.

The RMP recordings were rather stable around -70 mV (see Table 1). Initially, RMP values (RMP_i) were around -60 mV (range -40 to -71 mV), but after a few minutes these values stabilized to an $RMP = -69.5 \pm 2.4$ mV ($n=20$) and remained near that value for at least 15 min (see Table 1). A RMP of ~ -70 mV, not far above the calculated Nernst potential for the K^+ gradient (-84 mV), is consistent with a major role of I_{kir} -channels in establishing RMP.

R_m was measured in current-clamp with depolarizing 50- or 100-pA current pulses from RMP as well as with 10-mV depolarizing voltage-steps in voltage-clamp from a holding potential $V_h = -60$ mV: $R_m(rmp) = 111 \pm 67$ M Ω ($n=17$), while $R_m(-60) = 384 \pm 296$ M Ω ($n=20$) (Table 1) for the selected cells (criterion $R_m(-60) > 100$ M Ω), consistent with an RMP mainly resulting from activation of I_{kir} -channels.

C_m -values were obtained from capacitive current responses to 10-mV depolarizing voltage-clamp steps and were $C_m = 173 \pm 65$ pF ($n=20$) (Table 1). Thus, the membrane time constant of the cells around RMP was ~ 20 ms ($R_m(rmp) \cdot C_m$), implicating latency times around 20 ms for AP-generation with just-above threshold current stimuli, consistent with the records in Fig. 1b and 2b.

The measurements imply a variability, in which RMP is remarkably constant between myocytes with a variation coefficient of 3%, compared to coefficients of $R_m(rmp)$, $R_m(-60)$ and C_m of 60%, 77% and 38%, respectively.

Group-1 RVMCs with High-peak/Long-duration pulse-evoked action potentials (HL-APs)

The differences in AP-properties between example group 1, group 2 and the remaining cells with intermediate properties enabled us to analyze current-clamp behaviour (excitability) in terms of voltage-clamp properties for groups of RVMCs with different excitability.

The first example of excitability is that of a myocyte with a high-peak (at $+38$ mV) and long-duration AP (70-100ms at half height) (HL-AP) evoked by a short current pulse from a resting membrane potential $RMP \sim -72$ mV (Fig. 1b, c). The fast depolarizing and slow delayed repolarizing phase gives the typical asymmetrical shape of a mammalian cardiac AP with plateau-phase. Five out of 13 cells had APs of the HL-AP type further described below, i.e. with APPs of 30-40 mV and APDs of 50-110 ms at half-height (encircled as a group in the upper left corner of Fig. 4a).

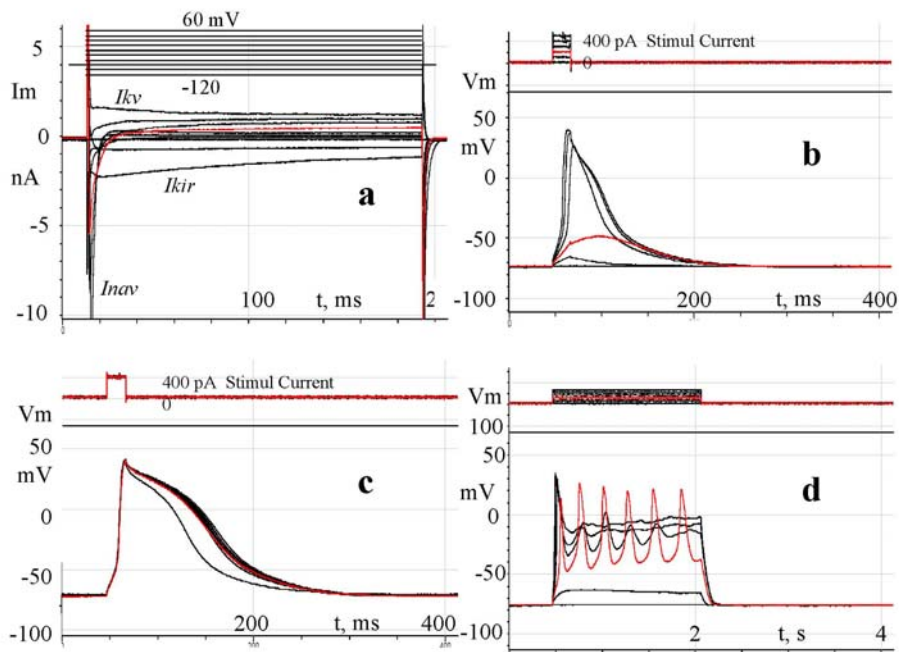


Fig. 1. Voltage- and current-clamp properties of an adult rat right ventricular myocyte (RVMC) with a high-peak and long-duration current-pulse evoked action potential (group 1 with HL-APs). All records are from the same cell.

(a) Superimposed voltage-clamp current-records from the cell evoked by voltage steps of 180 ms duration from the holding potential $V_h = -80$ mV to membrane potential (V_m) values of -120 mV and higher up to $+60$ mV, with increments of $+20$ mV. The resting intervals between the steps (at $V_h = -80$ mV) were 5 s. The voltage activated inward (negative) fast sodium current (I_{nav}) is large compared to the maximal currents of the inward rectifier potassium current (I_{kir}) and the voltage-activated (positive) potassium current (I_{kv}). The short current peaks preceding the I_{na} , I_{kv} and I_{kir} records are the rapid capacitive current transients charging the membrane capacitance to the applied potentials. The initial resting potential (RMP) was -68 mV but stabilized later between -72 and -76 mV. Seal resistance (R_{seal}) was 6 G Ω , membrane capacitance (C_m) was 150 pF, membrane resistance at -60 mV ($R_m(-60\text{mV})$) was 400 M Ω , and series resistance (R_{ser}) was 5 M Ω .

(b) Superimposed V_m records (bottom records) upon short (20 ms) current-pulse stimulations with increasing intensities (0 to 500 pA, with 100-pA increments, see top records). Resting interval between the pulses was 5 s. Notice that the V_m -threshold for evoking an AP is ~ 50 mV, while the current threshold is just above 100 pA. The first evoked AP is a bit shorter in duration than the two subsequent APs. The small instantaneous voltage changes in the records (order of 1 mV, consistent with an $R_{ser} = 5$ M Ω) at the start and stop of the pulses are the voltage changes over R_{ser} , which are also visible in Fig. 1c and 1d.

(c) Superimposed action potential (AP) records (bottom records), evoked by a 10-pulse/1-Hz train of 20-ms/400-pA current-pulses (top records). The shortest AP is the first AP, the 9 subsequent longer APs show some variation in repolarization time. Thus, the AP of this cell has largely adapted its APD to the train after ~ 1 s.

(d) Superimposed V_m records (bottom records) upon sustained depolarizing current stimulation with current steps of 1.6-s durations and increasing amplitudes with 50-pA increments from 0 to 250 pA (top records). Resting intervals between the current steps were 5 s. Notice that the amplitude and the number of waves in the damped oscillations decrease with increased current induced depolarization.

The voltage-clamp currents (Fig. 1a), evoked by voltage steps from a holding potential $V_h = -80$ mV, show various current types. First, a sustained inward-rectifier K^+ current (I_{kir} ; sustained over 180 ms with some degree of inactivation in this case) upon voltage steps downward to -100 and -120 mV. Second, a large and fast voltage-activated, transient inward Na^+ -current (I_{nav}) upon steps to ≥ -40 mV. The first signs of I_{nav} -activation are visible upon a depolarizing step to -60 mV, while maximal I_{nav} occurs at -40 mV with an I_{nav} -peak current (I_{navp}) more negative than -10 nA. Small sustained (over 180 ms) outward currents are visible at V_m -steps to > -20 mV and are considered here as K^+ -currents (I_{kv} , mainly the sustained I_{ss}), based on Pandit *et al.* (2001, 2003). Thus, in absolute value, the maximal I_{navp} is here much larger ($> 5x$) than the absolute value of the maximal inward-rectifier K^+ peak current ($I_{kirp} = -2.4$ nA at -120 mV) and the maximal voltage activated (outward-rectifier) K^+ current ($I_{ss} \sim +1.5$ nA at $+60$ mV). A small inward L-type voltage-activated calcium current (I_{caL}) must be present in the whole-cell currents (Pandit *et al.*, 2001) but cannot easily be recognized under these standard recording conditions, because it is masked by I_{nav} and I_{kv} (see Fig. 5). Furthermore, the outward currents do not show a prominent transient I_{kv} , I_t , as in the second example of a normal RVMC below. For an I-V curve representing the three main current components of this cell (I_{kir} , I_{nav} and I_{ss}) see Fig. 3.

Fig. 1b shows the excitable behaviour of the selected RVMC upon application of short (20ms) current pulses of increasing amplitude from 0 to 500 pA. For such a pulse-evoked AP (pAP), the firing threshold of the membrane potential was around -50 mV at ~ 200 -pA stimulation, consistent with activation of I_{nav} at ~ -50 mV in our voltage-clamp recordings (Fig. 1a) and with the literature (Pandit *et al.*, 2001). pAP depolarization accelerated with earlier threshold crossing by the stronger pulses, while the pulse-evoked action potential duration (pAPD at half height) increased by a decelerated repolarization at the stronger pulses.

Since APD often depends on the rate of AP firing (Pandit *et al.*, 2001), APD was measured in a train of 10 APs (tAPs) evoked with supramaximal pulses ($\sim 2x$ the threshold current pulse amplitude) at a frequency of 1 Hz (Fig. 1c). Supramaximal stimulation was evident from the constancy of the peak amplitudes of the tAPs (tAPP = 38 mV) and the absence of latency fluctuations. Fig. 1c shows indeed rate adaptation of tAPD to the train of 1 Hz by a significant tAPD increase after the first (shortest) tAP. This increase was not necessarily monotonic in a 1-Hz train. tAPD at 50% AP height of the 1st AP (tAP1D50) was 70 ms and increased to tAP10D50 = 90 ms at the 10th pulse after an overshoot of tAPD50max = 100 ms. The mean tAP1P, tAP1D50 and tAP10D50max of the 5 HL-APs were 33 mV, 70 ms and 92 ms, respectively.

Depolarizing-current induced automaticity in the HL-AP group

A peculiar type of RVMC excitability was seen as repetitive AP firing upon depolarizing the cell with a sustained (1.6-s lasting) current. This depolarizing-current induced automaticity (DIA) is shown in Fig. 1d. DIA occurred in all RVMCs tested ($n = 18$), was usually transient in nature (damped membrane potential oscillation), and was critically dependent on the degree of current-induced depolarization. The highest tendency to fire APs occurred at the lowest possible

depolarization just above -50 mV. Fig.1d shows that the higher depolarizations (at the higher sustained currents) cause stronger damped oscillations with fewer and smaller-amplitude APs or membrane potential waves. The oscillation at the lowest current amplitude (100 pA) occurs in this cell at a frequency of ~ 3.1 Hz. It starts with an initial depolarization, which develops too slowly to reach the threshold for triggering a fast full-blown sodium-channel based AP, because the Nav-channels largely inactivate before becoming activated (cf. Pandit *et al.*, 2001 for the properties of Nav-activation and inactivation). Nevertheless, the current-induced depolarization proceeds by closure of the inward-rectifier channels until the higher L-type calcium-channel threshold is reached around -30 mV (Pandit *et al.*, 2001). Because these calcium channels do not appreciably inactivate during the preceding depolarization, they are able to generate a typical slow calcium AP, which repolarizes by calcium channel inactivation and presumably by activation of residual (not yet inactivated) Kv-channels (cf. Pandit *et al.*, 2001, for the CaL and Kv-activation and inactivation properties). The duration of the first spontaneous AP, sAP, for 18 cells is sAP1D50 \sim 88 ms (see Table 1), thus in the range of durations of HL-APs (50-110 ms). However, the AP cannot return to the normal Kir-channel determined RMP, because of the applied sustained depolarizing current. This return of the membrane potential (V_m) to values of -50 to -30 mV allows recovery from CaL-channel inactivation causing repeated CaL-channel activation and generation of a repeated AP (Pandit *et al.*, 2001). Thus, this mechanism is similar to that of early afterdepolarizations (EADs) in the repolarizing phase of APs in ventricular myocytes of hypertrophic and failing hearts or from LQT-syndrome hearts (Rudy, 2000; Antzelevitch *et al.*, 2000). Therefore, the DIA may be seen as a series of repetitive EADs in normal heart cells.

Interestingly, DIA shows that Cav-channel excitability may be uncoupled from Nav-channel excitability in the slow onset of DIA and maintained during DIA when AP-firing continues above -50 mV, where all Nav-channels are inactivated (Pandit *et al.*, 2001; cf. Fig. 5b). At one higher applied current amplitude (150 pA), depolarization occurs fast enough to trigger an *Inav*-initiated AP as in Fig. 1b or c, but repolarization cannot be completed because of the sustained current, so that repeated APs can occur at the same frequency (~ 3.1 Hz) as at 100 pA, but with lower and sooner declining amplitudes and from a higher depolarized $V_m \sim -30$ mV, where more average CaL-channel inactivation occurs (Pandit *et al.*, 2001). A one-step higher depolarizing current (200 pA) shows such a strong damping of V_m -oscillation, that only one significant small wave is generated after the initial normal AP from a depolarized level of ~ -25 mV. At 250 pA the after-oscillation of the initial AP from a depolarized level of -20 mV is almost completely suppressed.

The average number of spontaneous APs or waves in the DIA during the 1.6-s sustained stimulation was 3.6 (range 2-6), a little higher than that in the general population (2.9, see Table 1).

Table 1. Electrophysiological properties of right ventricular myocytes of the adult rat.

	Average	SD	unit	n
RMP _i	-60.8	7.3	mV	20
RMP	-69.5	2.4	mV	20
C _m	172.9	65.2	pF	20
R _m (-60)	384.1	296.3	MΩ	20
R _m (rmp)	111.2	66.8	MΩ	17
<i>I</i> _{navp} (-40)	-7.1	3.2	nA	20
<i>I</i> _{kirp} (-120)	-2.9	1.0	nA	20
<i>I</i> _{kvp} (60)	2.9	1.6	nA	20
<i>I</i> _{ss} (60)	1.2	0.5	nA	20
<i>I</i> _{tp} (60)	1.7	1.3	nA	20
<i>I</i> _{tp} (60)/C _m	9.1	6.6	pA/pF	20
τ _{it} (60)	46.8	5.6	ms	6
tAP1P	19.6	17.3	mV	13
tAP1D50	41.0	28.4	ms	13
tAPD50max	61.2	44.2	ms	13
sAP1P	20.6	11.0	mV	18
sAP1D50	88.3	37.8	ms	18
sAPMDP	-31.2	9.2	mV	18
#sAPs/Waves	2.9	1.6		18

Table 1. Electrophysiological properties of right ventricular myocytes of the adult rat.

RMP_i, initial resting membrane potential (mV), measured within 1 min after whole-cell establishment.

RMP, stabilized resting membrane potential (mV), measured a few minutes after whole-cell establishment.

R_m(rmp), membrane resistance (MΩ) measured in current-clamp with a depolarizing 100-pA current step from RMP (~-70 mV).

C_m, membrane capacitance (pF), measured on-line in voltage-clamp with a 10-mV depolarizing voltage step from a holding potential V_h=-60 mV with the use of the pClamp-protocol MemTest.

R_m(-60), membrane resistance (MΩ) measured in voltage-clamp with a 10-mV depolarizing voltage step from a holding potential V_h=-60 mV (same protocol to measure C_m).

***I*_{navp}(-40)**, peak sodium current (nA), measured at -40 mV test potential.

***I*_{kirp}(-120)**, peak inward rectifier K⁺ current (nA), measured at -120 mV test potential.

***I*_{kvp}(60)**, peak voltage-activated outward K⁺ current (nA), measured at +60 mV test potential.

***I*_{ss}(60)**, sustained voltage-activated outward K⁺ current (nA), measured at +60 mV at t=180 ms, the time that the transient phase of *I*_{kvp} is largely over.

***I*_{tp}(60)**, the difference (nA) between *I*_{kvp}(60) and *I*_{kvs}(60).

***I*_{tp}(60)/C_m**, *I*_{tp}(60) normalized for variability in C_m.

τ_{it}(60), the time constant (ms) of decay of *I*_t at the 60-mV test potential, measured as the time elapsed between the peak of *I*_t and *I*_{tp/e}.

tAP1P, the peak amplitude (mV) of the first AP of a train of 10 APs, evoked by 20-ms supramaximal (>1.5 current threshold) current pulses at 1 Hz.

tAP1D50, the AP-duration at 50% AP-amplitude (APP-RMP) of AP1 of the 10-AP 1-Hz train of APs.

tAPD50max, the maximal AP50-duration (ms) of the 10-AP 1-Hz train of APs.

sAP1P, the peak amplitude (mV) of the first spontaneous AP after the initial current-step evoked AP or occurring at lower currents without an initial AP.

sAP1D50, the AP-duration (ms) at 50% AP-amplitude of sAP1.

sAP1MDP, the maximal (negative) diastolic potential (mV) after sAP1.

#sAPs/Waves, the number of spontaneous APs or waves during a 1.6-s sustained current stimulation, i.e. the broad APs or subsequent waves with >10-mV amplitude, measured from the interpolated MDPs after the APs/Waves, and occurring after the initial current-step evoked AP or occurring at lower currents without an initial AP.

Characteristic for all DIAs is a considerable gap between the maximal (-negative) diastolic potentials (MDPs) of the DIA-oscillations and the last preceding V_m -response in the protocol not giving rise to DIA (see also Fig. 2d). This must be due to depolarization-induced closure of the K_{ir} -channels causing an abrupt increase in the membrane resistance and thereby an abrupt increase in the current-step induced depolarization, as shown in Fig. 6c.

In conclusion, we found and compared two types of current-evoked excitation in a subset (group 1) of our normal RVMCs. The first one is represented by the classical short-pulse evoked I_{nav} -initiated and I_{caL} -extended HL-APs and the second one is represented by spontaneously occurring I_{nav} -independent, apparently I_{cav} -driven (see further evidence below) slow action potentials induced by sustained current stimulation.

Group-2 RVMCs with Low-peak/Short-duration pulse evoked action potentials (LS-APs)

Fig. 2 presents a quite different type of RVMC excitability: the cell has a strongly expressed I_{kv} combined with a low-peak/short-duration AP (LS-AP, see Fig. 2b,c), despite a relatively large I_{nav} (I_{navp} at -40 mV < -10 nA, Fig.2a). Nevertheless, DIA is preserved (Fig. 2d).

The voltage-clamp records (Fig. 2a) reveal an increased size of I_{kir} and I_{kv} , compared to the example group-1 RVMC in Fig. 1a, but now there is a pronounced expression of the transient component of I_{kv} , I_t . This makes the peak of I_{kv} at 60 mV more than 2x larger than that in the group-1 example RVMC (Fig. 1a). The more pronounced I_t in this group and in two other cells of the population allowed us to measure the time constant of inactivation of I_t at $+60$ mV for 7 cells, which was ~ 47 ms (see Table 1). I_{kir} has similar properties as in Fig. 1a, but the peak amplitude is almost doubled and the inactivation at -120 mV is less pronounced. The doubling of I_{kir} and I_{kv} in Fig. 2 compared to those presented in Fig.1 must be largely due to variability between the cells because C_m in Fig. 2 is only 7% larger and R_{ser} is only 8% smaller than in Fig. 1 (see Figure legends). Fig. 3 shows the I-V curve derived from the records in Fig. 2a with explanations below.

Analysis of the records in Fig. 2b gives a clue on the role of I_t in depressing and shortening the pAPs in group-2 RVMCs. A local response occurs upon a pulse of 300 pA (4th record from below) bringing V_m to a value around an increased firing threshold of ~ -40 mV. The low-peak AP-responses to the subsequent pulses of increasing strength repolarize faster than the local response to the 300 -pA pulse, which indicates that I_t has been activated during these pAPs. As the regenerative upswing of the pAP occurs relatively slowly, I_t is activated rapidly enough (Pandit et al., 2001) to antagonize excitation during the initial AP-development. Thus, the increased I_t expression appears to depress and shorten the AP in LS-AP myocytes around -70 mV.

The other three group-2 RVMCs showed a similar but more pronounced picture of reduced excitability. The pAPP-values were lower (-10 to 0 mV) and the APs were no longer all-or-nothing but rather graded responses, which repolarized earlier in the higher responses, consistent with progressive I_t activation at $V_m > -30$ mV (cf.

Fig. 2a). These responses looked rather aborted APs – through *I_t* activation- than depressed APs.

In one extra LS-RVMC the aborted AP with an APP=-10 mV and APD50=28 ms changed to a higher-peak and shorter AP (APP=12 mV and APD50=13 ms) when the RMP spontaneously hyperpolarized from RMP=-66 mV to -72 mV, indicating that the exact RMP-value around -70 mV is an important determinant of excitability. This observation was confirmed by similar effects of membrane hyperpolarizations evoked by steady current injections in 3 of the 4 LS-cells.

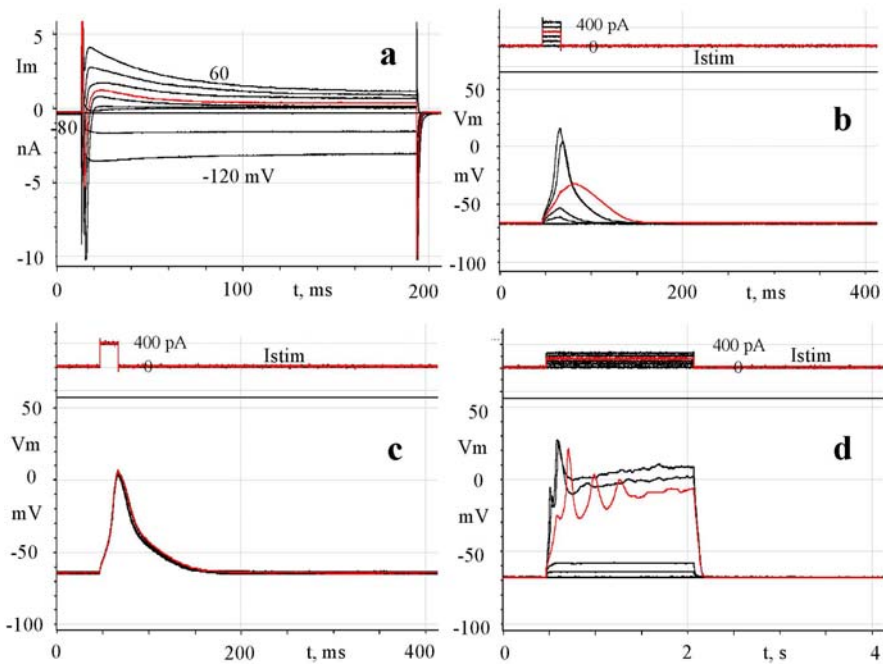


Fig. 2. Excitability of a group-2 RVMC with lowered and shortened pulse-evoked APs (LS-type) by strong *I_t* expression, but with preserved DIA.

(a) Voltage-clamp current records as in Fig. 1a. Notice the increased *I_t* expression compared with the HL-myocyte in Fig. 1a. The initial resting potential (RMP) was -60 mV but stabilized later between -65 and -68 mV (see Fig. 2b, c and d, with c preceding b in time). Rseal= 7 GΩ, Cm=161 pF, Rm (-60mV)=300 MΩ, Rser=4.6 MΩ.

(b) Vm records (bottom records) and applied-current records (top records) as in Fig. 1b. The APs have a low peak (0-10 mV) and short duration (LS-APs) compared to the APs in Fig. 1b, c. Notice a local response at liminal stimulation (3rd pulse) and that the subsequent APs upon the 4th and 5th pulse repolarize faster than the local response, indicating increased *I_{Kv}*-activation by those pulses.

(c) AP-records and current-pulse records during 10-pulse 1-Hz stimulation as in Fig. 1c. Notice the practical absence of frequency adaptation of the LS-type AP compared to that of the HL-type AP (cf. Fig. 1 c).

(d) Vm records and applied-current records to evoke DIA as in Fig. 1d. The Vm-oscillation is more damped than in Fig. 1d. Notice that a well-developed fast Nav-channel based AP is missing in the beginning of all records; but that slow Cav-channels based sustained-depolarization induced APs are present in the three upper records.

Reduced excitability around and above RMP=-70 mV is consistent with the inactivation curve of *Inav*, which shows already 80% inactivation at -70 mV, where inactivation of *It* is just beginning (Pandit *et al.*, 2001). Thus, the strongly increased *It* expression in LS-AP RVMCs depresses Nav-dependent excitability of these cells around -70 mV, which is in contrast to what happens in HL-APs (Fig. 1). Furthermore, the faster AP-repolarization upon steady hyperpolarizing LS-AP RVMCs from RMP>-70 to RMP<-70 mV must be at least partly due to making more *I_{ss}* channels available by de-inactivation (Pandit *et al.*, 2001). Another striking difference between AP-properties of group-2 and group-1 myocytes is the absence of frequency adaptation in group-2 cells as shown in Fig. 2c.

DIA in the LS-AP group

The depressed AP with the accelerated repolarization would prevent the generation of the slower Cav-channel based APs, if these Cav-channels would be present in the cell.

Fig. 2d indeed shows that this group-2 RVMC has these calcium channels expressed because it is able to generate slow *I_{caL}*-based APs during DIA. In all 4 LS-type RVMCs the DIA was transient with 2 or 3 APs/waves. The occurrence of the slow APs after the initial depressed AP at the beginning of the higher current steps can be understood from the stronger and longer-lasting current-induced depolarizations counteracting the repolarizing influence of *It*-activation and allowing *It*-inactivation.

In summary, a relatively strong *It* is able to inhibit the *Inav*-based beginning of the action potential of group-2 RVMCs by starting a premature repolarization process. This premature repolarization then prevents the generation of the *I_{caL}*-based slower AP-component. Thus, APD regulation by *It*-controlled *I_{caL}*-activation implies, at least partly, *It*-controlled *Inav*-activation. However, during continuous current-induced membrane depolarizations to $V_m > -40$ mV *It* inactivates and can no longer prevent the occurrence of the slow spontaneous APs during DIA.

I-V relationships

In order to better illustrate the voltage-dependencies of the main currents of our right ventricular myocytes, we show in Fig. 3 current-voltage (I-V) curves of the two myocyte types, having HL- or LS-APs. The curves were derived from the voltage-clamp records in Figs. 1a and 2a (see legend for further information). The I-V curves show the increased expression in the LS-myocyte of *I_{kv}* (best measured at +60 mV), in particular of *It*, and the range of *I_{kir}* sizes for both cell types at voltages <-80 mV. Activation of *It* in the LS-cell occurs at $V_m > -40$ mV, consistent with Pandit *et al.* (2001). The absolute size of the maximal *Inav* at around -40 mV is only a rough underestimation of the real current size due to inadequate voltage-clamp conditions (too large R_{ser} -values). Nevertheless, the curve reliably shows that *Inav* is activated at $V_m > -60$ mV, consistent with Pandit *et al.* (2001). *I_{caL}* is unrecognizable in the total whole-cell currents of the two cells plotted because of the presence of *I_{kv}*, but its presence can be revealed upon depolarizing voltage steps from a holding potential of -40 mV, as shown below in Fig. 5. For comparison, the I-V curve derived from that experiment has been

plotted in Fig.3 to illustrate how this hidden negative *IcaL* contributes to the total whole-cell current of a myocyte. The plot shows that *IcaL* activates in the same voltage range as *I_t*, consistent with Pandit *et al.* (2001). To visualize the real size of the outward (positive) *I_{kv}* current of a cell in the range of $-40 < V_m < 60$ mV, its negative *IcaL* (0 to -1.1 nA) should be subtracted from the total positive I-V curve in that *V_m*-range to obtain the real, more positive current of *I_{kv}*.

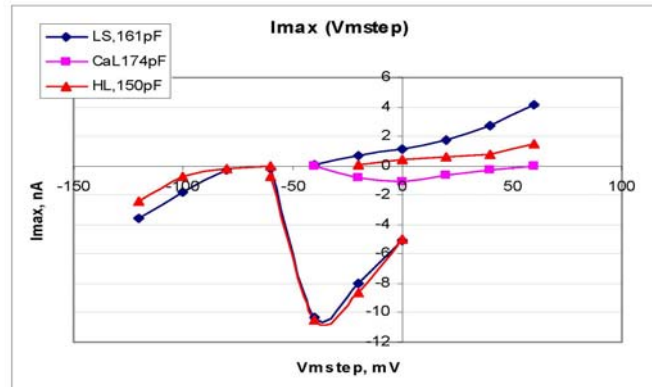


Fig. 3. I-V curves of the two types of myocytes with HL and LS-APs.

The curves consist of three unconnected parts, because the current amplitudes have been measured at different time points for different voltage ranges during the records. The left part (-120 to -80 mV) relates to that part of the I-V relationship representing maximal inward *I_{kir}*(*V_m*). The middle part (-60 to 0 mV) represents maximal inward *I_{nav}*(*V_m*), while the right part (-20 to $+60$ mV) represents maximal outward current, largely resulting from *I_{kv}*(*V_m*). The latter current is, however, mixed with the inward current *IcaL*, which deforms the records except at $+60$ mV ($\sim E_{CaL}$). For comparison, a *IcaL*(*V_m*) curve from another myocyte from the experiment of Fig. 5b has been added to the figure. All 3 cells plotted have comparable *C_m*-values (see legend in figure).

***I_t* affects pulse-evoked APs rather than DIA-APs**

Comparison of Figs. 1-2 suggests that an increase in *I_t* expression lowers and/or shortens pulse-evoked APs, but not the initial DIA-APs, consistent with the idea that *I_t* is largely inactivated during DIA (cf. Pandit *et al.*, 2001). This hypothesis was tested by plotting and comparing the peaks and durations of the first APs in the short 1-Hz trains (tAP1P and tAP1D50; Fig. 4a,b) and of the first spontaneous APs during DIA (sAP1P and sAP1D50; Fig. 4c,d) as a function of the peak of *I_t*, measured at 60 mV (*I_{tp60}*) and normalized to cell size by dividing *I_{tp60}* by the membrane capacity *C_m*.

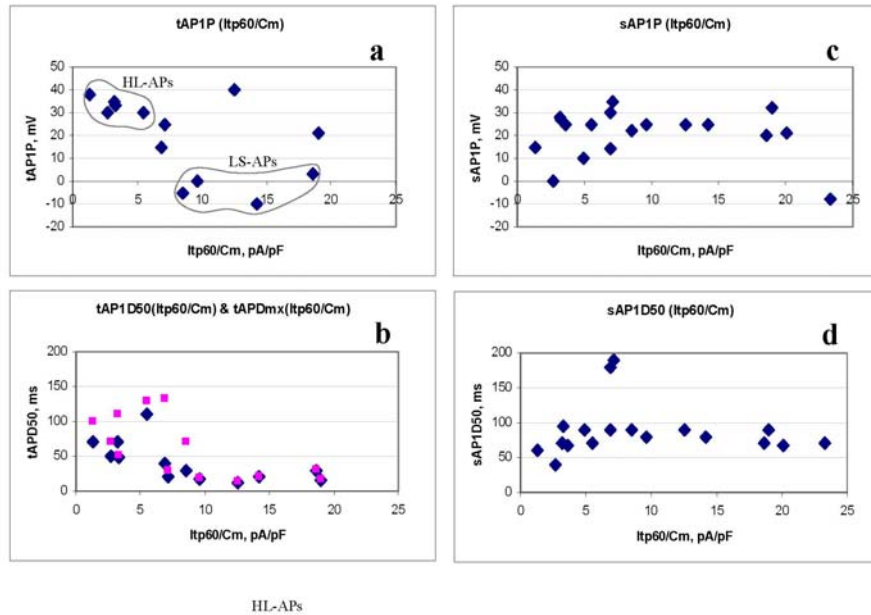


Fig. 4. The effect of *ltp*, normalized for cell-size (via Cm), at 60 mV on APP and APD for pulse-train evoked first APs (tAP1s, left frames, **a** and **b**) and for first spontaneous APs during DIA (sAPs, right frames, **c** and **d**) in the whole population. The two example-groups of myocytes with HL-APs and LS-APs are indicated in the figure. Notice the overall decline of tAP1P and tAP1D with an increase in normalized *ltp* and an absence of such a decline in the sAP1P and sAP1D values (for statistics see text). Notice also that the values of sAP1P and sAP1D are similar to the values of tAP1P and tAP1D at low normalized *ltp*-values. For definitions of the abbreviations, see the legend of Table 1.

The plots show lower tAP1P (Fig. 4a) and tAP1D50 (Fig.4b) values with an increase in *ltp60/Cm* (Spearman's correlation coefficient $r_s = -0.569$ and -0.817 , resp.). This correlation is absent in the corresponding plots of sAP1P (Fig. 4c) and sAP1D50 (Fig. 4d) ($r_s = 0.003$ and 0.168 , resp.). tAP1 peaks decline from values ~ 30 mV to values below 0 mV, while sAP1 peaks remain around 20 mV. Furthermore, tAP1 durations decrease from around 70 ms to values around 20 ms, while sAP1-durations remain high around 70 ms. This means that *ltp*-expression is an important determinant in APD regulation of pulse-evoked APs, but not in APD-regulation of DIA-APs. It also implies that, in general, the short pulse-evoked APs are not short as a result of a lack of *IcaL*-expression, as, if *ltp* inactivates under DIA-conditions, broad *IcaL*-based APs can appear. The location of the data points with the higher values of *ltp60/Cm* may need a right-shift because of underestimation of *ltp* due to imperfect voltage-clamp, but such a shift is not expected to affect the outcome of the used correlation test, because the Spearman test is based on rank correlation.

Fig. 4b shows another interesting property of pulse-evoked APs. They only show AP-lengthening in a 1-Hz train (frequency adaptation) for values of *ltp60/Cm*

below a certain value ($\sim 9\text{pA/pF}$), i.e. for APDs already longer than the short APD ($\sim 20\text{ ms}$) as observed at the higher I_{tp60}/C_m values.

***I_{caL}* measured under conditions of *I_{nav}* and *I_{kv}*-inactivation**

To establish the expression of L-type Cav-channels in our myocytes under our experimental conditions, we recorded *I_{caL}* under the standard/normal conditions of the AP-recordings of Figs. 1-2 at a holding potential of $V_h = -40\text{ mV}$. At that potential the masking effect of other currents on *I_{caL}* is minimal, because *I_{nav}* is completely inactivated, *I_t* largely and *I_{caL}* only slightly (cf. Pandit *et al.*, 2001).

Fig. 5 shows the results of such an experiment for a myocyte with properties intermediate between those of groups 1 and 2. In the control experiment of Fig. 5A it can be seen that *I_{kir}*, *I_{nav}* and *I_{kv}* dominate the recordings at $V_h = -80\text{ mV}$, making *I_{caL}* invisible. However, *I_{caL}* is clearly recognizable at $V_h = -40\text{ mV}$ in Fig. 5B, where *I_{nav}* is completely and *I_t* is largely inactivated. *I_{kir}* is not much affected, as expected. The inactivation of *I_{nav}* and *I_t* was largely reversible upon re-application of $V_h = -80\text{ mV}$ (see legend of Fig. 5).

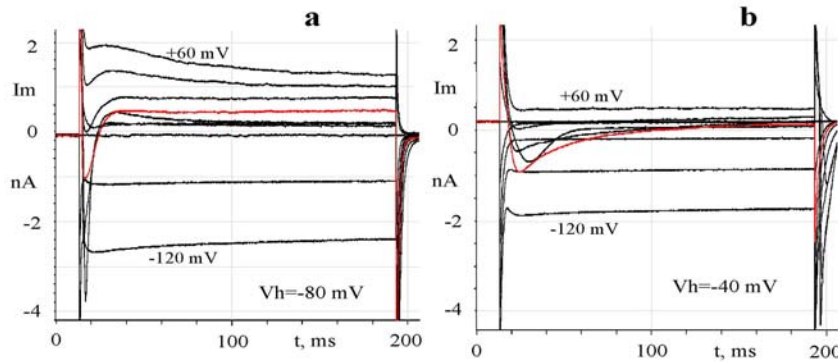


Fig. 5. Properties of *I_{caL}* measured under conditions of inactivation of *I_{nav}* and *I_{kv}* for a RVMC with properties intermediate between those of groups 1 and 2.

(a) Control recordings of membrane currents at a holding potential $V_h = -80\text{ mV}$, showing voltage-dependent activation of *I_{kir}*, *I_{nav}* and *I_{kv}* as in Fig. 2a. Conditions at the start of these recordings were: $RMP = -71\text{ mV}$, $C_m = 160\text{ pF}$, $R_m(-60) = 160\text{ M}\Omega$, and $R_{ser} = 12\text{ M}\Omega$.

(b) Membrane current recordings evoked as in (a), but from a $V_h = -40\text{ mV}$. At that V_h *I_{nav}* is completely inactivated and *I_{kv}* largely, but *I_{caL}* only slightly. *I_{caL}* is first clearly evoked at -20 mV , is maximal at 0 mV , becomes smaller at more depolarized potentials and is zero at 60 mV . The inactivating effect of $V_h = -40\text{ mV}$ on *I_{nav}* and *I_{kv}* was largely reversible upon return of V_h to -80 mV (not shown here). *I_{nav}* recovery was 57% and *I_{kv}* recovery 77%. *I_{kir}* did not recover, indicating a run down of the experimental conditions.

In this myocyte, *I_{CaL}* activates above -40 mV, is maximal at 0 mV and reverses at $+60$ mV. The I-V curve of this current is plotted in Fig. 3 for comparison with the total current I-V curves of a HL and LS-cell. The peak amplitude at $V_m=0$ mV, *I_{CaLp}(0)*, is -1.1 nA and this peak decays approximately exponentially with an inactivation time constant $\tau_{iCaL}(0)$ of ~ 35 ms. The precise course of the I-V curve may be slightly different from the plot in Fig. 3 because of incomplete inactivation of *I_t* at -40 mV.

Similar *I_{CaL}*-properties were found in one other cell and are consistent with other studies (Clark *et al.*, 1993; Lee *et al.*, 1997).

DIA involves L-type calcium-channel based excitability

Given the literature about DIA in various rodents (cf. Katzung, 1975; Malecot *et al.*, 1985; Peters *et al.*, 2000) and about the properties of expressed ion channels in rat ventricular myocytes (cf. Pandit *et al.*, 2001, 2003), cardiac L-type calcium channels (Cav1.2) are the primary candidate for generating the spontaneous slow APs during DIA in rat RVMCs. They even may provide the pacemaker mechanism for current-induced automaticity, or at least contribute to it. Therefore, we have studied the effect of the cardiac CaL-channel (Cav1.2) blocker nifedipine on DIA. The concentration used was $10 \mu\text{mol/L}$, because this concentration is supposed to inhibit almost 100% of the cardiac L-type Cav-channels at our resting membrane potentials of about -70 mV, without having disturbing aspecific effects on other channels (Hille, 2001).

Fig. 6 shows the results of such an experiment. The RVMC tested showed the three primary current types observed in the previous cell examples (*I_{kir}*, *I_{nav}* and *I_{kv}*), but resembled more to group-2 RVMCs than to group-1 RVMCs, because *I_{kv}* had a clear *I_t*-component (Fig. 6a). This caused a smaller APP (~ 13 mV) than in group 1. Application of $10 \mu\text{mol/L}$ nifedipine completely abolished DIA (Fig. 6c). The same stimulus protocol now resulted in *I_{kir}* and *I_{kv}* dominated responses of V_m . *I_{kir}* closure upon depolarization was now evident from the gap in the responses between zero current stimulation and stimulation with 50 -pA current. *I_{kv}* activation was evident from the abrupt stop in the time course of the current-step induced depolarization at voltages of -35 mV and higher. Inactivation of the *I_t* component is visible in the records at V_m values of -30 mV and higher as a delayed development of depolarization, consistent with the transient nature of *I_t* in the voltage-clamp responses in Fig. 6a. The survival in $10 \mu\text{mol/L}$ nifedipine of *I_{nav}*, *I_{kir}* and *I_{kv}* with its *I_t* component is visible in Fig. 6d for a different cell, recorded in the solution of the cell in Fig. 6a-c after losing that cell. The change in the precise initial time course of *I_{kv}* may be the result of the removal of the interference of *I_{CaL}* with the recorded *I_{kv}* or due to non-ideal voltage-clamp conditions.

These effects have been found in total for 4 cells and are consistent with comparable experiments on DIA in cardiomyocytes of other mammals (Peters *et al.*, 2000). We conclude therefore that L-type calcium channels provide the inward currents for the slow APs in the DIA. A second conclusion is that both the *I_{kir}* and *I_{kv}*-channels in some way contribute to the occurrence and mechanism of DIA. Kir-channels contribute, because it is the depolarization-induced closure of Kir-channels which brings the cell in the DIA-mode and a lack of reactivation keeps

the cell in the DIA-mode. Kv-channels must contribute in some way to DIA, because they are being activated and inactivated in the voltage range in which the slow APs occur. One significant role of I_t turns out to delay DIA, when a slow depolarization develops (cf. Fig. 6b).

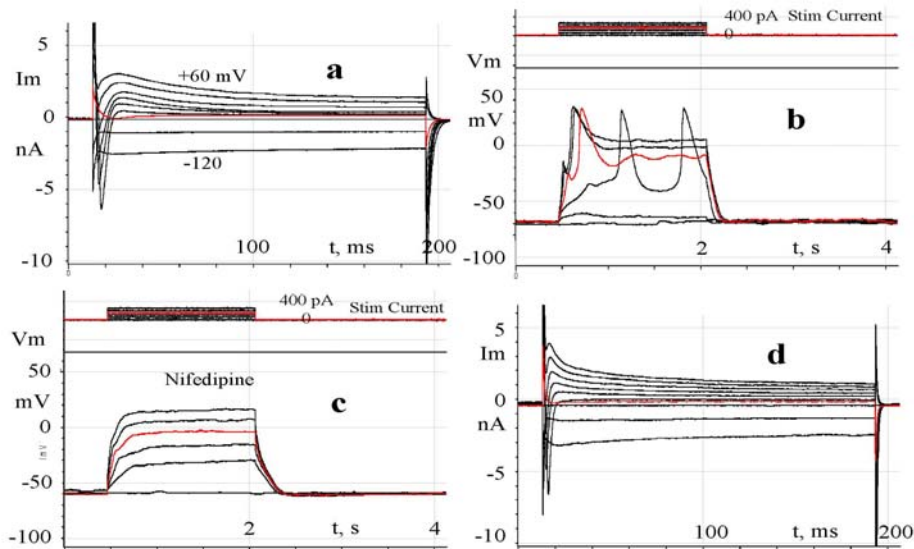


Fig. 6. The effect of 10 $\mu\text{mol/L}$ nifedipine on depolarizing-current induced automaticity (DIA) of a RVMC with AP-properties ($\text{APP} \sim 13\text{mV}$) between those of group 1 and 2. (a) Whole-cell voltage-clamp records, obtained as in Fig. 1a before addition of nifedipine. I_{Kir} , I_{Nav} and I_{Kv} with a I_t component are present. $R_{\text{seal}} > 1\text{G}\Omega$, $C_m = 233\text{pF}$, $R_m(-60\text{mV}) = 152\text{M}\Omega$, $R_{\text{ser}} = 7\text{M}\Omega$. (b) DIA with slow APs, evoked from $\text{RMP} = -70\text{mV}$. Records taken before the addition of nifedipine. The DIA inducing current steps were too small to evoke an initial full-size AP. (c) V_m responses upon the same stimulus protocol as in (b), after the addition of 10 $\mu\text{mol/L}$ nifedipine. RMP was decreased to $\sim -60\text{mV}$. (d) Voltage-clamp records, obtained as in (a), but from another RVMC in the presence of 10 $\mu\text{mol/L}$ nifedipine and serving as a voltage-clamp equivalent of the records in (c)

Exploring cardiomyocyte excitability mechanisms with a computer model

The main two questions studied were whether the model of Pandit *et al.* (2001, 2003) in its uncoupled membrane version of the RVMC is able to qualitatively reproduce (1) the changes in pAP-shape for different myocytes with variable I_t , as well as (2) the various types of DIA (weak and strong damping) observed in these cells. To answer these questions we ran simulation experiments with the model under conditions close to our experimental conditions (extra- and intracellular ion concentrations and R_{ser} , see legends of Fig. 7 and 8).

Fig. 7 concerns the first question and shows that a small- I_t RVMC has a much wider pAP with a higher plateau-phase than a large- I_t (epicardial) RVMC,

consistent with our observations (Figs 1-2 and 4) and consistent with the concept of a mechanism in which the approximate simultaneous activation of I_t with I_{CaL} (Pandit *et al.*, 2001; Fig. 3) after I_{NaV} -activation inhibits I_{CaL} and its depolarizing effect on V_m . However, the large- I_t RVMC does not show strongly reduced pAPPs as in Fig. 2b,c or aborted pAPs as in group-2 RVMCs with pAPPs < 0 mV. The latter failure could not be repaired by decreasing I_{NaV} or increasing I_t with a factor of 5 suggesting that the kinetics of I_{NaV} - and I_{Kv} -activation in the model is more separated in time than in the experiments, where I_{Kv} -activation can even suppress the initially developing I_{NaV} -driven pAP, thus preventing a I_{CaL} -driven second part of the AP. Frequency (0.5-5 Hz) adaptation of the AP (lengthening with higher pacing rate) was also produced by the model as a consequence of cumulative inactivation of I_t (not illustrated here).

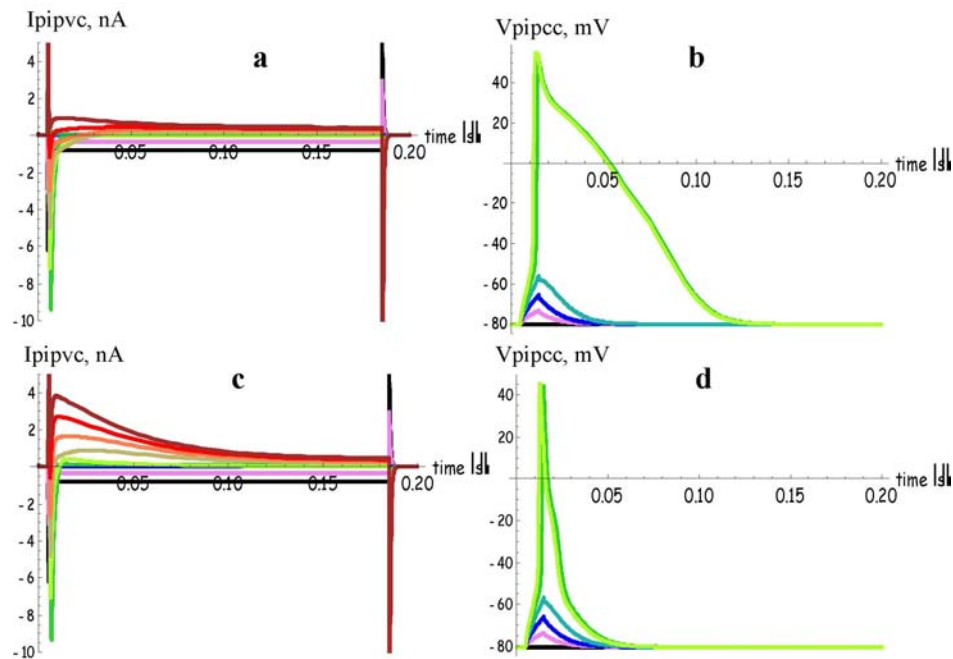


Fig.7. Correlation of I_t -expression in the model RVMC, as reflected in voltage-clamp simulation experiments (a, c), with pulse-evoked AP-shapes in current-clamp simulation experiments (b, d). The voltage-clamp and current-clamp simulations were carried out with a series resistance $R_{ser}=6\text{ M}\Omega$, the approximate average R_{ser} value in the experiments. External calcium concentration was as in our experiments (1.8 mmol/L). Intra- and extracellular K^+ and Na^+ concentrations were close to our experimental values. Properties of the various ion conductances in the membrane of the epicardial RVMC in (c) and (d) were as in Pandit *et al.* (2003). To simulate a small- I_t myocyte of the experiments (a) and (b), only I_t of the default epicardial cell was changed to 0.23x of the default value. The electrical behaviour of the myocyte membrane was uncoupled from intracellular ion- and calcium-dynamics by keeping $[Ca^{2+}]_i=79\text{ nmol/L}$, $[Na^+]_i=10.7\text{ mmol/L}$, and $[K^+]=139.3\text{ mmol/L}$.

A model myocyte with a high I_t and short AP (the default right epicardial model cell) had much less frequency adaptation at 2-5 Hz stimulation than that cell with a smaller I_t (e.g. 0.25x), consistent with the experimental result in Fig. 1b, 2b and 4b.

Fig. 8 illustrates the answer to the second question. An epicardial RVMC (with a large I_t) does not clearly exhibit DIA-behaviour when sustained-current stimulation with increasing intensities is applied (Fig. 8a). This can, however, be repaired by increasing I_{ss} with a factor of ~ 4 , allowing the generation of DIAs of 2 after-APs after the initial AP at intermediate stimulus intensities (Fig. 8b).

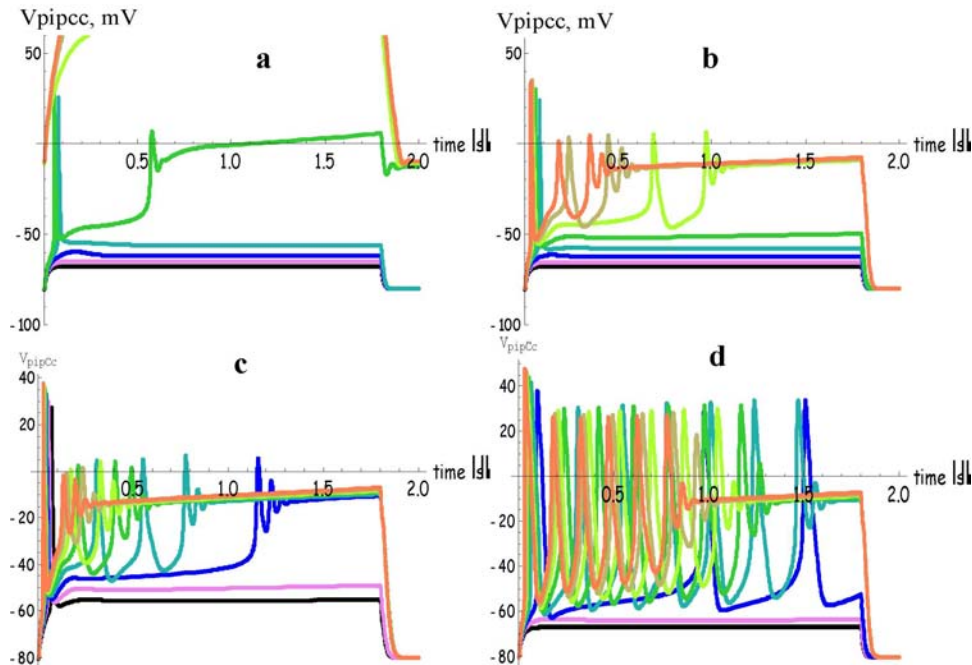


Fig. 8. Conditions required for the occurrence of DIA in the model of Pandit et al. (2001, 2003) of the RVMC of the adult rat (membrane uncoupled from the intracellular calcium dynamics). In all simulations $[Ca^{2+}]_i = 1.8$ mmol/L and $R_{ser} = 6M\Omega$, as in our experiments. The stimulation protocol started with a 1.8-s 0.1-nA current stimulus which was repeated with 5-s intervals (to obtain 8 records) and with current increments of 0.01 nA. Panel (a) shows the behaviour of the default epicardial RVMC (see Pandit et al. 2003) unable to generate DIA. After increasing I_{ss} with a factor of 4, the cell is able to generate DIAs at intermediate stimulation intensities (b). Reducing I_{kir} with 1/3 in panel (c) further facilitates DIA in the model cell of panel (b). In panel (d) I_t of the cell in panel (b) is reduced to 10%, causing a longer lasting DIA with broader and higher-amplitude APs.

A strong right-shift of the inactivation curve of I_{ss} has a similar effect. Additional simulations (not shown here) revealed that these sustained-stimulation induced

APs survive the removal of I_{nav} , disappear after removal of I_{caL} (consistent with the experimental result of Fig. 6) and are not or only slightly affected by the removal of I_f , I_{cap} , I_b , I_{naca} and I_{nak} . Thus, the induced APs are I_{caL} -driven and require sufficient I_{ss} expression. Increasing the time constant of inactivation of I_{ss} turned out to increase the number of APs in the DIA-transient. Removal of the window current of I_{caL} by shifting the inactivation curve of I_{caL} 10 to 15 mV to the left (not shown here) removes the sustained-current induced APs, indicating that the automaticity mechanism resides in the overlap of the activation and inactivation curve of I_{caL} . However, other K^+ currents than I_{ss} are also important in the generation of DIA. Fig. 8c shows that reduction of I_{kir} facilitates the occurrence of DIAs, because they occur at lower stimulation currents with more APs (less damped oscillation).

Finally, it seems to have an inhibitory effect on the DIAs, because reduction of I_t to 10% of the default value (Fig. 8d) makes the initial AP and subsequent ones broader and of larger amplitude and makes the train of induced APs longer (weakly damped oscillation).

These results imply that the variable DIA-phenotype observed in our experiments can be qualitatively reproduced from variable combinations of the main membrane currents playing a role in this phenomenon, I_{caL} , I_{ss} , I_{kir} and I_t . Thus, in principle, the mechanism of DIA resides in the membrane and does not require a connection of the membrane with the intracellular calcium (and other ion) dynamics. Naturally, such a connection can be expected to serve as an important regulator of DIA, for example because intracellular calcium can control I_{caL} through calcium-induced inactivation (cf. Antoons *et al.*, 2007), a mechanism included in a simple form in the complete model of Pandit *et al.* (2001, 2003).

A preliminary analysis of these results in terms of gating behaviour of the ion channels involved (not shown here) indicates that the automaticity mechanism of DIA resides in the window-current properties of I_{caL} in combination with the deactivation properties of I_{ss} . DIA requires AP-repolarization towards a membrane potential within the window current range to allow de-inactivation of I_{caL} to provide 'diastolic' depolarization by inward I_{caL} , which is then supported by 'diastolic' deactivation of I_{ss} to recover from activation during the preceding action potential. The strength of sustained stimulation in combination with the presence of other active currents, I_{kir} , I_t and the sum of the smaller currents, determine whether the membrane potential can land after the first AP in the window current range of the membrane potential. The slow inactivation of I_{ss} may then determine the length of the AP-train of the transient DIA. The differences regarding the phenotype between the DIAs of the different RVMCs of the heart may thus result from the variability in the expression of the various ion channels.

Discussion

The principal findings of the present experimental and model study concern **(1)** the role of the transient K^+ current I_t in RVMC action potential (AP) shaping, and **(2)** the roles of I_{kv} (I_t and I_{ss}) and I_{kir} (inward-rectifier K^+ current) in depolarizing-current induced automaticity (DIA).

I_t controls AP-duration by controlling I_{nav} as well as I_{caL} -activation

Under our conditions, the transient current I_t turned out to control the shape of current-pulse evoked APs, by starting an initial repolarization process as soon as the I_{nav} -initiated depolarization phase of the AP surpasses the activation potential of I_t around -30 mV (see our voltage-clamp currents and Pandit *et al.*, 2001). If I_t would be absent, the AP would develop an I_{nav} -driven AP lasting long enough to allow activation of the I_{caL} around -30 mV. I_{nav} -inactivation would then automatically remove the depolarizing influence of the Nav-channels. This influence is then replaced by that of the CaL-channels to generate the cardiac AP-plateau and lasts as long as I_{caL} -inactivation and activation of residual I_{kv} (I_{ss}) and background currents allow the CaL-channels to remain active. This situation approximates the conditions in the myocytes with HL-APs, where no or relatively little I_t is present, but some I_{ss} . If enough I_t -channels are present, they limit I_{nav} by activation above -30 mV and thereby the degree of depolarization by I_{nav} . At the same time the I_t -channels provide a hyperpolarizing force, against which I_{caL} -channels have to become activated. This limits the number of activated CaL-channels and the degree of depolarization these channels can contribute to the membrane. Thus, I_t -channels have a double-negative influence on CaL-channel induced membrane-depolarization during the AP, the first being hindrance of I_{nav} -induced depolarization and the second being hindrance of the depolarizing action of already-open CaL-channels. In this way, CaL-channel activation, and consequently APD, can be controlled by I_t -channels. In the extreme case, as in group-2 APs, I_t can be so strong, that it even aborts an I_{nav} -driven AP thereby also preventing I_{caL} -activation. In a functional myocyte, this would also mean electro-mechanical uncoupling.

This concept of the role of I_t in cardiomyocyte excitability applies to our preparation of rat RVMCs with their RMP ~ -70 mV, which is 5-10 mV more positive than reported by others (cf. Pandit *et al.*, 2003). This seems the reason that our simulation experiments with the model of Pandit *et al.* (2003) did not reproduce the depressed and aborted APs in the high- I_t cells (see below). At the more negative RMP ~ -80 mV I_{nav} is largely de-inactivated (Pandit *et al.*, 2001). At that potential the increased I_t expression in the LS-cells is no longer expected to affect APP, but only APD, as shown in our simulations with the Pandit model.

The above formulation of the mechanism of the regulation of APD by I_t follows from a careful comparison of current-clamp responses to voltage-clamp responses of the same cell under the same standard-normal conditions for diverse cases (from HL- to LS-APs). It may not be entirely novel, but an explicit formulation of this mechanism is required for a proper evaluation of changes of

ion channel expression during heart-failure associated remodeling of ion channel expression.

***Kir*-, *CaL*- and *Kv*-channels in the automaticity mechanism of DIA**

The experimental results show that DIA may occur in rat ventricular myocytes and indicate that *IcaL* and *Ikir* are important components in the automaticity mechanism. Preliminary observations indicate that DIA may also occur in left ventricular myocytes of the rat (not shown here). Closure of *Kir*-channels by current-induced depolarization may bring V_m in a voltage range where a *IcaL*-driven pacemaker ('automaticity') mechanism can arise based on the overlap of the activation and inactivation curves of *IcaL* in these cells (Pandit *et al.*, 2001). In this mechanism (see Ishikevich, 2005) the 'diastolic inward pacemaker current' would result from recovery of *IcaL*-inactivation in a voltage range where a fraction of the activation gates is still open. However, *Kv*-channels may also participate in this automaticity mechanism, but the observed slowly inactivating *Kv*-channels (*Kss*) are a more likely candidate than the rapidly inactivating *Kv*-channels (*Kt*; see for the inactivation properties of *Kt* and *Kss*, Pandit *et al.*, 2001). A minor role for *I_t* is consistent with our observation that a rapidly inactivating *Kv* can only transiently suppress and thereby delay DIA. The role of *Kss* could then be to make DIA transient of nature by slowly inactivating (over the course of a few seconds) after the onset of DIA. Obviously any other repolarizing or depolarizing background or voltage-dependent current would also contribute to the automaticity mechanism. Our model simulations indeed revealed that *I_{ss}* is an important participant in the automaticity mechanism of DIA (see below). Our view on *IcaL* as a 'diastolic pacemaker current' in DIA and on the accessory roles of *Kv*-channels in the generation of DIA is consistent with earlier interpretations of DIA-mechanisms described by Peters *et al.* (2000).

Origins of variability

The variability in expression of *I_t* between the myocytes was obvious from the initial overshoot of *I_{kv}* (*I_{kv}p*) over the sustained *I_{kv}* (*I_{ss}*, see Figs. 1a, 2a). The origin of this *I_{kv}p* variability may be assumed to reside largely in the variable histological (endo-, meso- and epicardial) origin of the cells (Clark *et al.*, 1993). The variability of *I_{kv}* below 60 mV may be influenced by variability in the expression of *IcaL* (Lee *et al.*, 1997), which current is present (though unrecognizable) in our whole-cell total current recordings (Fig. 5). How this *IcaL* variability affects *I_{kv}p* variability remains to be determined in pharmacological experiments. *R_{ser}*-variability is another source of variability affecting the higher *I_{kv}p*-values around 5nA at +60 mV.

A possibly important source of variability to be mentioned is the variability in *R_m* between the cells and within the cells in the course of an experiment. This variability affects RMP, excitability for current pulse stimulation, as well as inducibility of DIAs. The origin of *R_m*-variability is yet unclear, but may include variability in *R_{seal}*, in the expression of small unidentified membrane conductances and in cytoplasmic factors affecting ion channel function.

Besides I_{kv} variability we found variable I_{nav} and I_{kir} values. Although I_{nav} may be expected to be variably expressed in our cells (Pandit *et al.*, 2001), we did not quantify this variability, because of inadequate voltage-clamp conditions (too high R_{ser} values) for this purpose. We neither studied here I_{kir} variability, because our focus was primarily on the role of I_{kv} in action potential generation and depolarizing-current induced automaticity. However, the role of I_{kir} in both excitability phenotypes remains of interest because of its repolarizing role in pulse evoked action potentials and its permissive role in DIA.

Differences with other studies

Although our results with respect to the expression of the main ion channel types (Kir, Nav, CaL and Kv) generally agree with findings of others who studied adult rat RVMCs (see Pandit *et al.*, 2001), there are a few differences. For example our RMP is 5-10 mV more positive than reported by others (Lee *et al.*, 1997; Pandit *et al.*, 2003), while the APDs are often larger (e.g. 42 ms compared to 14 ms). The first difference, the slightly depolarized condition, may certainly explain a large part of the increased APDs, because APD is sensitive for depolarization above -80 mV, probably mainly due to inactivation of Kv-channels causing diminished repolarizing force (Pandit *et al.*, 2001). Preliminary results showed an average APD-increase of 2-3 ms per mV depolarization over the membrane potential range -80 to -40 mV. The reason of the slight depolarization of the resting membrane is unclear but may be due to a difference in experimental conditions.

Another difference is a larger C_m (~ 172 pF) than measured by others (e.g. ~ 90 pF in Lee *et al.*, 1997). This difference may result from several causes, including opposite differences in bias at the selection of cells or in the method of C_m measurement. Future experiments should evaluate these differences.

Model results

The simulations with the model of Pandit *et al.* (2001, 2003) in its cytoplasm-uncoupled membrane version qualitatively reproduced the experimentally observed dependency of AP-duration on I_t and that of DIA on I_{caL} and the strength of the depolarizing current, while the participation of I_{ss} was a new finding for the model DIA-behaviour. However, we are still far from a quantitative reproduction of AP-shapes in pulse-evoked APs and in repetitive AP-firing induced by sustained current stimulation. Depressed and aborted pAPs were not reproduced and DIA-reproduction required an increase in I_{ss} , despite the fact that DIA was a regular finding in almost all cells. Fixing these problems would require a careful inspection of the exact activation and inactivation kinetics of I_{nav} , I_{caL} , I_t and I_{ss} . These limitations of the model indicate that the model of Pandit *et al.* needs updating of its membrane conductance properties with more detailed voltage-clamp measurements, which may already be available in the recent literature. An example of a further improvement of Pandit's model for a better understanding of frequency adaptation of the ventricular myocyte AP is found in Salle *et al.* (2008). For the DIA the precise de-inactivation properties of I_{caL} and de-activation properties of I_{ss} are of crucial importance, because these currents appear to provide the automaticity mechanism of the DIA. However, the currents I_{kir} and I_t also need to be determined precisely because I_{kir} is permissive in

allowing DIA to occur, while I_t has both fast and slow components, which both may affect DIA, the fast component in initially inhibiting DIA and the slow component in contributing to DIA in a similar way as I_{ss} , e.g. in making DIA transient.

The reproduction by the model of the experimental finding that frequency adaptation is much more pronounced in small- I_t myocytes (see Fig. 4b) is of functional interest. Frequency adaptation may be considered as being largely due to cumulative inactivation of I_t (Salle *et al.*, 2008). This would imply that small- I_t (non-epicardial) myocytes (i.e. with large AP-durations) would be more sensitive to cumulative I_t -inactivation and would be more inclined to develop pathogenic AP-lengthening at high heart rates.

To our knowledge, this is the first time that the classical phenomenon of depolarizing-current induced automaticity, described since Katzung (1975) and later also by others in ventricular myocytes in various species of mammals, has been analyzed with the use of a quantitative membrane excitability model. The results indicate that this type of analysis may increase our understanding of the mechanism of abnormal automaticity of myocardial tissue.

Functional implications

The mechanism described above for the effect of I_t on APD may have a wider meaning than only for heart failure-related APD changes in the rat heart, since I_t is also important in shaping the human cardiac AP (Beuckelmann *et al.*, 1993). So far, emphasis in shaping the human cardiac AP was more on the slower acting I_{kv} 's, such as I_{kr} and I_{ks} , controlling APD by cutting off the terminal phase of the AP-plateau (Sanguinetti & Tristani Firouzi, 2006) instead of controlling APD by simultaneous inhibition of I_{caL} by I_t (see I-V curves in Fig. 3), as described here for the rat. An exception in this respect is the study of Greenstein *et al.* (2008), which ascribes an important role to I_t in controlling APD in canine ventricular cells

As described, we observed depressed and aborted APs in high- I_t myocytes with a 5-10 mV depolarized RMP~-70 mV (compared to the literature). This implies that areas of intact myocardial tissue of cells with increased I_t , such as epicardial cells, can become inexcitable when the membrane becomes 5-10 mV depolarized by whatever reason (hyperkalemia, ischemia). This would introduce heterogeneity in the tissue, allowing reentry and the development of ventricular arrhythmias. Down-regulation of I_t in hypertrophic and failing hearts, at risk of becoming locally depolarized by inadequate perfusion, may thus be seen as an adaptive response protecting the tissue against the development of abnormal heterogeneity in excitability.

The mechanism described for DIA may also have a wider meaning than for the rat heart alone. This mechanism may underlie DIA as well as EAD in greater mammalian species. Although the EAD-mechanism has been sought for in the properties of CaL -channels (Antoons *et al.*, 2007), studies so far have not pinpointed that mechanism to the intrinsic pacemaker properties of CaL -channels originating from the overlap between their activation and inactivation curves, which seems to apply to all mammalian ventricular myocytes. This may explain why EADs have the tendency to occur repetitively (Pogwizd and Bers, 2004). The

similarity between DIA and the V_m -oscillations during Torsade de Pointes (TdP) arrhythmias (Antzelevitch *et al.*, 2000) suggests that the automaticity-mechanism of DIA may also underly or contribute to TdP and in this way be responsible for the risk of sudden death in patients with long QT-intervals.

Perspective for Experimental Pulmonary Hypertension

The present study provides the control electrophysiological properties of adult rat RVMCs for a comparative study with RVMCs obtained from adult rats with experimental pulmonary arterial hypertension (PAH; cf. Lee *et al.*, 1997 and this thesis). Our results show great variability in excitability and ion channel expression, in particular of I_t , in adult rat RVMCs, probably arising from the precise histological origin of the cells from the right ventricle. In a preliminary electrophysiological study of RVMCs from rats treated with monocrotaline to induce PAH, we observed the same kind of variability as described here for control cells: HL-, LS- and intermediate types of action potentials were found in current-clamp and a similar variability of I_t expression in voltage-clamp experiments. Establishing statistical differences between these groups would require large groups of observations. Thus, it would be easier to establish statistical differences between the electrophysiological properties of control and PAH-cells by comparing subsets of cells of the same origin from the tissue, for example cells of mainly epicardial, mesocardial or endocardial origin (cf. Clark *et al.*, 1993). Variability remaining despite such a procedure could then be evaluated in plots such as Figs. 4.

The present results suggest to consider two possible roles of Kv-channel expression in the arrhythmogenicity of cardiac tissue of the hypertrophic and failing heart. One is the role of K_t -channel expression in creating inexcitable areas in the tissue (reentry) upon the occurrence of small depolarizations (~10 mV) and the other is the role of K_{ss} -channel expression in the automaticity response of the tissue (ectopic beats) upon the occurrence of larger depolarizations (~40 mV).

Acknowledgement

We thank Dr. W. Kolsters (Meander Hospital, Amersfoort, The Netherlands) for instructive and stimulating discussions.

References

1. Antoons G, Volders PG, Stankovicova T, Bito V, Stengl M, Vos MA, Sipido KR. Window Ca^{2+} current and its modulation by Ca^{2+} release in hypertrophied cardiac myocytes from dogs with chronic atrioventricular block. *J Physiol* 2007;579:147-60
2. Antzelevitch C, Yan G, Shimizu W, Burashnikov A. Electrical heterogeneity, the ECG, and Cardiac arrhythmias. In: Zipes and Jalife, *Cardiac electrophysiology from cell to bedside*, 3rd edition, W.B. Saunders Company, Philadelphia, PA, USA, 2000.
3. Beuckelmann DJ, Nabauer M, Erdmann E. Alterations of K^+ currents in isolated human ventricular myocytes from patients with terminal heart failure. *Circ Res* 1993;73:379-85
4. Cerbai E, Barbieri M, Li Q, Mugelli A. Ionic basis of action potential prolongation of hypertrophied cardiac myocytes isolated from hypertensive rats of different ages. *Cardiovasc Res* 1994;28:1180-7
5. Clark RB, Bouchard RA, Salinas-Stefanon E, Sanchez-Chapula J, Giles WR. Heterogeneity of action potential waveforms and potassium currents in rat ventricle. *Cardiovasc Res* 1993;27:1795-9
6. Greenstein JL, Wu R, Po S, Tomaselli GF, Winslow RL. Role of the calcium-independent transient outward current $I_{(to1)}$ in shaping action potential morphology and duration. *Circ Res* 2000 ;87 :1026-1033
7. Guo D, Zhao X, Wu Y, Liu T, Kowey PR, Yan GX. L-type calcium current reactivation contributes to arrhythmogenesis associated with action potential triangulation. *J Cardiovasc Electrophysiol* 2007;18:1-8
8. Hille B. *Ion channels of excitable membranes*, 3rd edition, Sinauer Associates, Inc. Publishers Sunderland, MA, USA, 2001.
9. Ishikevich EM. *Dynamical systems in neuroscience: The geometry of excitability and bursting*. The MIT Press, Cambridge, MA, USA, 2005.
10. Katzung BG. Effects of extracellular calcium and sodium on depolarization-induced automaticity in guinea pig papillary muscle. *Circ Res* 1975;37:118-27
11. Lee JK, Kodama I, Honjo H, Anno T, Kamiya K, Toyama J. Stage-dependent changes in membrane currents in rats with monocrotaline-induced right ventricular hypertrophy. *Am J Physiol Heart Circ Physiol* 1997;272:H2833-H2842
12. Malécot CO, Arlock P, Katzung BG. Amrinone effects on electromechanical coupling and depolarization-induced automaticity in ventricular muscle of guinea pigs and ferrets. *J Pharmacol Exp Ther* 1985;232:10-9
13. Oudit GY, Kassiri Z, Sah R, Ramirez RJ, Zobel C, Backx PH. The molecular physiology of the cardiac transient outward potassium current ($I_{(to)}$) in normal and diseased myocardium. *J Mol Cell Cardiol* 2001;33:851-72
14. Pandit SV, Clark RB, Giles WR, Demir SS. A mathematical model of action potential heterogeneity in adult rat left ventricular myocytes. *Biophys J* 2001;81:3029-51
15. Pandit SV, Giles WR, Demir SS. A mathematical model of the electrophysiological alterations in rat ventricular myocytes in type-I diabetes. *Biophys J* 2003;84:832-41
16. Peters NS, Cabo C, Wit AL. Arrhythmogenic mechanisms: Automaticity, triggered activity, and reentry. In: Zipes and Jalife, *Cardiac electrophysiology from cell to bedside*, 3rd edition, W.B. Saunders Company, Philadelphia, PA, USA, 2000.
17. Pogwizd SM, Bers DM. Cellular basis of triggered arrhythmias in heart failure. *Trends Cardiovasc Med*. 2004;14:61-6
18. Rudy Y. Ionic mechanisms of cardiac electrical activity. In: Zipes and Jalife, *Cardiac electrophysiology from cell to bedside*, 3rd edition, W.B. Saunders Company, Philadelphia, PA, USA, 2000.
19. Salle L, Kharche S, Zhang H, Brette F. Mechanisms underlying adaptation of action potential duration by pacing rate in rat myocytes. *Progr Biophys Mol Biol* 2008;96:305-20.

20. Sanguinetti MC, Tristani-Firouzi M. hERG potassium channels and cardiac arrhythmia. *Nature* 2006;440:463-9

Chapter 9

Summary, Conclusions, Future Perspectives and Samenvatting

Summary, Conclusions, Future Perspectives and Samenvatting

Summary of the thesis

The major objectives of research described in this thesis include investigation of molecular and cellular mechanisms of cardiac hypertrophy and failure. In a study on monocrotaline-induced pulmonary arterial hypertension in rats mesenchymal stem cell therapy was tested as a novel option to treat this disease.

Chapter 1 deals with general introduction of the thesis. It provides information about the molecular and cellular characteristics of the healthy heart, the heart with hypertrophy and the failing heart. Extracellular matrix (ECM) composition, synthesis and degradation, integrins and integrin signaling, nitric oxide synthases (NOSs) and NO are discussed in relation to normal, hypertrophic and failing myocardium. In addition, experimental models of myocardial hypertrophy and heart failure are described. Particularly, the characterization and pathology of right ventricular function in animals with monocrotaline-induced pulmonary hypertension are emphasized.

In **chapter 2** we hypothesized that pressure overload is “felt” by the myocardium through stretch-like effects imposed on integrins, the receptor by which cardiomyocytes are attached to the ECM. In the cell model of neonatal rat cardiomyocytes (NRCMs) *in vitro*, we activated the integrins by administration of a pentapeptide containing Arg-Gly-Asp (RGD) to test whether integrin stimulation leads to NRCM hypertrophy. The pro-hypertrophic effect of RGD-containing pentapeptide on NRCMs was compared with the well-known pro-hypertrophic effects of α_1 -adrenoceptor stimulation with phenylephrine. Saline-treated NRCMs were used as control. The hypertrophic response was quantified by measuring cell surface area (CSA). Phosphorylation of NO-synthase-1 (NOS1) was also assessed. CSA was increased by 38% with RGD and by 68% with PE versus control. A general NOS-inhibitor (L-NAME) inhibited RGD-induced hypertrophy completely, but had no significant effect on PE-induced hypertrophy. The L-NAME-induced inhibition of RGD-induced NRCM hypertrophy could be overcome, at least partly, by co-administration of a NO-donor, nitroprusside. Co-administration of a NO-donor had no effect on NRCMs incubated with PE + L-NAME. Ryanodine and BAPTA-AM inhibited RGD-induced hypertrophy completely but not that induced by PE, indicating the involvement of intracellular Ca^{2+} ions in the RGD-induced NRCM hypertrophy. NOS-1 phosphorylation was increased with RGD by 61%. Hence we concluded that integrin stimulation of NRCMs by RGD leads to hypertrophy. Abrogation of RGD-induced hypertrophic response upon NOS-inhibition and rescue of this hypertrophic effect by NO-donor suggest that integrin stimulation-induced hypertrophy of NRCMs depends upon NO, possibly derived from NOS1.

In **chapter 3** we demonstrated that ventricular failure may be associated with a disturbed myocardial collagen turnover. In patients with heart failure, myocardial collagen turnover can be assessed by serum concentrations of aminoterminal propeptides of type I and type III collagen (PINP and PIIINP) and carboxyterminal telopeptide of type I collagen (ICTP) that either represents measures of collagen synthesis (PINP, PIIINP) or collagen degradation (ICTP). We investigated the effects of cardiac resynchronization therapy (CRT) on myocardial collagen turnover in 64 patients with heart failure by comparing PINP, PIIINP and ICTP concentrations in serum obtained at baseline and after 6 months of CRT. We hypothesized that in patients with heart failure CRT leads to reverse ventricular remodeling, associated with a net collagen formation. Forty-six patients (72%) showed a >10% reduction in LV end-systolic volume at follow-up and were classified as responders to CRT, the other 18 patients (28%) were classified as non-responders. Responders demonstrated a mean increase of serum PINP and PIIINP during follow-up, by 42% and 12%, respectively. In non-responders, serum PINP and PIIINP remained unchanged during follow-up. At baseline, responders had significantly lower serum PINP than non-responders (by 21%). ICTP levels of responders at baseline tended to be higher than in non-responders (by 70%, $p=ns$), and in both groups ICTP levels did not change upon CRT. We concluded that reverse LV remodelling following CRT is associated with increased collagen synthesis rate in the first 6 months of follow-up.

It has been known for some time that monocrotaline (MCT)-induced pulmonary artery hypertension (PAH) and right ventricular (RV) failure are associated with the activation of matrix metalloproteinases (MMPs) in RV myocardium. In **chapter 4** we investigated whether NO plays any role in PAH-induced RV hypertrophy and failure. To that purpose, two doses of MCT were used that produced RV hypertrophy (RVH) only and RV hypertrophy and subsequent RV failure (RVF), respectively. In RVH and RVF, RV weight/ body weight increased by 36% and 109%, whereas RV ejection fraction decreased by 23% and 57% compared to control, respectively. A protein associated with integrins called focal adhesion kinase (FAK) became phosphorylated in RVH (2.5-fold compared to control) but slightly in RVF (1.15-fold compared to control). Phosphorylation of NOS1-P was increased in RVH (3.0-fold compared to control) and in RVF (3.3-fold compared to control). MMP-2 was highest in RVH and intermediate in RVF (3.5- and 1.8-fold compared to control, respectively). MMP-9 was elevated in RVH and RVF (2.4- and 2.9-fold compared to control, respectively). We concluded that activation of FAK in RVH points to an integrin-dependent hypertrophic response of the myocardium. Activation of NOS1 in failing RV suggests a role of excessive NO in the development of failure and activation of MMPs leading to ventricular remodeling.

Chapter 5 provides a comprehensive review of novel therapeutic approaches to treat PAH. PAH is a life-threatening disease with an important pulmonary component that may provide a target to direct therapy. These treatment options include a spectrum of pharmacotherapeutic agents. In addition, we discuss the emerging trends of using gene and cell therapy for the treatment of PAH. Finally, we discuss the possible applications of experimentally tested interventions for

therapeutic purposes in humans with PAH. The therapeutic agents include anti-mitogenic compounds, agents that have pro-endothelial function, agents with vasodilatory effects, compounds with pro-angiogenic effects, anti-inflammatory agents, agents with anti-oxidant effects, and agents that induce apoptosis of pulmonary artery smooth muscle cells.

Cell therapy is a novel treatment option and autologous mesenchymal stem cell (MSC) therapy is expected to be a safe and efficacious option to treat patients with PAH.

Chapter 6 describes a study on the effects of stem cell therapy on pulmonary pathology associated with MCT-induced PAH in rats. We demonstrated that MSCs from donor rats with PAH, injected i.v. into recipient rats that had MCT administration 14 days earlier, reduce pulmonary parenchymal damage, medial hypertrophy of pulmonary arterioles, and RV hypertrophy. At 28 days after MCT, rats had PAH (peak RV pressure had increased from 27.2 to 41.5 mmHg), and increased lung weight (by 73%). Lung histology revealed severe narrowing of precapillary arterioles, thickening of arteriolar walls (3.4-fold increased vs. control), thickening of alveolar septa (3.5-fold increased vs. control), and increased RV mass (by 63% vs. control). Treatment with MSCs attenuated PAH (to 30.7 ± 4.4 mmHg), and almost normalized lung weight (21% higher than control), wall thickness of arterioles (20% higher than control), thickness of alveolar septa (9% higher than control), and RV hypertrophy (RV mass 8% higher than control). Most beneficial effects of i.v. injected MSCs were less prominent or absent in MCT-treated rats i.v. injected with skin fibroblasts. We concluded that i.v. administration of MSCs from donor rats with PAH to recipient rats with PAH decreases RV peak systolic pressure, pulmonary arteriolar narrowing, alveolar septum thickening, and RV hypertrophy. These results suggest that autologous stem cell therapy may help alleviate pulmonary symptoms of patients with PAH.

In **chapter 7** the effects of MCT-induced PAH without and with cell therapy on the RV myocardium are described in more detail. At 28 days after MCT, rats had depressed LV ejection fraction (from 56 to 42%). In PAH rats treated with MSCs, RV ejection fraction was near normal (52%). In MCT-treated rats that had received i.v. skin fibroblasts, effects on RV peak systolic pressure, RVH and RV function were far less pronounced than in MCT-treated rats that had received MSCs. We concluded that i.v. administration of MSCs from donor rats with PAH to recipient rats with PAH decreases PAH, reverses RV hypertrophy, and improves RV function. These results suggest that patients with PAH may be treated successfully using autologous MSCs.

Chapter 8 presents the results of an exploratory study of the electrophysiologic properties of adult rat cardiomyocytes isolated from normal RV myocardium. We analyzed mechanisms of excitability of RV cardiomyocytes isolated from normal adult rat hearts, making use of the naturally occurring variability of excitability of these cells. We focused on the role of voltage-activated K^+ current (I_{kv}), including the transient current I_t and the sustained current I_{ss} , in shaping the current-pulse evoked action potential (AP) and in generating sustained depolarizing current-induced automaticity (DIA). Simulation experiments were carried out with a

computer model of the right ventricular myocyte of the rat. The model experiments reproduced the decrease of AP-duration with an increase in I_t and revealed a DIA-mechanism based on I_{CaL} deinactivation and I_{ss} deactivation at depolarized potentials.

The results provide the electrophysiological baseline-properties of the adult rat right-ventricular myocytes, which can serve as the control properties of these cells if taken from rats with pulmonary hypertension. A provisional comparison of excitability properties of normal RV myocytes with those of PAH RV myocytes showed no striking differences between these two cell types, e.g. DIA occurred in both groups.

Thus, to date it is still unknown whether and how this mechanism of DIA is involved in the high risk of arrhythmias in patients with heart failure.

Conclusions

1. Stimulation of integrin receptors on the cardiomyocyte membrane leads to cardiomyocyte hypertrophy by a nitric oxide-dependent mechanism.
2. Activation of signaling cascades involving the activation of FAK and NOS1 leads to the activation of MMPs in the failing right ventricular myocardium. Activated NOS1 in failing right ventricular myocardium suggests a role of (i) excessive NO in the development of heart failure, and (ii) MMPs leading to ventricular remodeling.
3. Reverse left ventricular remodeling following CRT in patients with congestive heart failure is associated with increased rate of collagen synthesis in the first 6 months of follow-up.
4. Intravenous therapy with mesenchymal stem cells from donor rats with MCT-induced PAH given to recipient rats with MCT-induced PAH reduces right ventricular hypertrophy and improves right ventricular function by improving lung pathology associated with PAH.
5. Insight in the membrane mechanism of depolarization-induced automaticity seems of importance for understanding the high risk of arrhythmias in patients with heart failure.
6. The experiments described in this thesis contribute to the knowledge about molecular and cellular characteristics of hypertrophic and failing myocardium, and may contribute to therapy of patients with PAH with autologous mesenchymal stem cells.

Future perspectives

1. Excessive NO production in the failing myocardium may be harmful and lead to nitrosylation of ryanodine receptors, rendering them dysfunctional as a consequence. More research is needed to define the exact role of (excessive) NO in the failing myocardium.
2. A variety of therapeutic modalities including drug therapy, gene therapy and cell therapy has been tested in several animal models of PAH including MCT-induced PAH in rats. Several of these therapeutic options have been shown to be effective also in PAH patients leading to improved life expectancy and a better quality of life. However, many patients still remain symptomatic despite therapy. Cell therapy is a novel treatment option, but more animal data should be collected to investigate optimal cell type, *in vitro* cell transduction, route of cell administration, and the number of cells to be injected. Autologous mesenchymal stem cell therapy is expected to be a safe and efficacious option to treat patients with PAH.

Samenvatting

De voornaamste doelstellingen van dit proefschrift betreffen het onderzoek naar moleculaire en cellulaire mechanismen die verantwoordelijk zijn voor harthypertrofie en hartfalen. In een onderzoek naar pulmonale hypertensie in ratten die zijn behandeld met monocrotaline is celtherapie getest met mesenchymale stamcellen met het oogmerk deze ziekte bij patiënten te genezen.

Hoofdstuk 1 is gewijd aan de inleiding van het proefschrift. Het geeft informatie over de moleculaire en cellulaire eigenschappen van het gezonde hart, het hypertrofische hart en het falende hart. De samenstelling, synthese en afbraak van de extracellulaire matrix (ECM), de integrines en bijbehorende signaleringspaden, stikstofoxide synthases (NOS) en stikstofoxide (NO) worden besproken in verband met het normale, hypertrofische en falende hart. Ook komen experimentele modellen die worden gebruikt voor de bestudering van harthypertrofie en hartfalen aan de orde. De nadruk ligt met name op de karakterisatie en pathologie van de rechterkamer functie in dieren met pulmonale hypertensie op basis van behandeling met monocrotaline.

In **hoofdstuk 2** is de hypothese dat drukoverbelasting van het hart door het myocard wordt "gevoeld" via rek-achtige effecten door de integrines, een familie van receptoren waarmee de cardiomyocyt gehecht is aan bestanddelen van het ECM. In het celmodel van neonatale rattenhart cardiomyocyten (NRCM) *in vitro* hebben we de integrines gestimuleerd met een pentapeptide dat het RGD-motief bevat, Arg-Gly-Asp, om te testen of integrine stimulatie leidt tot NRCM hypertrofie. Het pro-hypertrofische effect van het RGD-bevattende pentapeptide op NRCM is vergeleken met het goed gedocumenteerde pro-hypertrofische effect van α_1 -adrenoceptor stimulatie met fenylefrine (PE). NRCM die met fysiologisch zout zijn behandeld dienden als controle. De hypertrofische respons is gekwantificeerd door meting van het celoppervlak (CSA). Ook is gemeten hoeveel stikstofoxide synthase-1 (NOS1) gefosforyleerd is. Onder invloed van RGD steeg de CSA met 38% en onder invloed van PE met 68%, ten opzichte van controle. Een remmer van NOS, L-NAME, remde de door RGD gestimuleerde hypertrofie van NRCM volledig, maar had geen effect op de door PE gestimuleerde hypertrofie van NRCM. Remming van de door RGD gestimuleerde hypertrofie van NRCM met behulp van L-NAME kon, tenminste gedeeltelijk, worden doorbroken door toevoeging van een NO-donor, nitroprusside. Toevoeging van nitroprusside had geen effect op NRCM die met PE en L-NAME werden behandeld. Ryanodine en BAPTA-AM remden de door RGD gestimuleerde hypertrofie van NRCM volledig, maar niet de door PE gestimuleerde hypertrofie van NRCM, hetgeen betekent dat intracellulaire Ca^{2+} ionen betrokken zijn bij de door RGD gestimuleerde hypertrofie van NRCM. Onder invloed van RGD steeg het percentage gefosforyleerd NOS-1 met 61%. De conclusie van dit onderzoek was dat integrine stimulatie van NRCM met RGD leidt tot cardiomyocyt hypertrofie. Stopzetten van dit proces met behulp van een NOS remmer en het proces weer aan de gang krijgen met behulp van een NO-

donor doet ons vermoeden dat de door RGD gestimuleerde hypertrofie van NRCM afhankelijk is van NO, waarschijnlijk NO afkomstig van NOS1.

In **hoofdstuk 3** laten we zien dat hartfalen geassocieerd kan zijn met een verstoord collageen metabolisme. In patiënten met hartfalen kan de omzetting van collageen worden gemeten aan de hand van de serum concentraties van de aminoterminalen propeptiden van type I en type III collageen (resp. PINP en PIIINP) en het carboxyterminale telopeptide van type I collageen (ICTP) die maten zijn van hetzij collageen synthese (PINP, PIIINP) of collageen degradatie (ICTP). In 64 patiënten met hartfalen onderzochten wij de effecten van cardiale resynchronisatie therapie (CRT) op myocardiale collageen omzetting door meting van PINP, PIIINP en ICTP in serum verkregen vóór en 6 maanden na start van CRT. De hypothese was dat in patiënten met hartfalen CRT leidt tot kamerverkleining (na kamerdilatatie) die samen gaat met een toename van de myocardiale collageen concentratie. Zesenvestig patiënten (72%) vertoonden een >10% afname van hun linkerkamer eind-systolisch volume na 6 maanden en zij werden op basis hiervan responders genoemd. De andere 18 patiënten (28%) werden non-responders genoemd. Responders lieten een gemiddelde toename van serum PINP en PIIINP zien in de eerste 6 maanden, met resp 42% en 12%. In non-responders veranderden de serum PINP en PIIINP concentraties niet in de eerste 6 maanden. Voor aanvang van CRT hadden de responders significant lagere (met 21%) serum PINP concentraties dan non-responders. Serum ICTP concentraties van responders voor aanvang van CRT waren hoger (met 70%) dan die van non-responders, maar dit verschil was statistisch niet significant. In beide groepen veranderden de serum ICTP concentraties niet in de eerste 6 maanden. Onze conclusie was dat kamerverkleining (na kamerdilatatie) onder invloed van CRT geassocieerd is met een toegenomen myocardiale collageen synthese in de eerste 6 maanden van CRT.

Al lange tijd is bekend dat de door monocrotaline (MCT) opgewekte pulmonale hypertensie (PAH) en rechterkamer hypertrofie in ratten geassocieerd zijn met activatie van matrix metalloproteinases (MMP) in rechterkamer (RV) myocard. In **hoofdstuk 4** onderzochten wij of NO een rol speelt in de door PAH opgewekte RV hypertrofie en RV falen. Om dat te onderzoeken, gebruikten we twee doses MCT: een lage dosis om alleen RV hypertrofie te veroorzaken (RVH) en een hoge dosis om naast RV hypertrofie ook RV falen (RVF) te veroorzaken. In ratten met RVH en RVF was de ratio RV gewicht/lichaamsgewicht toegenomen met resp. 36% en 109%, terwijl de RV ejectiefractie was afgenomen met resp. 23% en 57%, ten opzichte van controle. In RV myocard van ratten met RVH steeg het fosforyleringspercentage van een met integrines geassocieerd eiwit, focal adhesie kinase (FAK), met een factor 2,5, maar in RV myocard van ratten met RVF steeg FAK-P met slechts 15%. De fosforylering van NOS1 in myocard van ratten met RVH en in myocard van ratten met RVF steeg met een factor van resp. 3,0 en 3,3. RV MMP-2 in ratten met RVH was toegenomen met een factor 3,5 en in ratten met RVF toegenomen met een factor 1,8 ten opzichte van controle. RV MMP-9 was toegenomen in ratten met RVH en RVF met een factor van resp. 2,4 en 2,9. Onze conclusie was dat FAK activatie in ratten met RVH wijst op een integrine-afhankelijke hypertrofische respons van het myocard. Activatie van

NOS1 in het falende RV doet ons vermoeden dat excessieve NO concentraties betrokken zijn bij de ontwikkeling van myocardfalen en de activatie van MMPs die de kamerdilatatatie inleiden.

Hoofdstuk 5 geeft een uitgebreid overzicht van therapieën van PAH in proefdieren waarover recent is gerapporteerd. PAH is een levensbedreigende ziekte waarbij de longen in belangrijke mate betrokken zijn. Deze betrokkenheid van de longen biedt een aangrijpingpunt voor therapie. De grote verscheidenheid aan therapieën berust voor een groot gedeelte op geneesmiddelen. Hiertoe behoren anti-mitogene middelen, stoffen met endotheel-beschermende werking, vasodilatoren, stoffen die de angiogenese bevorderen, anti-inflammatoire stoffen, anti-oxidanten en stoffen die de apoptose van gladdespiercellen in de pulmonaal arteriën bevorderen. Ook komen moderne therapieën van PAH aan de orde zoals gen- en celtherapie. Dit hoofdstuk wordt afgesloten met een bespreking van de mogelijke toepassingen van experimenteel geteste interventies op patiënten met PAH. Behandeling van patiënten met PAH met autologe mesenchymale stamcellen (MSCs) uit beenmerg is waarschijnlijk veilig en succesvol en zou in die patiëntengroep kunnen worden getest.

Hoofdstuk 6 beschrijft een onderzoek naar de effecten van stamcel therapie op de long pathologie van ratten met PAH die is opgewekt met MCT. Wij hebben aangetoond dat MSCs die zijn geïsoleerd uit beenmerg van donor ratten met door MCT opgewekte PAH, na intraveneuze inspuiting in ontvanger ratten die 14 dagen eerder waren behandeld met MCT leidden tot (1) minder schade aan het longparenchym, (2) minder hypertrofie van de pulmonale arteriolen en (3) minder RV hypertrofie, dan waargenomen in ratten met door MCT opgewekte PAH die geen stamcel therapie ondergingen. Op het moment van analyse, 28 dagen na behandeling met MCT was de piek-systolische druk in de pulmonaal arterie gestegen van 27.2 tot 41.5 mmHg en het longgewicht toegenomen met 73%. Histologische analyse van de longen liet ernstige vernauwing van de precapillaire arteriolen zien, verdikking van de wand van de arteriolen (toename met een factor 3,4), verdikking van de arteriolaire septa (toename met een factor 3,5), en een toename van het RV gewicht (met 63%), ten opzichte van controle. Behandeling van deze ratten met MSCs, 14 dagen na MCT behandeling, leidde tot verlaging van de piek-systolische druk in de pulmonaal arterie (30.7 ± 4.4 mmHg), een vrijwel normaal longgewicht (21% hoger dan controle), minder verdikking van de arteriolaire wand (20% hoger dan controle), minder verdikking van de alveolaire septa (9% hoger dan controle) en minder RV hypertrofie (RV gewicht 8% hoger dan controle). Naast ratten met PAH die wel of niet zijn behandeld met MSCs en controle ratten, is nog een vierde groep ratten bestudeerd. Deze groep is 14 dagen na MCT behandeling intraveneus ingespoten met huidfibroblasten van gezonde ratten. Deze ratten lieten veel minder grote reacties, of in het geheel geen reacties, zien op longpathologie, piek-systolische druk in de pulmonaal arterie en RV hypertrofie. Onze conclusie was dat intraveneuze toediening van MSCs, geïsoleerd uit beenmerg van donor ratten met PAH, aan ontvanger ratten met PAH leidde tot (1) lagere piek-systolische druk in de pulmonaal arterie, (2) minder ernstige long pathologie en (3) minder RV hypertrofie. Deze resultaten

ondersteunen een toekomstige toepassing van therapie met autologe MSCs in patiënten met PAH.

In **hoofdstuk 7** zijn de effecten van PAH op de rechterkamer functie van ratten die zijn behandeld met MCT, met of zonder celtherapie, beschreven. Op het moment van analyse, 28 dagen na behandeling met MCT, was de RV ejectiefractie gedaald van 56% naar 42%. In ratten met PAH waarbij 14 dagen na MCT MSCs zijn toegediend was de RV ejectiefractie vrijwel normaal (52%). Ratten waarbij 14 dagen na MCT behandeling huidfibroblasten zijn ingespoten, lieten minder grote verbeteringen op RV functie zien dan ratten die MSCs ingespoten kregen. Deze resultaten geven aan dat patiënten met PAH geholpen kunnen zijn met intraveneuze stamcel therapie gebruik makend van autologe MSCs.

Hoofdstuk 8 beschrijft een onderzoek naar de electrofysiologische eigenschappen van cardiomyocyten die zijn geïsoleerd uit RV myocard van gezonde ratten. Dit onderzoek moet de basis bieden voor een later onderzoek waarin electrofysiologische eigenschappen van cardiomyocyten die zijn geïsoleerd uit RV myocard van gezonde ratten worden vergeleken met electrofysiologische eigenschappen van cardiomyocyten die zijn geïsoleerd uit RV myocard van ratten met PAH. In RV cardiomyocyten van gezonde rattenharten maakten we gebruik van de normaal aanwezige variabiliteit in exciteerbaarheid van deze cellen. Wij concentreerden ons op de rol van de spanningsafhankelijke K^+ stroom (I_{kv}), inclusief de kort-durende stroom I_t en de lang-durende stroom I_{ss} , op de actiepotentiaal die wordt opgewekt door korte stroompulsjes en op de automaticiteit die wordt opgewekt door lange, depolariserende stroompulsen. In dit vooronderzoek zijn mogelijke mechanismen van door hartfalen geïnduceerde aritmieën onderzocht door meting van de exciteerbaarheid van cardiomyocyten die zijn geïsoleerd uit de RV van het normale rattenhart. Een biofysisch model van de RV cardiomyocyt van het rattenhart dat in 2001 in de literatuur gepubliceerd is was de basis voor het ontwikkelen van een computermodel waarmee de membraanstromen en membraanspanningen kunnen worden gesimuleerd. Met dit model hebben we de reciproke relatie tussen actiepotentiaalduur en I_t stroom gereproduceerd. Ook leverde dit model een mechanisme voor de automaticiteit die wordt opgewekt door lange, depolariserende stroompulsen. Met name de deactivatie van I_{caL} en de deactivatie van I_{ss} tijdens depolarisatie lijken voor deze automaticiteit verantwoordelijk. Het is nog niet bekend of dit mechanisme van automaticiteit verantwoordelijk is voor het hoge risico op aritmieën in patiënten met hartfalen.

Conclusies

1. Stimulatie van integrines op het membraan van cardiomyocyten bevordert hypertrofie van de cardiomyocyt via een mechanisme dat stikstofoxide afhankelijk is.
2. Signaaltransductie paden waarin activatie van focal adhesie kinase en stikstofoxide synthase-1 optreedt veroorzaken de activatie van matrix

- metalloproteinases in het falende rechter kamer myocard van ratten met pulmonale hypertensie. Geactiveerd stikstofoxide synthase-1 in het falende myocard doet vermoeden dat hartfalen geassocieerd is met (1) excessieve concentraties van stikstofoxide en met (2) geactiveerde matrix metalloproteinases die betrokken zijn bij het optreden van kamerdilatatie.
3. Kamerverkleining (na kamerdilatatie) als gevolg van cardiale resynchronisatie therapie in patiënten met hartfalen is geassocieerd met een toename van de myocardiale collageen synthese in de eerste 6 maanden na start van therapie.
 4. Intraveneuze toediening van mesenchymale stamcellen van donor ratten met door monocrotaline opgewekte pulmonale hypertensie aan ontvanger ratten met door monocrotaline opgewekte pulmonale hypertensie vermindert de bloeddruk in de pulmonaal arterie, vermindert de rechter kamer hypertrofie en verbetert de rechter kamer functie, verbeteringen die sterk gerelateerd zijn aan verbetering van de long pathologie.
 5. Inzicht in het membraanmechanisme van depolarisatie-geïnduceerde automatie lijkt van belang voor een beter begrip van het hoge risico op aritmieën in patiënten met hartfalen.
 6. De experimenten die in dit proefschrift zijn beschreven zijn bedoeld als bijdrage aan de kennis omtrent moleculaire en cellulaire mechanismen die verantwoordelijk zijn voor harthypertrofie en hartfalen. Wij hopen dat deze experimenten ook mogen bijdragen aan de introductie van stamceltherapie voor patiënten met pulmonale hypertensie met behulp van autologe mesenchymale stamcellen.

Toekomstperspectief

1. Overmatige stikstofoxide concentraties in het falende hart zijn waarschijnlijk schadelijk en kunnen leiden tot nitrosylering van o.a. ryanodine receptoren waardoor ze Ca^{2+} ionen lekken tijdens diastole. Het is aan te bevelen in de toekomst de effecten van overmatige stikstofoxide concentraties in en op het falende myocard te bestuderen.
2. Verscheidene therapeutische modaliteiten inclusief farmacotherapie, genterapie en celtherapie zijn getest in diermodellen van pulmonale hypertensie, zoals de door monocrotaline opgewekte pulmonale hypertensie in ratten. Een aantal van deze therapieën hebben hun waarde al in patiënten met pulmonale hypertensie bewezen, hetgeen geleid heeft tot een verbeterde levensverwachting en een betere kwaliteit van leven. Echter, vele patiënten met pulmonale hypertensie blijven symptomatisch ondanks therapie. Voor hen zou celtherapie een uitkomst kunnen zijn, maar vooralsnog is er behoefte aan meer onderzoek naar het optimale celtype, naar de vraag of de toe te dienen cellen *in vitro* nog een voorbehandeling moeten ondergaan, naar de route van celtoediening en naar het optimale aantal in te spuiten cellen. Niettemin verwachten wij dat intraveneuze therapie met autologe mesenchymale stamcellen veilig is en effectief voor patiënten met pulmonale hypertensie.

List of publications

- **Umar S**, Steendijk P, de Visser YP, Wagenaar GTM, Schutte CI, Bax WH, Pijnappels DA, Atsma DE, Schalij MJ, van der Wall EE, van der Laarse A. Intravenous cell therapy given to rats with monocrotaline-induced pulmonary artery hypertension reduces right ventricular hypertrophy and improves right ventricular function by restoring precapillary pulmonary artery patency (abstract). *Journal of American College of Cardiology* 2009; 53: A144-A197.
- **Umar S**, de Visser YP, Steendijk P, Schutte CI, Laghmani E, Wagenaar GTM, Bax WH, Mantikou E, Pijnappels DA, Atsma DE, Schalij MJ, van der Wall EE, van der Laarse A. Stem cell therapy attenuates right ventricular pressure overload, hypertrophy, and dysfunction by improving lung pathology in rats with pulmonary hypertension. *Submitted*, 2009.
- **Umar S**, van der Valk EJM, Schalij MJ, van der Wall EE, Atsma DE, van der Laarse A. Integrin stimulation-induced hypertrophy in neonatal rat cardiomyocytes is NO-dependent. *Molecular and Cellular Biochemistry* 2009;320:75-84.
- **Umar S**, van der Laarse A. Nitric oxide and nitric oxide synthase isoforms in the normal, hypertrophic and failing heart. *Submitted*, 2009.
- **Umar S**, Steendijk P, Ypey DL, Atsma DE, van der Wall EE, Schalij MJ, van der Laarse A. Novel approaches to treat pulmonary arterial hypertension. *Submitted*, 2009.
- Li Z, **Umar S**, Van der Valk EJM, Bax WH, Schutte CI, van der Laarse A. Integrin stimulation favors uptake of macromolecules by cardiomyocytes *in vitro*. *Submitted*, 2009.
- **Umar S**, Bax JJ, Klok M, van Bommel RJ, Hessel MHM, den Adel B, Bleeker GB, Henneman MM, Atsma DE, van der Wall EE, Schalij MJ, van der Laarse A. Myocardial collagen metabolism in failing hearts before and during cardiac resynchronisation therapy. *European Journal of Heart Failure* 2008;10:878-883.
- **Umar S**, van der Valk EJM, Schalij MJ, van der Wall EE, Atsma DE, van der Laarse A. Integrin stimulation-induced hypertrophy in neonatal rat cardiomyocytes is NO-dependent (abstract). *Journal of American College of Cardiology* 2008; 51: A35-A82.
- **Umar S**, Hessel M, Steendijk P, Bax W, Schutte C, Schalij M, van der Wall E, Atsma D, van der Laarse A. Activation of signaling molecules and matrix metalloproteinases in right ventricular myocardium of rats with pulmonary hypertension. *Pathology - Research and Practice* 2007; 203: 863-872.

- **Umar S**, Bax JJ, Klok M, Hessel MHM, den Adel B, Bleeker GB, Henneman MM, Atsma DE, van der Wall EE, Schalij MJ, van der Laarse A. Myocardial collagen metabolism in failing hearts before and during cardiac resynchronisation therapy (abstract). *Circulation* 2007; 116:II_690.
- **Umar S**, Hessel MH, Bax WH, Schutte CI, Steendijk P, van der Laarse A. Activation of focal adhesion kinase and neuronal nitric oxide synthase in right ventricular myocardium of rats with right-sided congestive heart failure (abstract). *Journal of American College of Cardiology* 2006; 47; 387A-418A.

Oral and poster presentations at international scientific conferences

- Poster presentation at **EUROPACE** conference in Berlin, Germany. Titled, "Making an extra beat: studying cellular arrhythmogenic activity with a computer model". van Meerwijk WPM, Umar S, van der Laarse A Pijnappels DA, Schalij MJ, Ypey DL, June 2009.
- Poster presentation at **The Netherlands Heart Society (NVVC)** Spring congress in Amsterdam, the Netherlands. Titled, "Intravenous administration of mesenchymal stem cells improves right ventricular function and restores right ventricular troponin I concentration in rats with pulmonary hypertension". Hoek TGT, Umar S, Steendijk P, Schutte CI, Bax WH, Pijnappels DA, Atsma DE, Schalij MJ, van der Wall EE, van der Laarse A, April 2009.
- Poster presentation at **The American College of Cardiology (ACC)** 58th Annual Scientific Sessions in Orlando, FL, USA, March 2009. Titled, "Intravenous cell therapy given to rats with monocrotaline-induced pulmonary artery hypertension reduces right ventricular hypertrophy and improves right ventricular function by restoring precapillary pulmonary artery patency". **Umar S**, Steendijk P, de Visser YP, Wagenaar GTM, Schutte CI, Bax WH, Pijnappels DA, Atsma DE, Schalij MJ, Van der Wall EE, van der Laarse A.
- Poster presentation at **The Netherlands Heart Society (NVVC)** Spring congress in Amsterdam, the Netherlands. Titled, "Intravenous cell therapy reduces right ventricular hypertrophy and right ventricular pressure overload in rats with pulmonary artery hypertension". **Umar S**, Steendijk P, Wagenaar GTM, Schutte CI, Bax WH, Pijnappels DA, Schalij MJ, van der Wall EE, Atsma DE, van der Laarse A, April 2008.

- Poster presentation at **The American College of Cardiology (ACC) 57th** Annual Scientific Sessions in Chicago, IL, USA, March 2008. Titled, "Integrin stimulation-induced hypertrophy in neonatal rat cardiomyocytes is NO-dependent". **Umar S**, van der Valk EJM, Schalij MJ, van der Wall EE, Atsma DE, van der Laarse A.
- Oral presentation at **The American Heart Association (AHA)** Annual Scientific Sessions in Orlando, FL, USA, November 2007. Titled, "Myocardial collagen metabolism in failing hearts before and during cardiac resynchronisation therapy". **Umar S**, Bax JJ, Klok M, Hessel MHM, den Adel B, Bleeker GB, Henneman MM, Atsma DE, van der Wall EE, Schalij MJ, van der Laarse A.
- Poster Presentation at **American College of Cardiology (ACC) 55th** Annual Scientific Sessions in Atlanta, GA, USA, March 2006. Titled, "Activation of Focal Adhesion Kinase and neuronal Nitric Oxide Synthase in right ventricular myocardium of rats with right-sided congestive heart failure". **Umar S**, Hessel MHM, Bax WH, Schutte CI, Steendijk P, van der Laarse A.
- Oral Presentation at **The National Institute of Cardiovascular diseases (NICVD)** International Congress of Cardiology in Karachi, Pakistan, December 2005. Titled, "Activation of signaling molecules and matrix metalloproteinases in right ventricular myocardium of rats with pulmonary hypertension". **Umar S**, Hessel MHM, Bax WH, Schutte CI, Steendijk P, van der Laarse A.
- Oral Presentation at **The Netherlands Heart Society (NVVC)** Autumn congress in Ermelo, the Netherlands, October 2005. Titled, "Activation of focal adhesion kinase and neuronal nitric oxide synthase in right ventricular myocardium of rats with right-sided congestive heart failure". **Umar S**, Hessel MHM, Bax WH, Schutte CI, Steendijk P, van der Laarse A.

Acknowledgements

I would like to thank all the colleagues and staff at the Department of Cardiology, LUMC, the Higher Education Commission (HEC) of Pakistan and the Netherlands Organization for International Cooperation in Higher Education (NUFFIC), the Hague, for their continuous support, especially Mrs. Loes Minkman from NUFFIC for her kind cooperation all the way.

I have utmost respect and gratitude for respected Mrs. Veling and her caring family. You took care of me like one of your own family members since the moment I arrived in the Netherlands. I can never forget your warmth, hospitality and the delicious meals that you cooked for me with motherly compassion. I sincerely wish future brings more happiness for your family.

A special word of thanks to my colleagues at the lab Cardiology, Lizet for your scientific help and introducing me to the Dutch culture every now and then. Minka and Robert, their bright young kids, my best friends Jochem and Martijn, hartelijk bedankt! Cindy for your enormous help all the way and in particular for the MCT project, you are such a good company, I really had a good time working with you. Ton for giving me occasional Dutch lessons and helping me with the cannulation of the hearts on the Langendorff, Margreet for your brilliant work for the project especially for your contribution to chapter 3 of this thesis. Brigit and Marleen for helping me out at the start of my PhD, and for being such nice colleagues, I wish you a lot of success in your respective future endeavors. Daniel and Arti for your continuous encouragement of my work and for our valuable friendship. I am sure both of you have a very bright future ahead of you. A special thanks to Daniel for valuable help with making the cover of this thesis. Dr. Li for your friendship and Chinese lessons.

Talitha and Lya for arranging all the documents necessary to start and continue my PhD and all the colleagues from the “tuin”. Colleagues from the Department of Paediatrics, Gerry and Yvonne for their collaboration in the stem cell therapy project.

My students Kei Nishioka from Japan and Eleni Mantikou from Greece for their extraordinary work at the lab and useful scientific discussions. Dr. Ton Baartscheer (Department of Molecular Cardiology, AMC, Amsterdam) for his valuable input regarding the cardiomyocytes isolation procedure, Mrs. Trudy van Kempen (MCB, LUMC) for helping with coating the glasses, Dr. Kees Swenne, Arie Maan and Sum-Che Man for helping analyze the ECGs, Wilbert for your amazing work with the computer model, I hope we take it further and expand our exploration.

To all my Pakistani friends in the Netherlands, especially Aamir, when I badly needed a friend, you were there for me. Asghar, Tariq, Hasnain bhai, Shahbaz, Jahangir, Qamar, Fraz and all the others, I thank you from the bottom of my heart and sincerely hope you guys finish your PhDs with a lot of success.

My international friends Nina, Victoria, Gaetano, Matteo, Chiara, Silvia and Rutger “grazie mille” for being such great friends and for the beautiful time we have had together and I wish you all the success in life and continuation of our friendship.

A special thanks to all the doctors and nurses who took great care of me at the Department of Haematology and short stay (LUMC), especially my doctor, Dr. Eefting.

On a personal note, I am indebted to my father, my biggest inspiration in life, my mother, my lifeline, my brothers Rehan and Adnan, without whom my

achievements are incomplete and my sister Asma, the little doctor of our family, I just could not have done anything without your constant support and encouragement.

And finally to my partner for life Federica, with you around nothing seems impossible, and with you it feels as if my life has just begun and my ambitions still young!

Curriculum vitae

Soban Umar, the author of this thesis, was born on June 24, 1979 in Multan, Pakistan. He completed his pre-medical studies from Govt. College Multan in 1997, standing 2nd in the board of Intermediate and Secondary Education. He completed his Bachelors in Medicine and Bachelors in Surgery (M.B.B.S) degree in 2002 with distinction from Nishtar Medical College Multan, Pakistan, securing first position in both the college as well as Bahauddin Zakariya University, Multan, Pakistan. He worked as a House Officer in the Departments of Surgery, Dermatology and Family Medicine of Nishtar Hospital Multan, Pakistan (2002-2005).

He passed the United States Medical Licensing Examinations (USMLE) Step-1 (2003), Step-2 Clinical knowledge (2004) and Step-2 Clinical Skills (2005) and became a certified M.D. by the Educational Commission for Foreign Medical Graduates, (ECFMG[®]) Philadelphia, PA, USA in 2005.

In 2005, he won the foreign PhD scholarship from the Higher Education Commission (HEC) of Pakistan and the Netherlands Organization for International Cooperation in Higher Education (NUFFIC) for completing a Doctoral Research Fellowship in Cardiology in The Netherlands. He pursued his PhD research at the Department of Cardiology, Leiden University Medical Center (LUMC), Leiden, the Netherlands (2005-2009) under the supervision of Prof.dr. A. van der Laarse. He has presented his research in prestigious conferences of Cardiology held in Atlanta (GA, USA), Orlando (FL, USA), Chicago (IL, USA), Karachi (Pakistan), Ermelo and Amsterdam (the Netherlands). He has been able to get his research papers published in international peer-reviewed journals.

